Mechanism of chiral symmetry breaking for three flavours of light quarks and extrapolations of Lattice QCD results

Guillaume Toucas

ED-517 Particules, Noyaux, Cosmos

THÈSE DE DOCTORAT

Présentée pour obtenir le grade de

Docteur ès Sciences de l'Université Paris-Sud 11

Spécialité: PHYSIQUE THÉORIQUE

par

Guillaume TOUCAS

Mécanisme de brisure de symétrie chirale pour trois saveurs de quarks légers et extrapolation de résultats de Chromodynamique Quantique sur réseau

Soutenue le 30 octobre 2012 devant le jury composé de:

Prof.	A. Abada	Président du jury
Dr.	V. Bernard	Directeur de thèse
Dr.	S. Descotes-Genon	Directeur de thèse
Prof.	J. Flynn	Rapporteur
Dr.	B. Kubis	Rapporteur
Dr.	C. Smith	Examinateur

Antoine

se renverse la tête.

Qui donc es-tu ?

Hilarion

Mon royaume est de la dimension de l'univers; et mon désir n'a pas de bornes. Je vais toujours, affranchissant l'esprit et pesant les mondes, sans haine, sans peur, sans pitié, sans amour et sans Dieu. On m'appelle la Science.

Antoine

se rejette en arrière :

Tu dois être plutôt... le Diable !

Hilarion

fixant sur lui ses prunelles :

Veux-tu le voir ?

Gustave Flaubert, *La tentation de Saint-Antoine*

Remerciements

Je remercie tout d'abord Henk Hilhorst, le directeur du Laboratoire de Physique Théorique d'Orsay, de m'avoir acceuillit au sein de son unité durant ces trois années marqué par un travail complexe et difficile. Par ailleurs, celui-ci n'aurait pu s'éffectuer sans l'aide de mes deux directeurs de thèse, Sébastien Descotes-Genon et Véronique Bernard, qui ont su trouver la patience infallible de mener à bien leur travail d'encadrement. Je les remercie de n'avoir jamais cédé au découragement.

Je voudrais maintenant adresser un grand merci à Benoît Blossier, qui partagea mon bureau ces trois années durant. Nos discussions politico-sociales passionnées sur l'actualité du monde seront pour moi un des meilleurs souvenirs humains de mes années de thèse.

Je remercie bien entendu tous les membres de mon jury, avec une mention particulière pour Asmaa Abada, du Laboratoire, qui en accepta le role de présidente, ainsi que pour ses précieux conseils concernant la tenue de la soutenance.

Enfin, cette thése n'aurait pu se terminer sans l'aide d'Olivier Pène, grâce à laquelle je su restreindre les inhibitions que j'entretenais à propos de la terrible QCD sur réseau, qui hanta mes cauchemars durant l'une des périodes les plus difficiles de l'écriture du manuscrit. Merci encore Olivier.

Ces quelques mots ne sauraient être complêts sans une adresse à tous mes camarades doctorants: Cédric, Julien, Joachim, Blaise, Charles, Andréas, Yannis, Antonin, Adrien, Antoine, Xavier, Bertrand, Jérémie, Julien... que ceux qui seraient oubliés hurlent très fort !... Hélas, ma mémoire commence serieusement à flancher !

Je remercie enfin tous les autres membres du Laboratoire de Physique Théorique: Philippe, Samuel, Damir, Odile, Mireille, Philippe, Jean-Pierre, Patricia ainsi que tout ceux que j'oublie. Je voudrais aussi adresser mes plus sincères salutations à Hagop Sazdjian, mon responsable d'enseignement des TDs de L1 que je dispensais chaque semaine avec grand plaisir.

Enfin, un tout dernier mot à l'attention de toute la famille grâce à son aide, je pu malgré tout traverser cette épreuve qui se termine enfin.

Contents

Introduction

The Standard Model of particle physics provides a very powerful and efficient description of the constituents of matter and their interactions − with its last element, the Higgs boson, likely to have been observed at CERN very recently. However, this does not mean that our understanding of the Standard Model is complete, nor that accurate predictions for all possible processes are available within this framework. Indeed, one of the three interactions, namely the strong interaction, has the particularity of becoming strongly coupled at low energies (below 1 GeV). The perturbative approach to QCD consisting in an expansion in powers of the strong coupling constant α_S is then no more relevant. One has to rely on alternative methods in order to probe hadronic phenomena at low energy. On one side, it is possible to build an Effective Field Theory (EFT) of QCD based on the main phenomenon occuring at low energies, i.e. the spontaneous breakdown of chiral symmetry (a flavour symmetry which is exact at the level of QCD lagrangian in the limit where the light quarks (u, d and s) are massless). In this effective theory, the fundamental degrees of freedom of QCD, quarks and gluons, are then replaced by *effective* degrees of freedom which can be identified to the eight pseudo-scalar light mesons of the QCD spectrum: $\pi^{+,0,-}$, $K^{+,-}$, $\bar{K^0}, K^0$ and η. The theory is an expansion of the hadronic observables in powers of the meson momentum and the quark masses: this is Chiral Perturbation Theory (χPT). On the other side, it is possible to rely on the numerical calculations of (some) low-energy hadronic observables. The 4-dimensional Minkowskian space-time is discretized into a 4-dimensional pseudo-euclidean discrete lattice, along with the quark and gluons fields. This leads to a path-integral "on the lattice", which can be evaluated through Monte-Carlo techniques: this is Lattice QCD (LQCD).

Those two methods, Effective Field Theory and Lattice QCD, are complementary: Chiral Perturbation Theory contain a certain amount of unknown parameters, called low-energy constants, which must be evaluated numerically using experimental and/or lattice data. Lattice QCD, even if a very powerful tool, is not always able to perform simulations at the physical values of the masses of the light quarks. Chiral Perturbation Theory is therefore used to extrapolate the "raw" lattice data to the physical point. But this is far from being a straightforward business: several lattice collaborations [96, 99, 100, 101, 102, 103] performing simulations with 2+1 dynamical quarks found difficulties in fitting their data when using Chiral Perturbation Theory built with three flavours of light quarks (u,d and s).

One may wonder whether this might be due only to intrinsic problems of the Lattice QCD approach, or if this might come from three-flavours χPT. Recent phenomenological analysis of experimental data (analysis of $\pi\pi$ and Kπ scattering [51, 52, 53, 54, 55, 56, 62, 63], fits to next-to-next-to-leading order χPT formulae [40], sum-rule estimate of low-energy constants [70, 71, 72]) suggest that there are indeed problems with the convergence chiral expansions built around the limit of three massless flavours. On the other hand, other experimental studies concerning the pion sector ($\pi\pi$ scattering from $K_{\ell 4}$ and $K \to 3\pi$ decays [53, 55, 56], lattice simulations for the pion mass and decay constant [96, 100, 101, 102, 103]) indicate that such problems do not occur within χPT built around the limit of two massless flavours, and dealing only with pions as degrees of freedom.

This set of results hints at a possible problem of convergence in the three-flavour chiral expansions themselves, in which the leading order (LO) would be in a numerical competition with the next-to-leading order (NLO), i.e. instead of the usual assumption that the leading order terms saturate almost the chiral expansions, there could be leading *and* next-to-leading order contributions with the same numerical weight (this problem being absent in the two-flavour theory). Such a scenario was advocated already some time ago [79]. The presence of massive $\bar{s}s$ pairs in the vacuum could have a significant of suppressing the chiral order parameters arising at LO in the three-flavours expansion, i.e. the quark condensate and the pseudoscalar decay constant in the limit $m_{u,d,s} \to 0$. This effect, related to the (observed) significant violation of the Zweig rule in the scalar sector, would affect the convergence of three-flavour chiral expansions leading to the problem encountered in both lattice and phenomenological analyses. On the other side, this scenario would still allow for a large condensate in the two-flavour chiral limit ($m_{u,d} \to 0$, m_s physical), leading to a good convergence of the expansions in m_u and m_d provided by two-flavour χPT. In order to cope with the numerical competition of leading and next-to-leading order in the three-flavour chiral expansions, a modified version of χPT, going under the name of Resummed Chiral Perturbation Theory (ReχPT), was designed. It was applied to the phenomenological analyses of $\pi\pi$ and πK scatterings [79, 81, 83, 84].

The main goal of this present thesis is therefore to extend this analysis to results from Lattie QCD simulations, with two different outcomes. First, we want to extract the pattern of chiral symmetry breaking in the limit of three massless flavours from lattice data, and check if the quark condensate and/or the pseudoscalar decay constant are indeed suppressed. Lattice data is complementary to experimental results in this respect, since the former probe the quark mass-dependence of pseudoscalar observables, which is out of reach for experiments.

Secondly, we want to determine how the extrapolation of lattice results to the physical quark masses is affected by alternative chiral expansions allowing for a suppression of LO contributions. This could constitute an additional and still poorly known systematics to the current lattice results, leading to significant changes in some of the tests of the Standard Model at low energy in the hadronic sector.

With these two questions in mind, we focus on observables that are accessible to lattice simulations and described by χPT, namely observables involving pseudoscalar mesons (decay constants, masses, electromagnetic and $K_{\ell 3}$ form factors) as well as topological quantities (topological susceptibility and fourth cumulant of the gluonic winding number).

The structure of this thesis is the following: in Chapter 1, we first make a presentation of QCD, its relevant symmetries (specifically chiral symmetry), and give an account regarding some aspects of its vacuum structure. In Chapter 2, we provide a short introduction to the concepts of Lattice QCD and Effective Field Theories, and make a detailed and thorough presentation of Chiral Perturbation Theory. Then in Chapter 3 we introduce Resummed χPT and explain why it could provide the proper treatment when chiral expansions are subjected to the convergence problems introduced above. In Chapter 4, we discuss the various fits we have performed over lattice data to (resummed) chiral expansions, for observables related to pseudoscalar mesons. Finally, in Chapter 5, we investigate the potentiality of topological quantities to constrain the pattern of chiral symmetry breaking, and in Chapter 6, we discuss other sets of fits that include lattice data concerning the topological susceptibility.

Chapter 1

QCD, Symmetries, and the Vacuum

1.1 Introduction

The Standard Model (SM) of Particle Physics is a theoretical description of the constituents of matter and their interactions at the most fundamental level. It dwells its theoretical foundations on Quantum Field Theory and Group Theory. Its powerfulness and elegance draw from a systematic use of symmetry principles, on one side to classify particles, on the other, to build the different interactions that occur between them. It is a result of a deeply interwoven work between experiment and theory, whose history spanned through nearly a half of the twentieth century, beginning in the 1930s with the birth of QuantumElectroDynamics (QED), and culminating in the early 1980s with the experimental discovery of the W and Z bosons, and the top quark in the mid 1990s. It accounts, up to a very good precision, for all the experimental observations that have been made until now. Finally it was announced in the 4th of July 2012 by the CERN commitee that a new signal around 126 GeV could be compatible with a Higgs-boson like particle. The new data provided by the ATLAS and CMS experiments at the Large Hadron Collider seems to point, at last, towards a long-awaited answer concerning the foundations of the Standard Model.

If a large part of the research about the Standard Model focuses on understanding the the electro-weak sector and the Higgs mechanism, another (substantial) part is devoted to the study of the strong interaction. This interaction shows a number of particular features, that put it somehow apart from the two other known interactions, the electromagnetic and the weak ones (besides the fact that no unification has (yet) been found between the electroweak and the strong sector). In the late sixties, the studies on the hadronic spectrum suggested that hadrons had an internal structure - that they were made of elementary fermionic particles: the quarks. In 1964, Murray Gell-Mann and George Zweig came with the quark model, postulating the existence of the three light quarks: the *up* u, the *down* d and the *strange* s. They were therefore able to explain the hadronic multiplets in terms of products of representations of doublets and triplets of quark flavour ($SU(2)$ and $SU(3)$ flavour symmetry). The quarks were subsequently discovered experimentally at SLAC in 1968. But the u d and s quarks were not the only ones to exist - the charm, the bottom and top quarks were latter discovered: in 1974, the charm was introduced to account for the existence of the J/ψ particle, the bottom and the top were postulated in the 1970s to explain $\mathcal{CP}$ violation in kaon decays - experimental evidence followed for the bottom in 1977 and in 1995 for the top, both at the Fermilab facility. But in the mid-sixties, shortly after the birth of Gell-Mann and Zweig's quark model, a mystery remained: how to account for the existence of the three-time

strange Ω baryon (sss) and the three-time up Δ^{++} baryon (uuu), which obviously seemed to violate the Fermi principle ? The answer to this puzzle was the introduction of another quantum number: the colour. The quarks were now bearers of a new degree of freedom and this lifted up the apparent degeneracy amongst the quarks in the Ω and the Δ^{++} baryons.

This gave rise to the $SU(3)$ colour gauge symmetry, which was one of the fundamental dynamical symmetries of particle physics, along with the $(SU(2)_L \times U(1)_Y)$ symmetry of the electroweak sector. In this framework, quarks interact through the mean of 8 gauge bosons, the gluons. This dynamics is described by Quantum ChromoDynamics (QCD), a Quantum Field Theory whose main parameter, beside the fields's masses, is the coupling constant α_S, which parametrize the strength of the quark-gluon and gluon-gluon interactions.

QCD possesses two peculiar properties: *confinement* and *asymptotic freedom*. The asymptotic freedom states that as energy increases, quark interactions becomes weaker and weaker. It means that at low energy, the usual perturbative expansion in terms of powers of the strong coupling constant, α_s, becomes irrelevant. There are however two main alternatives to this lack of viable analytical methods at the low-energy level:

First, one can construct an Effective Field Theory (EFT) of QCD in the low-energy limit, where quarks and gluons are replaced by effective degrees of freedom which are identified to the eight pseudo-scalar light mesons π, K and η. It is then possible to perform an expansion of the hadronic observables in powers of the meson momentum and the quark masses (therefore recovering some kind of perturbative method). This theory was coined Chiral Perturbation Theory, since it is built upon the spontaneous breaking of QCD chiral symmetry.

The second alternative relies on numerical calculations of hadronic observables. This technique consists in discretizing the 4-dimensional Minkowskian space-time into a 4-dimensional pseudo-euclidean discrete lattice. The quarks and gluons fields are themselves discretized, leading to a path-integral "on the lattice", which is then possible to evaluate with the help of the appropriate algorithms (Monte-Carlo techniques), and powerful computers. This is the domain of Lattice QCD (LQCD). The two methods, Effective Field Theory and Lattice QCD, are complementary − as it will be explained in details in Chapter 2.

This introductory chapter aims to provide a general account of Quantum Chromodynamics, its associated symmetries (sections 1.2 and 1.3), and its vacuum structure (section 1.4.5), before moving in the next chapter to a general presentation of Effective Field Theories and Lattice QCD.

1.2 QCD and Chiral Symmetry

1.2.1 The QCD lagrangian and asymptotic freedom

Quantum Chromodynamics is based upon a local colour symmetry group, $SU_C(3)$. This group is generated by the Gell-Mann matrices T^a, with $a = 1...8$. They have the following commutation relations: $\left[T^a, T^b\right] = if^{abc}T^c$, where f^{abc} are the structure constants defining the $SU(3)$ Lie algebra (for a full-fledged treatment of the $SU(3)$ group, see for example [10]). The quarks, carrying a colour charge, transform under its fundamental representation whereas the gluons (carrying both a colour and an anti-colour charge) transform, as gauge bosons, in the adjoint representation. Using gauge symmetry, one can divide the QCD lagrangian into three main sectors:

$$\mathcal{L}_{QCD} = \mathcal{L}_{quarks} + \mathcal{L}_{gluons} + \mathcal{L}_{topological} \tag{1.1}$$

Each of those "sub-lagrangians" is expressed in terms of the quarks fields (q for the light quarks u, d, s, and Q for the heavy quarks c, b, t) and the gluon fields A^μ:

$$\mathcal{L}_{quarks} = \sum_Q \bar{Q}(i\gamma_\mu D^\mu - M_Q)Q + \sum_q \bar{q}(i\gamma_\mu D^\mu - m_q)q \tag{1.2}$$

$$\mathcal{L}_{gluons} = -\frac{1}{4}G_a^{\mu\nu}G^a_{\mu\nu}, \quad \mathcal{L}_{topological} = -\frac{g^2}{32\pi^2}\theta_0\tilde{G}_a^{\mu\nu}G^a_{\mu\nu} \tag{1.3}$$

$\gamma_\mu D^\mu = \gamma_\mu(\partial^\mu - igA_a^\mu T^a)$ is the covariant derivative acting on the quark fields Q and q, $G^a_{\mu\nu} = \partial_\mu A^a_\nu - \partial_\nu A^a_\mu + g f^{abc} A^b_\mu A^c_\nu$ the gluon strength tensor, and its dual $\tilde{G}^{\mu\nu,a} = \frac{1}{2}\epsilon^{\mu\nu\rho\sigma}G^a_{\rho\sigma}$. $\mathcal{L}_{quarks}$ gathers the quarks-gluon dynamics through the covariant derivative, and the quark mass terms $m_q\bar{q}q$ and $M_Q\bar{Q}Q$. This separation is meant to reflect the hierarchy between the quark masses, and in particular that three of them (u,d,s) are light compared to the typical hadronic scale $\Lambda_\chi = 1$ GeV. $\mathcal{L}_{gluons}$ is the pure gluonic dynamics, telling how gluons would propagate and interact in an hypothetic quark-free world.

Finally, $\mathcal{L}_{topological}$, as its name suggests, corresponds to a topological term that does not enter equations of motion of quarks and gluons (it is not a dynamical term), but that is tied to the vacuum structure of the theory through its parameter, the vacuum angle θ_0. It introduces a violation of $\mathcal{CP}$ [7], which is usually neglected due to its smallness. Indeed, measurements performed on the neutron dipole electric moment lead to a very tiny bound on θ_0, of the order [1] of 10^{-10}. More shall be said about the topological term in sec. 1.4.5.

As was mentioned in the introduction, QCD possesses two very specific properties: *confinement* and *asymptotic freedom*. The confinement property states that the quarks are bound into hadrons, i.e. they can not be isolated nor individually observed. This is indeed the case since no experiment was able to observe free quarks (and also free gluons). Still, we get experimental evidence of those particules through the observations of jets. The asymptotic freedom, on the other side, is one of the most well-experimentally tested predictions of QCD dynamics: as the energy increase, interactions between quarks become weaker and weaker. This can be directly observed from the running of the coupling constant α_S cf. figure 1.1. This main prediction of QCD theory was discovered in 1970 by Politzer, Gross and Wilczek, which led to a Nobel prize in 2004.

The calculation of the running of α_s (an the subsequent theoretical observation of asymptotic freedom) can be performed using the usual Quantum Field Theory perturbative technics [6, 8, 9]. Confinement, however, as we stated before, can not be predicted from the theory. This "un-predictability" is due to the impossibility to get a satisfying description of QCD at low energies in terms of quarks and gluons (under the scale $\Lambda \sim 1$ GeV). Indeed the perturbative techniques rely on the expansion of QCD correlators describing the different hadronic observables in terms of an expansion in powers of α_S. It supposes that α_S remains reasonably small for this expansion to be valid. But in the low-energy regime, where α_S increases because of the asymptotic freedom property, a power expansion in terms of the coupling constant is no more relevant. Uses of effective field theoretic methods and numerical computations can prove viable alternatives to probe QCD at low energies.

1.2.2 Chiral symmetry

Apart from the $SU(3)$ colour gauge symmetry, the QCD lagrangian for the light quarks in the chiral limit: $m_{u,d,s} \to 0$ is also invariant under the global symmetry group $SU(3)_L \otimes SU(3)_R$

[1] Nothing in the Standard Model explains why this violation is so small. One remedy to this puzzle is the famous axion particle, introduced through the Peccei-Quinn mechanism [16, 17].

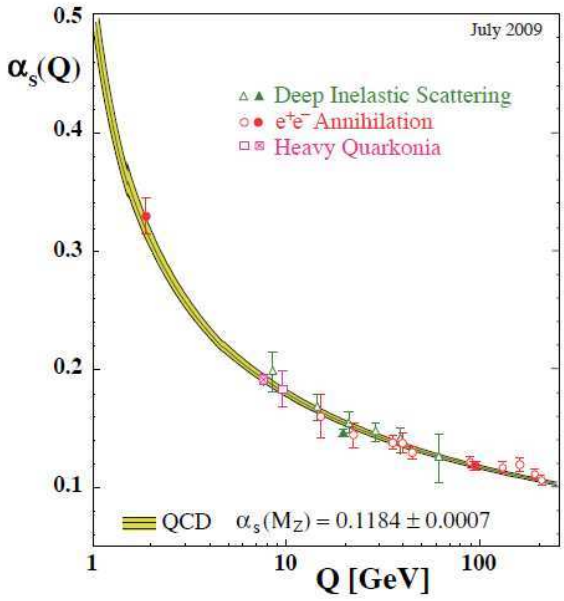

Figure 1.1: The running of the strong coupling constant α_S from the Particle Data Group [68].

which acts in flavour space on the right and left chiralities of the quark fields through the projection:

$$q_{R,L} = P_{R,L} q, \quad P_{R,L} = \frac{1 \pm \gamma^5}{2} \tag{1.4}$$

In the limit of a zero mass term, chirality is identified with helicity (projection of a particle's spin over its momentum) [2]. The "left" and "right" chiralities corresponds to the $\pm 1/2$ values of the helicity. Besides, chirality is always Lorentz invariant, whereas it happens only in the massless case for the helicity.

The massless quark lagrangian can therefore be split into the right and left chiralities:

$$\mathcal{L}^{m,}_{light\ quarks} = \sum_q \bar{q}_R (i\gamma_\mu D^\mu) q_R + \bar{q}_L (i\gamma_\mu D^\mu) q_L \tag{1.5}$$

We regroup the light quarks into a flavour triplet:

$$\psi_{R,L} = \begin{pmatrix} u_{R,L} \\ d_{R,L} \\ s_{R,L} \end{pmatrix} \tag{1.6}$$

Then, the QCD lagrangian is invariant under independent rotations of the chiralities in the space of light flavours:

$$\psi_{R,L} \rightarrow g_{R,L} \psi_{R,L}, \quad g_{R,L} \in SU(3)_{R,L} \tag{1.7}$$

If we add the vector phase invariance $U(1)_V$ (related to baryon number conservation), which is the same for the three light quarks (the triplet ψ transforms like $\psi \rightarrow e^{i\alpha}\psi$), we get the whole chiral group G that gathers the global symmetries of QCD:

[2] It is the mass term that breaks chiral symmetry, since the Dirac inner product mixes the right and left components of the quark bi-spinor : $m\bar{q}q = m(\bar{q}_R q_L + \bar{q}_L q_R)$.

$$G = SU(3)_L \otimes SU(3)_R \otimes U(1)_V \tag{1.8}$$

Up to that point, one should wonder why the rotations of the axial phase, $U(1)_A$ ($\psi \rightarrow e^{i\alpha\gamma^5}\psi$), have been omitted in G. The fact is, even if $U(1)_A$ is a symmetry of the classical theory, it is broken at the quantum level since the associated Noether current $J^{5,\mu} = \bar{\psi}\gamma^\mu\gamma^5\psi$ is no longer conserved [7]: $\partial_\mu J^{5,\mu} = 3g^2/(16\pi^2)\tilde{G}^{\mu\nu}_a G^a_{\mu\nu}$. This leads to the so-called axial anomaly (see sec. 1.4.5 for further details).

In this thesis, we shall be focusing mainly on the $SU(3)$ sector of the chiral group. Thus, unless stated otherwise, G is from now on identified as $SU(3)_L \otimes SU(3)_R$.

1.2.3 Currents and charges

We can associate to the group G the following Noether currents, both conserved at the classical and quantum levels in the chiral limit:

$$J^a_{L,\mu} = \bar{\psi}_L\gamma_\mu\lambda^a\psi_L, \qquad J^a_{R,\mu} = \bar{\psi}_R\gamma_\mu\lambda^a\psi_R \tag{1.9}$$

with the Gell-Mann matrices λ^a ($a = 1...8$) being the generators of $SU(3)$ in flavour space. $J^{a,\mu}_L$ and $J^{a,\mu}_R$ are themselves related to the axial and vector currents:

$$V^a_\mu = J^a_{L,\mu} + J^a_{R,\mu} = \bar{\psi}\gamma_\mu\lambda^a\psi, \qquad A^a_\mu = J^a_{R,\mu} - J^a_{L,\mu} = \bar{\psi}\gamma^5\gamma_\mu\lambda^a\psi \tag{1.10}$$

Out of the chiral limit, the vector and axial currents are only partially conserved:

$$\partial^\mu V^a_\mu = i\bar{\psi}[M,\lambda^a]\psi, \qquad \partial^\mu A^a_\mu = i\bar{\psi}\{M,\lambda^a\}\gamma^5\psi \tag{1.11}$$

where M is the light quark mass matrix.

These two divergences can be written in terms of the scalar and pseudo-scalar densities S^a and P^a:

$$S^a = \bar{\psi}\lambda^a\psi, \quad P^a = i\bar{\psi}\gamma^5\lambda^a\psi \tag{1.12}$$

$$\partial_\mu V^{a,\mu} = f^{abc}M_b S_c, \quad \partial_\mu A^{a,\mu} = d^{abc}M_b P_c \tag{1.13}$$

with $M^a = \langle M\lambda^a\rangle$, where $\langle ...\rangle$ is the trace in flavour space. f^{abc} and d^{abc} are the anti-symmetric and symmetric structure constants of $SU(3)$'s Lie algebra [10]:

$$[\lambda^a,\lambda^b] = if^{abc}\lambda_c \qquad \{\lambda^a,\lambda^b\} = \frac{1}{3}\delta^{ab} + d^{abc}\lambda^c \tag{1.14}$$

Finally, we define the Noether charges Q^a_V and Q^a_A relating to the vector and axial currents:

$$Q^a_V = \int J^{0,a}_V(x)d^3x \qquad Q^a_A = \int J^{0,a}_A(x)d^3x \tag{1.15}$$

They verify the following commutation relations:

$$[Q_V^a, Q_V^b] = if^{abc}Q_V^c \tag{1.16}$$
$$[Q_V^a, Q_A^a] = if^{abc}Q_A^c \tag{1.17}$$
$$[Q_A^a, Q_A^a] = if^{abc}Q_V^c \tag{1.18}$$

We point out that the vector charges Q_V^a define a sub-algebra of G, in fact the algebra of the diagonal subgroup $SU(3)_V$. This approach is the starting point of the analysis of low-energy QCD in terms of current algebra [12], which can be extended to an effective field theory described in details in Chapter 2.

1.3 Spontaneous breaking of chiral symmetry

1.3.1 Spontaneous symmetry breakdown and the QCD spectrum

As we presented in sec. 1.1, one of the most striking properties of QCD is the property of confinement. It is a direct consequence of the non-abelian colour symmetry, and it leads to the existence of bound states $\bar{q}q$ and qqq of quarks: the hadrons. Hadrons can be gathered into multiplets almost degenerate in mass. For the two light flavours of quarks u and d, one can mention the isospin multiplets like (n,p), (π^-, π^0, π^+), ($\Delta^-, \Delta^0, \Delta^+, \Delta^{++}$)... This symmetry is experimentally well-tested up to an accuracy of 5 % for the mass difference. When we also take into account the strange quark s, those multiplets can themselves be organized in octets like (π,K,η) or decuplets (Δ,Σ,Ξ,Ω). Here the mass differences are more significant - around 10% to 30%. An approximate $SU(3)_V$ flavour symmetry can account for this particular spectrum, since some of its irreducible representations correspond to the observed octets and decuplets. But no degeneracy have been observed between multiplets of opposite parity. Since chiral symmetry is broken at the level of the low energy hadronic spectrum, one can suspect that it undergoes a spontaneous symmetry breakdown (SSB):

$$SU(3)_L \otimes SU(3)_R \xrightarrow{SSB} SU(3)_V \tag{1.19}$$

What is left from the original group G is the unbroken vector sub-group $H = SU(3)_V$ ($g_R = g_L$). From the point of view of the Noether charges, it means that there exists an operator $\hat{O}$ such as:

$$\langle\Omega|[Q_V^a, \hat{O}]|\Omega\rangle = 0, \qquad \langle\Omega|[Q_A^b, \hat{O}]|\Omega\rangle \neq 0, \qquad a, b = 1...8 \tag{1.20}$$

where Q_V^a are the charges belonging to the unbroken *vector* generators, and Q_A^b the charges of the broken *axial* generators. This means that the theory's vacuum is no more invariant under the transformation of a broken charge: $Q_A|\Omega\rangle \neq |\Omega\rangle$ of the axial sub-group $SU(3)_A$. According to Goldstone theorem, the spontaneous breaking of a global, continuous symmetry give rise, for each broken generator, to a massless bosonic spin-0 particle, the so-called Goldstone bosons [36, 37]. This realization of symmetry, called the Nambu-Goldstone realization, which is non-linear, is different from the more "standard" linear one, i.e. the Wigner-Weyl realization (table 1.1). Let's take a matrix $u(\phi)$ gathering the Goldstone fields ϕ. Under G it transforms as:

$$u(\phi) \xrightarrow{G} g_R u(\phi) h(g,\phi)^{-1} = h(g,\phi)^{-1} u(\phi) g_L^{-1} \tag{1.21}$$

where the compensator field $h(g,\phi) \in SU(3)_V$ is an element of the un-broken sub-group [38]. In the case $g \in H$ ($g_R = g_L$), $h(g)$ is a simple unitary representation matrix,

independent of the Goldstone fields ϕ: this is the linear Wigner-Weyl realization. However, in the case of the chiral transformation $g_R \neq g_L$, we have $h = h(g, \phi)$, i.e. the compensator field depends on the Goldstone fields ϕ: this is the non-linear Nambu-Goldstone realization.

Wigner-Weyl realization	Nambu-Goldstone realization
linear	non-linear
G is the symmetry group.	G is spontaneously broken to subgroup H.
The vacuum state is unique.	The vacuum state is degenerate.
The excitations are massive.	The spontaneous breakdown of G give rise to massless excitations, the Goldstone bosons.
The states are gathered in multiplets of G.	The states are gathered in multiplets of H.

Table 1.1: Comparison between Wigner-Weyl and Nambu-Goldstone realizations.

In addition, the octet of light pseudoscalar mesons (pions, kaons and eta) stands out because of its masses lower than the hadronic scale. The lightest multiplet in the QCD spectrum is an octet of pseudo-scalar mesons ($J^P = 0^{-1}$), with fairly non-degenerate masses but light compared to Λ_χ. If those mesons were to possess a vanishing mass, they could be identified with Goldstone bosons emerging from the spontaneous breakdown of a continuous global symmetry − namely G. Then, $SU(3)_V$ mentioned above would act as a residual symmetry group responsible for the degeneracy of the hadronic multiplets.

Hadrons	Flavour structure	Masses (MeV)
Pions	π^+/π^- $(u\bar{d},\, d\bar{u})$, π^0 $(u\bar{u} - d\bar{d})/\sqrt{2}$	~ 137
Kaons	K^+/K^- $(u\bar{s},\, s\bar{u})$, K^0/K^0 $(d\bar{s},\, s\bar{d})$	~ 495
Eta	η $(c_1(u\bar{u} + d\bar{d}) + c_2 s\bar{s})$	~ 547

Table 1.2: Octet of light pseudo-scalar mesons with quark content and masses (from PDG [68]). c_1 and c_2 are coefficients of the linear combinations of quarks for the η meson coming from the η/η' mixing. We have $c_1 = 1/\sqrt{3}$, $c_2 = -c_1$ in the simple model described in ref. [42].

1.3.2 The Goldstone theorem

The Goldstone theorem makes the link between the spontaneous breaking of a global continuous symmetry with the appearance in the theory of massless spin-0 fields, i.e. the Goldstone bosons. In what follows, we outline a proof of the theorem [6, 8].

As a preliminary example, we take the usual $SO(N)$ scalar model with a quartic ϕ^4 interaction:

We define $\Phi = (\phi_1, ..., \phi_N)$ a vector of dimension N, where Φ is a Lorentz-invariant scalar field. We write g an element belonging to $SO(N)$. The lagrangian of the theory is:

$$\mathcal{L}_\Phi = \frac{1}{2}\partial_\mu \phi_i \partial^\mu \phi^i - \frac{m^2}{2}\phi_i \phi^i - \lambda(\phi_i \phi^i)^2 \tag{1.22}$$

with the parameter $\lambda > 0$. The associated potential is given by $V[\phi_i] = \frac{m^2}{2}\phi_i\phi^i + \lambda(\phi_i\phi_i)^2$ (cf. figure 1.2).

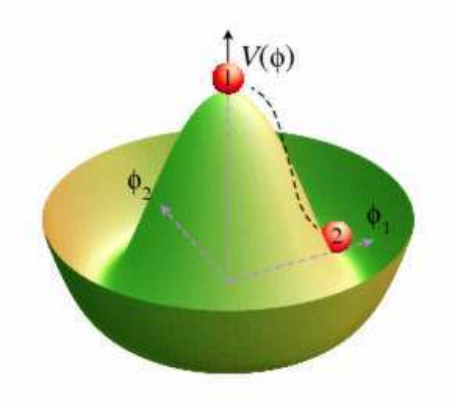

Figure 1.2: A representation of the quartic potential $V[\phi_i]$ in the $SO(2)$ case, for $m^2 < 0$.

It is invariant under the transformation $V[\phi_i] \to V[g\phi_i]$. One defines the minimum of $V[\phi_i]$ for a field configuration Φ_0 by:

$$\frac{\partial V}{\partial \phi_i}|_{\Phi=\Phi_0} = 0 \tag{1.23}$$

In terms of the components ϕ^i:

$$\left[\frac{m^2}{2} + 2\lambda(\phi_k \phi^k)\right]\phi^i = 0 \tag{1.24}$$

For $m^2 > 0$, the solution of (1.24) is trivially $\phi_0^{i=1...N} = 0$. However, if $m^2 < 0$ we have the solution:

$$|\Phi_0| = \sqrt{\frac{|m^2|}{4\lambda}} \tag{1.25}$$

Φ_0 is not invariant under the whole group $SO(N)$. However, there is a subgroup $H \equiv SO(N-1)$ of G, so that Φ_0 is invariant. Since the condition on the minimum of V is only given by the norm of Φ_0, we are free to choose its direction: we set $\Phi_0 = (0, ..., 0, \phi_0^N \equiv v)$, so that it points along the N-th direction.

We can now shift the components ϕ^i of Φ from its vacuum value v: $\Phi = (\pi_1, ..., \pi^{N-1}, \sigma + v)$. The lagrangian (1.22) is thus written in terms of the π fields $\pi^{i=1...N-1}$ and the σ field:

$$\begin{aligned} &\mathcal{L} = \frac{1}{2}(\partial_\mu \pi^k)^2 + \frac{1}{2}(\partial_\mu \sigma)^2 + (-m^2)\sigma^2, \qquad k = 1...N-1 \\ &-m\sqrt{\lambda}\sigma^3 - m\sqrt{\lambda}(\pi^k)^2\sigma - \frac{\lambda}{4}(\pi_k\pi^k)\sigma^4 - \frac{\lambda}{2}(\pi^k)^2\sigma^2 - \frac{\lambda}{4}(\pi_k\pi^k)^2\sigma^2 \end{aligned} \tag{1.26}$$

We observe that only the field σ along the broken axis N acquire a mass $-m^2 > 0$, while the $N-1$ fields π^k form a multiplet of $SO(N-1)$, the un-broken subgroup H. The latter are thus the $N-1$ Goldstone bosons of the spontaneous symmetry breaking of $SO(N)$ to $SO(N-1)$. $SO(N)$ has $N(N-1)/2$ symmetries (which correspond to the number of generators of its Lie algebra). For $SO(N-1)$, there are $(N-1)(N-2)/2$ symmetries. The difference is $N-1$, which correspond to the number of *broken* symmetries. The Goldstone

theorem then states that for each of these broken symmetries, a massless particle must appear. It is the same phenomenon that happens for the spontaneous breakdown of the chiral symmetry of QCD, even if in this case the non-perturbative nature of the theory at low energy forbids to get the precise details of the mechanism. It is also possible to parametrize Φ using a "polar" representation: $\Phi = e^{it_a\pi^a}(0,\ ...\ 0, \sigma + v)$, where the t_a are the generators of $SO(N-1)$. In this case, the massless π^a fields get derivative interactions only:

$$\mathcal{L} = \frac{1}{2}(\partial_\mu \pi^k)^2 + \frac{1}{2}(\partial_\mu \sigma)^2 + (-m^2)(v+\sigma)^2 - \lambda(v+\sigma)^4 \tag{1.27}$$

We observe therefore that the Goldstone modes π^a do not interact in the limit of zero momentum, a fact that was not obvious from the representation (1.26), but which correspond to a general feature of Goldstone bosons.

In a more general way, for a field configuration Φ_0 that minimizes V, we expand the potential around its minimum value $V[\Phi_0]$:

$$V[\Phi] = V[\Phi_0] + \frac{1}{2}(\phi - \phi_0)^i(\phi - \phi_0)^j \Big(\frac{\partial^2 V}{\partial\phi^i \partial\phi^j}\Big)_{\Phi=\Phi_0} + O(\Phi^3) \tag{1.28}$$

The eigenvalues of the matrix $\partial^2 V/(\partial\phi^i\partial\phi^j)_{\Phi_0}$ give the masses of the fields. Because Φ_0 is a minimum, those eigenvalues, and thus the field masses are positive or zero. We apply a transformation $\Phi \to \Phi + i\alpha\delta\Phi$ to V, α being a small parameter. Because V is invariant under such a transformation, we have:

$$V[\Phi] = V[\Phi + i\alpha\delta\Phi] \tag{1.29}$$

Or equivalently:

$$\delta\phi^i \frac{\partial V}{\partial \phi^i} = 0 \tag{1.30}$$

Differentiating (1.30) by ϕ^j, and setting $\Phi = \Phi_0$, we have:

$$\left(\frac{\partial(\delta\phi^i)}{\partial\phi^j}\right)_{\Phi=\Phi_0}\left(\frac{\partial V}{\partial\phi^i}\right)_{\Phi=\Phi_0} + \delta\phi_0^i\left(\frac{\partial^2 V}{\partial\phi^i\partial\phi^j}\right)_{\Phi=\Phi_0} = 0 \tag{1.31}$$

The first term cancels because we are set at the minimum of V. Therefore, the second term is zero. We have then an eigenvector $\delta\phi_0^i$ with 0 eigenvalue for each index i belonging to the broken part of G. Therefore the matrix $\partial^2 V/\partial\phi^i\partial\phi^j$ is a null-eigenvalue matrix, for i corresponding to a broken generator of the group. This means that there are as many Goldstone bosons with vanishing mass as there are broken generators. The argument, presented here at the classical level, can be generalized to include quantum corrections through the formalism of the effective action [6, 9].

So in the case of $SU(3)_L \otimes SU(3)_R$ going to $SU(3)_V$, we expect eight massless fields to appear in the spectrum after a spontaneous symmetry breakdown. Those fields can in fact describe the eight pseudo-scalar light mesons, under the addition fo a small mass term. Those eight pseudoscalar Goldstone bosons $|\phi^a(p)\rangle$ are organized in an octet according to the residual symmetry group H:

$$Q_V^a|\phi^b(p)\rangle = if^{abc}Q_V^a|\phi^c(p)\rangle \tag{1.32}$$

They are coupled to the vacuum $|\Omega\rangle$ through the axial current $A_\mu^a(x)$:

$$\langle \Omega | A^a_\mu(x) | \phi^b(p) \rangle = i\delta^{ab} F(3) p_\mu e^{ip.x} \tag{1.33}$$

This coupling is described by the single decay constant $F(3)$, where the 3 indicates that it is here defined in the chiral limit $m_{u,d,s} \to 0$.

Now we have seen that chiral symmetry is spontaneously broken, but we would like to describe in more detail this (non-perturbative) feature of the QCD vacuum.

1.4 The QCD vacuum

1.4.1 Order parameters: overview

The notion of spontaneous symmetry breaking is a very standard issue in physics. The traditional example consists in a ferromagnetic system undergoing a (second-order) phase transition to a paramagnetic phase when heating the system above a critical temperature T_C (the Curie temperature).

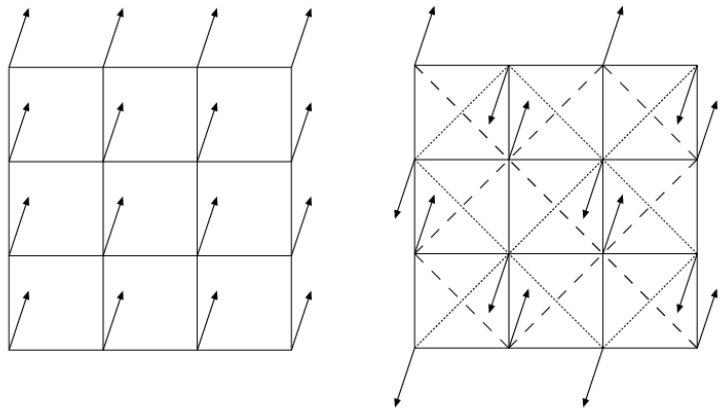

Figure 1.3: Ferromagnetic spin system (left) versus Anti-ferromagnetic (right)

The ferromagnet can be modeled by a lattice of spins (figure 1.3), whose interactions lead to a global alignment, which in turn gives rise to a *spontaneous* magnetization $\mathcal{M}$ (it is defined as the sum of all the spins in the system). This holds as long as the temperature T stays below T_C: the spins are in an ordered phase, which is not invariant under a rotation of $SO(3)$, because a particular direction of alignment has been privileged. But when $T > T_C$, the thermal energy become sufficient to overcome the interactions amongst spins, thus spoiling their alignment and therefore making the spontaneous magnetization $\mathcal{M}$ vanish. The spins are disordered, and the rotational symmetry is recovered (since our disordered system of spins looks the same in every direction). We observe that the spontaneous magnetization $\mathcal{M}$ vanishes in the paramagnetic, high temperature phase, while it is different from zero in the ferromagnetic, low-temperature phase: $\mathcal{M}$ is an *order parameter* of the ferro-paramagnetic phase transition. Moreover, an hamiltonian for this system would be of the form: $\mathcal{H} = -J \sum_{<i,j>} \sigma_i . \sigma_j$, where σ is a spin, J a constant and $< ... >$ denotes the nearest neighboring spins. This hamiltonian is of course invariant under $G \equiv SO(3)$, while in the ferromagnetic phase the fundamental state of the system breaks the symmetry into the subgroup $H \equiv SO(2)$: under T_C, it is therefore spontaneously broken. We have the following implication that for a non-zero order parameter $\mathcal{O}$ like the spontaneous magnetization, the system undergoes a spontaneous symmetry breaking:

$$\mathcal{O} \neq 0 \Rightarrow \text{SSB} \tag{1.34}$$

In principle, the number of order parameters is infinite. One must point out that the converse of relation (1.34) *is not* true. The system can be spontaneously broken whilst some of its order parameters are still zero. This is for example the case in anti-ferromagnetic systems: in the (anti)-ferromagnetic phase, the lattice made of anti-parallel spins yields a vanishing magnetization $\mathcal{M}$. A relevant order parameter would be the difference of the magnetization of the two sub-lattices: $\mathcal{D} = \mathcal{M}_+ - \mathcal{M}_-$ (in figure 1.3 $\mathcal{M}_+$ correspond to the dashed lattice, while $\mathcal{M}_-$ stands for the dotted lattice). This illustrates the fact that the study of order parameters is of particular importance since it provides information about the mechanism of symmetry breaking.

1.4.2 Order parameters of the chiral spontaneous symmetry breaking

We can point out two order parameters that play an essential role in the investigation of chiral symmetry breaking: the decay constant of the pion F, and the quark condensate $\langle\bar{q}q\rangle$.

The pion decay constant F is very specific since it attests without ambiguity the breaking of chiral symmetry [73]; i.e. the relation (1.34) is modified into:

$$F \neq 0 \Leftrightarrow \text{Chiral SSB} \tag{1.35}$$

To understand why, let's have a look at a more general order parameter of chiral SSB, the two-point Green function of the axial and vector currents:

$$\Pi^{ab}_{\mu\nu}(q) = i \int d^4x e^{iq.x} \langle\Omega| T \left\{ V^a_\mu(x) V^b_\nu(0) - A^a_\mu(x) A^b_\nu(0) \right\} |\Omega\rangle \tag{1.36}$$

In the $N_f = 3$ flavour case, assuming that the chiral symmetry is broken, we consider Π in the chiral limit. The Green function (1.36) has poles which correspond to one-particle states:

$$\Pi^{ab}_{\mu\nu}(q) = q_\mu q_\nu \delta^{ab} \left[- \frac{F(3)^2}{q^2} - \sum_V \frac{F_V^2}{M_V^2 - q^2} + \sum_A \frac{F_A^2}{M_A^2 - q^2} \right] + ... \tag{1.37}$$

where $F(3)$ is the decay constant of the pion in the chiral limit for the three flavour case. The first term corresponds to the Goldstone boson stemming from the breakdown of chiral symmetry, the second and third terms correspond respectively to massive vector V and axial A resonances, and the ellipsis denotes non-holomorphic structures that arise at higher energies. $F(3)$, F_V and F_A can be seen as the couplings of the one-particle states to the vector and axial currents (or equivalently their decay constants). For vanishing momentum $q_\mu = 0$, only the Goldstone bosons contribute to eq. (1.37):

$$\Pi^{ab}_{\mu\nu}(0) = -\frac{1}{4} g_{\mu\nu} \delta^{ab} F^2(3) \tag{1.38}$$

$\Pi^{ab}_{\mu\nu}(0)$ only contains contributions from Goldstone bosons. If chiral symmetry is broken then $\Pi^{ab}_{\mu\nu}(0) \neq 0$ which implies $F(3)^2 \neq 0$. The double implication (1.35) follows. In that sense, F can be considered as the "main" order parameter of chiral symmetry breaking.

A second order parameter of importance to the chiral symmetry breaking is the quark condensate $\langle\bar{q}q\rangle$ in the chiral limit. Its importance is actually made clearer once one moves away from the chiral limit. The quark condensate appears in the expansions of the pseudoscalar mesons masses (neglecting isospin breaking $m_u \neq m_d$):

$$F_\pi^2 M_\pi^2 = 2m\Sigma(3) + O(m_q^2) \tag{1.39}$$
$$F_K^2 M_K^2 = (m + m_s)\Sigma(3) + O(m_q^2) \tag{1.40}$$
$$F_\eta^2 M_\eta^2 = \frac{2}{3}(m + 2m_s)\Sigma(3) + O(m_q^2) \tag{1.41}$$

where $\Sigma(3)$ is the quark condensate in the chiral limit ($N_f = 3$): $\Sigma(3) \equiv -\langle \bar{u}u \rangle_{m_{u,d,s} \to 0}$. Those equations relate the order parameter $\Sigma(3)$ to the masses of the pseudo-scalar mesons which stem from the breakdown of chiral symmetry. Since the quark masses are treated here as a perturbation, the quark condensate induces a linear response to this same perturbation, in a way similar to the spontaneous magnetization of a ferromagnet in an exterior magnetic field. To avoid negative pseudoscalar masses for very small quark masses (condition of vacuum stability), the quark condensate must itself be negative or zero.

At that point, we make a first stop at the expansions (1.39)-(1.41). One can ask the question about how the higher orders hidden in the $O(m_q^2)$ are to be compared to the leading order (i.e. the size of the quark condensate). The usual assumption is that these higher-order corrections are rather small for physical quark masses. This would mean that the ratio:

$$X(3) = \frac{2m\Sigma(3)}{F_\pi^2 M_\pi^2} \tag{1.42}$$

which measures the relative size of the quark condensate with respect to the physical value is close to 1, so the expansions (1.39)-(1.41) are to be treated like any usual Taylor expansion where the higher orders are expected to become smaller and smaller. In this manner the quark condensate would play an essential role in the description of chiral symmetry breaking, compared to all the other order parameters (excepting, of course, F). We shall see from Chapter 3 that this is not necessarily the case.

1.4.3 The chiral limits $N_f = 2$ and $N_f = 3$

Up to now we have considered only the chiral limit where the u, d and s quark masses vanish. Because of the mass hierarchy $m_u \sim m_d \ll m_s \ll \Lambda_{QCD}$, we can consider two chiral limits of interest (fig. 1.4):

- $N_f = 3$ chiral limit (breaking of $SU(3)_R \otimes SU(3)_L$ into $SU(3)_V$): $m_{u,d,s} \to 0$, giving rise to an octet of Goldstone bosons that is identified with the light pseudoscalar octet (π, K, η).
- $N_f = 2$ chiral limit (breaking of $SU(2)_R \otimes SU(2)_L$ into $SU(2)_V$): $m_{u,d} \to 0$ whereas m_s is kept at his physical value, giving rise to a triplet of Goldstone bosons identified with the pion triplet.

In the case of the $N_f = 2$ limit, the masses of the u and d quarks go indeed to zero, but the mass of the strange quark m_s remains at its physical value. Therefore, the breaking of the chiral symmetry in the two-flavour case involves the order parameters of $SU(2)_R \otimes SU(2)_L$, in which an implicit dependence on m_s is contained. Now we define in both chiral limits our two main order parameters of chiral symmetry breaking, the pseudoscalar decay constant and the quark condensate:

$$F(2)^2 = \lim_{m_u, m_d \to 0} F_\pi^2, \quad F(3)^2 = \lim_{m_u, m_d, m_s \to 0} F_\pi^2, \quad \lim_{m_s \to 0} F^2(2) = F(3)^2 \tag{1.43}$$

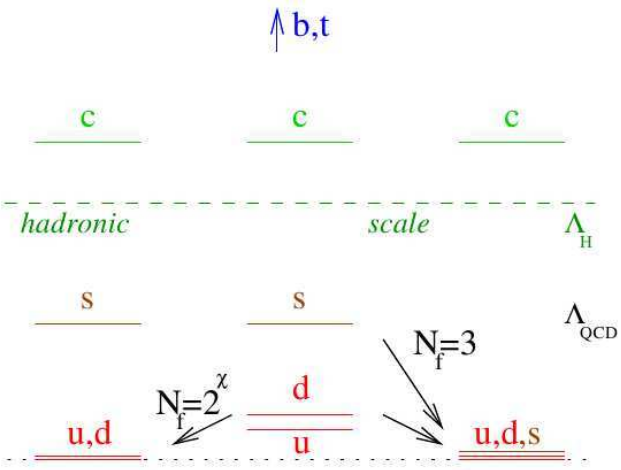

Figure 1.4: Sketch presenting our two chiral limits of interest $m_{u,d} \to 0$, m_s *physical* and $m_{u,d,s} \to 0$.

$$\Sigma(2) = \lim_{m_u,m_d\to 0} -\langle\Omega|\bar{u}u|\Omega\rangle, \quad \Sigma(3) = \lim_{m_u,m_d,m_s\to 0} -\langle\Omega|\bar{u}u|\Omega\rangle, \quad \lim_{m_s\to 0}\Sigma(2) = \Sigma(3) \tag{1.44}$$

The two rightmost limits are of particular importance since they relate F and Σ in the two chiral limits. Indeed, the values of $\Sigma(N_f)$ and $F(N_f)$ can in principle be different in the $N_f = 2$ and $N_f = 3$ limits. $\Sigma(2)$ being a function of m_s, we have:

$$\frac{\partial\Sigma(2)}{\partial m_s} = \lim_{m\to 0} i\int d^4x\langle T\{\bar{u}u(x)\bar{s}s(0)\}\rangle^c \equiv \Pi_Z(m_s) \tag{1.45}$$

c stands for the connected Green function. Since $\Sigma(2) \to \Sigma(3)$ for $m_s \to 0$, we have the following expression for $\Sigma(2)$:

$$\begin{aligned}\Sigma(2) &= \Sigma(3) + \int_0^{m_s} d\mu\Pi_Z(m_s) \\ &= \Sigma(3) + m_s \lim_{m_u,m_d\to 0} i\int d^4x\langle\Omega|\bar{u}u(x)\bar{s}s(0)|\Omega\rangle + O(m_s^2)\end{aligned} \tag{1.46}$$

We can interpret this expression the following way: $\Sigma(2)$ receives two different contributions – the first comes from the "genuine" $N_f = 3$ condensate $\Sigma(3) = -\langle\bar{u}u\rangle_{m_{u,d,s}\to 0}$, the second from the "induced" condensate corresponding to the effect of the strange sea-pairs through the correlator $\langle\Omega|\bar{u}u(x)\bar{s}s(0)|\Omega\rangle$ (cf. figure 1.5).

1.4.4 Order parameters and the spectrum of the euclidean Dirac operator

Analysing the issues concerning the spectrum of the Euclidean Dirac operator $\not{D}$ can be interesting to better understand the behavior of the quark condensates $\Sigma(3)$ and $\Sigma(2)$, as described in the preceding section. We perform a Wick rotation to work with an Euclidean metric, in a finite volume V. For any given gluonic configuration, the Dirac operator is hermitian and can be diagonalized [113]:

$$\not{D}[G]\psi_n = \lambda_n[G]\psi_n, \quad \lambda_n \in \mathbb{R} \tag{1.47}$$

with $\{\psi_n\}$ a complete basis of orthonormal states:

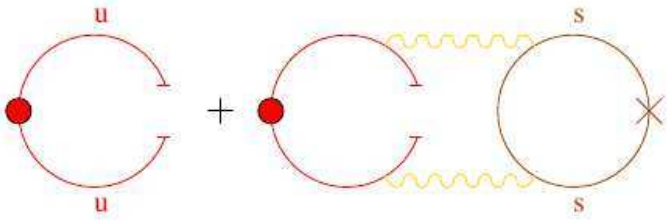

Figure 1.5: OPE-like diagrammatic representation of expression (1.46). The left term corresponds to the "genuine" condensate $\Sigma(3)$ while the right term corresponds to the "induced" part - second term of eq. (1.46). The broken lines correspond to non-perturbative contributions from the vacuum, while the cross stands for an insertion of the strange quark mass m_s

$$\int d^4\psi_m^\dagger(x)\psi_n(x) = \delta_{mn}, \quad \sum_m \psi_m^\dagger(x)\psi_m(y) = \delta(x-y) \tag{1.48}$$

Furthermore, we have the symmetry property that for any eigenvector and eigenvalue $\{\psi_n, \lambda_n\}$, we have the eigenvector $\gamma^5\psi_n$ with eigenvalue $-\lambda_n$. We write ν the number of exact zero-modes of $\not{D}$ (related to topological considerations, see next section 1.4.5). This is due to the simple fact that γ^5 and $\not{D}$ anti-commute. Vafa and Witten [20] derived the existence of a uniform bound on the eigenvalues:

$$|\lambda_n[G]| < C\frac{n^{1/d}}{V^{1/4}} \equiv \omega_n, \quad \omega_n \text{ independent of the configuration G} \tag{1.49}$$

for a gluonic configuration G, with $d = 4$ the space-time dimension, C a constant independent of G and the space-time volume V. We observe that as the volume grows, the eigenvalues λ_n accumulate around zero.

$S(x, y|G)$ is the light-quark propagator for a gauge configuration G:

$$S(x,y|G) = \sum_n \frac{\psi_n^\dagger(x)\psi_n(y)}{M - i\lambda_n[G]}, \quad M = \text{Diag}(m_1, ..., m_{N_f}) \tag{1.50}$$

We can use this basis to describe any correlator integrating over fermionic fields, leading to the gluonic average $< ... >$:

$$< \mathcal{O} >= \frac{\int [dG]\mathcal{O}e^{-S[G]}\Delta[G]}{\int [dG]e^{-S[G]}\Delta[G]} \tag{1.51}$$

The fermion determinant $\Delta[G]$ reads:

$$\Delta[G] = \prod_i \Delta(m_i|G), \quad \Delta(m|G) = m^{|\nu|}\prod_{n>0}\frac{m^2+\lambda_n^2[G]}{m^2+\omega_n^2} \tag{1.52}$$

where ω_n introduces a normalization independent of the gauge configuration. We take the N_f chiral limit: $m_1, ..., m_{N_f} \to 0$, keeping the remaining N_h quarks massive: $m_{N_f+1}, ..., m_{N_h} \neq 0$. In this limit the quark condensate $\langle\bar{u}u\rangle \equiv -\Sigma(N_f)$ is given by:

$$\Sigma(N_f) = \lim \frac{1}{V} < \int d^4x Tr\{S(x,x|G)\} > = \lim \frac{1}{V} < \sum_{n=-\infty}^{+\infty} \frac{m}{m^2+\lambda_n^2} > \tag{1.53}$$

where "lim" stands for the large volume limit $V \to \infty$, followed by the N_f chiral limit[3]. Some calculations bring us to:

$$\begin{aligned}\Sigma(N_f) &= \lim \frac{1}{V} < \sum_n \frac{m}{m^2+\lambda_n^2} > \\ &= \lim_{m\to 0} \int_{-\infty}^{+\infty} d\epsilon \frac{m}{m^2+\epsilon^2} \lim_{V\to\infty} \frac{1}{V} < \delta(\epsilon-\lambda_n) > \\ &= 2 \lim_{m\to 0} \int_0^{\infty} du \frac{1}{u^2+1} \frac{1}{V} < \rho(mu) >\end{aligned} \tag{1.54}$$

with $\rho(\epsilon)$ the eigenvalue density $\rho(\epsilon) = \sum_n \delta(\epsilon - \lambda_n)$. The same applies for the decay constant F [73]:

$$F^2(N_f) = \lim \frac{1}{V} < \sum_{k,n} \frac{m}{m^2+\lambda_k^2} \frac{m}{m^2+\lambda_n^2} J_{kn} >, \quad J_{kn} = \frac{1}{4} \sum_\mu |\int d^4x \psi_n^\dagger(x) \gamma_\mu \psi_n(x)|^2 \tag{1.55}$$

We can observe that those two quantities depend on the small Dirac eigenvalues - the infrared end of the Dirac spectrum - or, to put it differently, that they are tied to the accumulation of eigenstates around 0 as the volume $V \to \infty$ (eq. 1.49).

We now assume that the lightest of the massive quarks (the strange quark s in the $N_f = 2$ case), has a non-zero mass much smaller than the other ones and the scale Λ_χ, so in the chiral limit it would be of interest. We therefore isolate it from the other massive contributions and we get the following average over gluonic configurations:

$$< \mathcal{O} >= Z^{-1} \int [\mathcal{D}G] \mathcal{O} \Delta^{N_f}(m|G) \Delta(m_s|G) \prod_{i>N_f+1}^{N_f+N_h} \Delta(m_i|G) e^{-S[G]} \tag{1.56}$$

By choosing a cut-off Λ and defining an integer K such that $\omega_K = \Lambda$ (all of which are independent from the gluonic configuration), we can separate the fermion determinant into its infrared and ultraviolet contributions:

$$\Delta(m|G) = m^{|\nu|} \Delta_{IR}(m|G) \Delta_{UV}(m|G) \tag{1.57}$$

Then the infrared contribution has the following expression:

$$\Delta_{IR}(m|G) = \prod_{n=1}^{K} \frac{m^2+\lambda_n^2[G]}{m^2+\omega_n^2} < 1 \tag{1.58}$$

the bound $\Delta_{IR}(m|G) < 1$ coming from the relation (1.49). In the expression (1.56), the determinants $\Delta(m_i|G)$ containing the contributions of the massive quarks are dependent on the masses m_i unaffected by the chiral limit. Therefore their contributions are insensitive to small eigenvalues $\lambda \ll m_i$. Since Σ is dominated by small eigenvalues, the infrared contribution Δ_{IR} should dominate in the gluonic average eq. (1.56). Δ_{IR} is an increasing function of the masses:

$$m < m_s \Rightarrow \Delta_{IR}(m|G) < \Delta_{IR}(m_s|G) \tag{1.59}$$

so that taking the limits $m \to 0$ and $m_s \to 0$ (for the $N_f = 3$ chiral limit) would lead to a decrease of the chiral order parameters Σ and F:

[3]The order into which those two limits are taken is of particular importance, since spontaneous symmetry breaking does not happen in a finite volume [9].

$$\Sigma(3) < \Sigma(2), \quad F^2(3) < F^2(2) \tag{1.60}$$

Of course, the strength of the effect shall depend on the sensitivity of those parameters on the smallest Dirac eigenvalues. This affects essentially quantities sensitive to the infrared end of the Dirac spectrum (like the chiral order parameters), but not many others (quantities related to the dynamics of vector mesons, excited states, heavy-light systems, the baryon masses...).

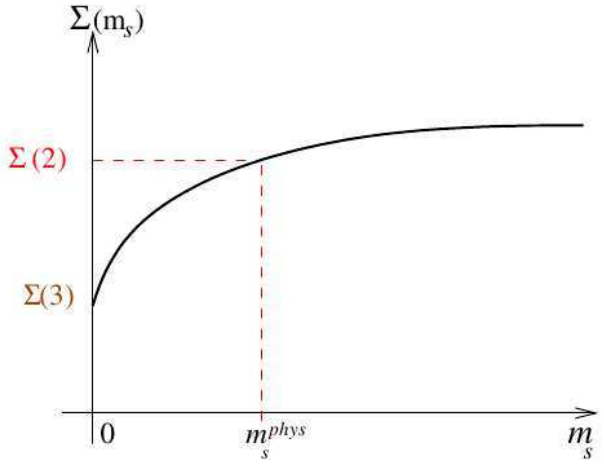

Figure 1.6: Possible dependence of the quark condensate Σ on the mass of strange quark m_s. $\Sigma(3)$ is the three-flavour condensate, $\Sigma(2)$ stands for its value in the two-flavour chiral limit.

As seen in the previous section, this difference between the values of $\Sigma(3)$ and $\Sigma(2)$ could be related to the fact that their difference, $\langle(\bar{u}u)(\bar{s}s)\rangle$, is connected to the violation of the Zweig rule in the scalar sector ($J^{PC} = 0^{++}$), effect which disappears in the large N_c limit. There are two possible scenarios: if $\Sigma(3) \sim \Sigma(2)$, then $\langle(\bar{u}u)(\bar{s}s)\rangle$ is small and the Zweig rule is verified. However, if the $N_f = 3$ condensate is suppressed $\Sigma(3) < \Sigma(2)$ (figure 1.6) and $\langle(\bar{u}u)(\bar{s}s)\rangle$ violates the Zweig rule, therefore enhancing the effects of the strange sea-pairs. A similar situation also happens for the decay constant F, having $F^2(3) < F^2(2)$. The value of the correlator $\langle(\bar{u}u)(\bar{s}s)\rangle$ was studied in details in [70, 71, 72] using dispersive methods, highlighting the importance of the $f_0(980)$ resonance for the estimate of this correlator since it strongly couple to $\bar{u}u$ and $\bar{s}s$ densities − concluding to an important dependence of the quark condensate and the decay constant on the number of quark flavours N_f. That fact was latter corroborated by some lattice collaborations (PACS-CS, MILC) [96, 102, 103] (see sec. 2.7.3). Again, the precise study of this phenomenon could provide valuable information about the chiral structure of the QCD vacuum, and the pattern of chiral symmetry breaking. This comparison will be a significant part of the work presented in this thesis.

1.4.5 The vacuum angle

• **Winding number and the QCD vacuum:**

We recall that the QCD lagrangian (1.1) contains the topological term:

$$\mathcal{L}_{topological} = -\frac{g^2}{32\pi^2}\theta_0 \tilde{G}^{\mu\nu}_a G^a_{\mu\nu} \tag{1.61}$$

Again, this term is peculiar in the sense that it does not appear in the equations of motion, but nevertheless, it affects QCD physics through the axial anomaly from the $U_A(1)$ transformation.

To a given configuration of the gauge fields, it is possible to associate a topological charge called the *winding number* [7, 113]:

$$\nu = \int d^4x \; \omega(x) \tag{1.62}$$

where $\omega(x)$ is the winding number density:

$$\omega(x) = \frac{g^2}{32\pi^2} \tilde{G}_a^{\mu\nu}(x) G_{\mu\nu}^a(x) \tag{1.63}$$

ν is a topological invariant, and can be used to classify the different gluonic configurations according to their topological sector, itemized by their winding number. Preeminent examples of configurations with non-zero winding number are the famous *instanton* configurations [9].

It is possible to relate the winding number ν to the right and left zero-eigenstates of the Dirac operator (i.e. with eigenvalues $\lambda = 0$): for a suitable basis consisting of n_+ right-handed eigenstates and n_- left-handed eigenstates, then we have the following relation $\nu = n_+ - n_-$. This is the famous Atiyah-Singer index theorem [19]. It also shows that ν is an integer when the fermions of the theory are in the fundamental representation [113].

The vacuum of QCD is characterized by configurations of gluon fields that are grouped according to their winding number ν. The different vacuum states $|\Omega_\nu\rangle$ are separated by potential barriers connected through tunneling effects (for example, instantons provide a description for the "jumps" between those barriers, i.e. from one topological sector to the other). For a gauge transformation with winding number 1 the states $|\Omega_\nu\rangle$ and $|\Omega_{\nu+1}\rangle$ are related by a gauge transformation $U_1|\Omega_\nu\rangle = |\Omega_{\nu+1}\rangle$. So a gauge invariant vacuum state is a superposition of all the topological classes:

$$|\theta_0\rangle = \sum_\nu e^{-i\nu\theta_0} |\Omega_\nu\rangle \tag{1.64}$$

which is gauge-invariant up to a phase:

$$U_1|\theta_0\rangle = e^{i\theta_0}|\theta_0\rangle \tag{1.65}$$

We stress that different values of θ_0 are associated with different vacua, i.e. $\langle\theta_0^{'}|\theta_0\rangle = \delta_{\theta_0^{'}\theta_0}$. In the case of a vacuum-to-vacuum transition amplitude $\langle\theta_0|\mathcal{O}|\theta_0\rangle$, we have the presence of a phase:

$$\langle\theta_0|\mathcal{O}|\theta_0\rangle = \sum_{\nu,\nu^{'}} e^{i(\nu-\nu^{'})\theta_0} \langle\nu|\mathcal{O}|\nu^{'}\rangle \tag{1.66}$$

that can be taken into account in the generating functional by:

$$\begin{aligned} \langle\theta_0|\mathcal{O}|\theta_0\rangle &= \int [\mathcal{D}G][\mathcal{D}\bar{\psi}][\mathcal{D}\psi]\mathcal{O}e^{-i\int \mathcal{L}_{QCD} + \frac{g^2}{32\pi^2}\theta_0 \tilde{G}_a^{\mu\nu} G_{\mu\nu}^a} \\ &= \sum_{\nu,\nu^{'}} e^{i(\nu-\nu^{'})\theta_0} \langle\nu|\mathcal{O}|\nu^{'}\rangle \end{aligned} \tag{1.67}$$

The phase $e^{i(\nu-\nu^{'})\theta_0}$ is equivalent to the presence of the topological term (1.61) in the path-integral.

• **Relationship between θ_0 and the axial anomaly:**

As was introduced in sec. 1.2.2, the *massless* QCD lagrangian is invariant under the axial phase transformation:

$$\psi \to e^{i\alpha\gamma^5}\psi, \quad \psi_R \to e^{i\alpha}\psi_R, \quad \psi_L \to e^{-i\alpha}\psi_L \tag{1.68}$$

where $e^{i\alpha\gamma^5}$ is any element of $U_A(1)$. As for any other symmetry at the classical level, one would therefore expect that the Noether current $J^{5,\mu} = \bar{\psi}\gamma^\mu\gamma^5\psi$ is classically conserved:

$$\partial_\mu J^{5,\mu} = 0 \quad \text{(Classical)} \tag{1.69}$$

But the above relation (1.69) is *incorrect* at the quantum level. As a first approach, this can be shown explicitly by evaluating anomalous correlators such as $\langle\Omega|\, T\{J^5_\mu(x)J^a_\nu(y)J^b_\sigma(z)\}\,|\Omega\rangle$ [7] at one loop, showing an ambiguity in their value. It turns out that it is not possible to define all the correlators while preserving the corresponding chiral Ward identities − the involved symmetry being called anomalous. In our case it is the axial anomaly that is "sacrified" in order to cope with this problem.

A more general approach taken by [18] shows that the reason for the existence of the axial anomaly was in fact *intrinsic* to the structure of QCD at the quantum level: simply stated, the measure of the theory's generating functional is not invariant under the transformation (1.68):

$$[\mathcal{D}\bar{\psi}\mathcal{D}\psi] \to [\mathcal{D}\bar{\psi}][\mathcal{D}\psi]\exp\left[i\int d^4x\ \alpha\ N_f\ \frac{g^2}{16\pi^2}\tilde{G}^{\mu\nu}_a G^a_{\mu\nu}\right] \tag{1.70}$$

for a given number N_f of quark flavours. This can be explained by the fact that the divergence of $J^{5,\mu}$ is non-zero:

$$\partial_\mu J^{5,\mu} = N_f\frac{g^2}{16\pi^2}\tilde{G}^{\mu\nu}_a G^a_{\mu\nu} \quad \text{(Quantum)} \tag{1.71}$$

into which we can recognize the topological term (1.61). We invite the reader to refer to [7] and [18] for the details of the (somehow) technical calculation leading to (1.70). When the quarks are massive, the full divergence is given by:

$$\partial_\mu J^{5,\mu} = 2i\sum_q m_q\bar{q}\gamma^5 q + N_f\frac{g^2}{16\pi^2}\tilde{G}^{\mu\nu}_a G^a_{\mu\nu} \tag{1.72}$$

where the mass part comes from the lagrangian itself (which is not $U_A(1)$ invariant for non-zero masses) and the topological part comes from the anomalous behaviour of the generating functional under the $U_A(1)$ symmetry.

Now how does the theta vacuum $|\theta_0\rangle$ behave under chiral transformations ? This issue is in fact connected to the axial anomaly. Since $\tilde{G}^{\mu\nu}_a G^a_{\mu\nu}$ corresponds to a total divergence (eq. (1.71)), one can define a conserved current:

$$\tilde{J}^{5,\mu} = J^{5,\mu} - N_f\frac{g^2}{16\pi^2}K_\mu \tag{1.73}$$

where K_μ is a gauge-dependent current verifying $\partial_\mu K^\mu = \tilde{G}^{\mu\nu}_a G^a_{\mu\nu}$ [7]. From the "new" axial current $\tilde{J}^{5,\mu}$ we define the corresponding Noether charge:

$$\tilde{Q}^5 = \int d^3x\tilde{J}^{5,0}(x) \tag{1.74}$$

Under the gauge transformation U_1 (1.65), $\tilde{Q}^5$ transforms like:

$$\tilde{Q}^5 \to U_1 \tilde{Q}^5 U_1^{-1} = \tilde{Q}^5 - 2N_f \tag{1.75}$$

Providing that we work in the massless case, each of the different theta vacua are therefore related by a chiral $U(1)$ transformation. We have:

$$\begin{aligned} U_1 e^{i\alpha\tilde{Q}^5}|\theta_0\rangle &= U_1 e^{i\alpha\tilde{Q}^5} U_1^{-1} U_1 |\theta_0\rangle \\ &= e^{i(\theta_0 - 2\alpha N_f)} e^{i\alpha\tilde{Q}^5}|\theta_0\rangle \end{aligned} \tag{1.76}$$

By writing $e^{i\alpha\tilde{Q}^5}|\theta_0\rangle = |\theta_0'\rangle$ we see from eq. (1.65) that:

$$e^{i\alpha\tilde{Q}^5}|\theta_0\rangle = |\theta_0 - 2\alpha N_f\rangle \tag{1.77}$$

We observe that a $U(1)$ chiral transformation implies a shift in the coefficient of the topological term (1.61), i.e. the vacuum angle θ_0:

$$\theta_0 \to \theta_0 - 2\alpha N_f \tag{1.78}$$

It is therefore possible to rotate away the dependence of the lagrangian on the vacuum angle by an axial phase transformation. This does not hold for massive quarks since the chiral symmetry is then explicitly broken.

• Introduction to topological quantities

Going further, it is possible to split the QCD generating functional $Z[\theta_0]$ (see sec. 2.4.1) into the sum of the contributions from each different topological sector itemized by ν:

$$Z[\theta_0] = \sum_\nu e^{i\theta_0\nu} Z_\nu \tag{1.79}$$

with $Z_\nu = \int [\mathcal{D}G] e^{S[G]} \mathrm{Det}[-i\not{D} + \mathcal{M}]$, $S[G]$ being the classical gluonic action of a given topological configuration of winding number ν. The distribution of the winding number is also characterized by its mean square:

$$\langle \nu^2 \rangle = \sum_\nu \frac{Z_\nu}{Z} \nu^2 \ (= V\Sigma m \text{ in the } N_f = 1 \text{ case.}) \tag{1.80}$$

This winding number is related to the non-perturbative structure of the QCD vacuum, and we are able to describe some of its features in the simplifying case $N_f = 1$ (which is not exactly identical to the $N \geq 2$ case since the quark condensate does not have any symmetry in the case $N_f = 1$). We obtain [113]: $\langle \nu^2 \rangle = V\Sigma m$.

Setting $\theta_0 = 0$, in the case of large volumes, $V\Sigma m >> 1$, for winding numbers $\nu << \langle \nu^2 \rangle$, we have a Gaussian distribution:

$$\frac{Z_\nu}{Z} = \frac{1}{\sqrt{2\pi\langle \nu^2 \rangle}} \exp \frac{-\nu^2}{2\langle \nu^2 \rangle} \tag{1.81}$$

Configurations with low ν have the same probablity of occuring, whereas configurations with $\nu \gtrsim \langle \nu^2 \rangle$ become highly suppressed.

For small volumes $V\Sigma m \ll 1$, the distribution is all concentrated around $\nu = 0$, i.e. non-trivial topologies with $\nu \neq 0$ are rare. The mean value of $\langle \nu^2 \rangle$ stems from configurations with $\nu = \pm 1$, which also dominate the quark condensate. This in fact hinders the capacity of

lattice simulations to jump from one topological sector ν to the next, the non-trivial sectors being difficult to reach.

For the theory with more than 1 flavour evaluating $Z[\theta_0]$ directly is much more difficult and one has to use an effective theory of QCD to extract information on its mass and volume dependence (see ref. [113]).

The previous discussion highlights the importance of a quantity called the *topological susceptibility* (χ_t) directly tied to the vacuum structure of QCD. This (un-physical) quantity is defined by the mean square winding number per unit volume: $\chi_t = \langle \nu^2 \rangle / V$. This is an interesting quantity since it does have a sensitivity on the quark condensate Σ, which becomes explicit in the low-energy effective theory of QCD. In the one flavour case, it is simply given by $\chi_t^{N_f=1} = \langle \nu^2 \rangle / V = \Sigma m$. We observe that it is independent of the volume and that it vanishes in the chiral limit $m \to 0$ (which is always true for an arbitrary number of flavours when any of the masses tends to zero $m_f \to 0$). Using the generating functional:

$$Z[\theta_0] = e^{-W[\theta_0]V} \tag{1.82}$$

with $W[\theta_0]$ the (vacuum) energy density, the topological susceptibility is taken as $W[\theta_0]$ second derivative in the expansion of $W[\theta_0]$ as a series in θ_0:

$$\begin{aligned} W[\theta_0] &= W[0] + \frac{\theta_0^2}{2} \frac{d^2 W[\theta]}{d\theta^2}|_{\theta=\theta_0} + \frac{\theta_0^4}{4!} \frac{d^4 W[\theta]}{d\theta^4}|_{\theta=\theta_0} + O(\theta_0^6) \\ &= W[0] + \frac{\theta_0^2}{2}\chi_t + \frac{\theta_0^4}{4!} c_4 + O(\theta_0^6) \end{aligned} \tag{1.83}$$

with all the odd-derivatives being 0 ($\theta_0 = 0$ is a minimum of $W[\theta_0]$). We see that χ_t can be understood as the second-order coefficient of the expansion of $W[\theta_0]$, and from the definition $\chi_t = \langle \nu^2 \rangle / V$, as the second cumulant of the gluonic winding number ν. Similarly at fourth order, the coefficient $c_4 = [\langle \nu^4 \rangle - 3\langle \nu^2 \rangle^2]/V$ corresponds to the fourth cumulant of ν. Both can be evaluated through the means of lattice simulations, with the possibility to extract information about the quark condensate.

We can make a link between these two topological quantities and any arbitrary correlation function $G(\theta_0) = \langle \theta_0 | O_1 ... O_n | \theta_0 \rangle$, defined in the case of a fixed winding number ν: in the same manner as eq. (1.79), we have the Fourier coefficient of $G(\theta_0)$ [118]:

$$G_\nu = \frac{1}{2\pi Z_\nu} \int d\theta Z(\theta) G(\theta) e^{i\theta\nu} \tag{1.84}$$

If the correlator G is $\mathcal{CP}$-even, it is an even function of θ - conversely if G is $\mathcal{CP}$-odd. Expanding G_ν in a series in θ we therefore obtain:

$$\begin{aligned} G_\nu^{even} &= G(0) + G^{(2)}(0) \frac{1}{2\chi_t V} \Big(1 - \frac{\nu^2}{\chi_t V} - \frac{c_4}{2\chi_t^2 V} \Big) + G^{(4)}(0) \frac{1}{8\chi_t^2 V^2} + O(V^{-3}) \\ G_\nu^{odd} &= G^{(1)}(0) \frac{i\nu}{\chi_t V} \Big(1 - \frac{c_4}{2\chi_t^2 V} \Big) + G^{(3)}(0) \frac{i\nu}{2\chi_t^2 V^2} + O(V^{-3}) \end{aligned} \tag{1.85}$$

From the previous equations (1.85), we can obtain an estimate of the size effects due to a fixed winding number. We see that the leading order correction is of order $O(1/V)$. Those finite-volume corrections are supressed when the quark masses are larger than $1/(\Sigma V)$, but they become significant when the masses are of order $m \sim 1/(\Sigma V)$.

Furthermore, χ_t is related to the value at zero of the correlation function:

$$\chi(p^2) = -i \int d^4x\, e^{ip\cdot x} \langle 0|T\omega(x)\omega(0)|0\rangle \tag{1.86}$$

which can be obtained from the generating functional of QCD by performing two derivatives with respect to the local source corresponding to the vacuum angle $\theta(x)$. As discussed in ref. [114], this correlation function is too singular in QCD for the integral to exist, so that eq. (1.86) is an ambiguous notion and has to be renormalized. This problem however does not affect the value of $\chi(p^2)$ at zero momentum transfer and per unit volume $\chi \equiv \chi(0)/V \equiv \chi_t$, i.e. the topological susceptibility. Indeed, $\chi(0)$ can be related through Ward identities to correlators requiring no renormalization:

$$\chi(0) = -\frac{i}{6} \int dx \langle \Omega|T\sigma_0(x)\sigma_0(0)|\Omega\rangle - \frac{1}{9}\langle \Omega|\bar{q}mq|\Omega\rangle\,, \qquad \sigma_0 = \sqrt{\frac{2}{3}}\bar{q}i\gamma_5 mq \tag{1.87}$$

The two terms on the right-hand side of this Ward identity (written in the case of degenerate masses among quarks collected in a flavour multiplet ψ (see ref. [114]) shows the connection of the topological susceptibility with the determination of the quark condensate ($\langle \Omega|\bar{q}mq|\Omega\rangle$) and the propagation of flavour-singlet Goldstone bosons respectively (σ_0). It is thus of no surprise that this quantity, related to topological properties of QCD, is also exploited to determine the quark condensate on the lattice [120, 121, 122, 123, 124].

1.5 Summary

After a (very) short introduction to the Standard Model, we have given a presentation of QCD, focusing mainly on the aspects of chiral symmetry, which arises in the (chiral) limit of zero quark masses $m_q \to 0$, for either two (u and d) or three flavours (u, d and s). We detailed the notion of spontaneously broken global symmetry and the subsequent Goldstone theorem. We saw in particular that chiral symmetry breaking generates eight Goldstone bosons that can be identified with the eight pseudo-scalar mesons $\pi^{+,0,-}$, $K^{+,-}$, $\bar{K^0}, K^0$ and η of QCD low-energy spectrum.

From there, we moved to a description of the QCD vacuum, where we introduced the important concept of order parameter for a spontaneous symmetry breaking. We have seen that for chiral symmetry, there exist two main order parameters: the decay constant F and the quark condensate Σ. We shown that those order parameters could undergo a decrease when one moved from the theory with two massless flavours to the theory with three massless flavours: $\Sigma(3) < \Sigma(2)$, $F(3)^2 < F(2)^2$, this effect comes from the presence of massive $\bar{s}s$ in the vacuum being related to a violation of the Zweig rule in the scalar sector.

The second part of our description of the QCD vacuum involved topological considerations, stemming from the presence of the topological term $-g^2/(32\pi^2)\theta_0 \tilde{G}_a^{\mu\nu} G_{\mu\nu}^a$ in the QCD lagrangian. We introduced the winding number ν of gluonic configurations, and gave a classification of the vacuum states according to this number. We also gave relations between the $U_A(1)$ axial anomaly and the vacuum angle θ_0. Finally, we discussed two quantities describing the distribution of the winding number: the topological susceptibility χ_t and the fourth cumulant c_4 defined from an expansion of QCD's energy density in powers of θ_0. These two topological quantities (even if "un-physical") being interesting objects because of their dependence on the quark condensate, whose better understanding could help us to probe the pattern of chiral symmetry breaking.

In the second chapter, we shall introduce the two alternative techniques aimed at studying QCD at low energies in the non-perturbative regime: Lattice QCD and Effective Field Theories. Then, we will give a detailed presentation of Chiral Perturbation Theory, the effective theory of low-energy QCD.

Chapter 2

Lattice QCD, Effective Field Theories, and Chiral Perturbation Theory

2.1 Introduction

At low energies below the chiral symmetry breaking scale $\Lambda_\chi \approx 1$ GeV, quarks and gluons interact so strongly that the usual perturbative approach of QCD is no longer relevant. Indeed, the value of the strong coupling constant becomes too high for the perturbative expansion in powers of α_s to be still valid. Thus, the whole machinery of perturbative diagrammatical techniques with quarks and gluons can no longer be used: getting analytical results (even approximate) for hadronic processes in terms of quark-gluon interaction is no longer possible. But, as was introduced in sec. 1.1, two alternatives exist to cope with that issue:

On one side, we can make use of numerical simulations to extract relevant information about QCD observables: this is the purpose of Lattice QCD. On the other side, in order to stick with an analytical approach, it is possible to construct an Effective Field Theory of QCD in the low-energy limit, based on the fact that the "failure" of low-energy QCD with quarks and gluons may be a sign that below Λ_χ, quarks and gluons can not anymore be considered as the "good" degrees of freedom of the theory. We then have to find another class of degree of freedom more suited to energy domains under 1 GeV: this role shall be devoted to the octet of light pseudo-scalar mesons $\pi^{+,0,-}$, $K^{+,-}$, $\bar{K}^0$, K^0, and η. The resulting effective theory, called Chiral Perturbation Theory, or χPT for short, is fully workable within a perturbative framework.

The first two sections of this chapter shall be devoted to a global overview of Lattice QCD, followed by an introductory presentation of Effective Field Theories. Then in the remaining sections we shall give a detailed account of Chiral Perturbation Theory.

2.2 Lattice QCD

One method used to probe the dynamics of QCD at energy scales for which perturbation theory in α_s breaks down is Lattice QCD (LQCD). To put it as concisely as possible, it consists in performing numerical calculations of observables (i.e. correlators) over discrete space-time.

From a theoretical point of view, the main issue of this method is how to discretize the generating functional in order to make numerical calculations possible. Since it is not possible to perform calculations over a discretized $3+1$ Minkowskian space-time, one has

first to perform a Wick rotation into a 4-dimensional Euclidean space with imaginary time $\tau \equiv it$. We have moved from a Quantum Field Theory in Minkowski space to a Classical Theory at Equilibrium (CTE), i.e. a statistical field theory in Euclidean space [23]. Writing $e^{-iS[\bar{\psi},\psi,G]}$ the QCD action, the generating functional in QFT:

$$Z_{QFT} = \int [\mathcal{D}\bar{\psi}][\mathcal{D}\psi][\mathcal{D}G]\ e^{-iS[\bar{\psi},\psi,G]} \tag{2.1}$$

becomes a partition function in CTE:

$$Z_{CTE} = \int [\mathcal{D}\bar{\psi}][\mathcal{D}\psi][\mathcal{D}G]\ e^{-S[\bar{\psi},\psi,G]} \tag{2.2}$$

For a given correlator we get:

$$\langle \mathcal{O}(\bar{\psi},\psi,G)\rangle = \frac{\int [\mathcal{D}\bar{\psi}][\mathcal{D}\psi][\mathcal{D}G]\ \mathcal{O}(\bar{\psi},\psi,G)\ e^{-S[\bar{\psi},\psi,G]}}{\int [\mathcal{D}\bar{\psi}][\mathcal{D}\psi][\mathcal{D}G] e^{-S[\bar{\psi},\psi,G]}} \tag{2.3}$$

which can be thought of as a probabilistic average over the field configurations with a weight $e^{-S[\bar{\psi},\psi,G]}$. Furthermore, it is possible to separate the fermionic contribution from the bosonic one (as in eq. 1.51):

$$\langle \mathcal{O}\rangle = \frac{\int \tilde{\mathcal{O}}(G) e^{-S[G]} \prod_f \mathrm{Det}[i\ \not{D} - m_f]}{\int e^{-S[G]} \prod_f \mathrm{Det}[i\ \not{D} - m_f]} \tag{2.4}$$

where $\mathrm{Det}[i\ \not{D} - m_f]$ is the fermion determinant for a given flavour in the case of massive quarks (equation (2.4) is the lattice counterpart of equation (1.51) defined in sec. 1.4.4). There is a further separation between the quarks that is made in eq. (2.4): the operator $\tilde{\mathcal{O}}$ contains the contribution of the valence quarks, while the determinant $\mathrm{Det}[i\ \not{D} - m_f]$ gathers the sea-quark dynamics.

The discrete space-time in which we work is an hypercube of space length L in the space directions, and of length T in the "time" direction. Each vertex x on the hypercube is separated by a lattice spacing a. The vertices are linked to their neighbours by a gauge matrix $U_\mu(x) \in SU(3)$, which represent the gluonic fields on the lattice. μ is an index corresponding to a unit vector $\hat{\mu}$ in the direction $\mu = 1, ..., 4$. An action of LQCD is invariant under gauge transformations which are defined as follows: for an arbitrary set of matrices $g(x)$ located on the sites of the lattice the gauge fields, as well as the fermion fields, transform as:

$$U_\mu \to g(x) U_\mu g^{-1}(x+\hat{\mu}), \quad \psi(x) \to g(x)\psi(x) \tag{2.5}$$

All the physcial observables are of course gauge invariant. The set of all the matrices $U_\mu(x)$ on each vertex is called the *gauge configuration* of the lattice. They are numerically evaluated by means of the usual Monte-Carlo method using the weight $e^{-S[G]}$ [25]. The action which is used is the gluonic Wilson action:

$$S_G[\{U\}] = \frac{1}{3}\int d^4x\ Tr\{1 - P_{\mu\nu}(x)\} \tag{2.6}$$

with the matrix product $P_{\mu\nu}(x) = U_\mu(x) U_\nu(x + a\hat{\mu}) U_{-\mu}(x + a\hat{\mu} + a\hat{\nu}) U_{-\nu}(x + a\hat{\nu})$, called a *plaquette*. In the limit $a \to 0$ the continuous gluonic action $-\frac{g^2}{36}\sum_{a=1...8}\int \frac{1}{4} G_a^{\mu\nu} G^a_{\mu\nu}$ is recovered. The fact of having put the theory on a lattice results in discretization effects, i.e. the simulated observables come with numerical artefacts of order of the size of the lattice spacing a.

For the quarks the problem is much more difficult since the numerical evaluation of the fermionic determinant $\mathrm{Det}[i\ \not{D} - m_f]$ is a tremendous calculational task. Indeed, it stems from a huge matrix whose size amounts to the product (number of sites on the lattice) $\times$

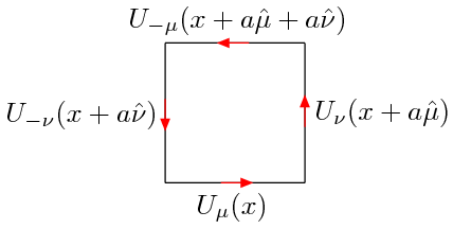

Figure 2.1: A *plaquette* representing the matrix product $P_{\mu\nu}(x)$. Each vertex is linked to its neighbours by a matrix $U_\mu(x)$. The red arrows indicate the direction of the rotation around the plaquette.

(quark colour)×(quark spin). One then uses a modified version of the Monte-Carlo algorithm called Hybrid Monte-Carlo [26] − a recent technique used to make an evaluation of the fermionic determinant at a reasonable calculational cost.

The basic (naive) action for the quarks is the following:

$$\frac{1}{2a}\int d^4x\ \bar{\psi}(x)\sum_{\mu}\gamma_\mu[U_\mu(x)\psi(x+\hat{\mu}) - U_\mu^\dagger(x-\hat{\mu})\psi(x-\hat{\mu})] + \sum_x m_q\bar{\psi}(x)\psi(x) \tag{2.7}$$

As one expects, the usual Dirac action $\int \bar{\psi}(\not{D} - m)\psi$ is recovered in the limit $a \to 0$. The problem is that this action gives rise to 16 duplicate quark modes (the so-called doubler modes) in the continuum limit. To overcome this problem, one can define the Wilson action [24]:

$$\begin{aligned}\frac{1}{2a}\int d^4x\ \bar{\psi}(x)\sum_{x,\mu}[(\gamma_\mu - 1)U_\mu(x)\psi(x+\hat{\mu}) - (\gamma_\mu + 1)U_\mu^\dagger(x-\hat{\mu})\psi(x-\hat{\mu})] \\ + \frac{m_q a + 4}{a}\sum_x \bar{\psi}(x)\psi(x)\end{aligned} \tag{2.8}$$

This action (2.8) however breaks chiral symmetry, since it adds another "mass" term $4/a$ to lift degeneracy among the doublers. It is possible to define other actions, most of them derived from the Dirac operator of Wilson's action, like for example "Wilson clover" [30] and "Wilson twisted" [31], which have $O(a^2)$ artefacts due to finite lattice spacing, much better than the $O(a)$ artefact of eq. (2.8). Actions with the appropriate chiral properties needed to study light quark dynamics are also derived from Wilson's Dirac operator, such as the "domain wall" [27] and "overlap" [28, 29] actions − the latter having very good chiral properties but leading to very heavy calculations when the volume increases, so that it is almost impossible to perform them on large volumes.

Now the generating functional of lattice QCD can be summarized as such:

$$\langle\mathcal{O}\rangle_{lattice} = \frac{\int_{\{U\}}\tilde{\mathcal{O}}e^{-\beta S_G[\{U\}]}\prod_f \mathrm{Det}[i\ \not{D} - m_f]}{\int_{\{U\}} e^{-\beta S_G[\{U\}]}\prod_f \mathrm{Det}[i\ \not{D} - m_f]} \tag{2.9}$$

with $\{U\}$ a gauge configuration, and $1/\beta = g^2/6$, which can be thought as the equivalent of the temperature T of a thermal bath. In the early times of lattice QCD, one would neglect the effect of the fermionic determinant, i.e. one would consider a situation for which the sea-quark pairs are neglected. From a diagrammatic point of view, this means that only gluons contribute as internal lines: it is the *quenched* QCD. In particular, it encouters severe problems of unitarity, and it is no more used nowadays. Another situation consists

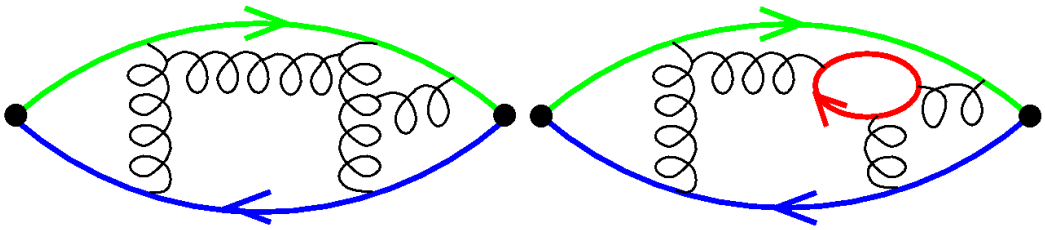

Figure 2.2: Illustration of the three situations quenched (A), and full (B) in lattice QCD. The black dots represent the valence quarks and the connecting gray lines their propagation. The internal curvy lines stand for the gluons while the loop illustrate a sea-quark effect.

in taking into account the dynamics of the sea-quarks, but in setting a mass for the sea-quarks different from the mass of the valence quarks, this is called the *partially-quenched* QCD, with similar problems concerning unitarity. Finally, the last situation correspond to the full QCD with dynamical quarks verifying $m_{sea} = m_{valence}$ (see figure 2.2). The calculations with sea-quarks are much heav ier than the quenched calculations: they are becoming more and more demanding as the light quark masses (and consequently the pion mass) decrease. Many different simulations have been performed over the years, for instance 2 [33], $2+1$ [96, 97, 98, 99, 100, 101, 102, 103] and $2+1+1$ dynamical quarks [34] (the charm quark being introduced in the latter).

It must be stressed that most of the simulations are made for masses that are larger than the actual physical masses. Currently, the BMW collaboration [32] has reached the physical pion mass $\tilde{M}_\pi \sim M_\pi$ ($\tilde{O}$ denotes an observable on the lattice). The lower bound the other collaborations have reached is at $\tilde{M}_\pi \gtrsim 250$ GeV [69]. This restriction is due to the fact that small masses need larger volumes (otherwise the light particles would extend beyond the box's boundaries − and one would not be able to tame the finite volume effects), and larger volumes mean more costly simulations in terms of calculation time. The space-time volumes used currently revolve around $L^3 \times T = 32^3 \times 64$ (or 24^3 for a coarser lattice, see for example [122]), with lattice spacing of the order $a \sim 0.1$ fm.

We must stress that the whole lattice "procedure" brings up sources of uncertainties, stemming from all the different steps performed:

- the first source of uncertainties comes from the numerical calculations themselves: the sampling of gluonic configurations from the Monte-Carlo method leads to statistical uncertainties.

- It is necessary to know the value of the lattice spacing a, which can not be determined from lattice simulations themselves, but by comparing the value of an observable on the lattice (in units of a) and in the physical world (in units of GeV). This determination suffers from scale uncertainties, since there is an arbitrariness in the choice of this observable − and also for the reason that the simulations are not performed for physical quark masses.

- Finite-volume effects can be estimated by introducing terms describing the modification of the propagation in a box with periodic boundary conditions (see sec. 6.2.2 for an example).

- Moreover, since Lattice QCD is a *field* theory, it can not escape the issue of renormalization: observables evaluated on the lattice also need renormalization. Those observables $\tilde{O}$ are dependent on the lattice spacing a as a UV cut-off. The main point is to link $\tilde{O}(a)$ to the quantity in the continuum $O(\mu^2)$, evaluated using a continuum renormalization scheme, such as $\overline{MS}$ (μ^2 being the associated renormalization scale). It is therefore necessary to build a "dictionary", i.e. to define a renormalization factor Z such as: $\tilde{O}(a^2)Z(\mu^2, a^2) = O^{\overline{MS}}(\mu^2) + O(a^2)$. The Z factor is itself evaluated from the lattice generally using a non-perturbative scheme, usually the MOM scheme.

- Finally, since most lattice simulations are not able to reach the actual physical values (for example the pion mass quoted above), one must therefore rely on extrapolations to reach it. A last source of uncertainties stems from this extrapolation to the physical masses. For low energy observables like the pion and the kaon masses or their decay constants, it is necessary to rely on Effective Field Theory to perform these extrapolations.

2.3 Some generalities about Effective Field Theories

We have seen at the very end of the previous section that, in order to extract relevant information from lattice data, it was necessary to perform extrapolations since most of the simulations could not be performed at the actual physical values. We therefore rely on Effective Field Theories (EFT) to perform them. The concept of EFT is very broad: Physics by itself is a collection of effective theories, each valid in its particular scale domain. Particle Physics does not escape this fact; on the contrary, it contains some quintessential examples of what makes up an effective theory. To mention but only one, the Standard Model by itself is an effective theory. If this very fundamental notion had to be summarized into one short sentence, it would be stated as such: *An effective theory is a theory representing the low energy limit of an underlying theory said to be complete (valid at higher energies).*

The phenomenological ideas at the root of the effective concept are fairly simple [13]: specific physical phenomena arise only at a given range of energy (or length) scale E, and should be represented in the theory by degrees of freedom adapted to that particular scale. Those which are no more relevant at low energy are integrated out into the parameters of the effective theory. This means that we do not have to bother anymore about the details of the physics at higher energies: in some sense, what is left of their proper dynamics is an overall averaging into single numbers, and the symmetries of the underlying theory which is verified in the structure of the effective operators. We call the *low-energy constants* (LECs) those numbers implicitly containing the physics of higher energy. They can be calculated either by the means of the underlying theory (if possible) or evaluated from experimental measurements and/or numerical simulations.

From the more specific point of view of Quantum Field Theory (QFT), given an energy scale E with $E << \Lambda$, for Λ any energy sufficiently high, one will only see the propagation of particles of mass $m \sim E$. The heavier particles, those with masses $M >> \Lambda$, are integrated out. Even if they still manifest themselves through the particular values of the low-energy constants, they do not play anymore a role as degrees of freedom. An Effective Field Theory possesses all the properties of a Quantum Field Theory [9], in particular, the resulting S-matrix for all possible processes is then consistent with causality, analyticity, unitarity, cluster decomposition, and must also satisfies all of the symmetry principles of the underlying theory.

The endeavour of building an Effective Field Theory from those fundamental principles is in fact simple, since a systematic recipe exists:

- State the energy scale E at which the physical phenomena you study occurs.
- Define a scale $\Lambda > E$ which corresponds to the frontier of high energy.
- Give the particle content of your low energy effective theory.
- Build an effective lagrangian $\mathcal{L}_{eff}$ by making an expansion in powers of E/Λ. This lagrangian must satisfy all the symmetries of the underlying theory.

The lagrangian you choose to use should be the most general one, consistent with *all* the symmetries of the underlying theory. Then, you shall end up with a collection of effective operators describing the dynamics of low energy degrees of freedom:

$$\mathcal{L}_{eff} = \sum_i C_i \times \hat{O}^i \tag{2.10}$$

where the $\hat{O}^i$ are the operators and C_i the effective couplings (i.e. the low energy constants). The sum is organized in growing powers of the dimension d_i of the operators $\hat{O}_i$. We can distinguish between two types of EFT: decoupling, and non-decoupling. Their main difference is about how the low energy degrees of freedom are related to the ones of the underlying theory.

2.3.1 Decoupling EFT

A first case is the situation where the integration of the degree of freedom can be explicit: one can identify the EFT's degrees of freedom with the low-momentum modes of the fields of the underlying theory. The Fermi theory of the weak interactions and the Standard Model are good examples of such decoupling theories. In that case, it is possible to organize the EFT in terms of the ultraviolet dimension (identical to the one used for the renormalization power counting) of the operators. Thus the dimension for the couplings are of the form $[C_i] = \Lambda^{4-di}$. The differents operators are therefore classified according to their dimensionality:

- Relevant ($d_i < 4$)
- Marginal ($d_i = 4$)
- Irrelevant ($d_i > 4$)

This classification corresponds in fact to the behavior under E/Λ. The C_i of the relevant operators scale as powers of $(E/\Lambda)^{-1}$: they become important at low energy. C_i of marginal operators scale as $\log(\Lambda)$; they influence both the infrared and ultraviolet behavior of the theory (the Standard Model is an example of a theory built from marginal operators for the interaction part of the lagrangian). Finally, the C_i of irrelevant operators scale as powers of E/Λ. That is why they are supressed at low energy. The usual approach in Quantum Field Theory consists in keeping only the relevant and marginal operators. It guarantees renormalizability at all orders of the theory, since the dimensionality of the lagrangian coupling constants into which infinities are re-absorbed are at least zero. So, only a finite number of counter-terms is needed to get finite predictions. The usual approach to consider only renormalisable theories is supported by this view of EFT: irrelevant operators disappear at low energy, so that only renormalizable terms remain whatever the underlying theory.

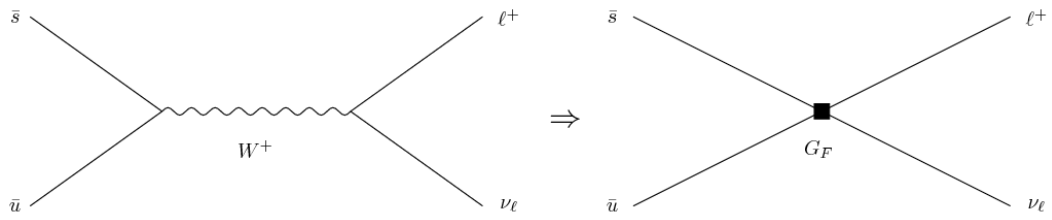

Figure 2.3: The Fermi theory: droping from high to low energies.

One of the most basic examples of such effective decoupling theory is the Fermi Theory of weak interactions, in which the W bosons are integrated out, letting quarks and leptons to interact through effective vertices. It corresponds to the low-energy limit of the theory of weak interactions, based on the $V - A$ interaction, with the typical heavy scale of order $\Lambda = O(M_W)$. The effective coupling (i.e. the low energy constant) is the Fermi constant G_F, related to the parameters of the underlying theory by $G_F/\sqrt{2} = g^2/(8M_W^2)$.

The effective lagrangian reduces to a 4-fermions operator:

$$\mathcal{L}_{eff} = \frac{G_F}{2} J_\mu J^{\mu\dagger} \tag{2.11}$$

with the charged current:

$$J^\mu = \sum_{ij} \bar{u}_i \gamma^\mu (1 - \gamma^5) V_{ij} d_j + \sum \bar{\nu}_\ell \gamma^\mu (1 - \gamma^5) \ell \tag{2.12}$$

V_{ij} is an element of the CKM matrix and $i,\ j$ are the family indices.

In the low energy regime $E << M_W$, the W particle can not propagate over large distances, so the associated field disappears in the effective theory and the information about its interaction with the other fields (namely the weak coupling g and its mass M_W) is then contained in G_F (illustrated in figure 2.3).

2.3.2 Non-decoupling EFT

A non-decoupling EFT distinguishes from a decoupling one by the presence of a *phase transition*, occuring via the spontaneous breakdown of one of the underlying symmetries. This breakdown generates a set of Goldstone bosons which constitutes the effective theory's degrees of freedom. Because of their "Goldstone nature", they are derivatively coupled (see sec. 1.3.2) − furthermore, the symmetries connect processes with a different number of Goldstone bosons. We thus organise the successive terms in the lagrangian by the number of derivatives they contain, contrarily to the decoupling theories where this role was fulfilled by dimensionality of the operators. In turn, the realization of the broken symmetry tightly constrains the interactions between the effective degrees of freedom. Also, we must stress that there is no guarantee of renormalizability to all orders, compared to the case of the decoupling effective field theories. But, because of the constraint imposed by symmetry, we can achieve a renormalization order-by-order: the loops at a given order in the derivative counting can be renormalized by the low-energy constants of the theory at this particular order, which therefore act as the counter-terms. An example of such theory is Chiral Perturbation Theory (χPT), an effective theory of QCD at low energies $E < 1$ GeV. The following sections aim to provide a detailed presentation of this theory.

2.4 Chiral Perturbation Theory: foundations

2.4.1 Generating functional

Our program is thus to build an effective theory for QCD that incorporates chiral symmetry and describes its spontaneous breaking, and to which it is possible to apply a perturbative expansion. Since the effective theory is built upon the symmetries of the underlying one, we must begin by the most fundamental object containing this piece of information: the generating functional, which allows one to generate all the Ward identities among correlators encoding all the symmetries of the theory. In QCD it is expressed by:

$$Z[v^\mu, a^\mu, s, p, \theta] = \int \mathcal{D}G\mathcal{D}\bar{\psi}\mathcal{D}\psi \; exp\left[i \int d^4x \mathcal{L}_{QCD}[G, \psi, \bar{\psi}, v^\mu, a^\mu, s, p, \theta] \right] \tag{2.13}$$

with the QCD lagrangian in the presence of the classical sources v^μ, a^μ, s, p and θ:

$$\mathcal{L}_{QCD}[G, \psi, \bar{\psi}, v^\mu, a^\mu, s, p, \theta] = \mathcal{L}_{QCD}[0] + \sum_f \bar{\psi}_f [\gamma_\mu (v^\mu + \gamma^5 a^\mu) + s + i\gamma^5 p]\psi_f \tag{2.14}$$
$$- \frac{g^2}{32\pi^2}\theta \tilde{G}_a^{\mu\nu} G^a_{\mu\nu}$$

where $\mathcal{L}_{QCD}[0]$ is the source-free lagrangian eq. (1.1) in the chiral limit. We can use Z to compute the Green functions of vector and axial currents, and scalar and pseudoscalar densities, and take the LSZ reduction formula to extract the amplitudes related to incoming and outgoing states of pseudoscalar mesons[1]. The Green functions are obtained by differentiating Z with respect to the sources, and set $v^\mu = a^\mu = p = 0$ and $s = M$ and $\theta = \theta_0$ (for an non-vanishing vacuum angle). Recall that M is the light quark mass matrix introduced in sec. 1.2.3.

It is usual to combine the vector and axial-vector sources into right and left components:

$$r_\mu = v_\mu + a_\mu, \quad l_\mu = v_\mu - a_\mu \tag{2.15}$$

so r_μ and l_μ can be used to identify related QCD correlators involved in electroweak processes, through the following relations:

$$r_\mu = e\mathcal{Q}A_\mu + ..., \quad l_\mu = e\mathcal{Q}A_\mu + \frac{e}{\sqrt{2}\sin\theta_W}(W_\mu T_+ + h.c.) + ... \tag{2.16}$$

$$\mathcal{Q} = \frac{1}{3}\mathrm{Diag}(2, -1, -1), \quad T_+ = \begin{pmatrix} 0 & V_{ud} & V_{us} \\ 0 & 0 & 0 \\ 0 & 0 & 0 \end{pmatrix} \tag{2.17}$$

2.4.2 Ward Identities

One wants to build a generating functional in terms of the low-energy degrees of freedom, and respecting the same symmetries as the QCD generating functional. The effective generating functional describing χPT is identified with that of QCD, up to a certain order in a low-energy expansion to be defined in the later section 2.5:

[1] The same ideas can be applied to the interaction of Goldstone bosons with other fields (nucleons, heavy-light mesons...)

$$Z_{\chi PT}[v^\mu, a^\mu, s, p, \theta] = \int \mathcal{D}U \; exp\left[i \int d^4x \mathcal{L}_{\chi PT}[U, v^\mu, a^\mu, s, p, \theta] \right] \equiv Z_{QCD}[a^\mu, v^\mu, s, p, \theta] + ... \tag{2.18}$$

where U is a matrix gathering the effective degrees of freedom. The ellipsis ... keeps track of the fact that the above equality (2.18) between QCD and the corresponding effective theory holds up to a given order in the low energy expansion. Chiral symmetry will act on the Green functions derived from $Z_{\chi PT}$ by constraining their structures through Ward identities. We can write the generating functional as:

$$Z_{\chi PT}[a^\mu, v^\mu, s, p, \theta] = e^{i\Gamma_{\chi PT}[v^\mu, a^\mu, s, p, \theta]} \tag{2.19}$$

making the effective action $\Gamma_{\chi PT}$ appear explicitly [6]. The set of all the Ward identities can then be derived by requiring the effective action must be invariant under *local* chiral transformations of the sources [6, 9] $S = [v^\mu, \; a^\mu, \; s, \; p, \; \theta]$:

$$S \overset{G \; local}{\longrightarrow} S', \; G = SU(3)_R \times SU(3)_L \tag{2.20}$$

$$\Gamma[S'] = \Gamma[S], \quad S' = T(g(x))S, \quad g(x) \in G \tag{2.21}$$

$T(g(x))$ belonging to a representation of G for the sources. We have the following local transformations of $v^\mu, \; a^\mu, \; s$ and p:

$$\begin{aligned} s + ip &\to g_L(s + ip)g_R^\dagger \\ r_\mu &\to g_R r_\mu g_R^\dagger + i g_R \partial_\mu (g_R^\dagger) \\ l_\mu &\to g_L l_\mu g_L^\dagger + i g_L \partial_\mu (g_L^\dagger) \end{aligned} \tag{2.22}$$

Furthermore, expanding $g_R(x)$ and $g_L(x)$ around the identity leads to:

$$\begin{aligned} g_R(x) &= 1 + i\alpha(x) + i\beta(x) + O(\alpha^2, \beta^2, \alpha\beta) \\ g_L(x) &= 1 + i\alpha(x) - i\beta(x) + O(\alpha^2, \beta^2, \alpha\beta) \end{aligned} \tag{2.23}$$

where $\alpha(x)$ and $\beta(x)$ are two hermitean zero-trace matrices collecting the rotations of the vector and axial parts of G respectively. The corresponding infinitesimal transformations then read:

$$\begin{aligned} \delta v_\mu(x) &= \partial_\mu \alpha(x) + i[\alpha(x), v_\mu(x)] + i[\beta(x), a_\mu(x)] \\ \delta a_\mu(x) &= \partial_\mu \beta(x) + i[\alpha(x), a_\mu(x)] + i[\beta(x), v_\mu(x)] \\ \delta s &= i[\alpha(x), s(x)] - \{\beta(x), p(x)\} \\ \delta p &= i[\alpha(x), p(x)] + \{\beta(x), s(x)\} \end{aligned} \tag{2.24}$$

At that point, one would wish to include the Green functions for the singlet vector and axial currents. The group G must therefore be extended to $G = U(3)_R \times U(3)_L$ (meaning $\langle\alpha\rangle \neq 0, \; \langle\beta\rangle \neq 0$). This leads to the anomaly described in sec. 1.4.5 for $U_A(1)$, with $\langle\beta\rangle \neq 0$. Fixing the corresponding ambiguities leads some Ward identities to become anomalous, and some of the symmetry constraints must therefore be changed when going from the classical

to the quantum level. We then expect the relation (2.21) to be modified. $\Gamma[S]$ is therefore written as the sum of two contributions:

$$\Gamma[S] = \Gamma^0[S] + \Gamma^{WZW}[S] \tag{2.25}$$

with $\Gamma^{WZW}[S]$ gathering the terms that correspond to the anomalous Ward identities, and Γ^0 the general solution of the invariance equation (2.21):

$$\Gamma^0[S^{'}] = \Gamma^0[S] \tag{2.26}$$

In particular, the presence of those anomalous identities leads to the local transformation law for the source $\theta(x)$ corresponding to the vacuum angle (see eq. (1.78)), that have to be added to the list (2.24):

$$\theta(x) \to \theta(x) - 2\langle\beta(x)\rangle \tag{2.27}$$

where $\langle ...\rangle$ is the trace over flavour space. Any lagrangian that verifies the chiral Ward identities will obey the splitting (2.25). A lagrangian, written in terms of the matrix U and the sources v_μ and a_μ taking the chiral anomaly into account was built by Wess, Zumino [21], and then Witten [22]. Now all that remains is to build explicitly the corresponding lagrangian to the effective action $\Gamma^0[S]$.

2.4.3 Goldstone bosons

A systematic approach to describe the effective degrees of freedom and their dynamics in the case of a SSB mechanism was invented by Callan, Coleman, Wess and Zumino [38] in the late sixties. Recall from eq. 1.7 that quark fields transform linearly under G:

$$\psi_{R,L} \xrightarrow{G} g_{R,L}\psi_{R,L} \tag{2.28}$$

However, in the effective theory, G will act non-linearly on the Goldstone fields ϕ^a representing the effective degrees of freedom:

$$\phi^a \xrightarrow{G} \Theta^a(g,\phi) \tag{2.29}$$

where the non-linear representation Θ is constrained by the composition law [38]:

$$\Theta(g_1, \Theta(g_2,\phi)) = \Theta(g_1 g_2, \phi) \tag{2.30}$$

We can check this statement the following way: We begin by considering the origin $\Theta(g,0)$. The set of elements that leave the origin invariant is a subgroup H of G. In particular we have: $\Theta(gh,0) = \Theta(g,0)$ for $g \in G$ and $h \in H$. The function $\Theta(g,0)$ then belongs to the coset space G/H, obtained by identifying the elements g and $g^{'}$ which only differ by an element h of H: $g^{'} = gh$. Furthermore, this mapping is invertible: if $\Theta(g_1,0) = \Theta(g_2,0)$, then $g_1 g_2^{-1} \in H$, so in the coset G/H we have $g_1 \equiv g_2$. Then, the Goldstone fields ϕ^a can be viewed as the coordinates of the coset space G/H. Moreover, we choose a representative element k of each of the equivalence classes $\{gh, h \in H\}$, so an element g of G can be uniquely decomposed as $g = kh$. The composition law (2.30) shows that the image $k^{'}$ of k under a transformation $g \in G$ is obtained by decomposing the product gk into $k^{'}h$: this corresponds to the action of G on G/H. In the $SU(3)$ case we have simply: $G = SU(3)_L \otimes SU(3)_R$ and $H = SU(3)_V$. G consists then in pairs $g = (g_R, g_L)$, while H contains equal pairs $g_R = g_L$.

We can choose $k = (U,1)$ as a representative of the equivalence classes. The composition law (2.30) is therefore:

$$gk = (g_R, g_L)(U,1) = (g_R U, g_L) = (g_R U g_L^\dagger, 1)(g_L, g_L) = k^{'}h \tag{2.31}$$

Then the Goldstone fields transform as:

$$U(x) \to g_L U(x) g_R^\dagger \tag{2.32}$$

We finally define a parametrization for the unitary matrix $U(x)$:

$$U(x) = e^{i\frac{\sqrt{2}}{F_0}\lambda^a \phi(x)_a} \tag{2.33}$$

with ϕ_a the Goldstone fields, λ^a the eight broken generators of $SU(3)_A$, and F_0 a real number that is identified with the pion decay constant in the $N_f = 3$ chiral limit. It is also convenient to define a matrix $\Phi(x) = \lambda_a \phi^a(x)$. In the case of isospin limit $m_u = m_d$, the matrix $\Phi(x)$ can then be explicitly written as:

$$\lambda^a \phi_a(x) = \begin{pmatrix} \frac{\pi^0}{\sqrt{2}} + \frac{\eta}{\sqrt{6}} & \pi^+ & K^+ \\ \pi^- & -\frac{\pi^0}{\sqrt{2}} + \frac{\eta}{\sqrt{6}} & K^0 \\ K^- & \overline{K^0} & -\frac{2\eta}{\sqrt{6}} \end{pmatrix} \tag{2.34}$$

We will see in the later section 2.5.2 that the different fields π, K and η can be identified to the actual pseudo-scalar mesons of the same name. Notice at that point that the Goldstone character of the mesons forbids them to get any mass from the spontaneous symmetry breaking. The mass term should be treated as a perturbative *explicit* symmetry-breaking term to the effective lagrangian of χPT.

2.5 Chiral Perturbation Theory for three flavours

2.5.1 Power counting

In principle, effective lagrangians contain an infinite number of terms: *a priori*, owing to the symmetry principles, it is possible to build an infinite tower of invariants (see sec. 2.3). But how shall they be organized ? For the lagrangian of Chiral Perturbation Theory, one can propose a counting criterion, based on the fact that at zero momentum transfer and in the chiral limit, hadronic interactions tend to zero: first, the pseudo-Goldstone character of the light mesons tells us that because of derivative couplings, soft mesons have interactions that vanish with their momentum. Secondly, light quark masses are considered sufficiently small for the mass term to be treated as a perturbation. Thus, the χPT lagrangian $\mathcal{L}_{eff}$ corresponds to an expansion in powers of the momenta p and the quark masses m_p:

$$\mathcal{L}_{eff} = \sum_n \mathcal{L}^{(2n)}, \quad \mathcal{L}^{(2n)} \sim q^k m_p^l, \quad n = (k+l)/2 \tag{2.35}$$

This yields in fact a double expansion both in momenta and masses, but p, m are to be compared according to a single index. Under the hypothesis of a large quark condensate, we can make the approximation that M_π^2 has a linear dependence on the quark masses, so m_p must count as two powers of p: $p^2 \sim m_p$. This is the counting rule of Standard Chiral Perturbation Theory proposed by Gasser and Leutwyler [1, 2]:

$$U \sim 1, \quad s,\ p \sim q^2,\ v_\mu,\ a_\mu,\ D_\mu \sim q \tag{2.36}$$

We mention that in the case of a small quark condensate, one can organize the expansion around $\langle \bar{q}q \rangle = 0$, $m_q = 0$. One counts differently the scalar/pseudoscalar sources: instead

of two powers of p, one can set $s,\ p \sim p$ and $\langle \bar{q}q \rangle \sim p$, as it corresponds to an expansion around $\langle \bar{q}q \rangle = 0$. By performing this counting we obtain the Generalized Chiral Perturbation Theory, as proposed by Fuchs, Knecht, Moussalam, Sazdjian and Stern in [4, 5]. Such an expansion takes into account in a well-defined framework all the corrections counted as higher orders in the Standard framework, but significant in the case of a small condensate. The very general nature of this framework led to a restricted range of predictions compared to Standard χPT. In the present thesis, triggered by the considerations from Chapter 1 we investigate an intermediate case (see chapter 3), for which only the leading and next-to-leading orders of the standard expansion compete. We will thus use the counting (2.36), with some further assumptions discussed in the next chapter concerning the convergence the chiral series.

2.5.2 Effective lagrangian at lowest order

In order to build our effective lagrangian, we have to look for the most general expression $\mathcal{L}_{eff}$ corresponding to the generating functional described in the previous sections 2.4.1 and 2.4.2, eqs. (2.18) and (2.19).

The effective action is again $\Gamma = \Gamma^0 + \Gamma^{WZW}$ (eq. (2.25)), Γ being invariant under local transformations of the sources $v^\mu, a^\mu, s, p, \theta$ according to the principles of sec. 2.4.2. Since the anomalous part Γ^{WZW} is known, what is left is to find the solution Γ^0. The path-integral measure $\mathcal{D}U$ being itself invariant under the local transformations, what remains is simply to write down the most general effective lagrangian $\mathcal{L}_{eff}$ function of $U,\ v^\mu,\ a^\mu,\ s,\ p$ and θ invariant under relations (2.22) and (2.27), consistent with Lorentz invariance, chiral symmetry, and parity. According to the previous section, this lagrangian is organized in growing powers of momentum (i.e derivatives):

$$\mathcal{L}_{eff} = \sum_n \mathcal{L}^{(2n)}[U, v^\mu, a^\mu, s, p, \theta] \tag{2.37}$$

The vector and axial sources v_μ and a_μ enter the chiral lagrangian through covariant derivatives:

$$D_\mu U = \partial_\mu U - iUr_\mu + il_\mu U, \quad (D_\mu U)^\dagger = (\partial_\mu U)^\dagger + iU^\dagger r_\mu - il_\mu U^\dagger \tag{2.38}$$

With their local transformation law:

$$D_\mu U \to g_R D_\mu U g_L^\dagger, \quad (D_\mu U)^\dagger \to g_L (D_\mu U)^\dagger g_R^\dagger \tag{2.39}$$

We define furthermore the associated curvature tensors:

$$F_{\mu\nu}^{R,L} = \partial_\mu F_\nu^{R,L} - \partial_\nu F_\mu^{R,L} - i[F_\mu^{R,L}, F_\nu^{R,L}], \quad F_\mu^{R,L} = r_\mu, l_\mu \tag{2.40}$$

For θ the covariant derivative is:

$$D_\mu \theta = \partial_\mu \theta + 2\langle a_\mu \rangle \tag{2.41}$$

where $\langle ... \rangle$ is again the trace operator over flavour space. We limit ourselves to a constant θ for the remainder of this thesis.

The sources $s,\ p$ and θ do not have independent transformation laws. Under a given chiral transformation, we can have:

$$\begin{aligned} s + ip = M \quad &\to \quad s = \mathcal{M},\ p = 0 \\ \theta = \theta_0 \quad &\to \quad \theta = \theta_0 + arg(det[M]) = \bar{\theta} \end{aligned} \tag{2.42}$$

M is the general quark mass matrix, and $\mathcal{M}$ is its diagonalized form with real and positive eigenvalues $m_{u,d,s}$. $\bar{\theta}$ is the chirally invariant vacuum angle $\bar{\theta} = \theta + arg(det[s+ip])$. Therefore, the effective action depends only (apart from vector and axial sources) on the quark masses and the invariant vacuum angle $\bar{\theta}$. Conversely it is possible to set $\theta = 0$; in that case the mass matrix is rotated into:

$$\begin{aligned} s + ip = \mathcal{M} \quad &\rightarrow \quad s + ip = \mathcal{M} e^{i\theta_0/N_f}, \quad (N_f = 3) \\ \theta = \theta_0 \quad &\rightarrow \quad \theta = 0 \end{aligned} \tag{2.43}$$

We can thus build a lagrangian at $\theta = 0$ with a generic mass term, and infer the corresponding lagrangian at $\theta = \text{Cst}$ by changing the mass term $\mathcal{M}$ with $e^{i\theta/3}\mathcal{M}$. In the case where θ is not constant, the construction of this lagrangian has been discussed in greater details in the large N_c limit, where $U_A(1)$ stops being anomalous, and θ being promoted to the dynamical η' field, the ninth Goldstone boson [114, 116].

Of course, if one wishes to study correlators not containing the winding number density $\omega(x)$ (1.63) from the start, it is always possible to set $\theta = 0$.

It is usual to group the scalar and pseudo-scalar sources s and ip into one single entity:

$$\chi = 2B_0(s + ip) \tag{2.44}$$

where the parameter B_0 is a low energy constant that will be discussed later. Taking into account the source θ corresponds to the change:

$$\chi \quad \rightarrow \quad e^{i\theta/3}\chi \tag{2.45}$$

We are now ready to write the most general expression for the ($O(p^2)$) lagrangian at lowest order:

$$\mathcal{L}^{(2)} = \frac{F_0^2}{4}\Big[\langle D_\mu U^\dagger D^\mu U\rangle + \langle e^{i\theta/3}\chi U^\dagger + e^{-i\theta/3}\chi^\dagger U\rangle\Big] \tag{2.46}$$

The factor $F_0^2/4$ is a constant used to retrieve the proper normalization of the kinetic term once U is expressed in terms of the fields ϕ_a (eq. (2.34)).

To express the lagrangian in terms of the meson fields, it is necessary to expand the matrix $U(x)$ in powers of $\Phi(x)$:

$$U = \mathbb{1} + i\frac{\sqrt{2}}{F_0}\Phi - \frac{1}{F_0^2}\Phi^2 - i\frac{\sqrt{2}}{3F_0^3}\Phi^3 + \frac{1}{6F_0^2}\Phi^4 + O(\Phi^5) \tag{2.47}$$

Thus, for $\mathcal{L}^{(2)}$, taking $\chi = 2B_0\mathcal{M}$ and setting $\theta = 0$:

$$\begin{aligned} \mathcal{L}^{(2)} = &\frac{1}{2}\langle\partial^\mu\Phi\partial_\mu\Phi\rangle + \frac{1}{12F_0^2}\langle(\Phi\partial_\mu\Phi + (\partial_\mu\Phi)\Phi).(\Phi\partial^\mu\Phi + (\partial^\mu\Phi)\Phi)\rangle \\ &+ B_0\Big(-\langle\mathcal{M}\Phi^2\rangle + \frac{1}{6F_0^2}\langle\mathcal{M}\Phi^4\rangle\Big) + O\Big(\frac{\Phi^6}{F_0^4}\Big) \end{aligned} \tag{2.48}$$

We have a tower of interaction terms which at each order involve an increasing number of fields. We can observe further that different processes with different numbers of meson fields are described in the chiral limit by the single constant F_0, a prominent feature of the Goldstone bosons interactions.

After taking the trace, isolating all the bilinear terms $\partial_\mu\phi_a\partial^\mu\phi_b$ and $\phi_a\phi_b$ leads to a Klein-Gordon-type lagrangian for the kinematical part:

$$\begin{aligned}\mathcal{L}^{(2)}_{eff,KG} = &\frac{1}{2}(\partial\pi^0)^2 + \frac{1}{2}(\partial\eta)^2 + \partial^\mu\pi^+\partial_\mu\pi^- + \partial^\mu\bar{K^0}\partial_\mu K^0 + \partial^\mu K^+\partial_\mu K^- \\ &- B_0\left((m_u+m_d) - \frac{4}{3}(m_s-m)\frac{\sin^2\epsilon}{\cos 2\epsilon}\right)(\pi^0)^2 \\ &- B_0\left(\frac{2}{3}(m+2m_s) + \frac{4}{3}(m_s-m)\frac{\sin^2\epsilon}{\cos 2\epsilon}\right)\eta^2 \\ &- B_0(m_u+m_d)\pi^+\pi^- - B_0(m_u+m_s)K^+K^- - B_0(m_d+m_s)\bar{K^0}K^0 \\ &+ O(\phi_a^4)\end{aligned} \tag{2.49}$$

ϵ accounts for the mixing between the η and π^0 fields at leading order:

$$\tan 2\epsilon = \frac{\sqrt{3}}{2}\frac{m_d-m_u}{m_s-m}, \quad m = \frac{m_u+m_d}{2} \tag{2.50}$$

We have the masses at leading order:

$$\overset{\circ}{M}{}^2_{\pi^0} = B_0\left((m_u+m_d) - \frac{4}{3}(m_s-m)\frac{\sin^2\epsilon}{\cos 2\epsilon}\right) \tag{2.51}$$

$$\overset{\circ}{M}{}^2_{\eta} = B_0\left(\frac{2}{3}(m+2m_s) + \frac{4}{3}(m_s-m)\frac{\sin^2\epsilon}{\cos 2\epsilon}\right) \tag{2.52}$$

$$\overset{\circ}{M}{}^2_{\pi^\pm} = B_0(m_u+m_d) \tag{2.53}$$

$$\overset{\circ}{M}{}^2_{K^0} = B_0(m_u+m_s) \tag{2.54}$$

$$\overset{\circ}{M}{}^2_{K^\pm} = B_0(m_d+m_s) \tag{2.55}$$

(For the remainder of the manuscript, $\overset{\circ}{M}{}^2_P$ will denote the masses at leading order). In the isospin limit $m_u = m_d$, which we shall be dealing with in most of the thesis, the expressions for the masses take a much reduced form:

$$\overset{\circ}{M}{}^2_{\pi} = 2B_0 m \tag{2.56}$$

$$\overset{\circ}{M}{}^2_{K} = B_0(m+m_s) \tag{2.57}$$

$$\overset{\circ}{M}{}^2_{\eta} = B_0\frac{2}{3}(m+2m_s) \tag{2.58}$$

From the previous equations we can retrieve the famous Gell-Mann-Okubo formula, which, at leading order, gives an exact relation between the three masses:

$$\overset{\circ}{M}{}^2_{\eta} = \frac{4}{3}\overset{\circ}{M}{}^2_{K} - \frac{1}{3}\overset{\circ}{M}{}^2_{\pi} \tag{2.59}$$

Now we can evaluate in χPT at lowest order the coupling of the pion to the axial current eq. (1.33) and the quark condensate $\langle\bar{u}u\rangle$ out of the chiral limit:

$$\begin{aligned}\langle\Omega|\bar{d}\gamma_\mu(x)\gamma^5 u|\pi^+(p)\rangle &= iF_0 p_\mu e^{ip.x} + O(m_q) \\ \langle\bar{u}u\rangle &= -F_0^2 B_0 + O(m_q)\end{aligned} \tag{2.60}$$

Higher orders will come from contributions proportional to the quark mass. Therefore in the chiral limit, the relation of the two low energy constants F_0 and B_0 to the two main order parameters of the $SU(3)$ chiral spontaneous symmetry breaking follows easily (see sec. 1.4.3):

$$F_0 \equiv F(3), \quad B_0 F_0^2 \equiv \Sigma(3) \tag{2.61}$$

2.5.3 Higher Orders and Renormalization

At next-to-leading order (NLO), we expect the terms to be of order $O(p^4)$. Always following the prescription dictated by symmetry principles, we need a lagrangian compatible with Lorentz invariance and chiral symmetry: The most general lagrangian at $O(p^4)$ is a sum of 12 terms:

$$\begin{aligned}\mathcal{L}_{eff}^{(4)} =& L_1\langle D_\mu U D^\mu U^\dagger\rangle^2 + L_2\langle D_\nu U D^\mu U^\dagger\rangle\langle D_\mu U D^\nu U^\dagger\rangle \\ &+ L_3\langle D_\mu U D^\mu U^\dagger D_\nu U D^\nu U^\dagger\rangle + L_4\langle D_\mu U D^\mu U^\dagger\rangle\langle\chi^\dagger U + U^\dagger\chi\rangle \\ &+ L_5\langle D_\mu U D^\mu U^\dagger(\chi^\dagger U + U^\dagger\chi)\rangle + L_6\langle U^\dagger\chi + \chi^\dagger U\rangle^2 \\ &+ L_7\langle U^\dagger\chi - \chi^\dagger U\rangle^2 + L_8\langle U^\dagger\chi U^\dagger\chi + \chi^\dagger U\chi^\dagger U\rangle \\ &- iL_9\langle D_\mu U D_\nu U^\dagger F_r^{\mu\nu} + F_l^{\mu\nu} D_\mu U D_\nu U^\dagger\rangle + L_{10}\langle U F_l^{\mu\nu} U^\dagger F_{r,\mu\nu}\rangle \\ &+ H_1\langle F_{r\mu\nu}F_r^{\mu\nu} + F_{l\mu\nu}F_l^{\mu\nu}\rangle + H_2\langle\chi^\dagger\chi\rangle\end{aligned} \tag{2.62}$$

for $\theta = 0$. The L_i are the ten next-to-leading order low energy constants, containing information about short-distance dynamics (see sec. 2.3). $F_{r,l}^{\mu\nu}$ is the field strength of the external sources, and the H_i are two high energy counter-terms not containing any dynamics associated with the light mesons. At next-to-next-to-leading order (NNLO) for $\theta = 0$, the lagrangian $\mathcal{L}^{(6)}$ contains ninety low energy constants (written C_i) and four high energy counter-terms. Up to that point, χPT has been investigated up to NNLO [35]. We must stress that it is not possible to evaluate the values of all the low-energy constants from experiment, and one has to rely on analytic estimates like resonance saturation, or numerical estimates from lattice simulations. We must add to this lagrangian another one, accounting for the anomalous parts of the Ward identities [21, 22], involving only vector and axial sources.

Now, in order to get observables, one has to compute correlators, which, from the point of view of Quantum Field Theory, can be done computing Feynman diagrams. In practice, $O(p^2)$ calculations is a rather easy business, since it only involves tree-level graphs: once we get the vertices, everything is (virtually) done. Pushing the calculation to $O(p^4)$ is more tricky: because of the presence of loops, infinities emerge, and, unless we find a mean to re-absorb them, the theory will have no meaning at all.

When calculating a process up to a given order $O(p^{2n})$, where p is any relevant external momentum, we need to truncate the chiral lagrangian at the desired power $\mathcal{L}_{eff}^{(2n)}$, and then generate all the contributing diagrams. Except for the lowest order which is generally tree-level, those diagrams contain loops. Their amplitudes are of the form:

$$\int (d^4k)^{N_L} \frac{1}{(k^2)^{N_I}} \prod_n (k^n)^{N_n} \tag{2.63}$$

where N_I is the number of internal lines, and k a momentum. A loop contributes with an integration factor $\int (d^4k)$, an internal line with $\frac{1}{k^2}$, and k^n accounts for a vertex of dimension n. The counting rules giving the total order of a diagram have been introduced by Weinberg in [39]. The total order N_T of the diagram reads:

$$N_T = 2 + 2N_L + \sum_{n \geq 2} (n-2) N_n \tag{2.64}$$

where N_n is the number of vertices of order n, and N_L the number of loops. The proof can be found in [35]. Chiral symmetry puts a lower bound on N_T, explaining why lagrangians of order $2n$ start contributing only for computations performed at $n-1$ loops or higher, as shown in table 2.1. At order $O(p^2)$, χPT computations involve only tree diagrams from $\mathcal{L}^{(2)}$, at order $O(p^4)$, they involve 1-loop diagrams from $\mathcal{L}^{(2)}$ and tree diagrams from $\mathcal{L}^{(4)}$, and so on: there is in fact a one-to-one correspondance between the order of a diagram and its number of loops. This process is summarized in table 2.1 up to $O(p^6)$.

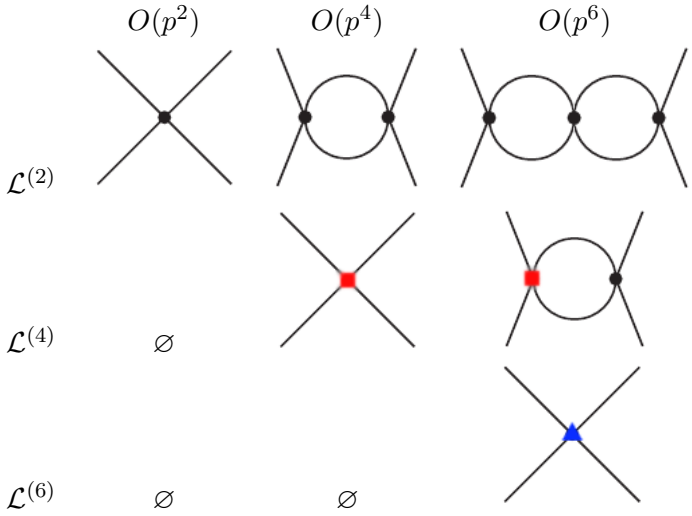

Table 2.1: Counting rules for diagrams in χPT up to $O(p^6)$: example with *some* of the graphs for $\pi\pi$ scattering. The black dots represent vertices from $\mathcal{L}^{(2)}$, red squares vertices from $\mathcal{L}^{(4)}$, and the blue triangle a vertex from $\mathcal{L}^{(6)}$.

In order to keep the symmetries explicit, we regularize the theory using dimensional regularization, toghether with the minimal substraction scheme to re-absorb divergences. Since chiral symmetry is preserved by such a choice, the counter-terms needed to renormalize a computation at $n-1$ loops will be of order $O(p^{2n})$ as well as to observe the symmetries of the lagrangian. By construction they are all already contained in $\mathcal{L}^{(2n)}$, so the divergences stemming from loops can be re-absorbed thanks to $O(p^{2n})$ terms of the chiral lagrangian. For example, a process to order $O(p^4)$ would involve a 1-loop graph with vertices from $\mathcal{L}^{(2)}$, and a tree-level graph with counter-terms from $\mathcal{L}^{(4)}$ (see table 2.1 for example). The theory is systematically renormalizable in the sense that for a given order in the chiral counting, only a finite number of counter-terms are needed to re-absorb the divergences at this order and are already present in the lagrangian of the theory. It is the symmetry structure of χPT that strongly constrains (and allows) its renormalizabilty *order-by-order*. For a next-to-leading order calculation, the low-energy constants L_i play the role of renormalization counter-terms, which must be redefined according to Ward identities [2] to properly cancel the divergences (see Appendix D.1). The low-energy constants are then functions of the

renormalization scale μ, for example $L_i^r = L_i^r(\mu)$. The scale μ can be interpreted as the separation scale between the low-energy dynamics given by the effective operators and the high energy dynamics summed up in the low-energy constants (see sec. 2.3). The generating functional and all the derived correlators are μ-independent at the concerned order in the chiral counting.

2.5.4 The generating functional at 1-loop

When evaluating an amplitude for a given process, it is possible to tackle the calculation by two different ways: first, we can derive the Feynman rules for propagators and vertices directly from the lagrangian, write out the corresponding diagrams, and apply the rules. This corresponds to the straightforward "textbook" approach. On more general grounds, a second strategy consists in the systematic analysis of the generating functional [1, 2]. It consists in integrating the degrees of freedom of the path-integral Z to obtain a quantity containing only propagators, loop integrals and sources. To retrieve the relevant terms corresponding to a given correlator, one has then simply to differentiate Z with respect to the appropriate sources. For $N_f = 3$ χPT the formula was derived at one loop in [2]:

$$Z = Z_t + Z_u + Z_A + ... \tag{2.65}$$

Z_t is the generating functional for diagrams at tree-level ($O(p^2)$ and $O(p^4)$) and tadpole contributions, Z_u gathers the 1-loop unitarity corrections for the graphs with two $O(p^2)$ vertices and the non-analytic contributions (cuts) - and Z_A is the Weiss-Zumino functional collecting the anomalous terms. The ellipsis ... stands for the higher orders. The expressions for Z_t read:

$$\begin{aligned} Z_t =& \sum_P \int dx \frac{F_0^2}{6} \left(1_{|(LO)} - \frac{3}{16\pi^2} \frac{\overset{\circ}{M}{}_P^2}{F_0^2} \log \frac{\overset{\circ}{M}{}_P^2}{\mu^2}{}_{|(NLO)} \right) \sigma^{\Delta}_{PP} \\ &+ \sum_P \int dx \frac{3F_0^2}{6} \left(1_{|(LO)} - \frac{3}{6\pi^2} \frac{\overset{\circ}{M}{}_P^2}{F_0^2} \log \frac{\overset{\circ}{M}{}_P^2}{\mu^2}{}_{|(NLO)} \right) \sigma^{\chi}_{PP} + \int dx \mathcal{L}^{(4),r}{}_{|(NLO)} \end{aligned} \tag{2.66}$$

The quantities σ^{Δ} and σ^{χ} gather the source terms respectively for vector/axial currents and scalar/pseudoscalar densities. $\mathcal{L}^{(4),r}$ is the $O(p^4)$ lagrangian with the renormalized constants L_i^r and H_i^r, and $\overset{\circ}{M}{}_P^2$ are the pseudoscalar masses at $O(p^2)$. The subscripts LO (leading order) and NLO (next-to-leading order) indicate to which order the terms belong.

The tadpole "bubble" $\Delta^P(0)$, leading to the chiral logarithms $\frac{\overset{\circ}{M}{}_P^2}{16\pi^2} \log \frac{\overset{\circ}{M}{}_P^2}{\mu^2}$ after renormalization, is regularized as follows:

$$\Delta^P(0) = \frac{\overset{\circ}{M}{}_P^2}{16\pi^2} \left[\log \frac{\overset{\circ}{M}{}_P^2}{\mu^2} - \frac{2}{\epsilon} - \ln 4\pi + \gamma - 1 + \ln \mu^2 + O(\epsilon) \right], \quad \epsilon = 4 - d \tag{2.67}$$

where $\overset{\circ}{M}{}_P^2$ is the leading-order mass of any meson P running in the loop, eqs. (2.56) and γ is the Euler-Mascheroni constant [6, 8].

The ϵ divergence is re-absorbed by the counter-terms from the $\mathcal{L}^{(4)}$ lagrangian, eq. (2.62), under a suitable redefinition of the low-energy constants L_i (see sec. 2.5.3) in the $\bar{M}S$ scheme:

$$L_i = L_i^r + \kappa \Gamma_i, \quad \kappa = \frac{\mu^{-\epsilon}}{16\pi^2} \Big[\frac{1}{-\epsilon} - \frac{1}{2} (\ln 4\pi - \gamma + 1) \Big] \tag{2.68}$$

The coefficients Γ_i are fixed by the Ward identities [2] and given numerically by:

$$\begin{aligned}\Gamma_1 = \frac{3}{32},\ \Gamma_2 = \frac{3}{16},\ \Gamma_3 = 0,\ \Gamma_4 = \frac{1}{8},\ \Gamma_5 = \frac{3}{8},\\ \Gamma_6 = \frac{11}{144},\ \Gamma_7 = 0,\ \Gamma_8 = \frac{5}{48},\ \Gamma_9 = \frac{1}{4},\ \Gamma_{10} = -\frac{1}{4}.\end{aligned} \tag{2.69}$$

Finally, we have for Z_u:

$$\begin{aligned}Z_u = &\sum_{P,Q}\int dxdy\Big[\Big((\partial_{\mu\nu} - g_{\mu\nu}\Box)M^r_{PQ}(x-y) - g_{\mu\nu}L_{PQ}(x-y)\Big)\hat{\Gamma}^{\mu}_{PQ}(x)\hat{\Gamma}^{\nu}_{QP}(x) \\ &- \partial_\mu K_{PQ}(x-y)\hat{\Gamma}_{PQ}(x)^\mu\bar{\sigma}_{QP}(y) + \frac{1}{4}J^r(x-y)\bar{\sigma}_{PQ}(x)\bar{\sigma}_{QP}(y)\Big]\end{aligned} \tag{2.70}$$

where J, K, L, M are renormalized functions defined from the 1-loop scalar integral with P and Q any mesons propagating in the loop. They encode the non-analytic structure of the amplitudes. Γ^μ and $\bar{\sigma} = \sigma^\Delta + \sigma^\chi$ collect the source terms and involve the solution $\bar{U}$ of the equation of motion [1] derived from the leading order χPT lagrangian in the presence of sources (see Appendices A.1 and A.2). To get a specific correlator, one simply has to differentiate the generating functional Z with respect to the different sources. The dependence on the renomalization scale μ in the tadpole and unitarity terms cancels the dependence of the $O(p^4)$ counter-terms of $\mathcal{L}^{(4),r}$.

2.6 Chiral Perturbation Theory for two flavours

All of the preceeding discussion for $N_f = 3$ Chiral Perturbation Theory is also valid for two flavours $N_f = 2$. In this case, the theory accounts for very low energies at which only pions are the relevant degrees of freedom [1]: $m_u, m_d \ll m_s$, $p_\pi^2 \ll M_{K,\eta}^2$. Similarly to $SU(3)_L \otimes SU(3)_R$, the lagrangian at lowest order takes the form:

$$\mathcal{L}^{(2)}_{N_f=2} = \frac{F^2}{2}\langle D_\mu U^T D^\mu U + 2\chi^T U\rangle \tag{2.71}$$

where T is the transpose. Here the object U gathering the meson fields can be chosen as a real 4-component orthogonal vector $U(x) = (U^0(x), U^{i=1,2,3}(x))$, with $U^0 = \sqrt{1 - \sum_i (U^i)^2}$. It is possible to make this choice for U because one can identify $SU(2)_L \times SU(2)_R$ and $O(4)$ at the level of their Lie algebras. Its covariant derivatives are defined as:

$$\begin{aligned}D_\mu U^0(x) &= \partial U^0(x) + a^i_\mu(x)U_i(x) \\ D_\mu U^i(x) &= \partial U^i(x) + \epsilon^{ijk}v^j_\mu(x)U^k - a^i_\mu(x)U_0(x)\end{aligned} \tag{2.72}$$

where v_μ and a_μ are the usual vector and axial sources, and $\chi(x) = 2B(s^0(x), p^i(x))$. The scalar and pseudo-scalar sources s and p have been decomposed over the set of Pauli matrices τ^i plus the identity τ^0:

$$s(x) = s^0\tau^0 + s^i(x)\tau^i, \quad p(x) = p^0\tau^0 + p^i(x)\tau^i \tag{2.73}$$

The two low energy constants F and B play the same roles as in the $N_f = 3$ theory, namely they correspond to the pion decay constant $F(2)$ and the quark condensate $\Sigma(2)$ in the chiral limit (sec. 1.4.3) with two massless flavours:

$$F^2 = \lim_{\substack{m_{u,d}\to 0,\\ m_s \ physical}} F_\pi^2 \equiv F(2)^2 \tag{2.74}$$

$$BF^2 = -\lim_{\substack{m_{u,d}\to 0,\\ m_s \ physical}} \langle 0\,|\bar{u}u|\,0\rangle \equiv \Sigma(2) \tag{2.75}$$

At $O(p^4)$ the lagrangian is given by (for $\theta = 0$):

$$\begin{aligned}\mathcal{L}^{(4)}_{N_f=2} &= l_1\langle D_\mu U D^\mu U^T\rangle^2 + l_2\langle D_\nu U D^\mu U^T\rangle\langle D_\mu U D^\nu U^T\rangle \\ &+ l_3\langle \chi^T U\rangle^2 + l_4\langle D^\mu\chi^T D_\mu U\rangle \\ &+ l_5\langle U^T F_{\mu\nu}F^{\mu\nu}U\rangle + l_6\langle D^\mu U^\dagger F_{\mu\nu}D^\nu U\rangle \\ &+ l_7\langle\tilde{\chi}^T U\rangle^2 + h_1\langle\chi^T\chi\rangle + h_2\langle 2F_{\mu\nu}F^{\mu\nu}\rangle + h_1\langle\tilde{\chi}^T\tilde{\chi}\rangle\end{aligned} \tag{2.76}$$

with $\widetilde{\chi}= 2B(p^0, s^i)$. The tensor $F_{\mu\nu}$ is defined by the relation:

$$[D_\mu, D_\nu]U = F_{\mu\nu}U \tag{2.77}$$

We have thus 7 low energy constants l_i and 3 high energy counter-terms h_i. At next-to-next-to leading order, the lagrangian $\mathcal{L}^{(6)}_{N_f=2}$ contains 54 low energy constants and 4 high energy counter-terms. All of those LECs, defined in the chiral limit $N_f = 2$, are dependent on the strange quark mass that has been kept at its physical value. We must stress that the previous discussion of sec. 2.5 concerning the generating functional of the $SU(3)$ theory also applies in the $SU(2)$, as well as the chiral counting of loops and the renormalization of the low-energy constants.

The $N_f = 2$ and $N_f = 3$ chiral perturbation theories can be matched in the very low energy domain of (very) soft pions where they both apply. In particular, at one loop, we have for the two order parameters $F(2)$ and $\Sigma(2)$:

$$F(2)^2 = F(3)^2\Big(1 - \frac{m_s B_0}{16\pi^2 F(3)^2}\log\frac{\bar{M}_K^2}{\mu^2} - 16\frac{m_s B_0}{F(3)^2}L_4^r(\mu)\Big) \tag{2.78}$$

$$\Sigma(2) = \Sigma(3)\Big(1 + \frac{m_s B_0}{16\pi^2 F(3)^2}\log\frac{\bar{M}_K^2}{\mu^2} + \frac{m_s B_0}{96\pi^2 F(3)^2}\log\frac{\bar{M}_\eta^2}{\mu^2} - 32\frac{m_s B_0}{F(3)^2}L_6^r(\mu)\Big) \tag{2.79}$$

$\bar{M}_P$ being the leading-order mass in the limit $m_u = m_d = 0$. These two expressions correspond, in the language of Chiral Perturbation Theory, to the statement of sec. 1.4.3 that the order parameters for $N_f = 2$ are functions of the order parameters for $N_f = 3$ *plus* a function of the strange quark mass: the NLO part of eq. (2.79), which contains L_6, is to be identified with the term corresponding to the induced condensate of eq. (1.46). The same holds for L_4 in the case of the decay constant, those two low-energy constants being related to the correlators $\langle(\bar{u}u)(\bar{s}s)\rangle$ and $\langle(\bar{s}s)(VV - AA)\rangle$ respectively. They indicate the role of $\bar{s}s$ sea-pairs in the chiral expansions. In the same manner, we give the expressions for the next-to-leading order low energy constants l_3^r and l_4^r:

$$l_3^r = -8L_4^r - 4L_5^r + 16L_6^r + 8L_8^r - \frac{1}{576\pi^2}(\log\frac{\bar{M}_\eta^2}{\mu^2} + 1) \tag{2.80}$$

$$l_4^r = 8L_4^r + 4L_5^r - \frac{1}{64\pi^2}(\log\frac{\bar{M}_K^2}{\mu^2} + 1) \tag{2.81}$$

Those low energy constants encode the u and d quark mass dependence [1] of the decay constant and the mass of the pion in the $SU(2)$ theory:

$$F_\pi = F(2)\Big(1 + \frac{2mB}{F(2)^2} l_4^r(\mu) - \frac{2mB}{16\pi^2 F(2)^2} \log\frac{2mB}{\mu^2} + O(m^4)\Big) \tag{2.82}$$

$$M_\pi^2 = 2mB\Big(1 + \frac{4mB}{F(2)^2} l_3^r(\mu) + \frac{2mB}{32\pi^2 F(2)^2} \log\frac{2mB}{\mu^2} + O(m^4)\Big), \tag{2.83}$$

in the isospin limit $m_u = m_d$.

2.7 Review of numerical results for χPT low energy constants

We are now in possession of a framework that takes into account all the symmetry considerations, but that is unable to provide values for its parameters, i.e. the low energy constants (sec. 2.3). Those need to be determined if the theory is to make any *numerical* predictions.

Therefore in this section, we aim to provide a short review of the numerical determination of χPT's low energy constants L_i^r and l_i^r. Those constants are to be determined through experimental measurement and lattice simulations. Each of the LECs is related to some specific observables, hence their precise determination is strongly dependent on our ability to gain information about those same observables, and to constrain the rate of convergence of the chiral series.

2.7.1 $N_f = 3$

We state here the list of the different $SU(3)$ low energy constants L_i^r along with their associated observables that are simple to obtain from experiments and/or lattice calculations:

- L_1, L_2, L_3 : $K_{\ell 4}$ form factors
- L_4, L_5 : π and K decay constants
- L_6, L_8 : π and K masses
- L_7 : η mass and decay constant
- L_9 : Pion electromagnetic form factor
- L_{10} : $\pi \to e\nu\gamma$ form factor and τ spectral functions

We can distinguish between two groups of $O(p^4)$ LECs: the first one (L_1, L_2, L_3, L_9, L_{10}) involves operators containing only derivatives. The associated correlators are more accessible experimentally through the energy-dependence of form factors and scattering amplitudes. Conversely, it is more difficult to evaluate from experiment the LECs of the second group (L_4, L_5, L_6, L_7, L_8) since the operators in the lagrangian also involve quark masses (i.e. scalar and pseudo-scalar densities). They can otherwise be accessed by lattice simulations, which permits one to probe the quark mass dependence of the correlators. We will focus on the latter in the following.

In [2], first estimates of the next-to-leading order low-energy constants were provided, using the available information at that time. A summary is presented in table 2.2. The work from [40] involves computations up to NNLO and a subsequent fit to experimental results from masses, decay constants, $K_{\ell 4}$, $\pi\pi$ and πK scattering observables lengths and slopes and the slope of the pion scalar form factor. To fix the values of the NNLO low energy constants C_i, they used models of resonance saturation in the vector and scalar

channels. They also relaxed the constraint corresponding to fixing L_4^r and L_6^r to zero at a particular scale. Finally, they probed the dependence of their results on the models they used to evaluate the C_i counter-terms. They observed that the value they obtained of the L_i^r depended on the assumptions made for the C_i, with fits being of the same (good) quality (see table 2.2). No conclusion gave greater importance to a given model. We observe that the resulting values for L_4 and L_6 are positive.

L_4 and L_6 account for the effect of $\bar{s}s$ sea pairs on the chiral structure of the QCD vacuum, since they are tied to the Zweig rule because they correspond to products of traces in the lagrangian $\mathcal{L}_{eff}^{(4)}$ (2.62). This is reflected in expressions (2.78)-(2.79) where we can observe that they are the low energy constants that indicate the m_s-dependence of the low energy observables in the chiral perturbation theory framework at one loop. It is thus more difficult to determine them than to determine for instance L_5 or L_8, which impact differently on observables related to π and K.

Following the Zweig rule, it is common to set L_4 and L_6 to zero (at a certain scale), thus minimizing the impact of a dynamical strange quark on the pattern of chiral spontaneous symmetry breaking. In ref. [2] it was chosen to set them to zero at the scale of the η mass: $L_{4,6}^r(\mu_0 = M_\eta) = 0$. But a different choice of μ_0 would then modify the value of $L_{4,6}^r$ at the ρ mass:

$$\mu_0 = M_\eta \rightarrow \qquad L_4^r(M_\rho) = -0.27 \times 10^{-3}, \qquad L_6^r(M_\rho) = -0.17 \times 10^{-3} \tag{2.84}$$

$$\mu_0 = M_\rho \rightarrow \qquad L_4^r(M_\rho) = 0, \qquad L_6^r(M_\rho) = 0 \tag{2.85}$$

$$\mu_0 = 1 \text{ GeV} \rightarrow \qquad L_4^r(M_\rho) = 0.21 \times 10^{-3}, \qquad L_6^r(M_\rho) = 0.13 \times 10^{-3} \tag{2.86}$$

In addition to this uncertainty on the scale where these low-energy constants vanish, a violation of the Zweig rule in the scalar sector could make such estimates completely inaccurate.

L_i	Source (in [2])	[2]	[40] $O(p^4)$	[40] All $O(p^6)$
L_1	$K_{\ell 4}$, D-wave $\pi\pi$, Zweig rule	0.7 ± 0.3	1.12	0.88 ± 0.09
L_2	$K_{\ell 4}$, D-wave $\pi\pi$, Zweig rule	1.3 ± 0.7	1.23	0.61 ± 0.20
L_3	$K_{\ell 4}$, D-wave $\pi\pi$, Zweig rule	-4.4 ± 2.5	-3.98	-3.04 ± 0.43
L_4	Zweig rule	-0.3 ± 0.5	1.50	0.75 ± 0.75
L_5	F_K/F_π	1.4 ± 0.5	1.21	0.58 ± 0.13
L_6	Zweig rule	-0.2 ± 0.3	1.17	0.29 ± 0.85
L_7	GMO, L_5, L_8	-0.4 ± 0.15	-0.36	-0.11 ± 0.15
L_8	$M_{K^0}^2 - M_{K^+}^2$, L_5, $\frac{m_s - \hat{m}}{m_d - m_u}$	0.9 ± 0.3	0.62	0.18 ± 0.18
L_9	$\langle r^2 \rangle_\pi^V$	6.9 ± 0.7		
L_{10}	$\pi \rightarrow e\nu\gamma$	-5.5 ± 0.7		

Table 2.2: Estimates of $N_f = 3$ low-energy constants $L_i.10^3$ at M_ρ. [2] is the initial NLO estimate, while [40] are fits to NLO and NNLO expressions.

Furthermore, large values of L_4 and/or L_6 have been obtained in several earlier works: dispersive analysis of scalar form factors [88, 89], dispersive treatment of $K\pi$ scattering [90], J/ψ decay into a vector meson and two pseudo-scalar [91] (with a value of L_6 compatible with zero), preliminary next-to-next-to-leading order $N_f = 3$ fits to pseudoscalar masses, decay constants, $K_{\ell 4}$ decay and πK scattering data [111].

The values of the L_i can also be determined by lattice simulations with $2 + 1$ dynamical light quarks (see sec. 2.2), for observable like masses, decay constants, and $K_{\ell 3}$ form factors (see Chapter 4). Once these values are known, they can be re-inserted into the chiral series to obtain the values of the observables at the physical point. This procedure is sensitive to

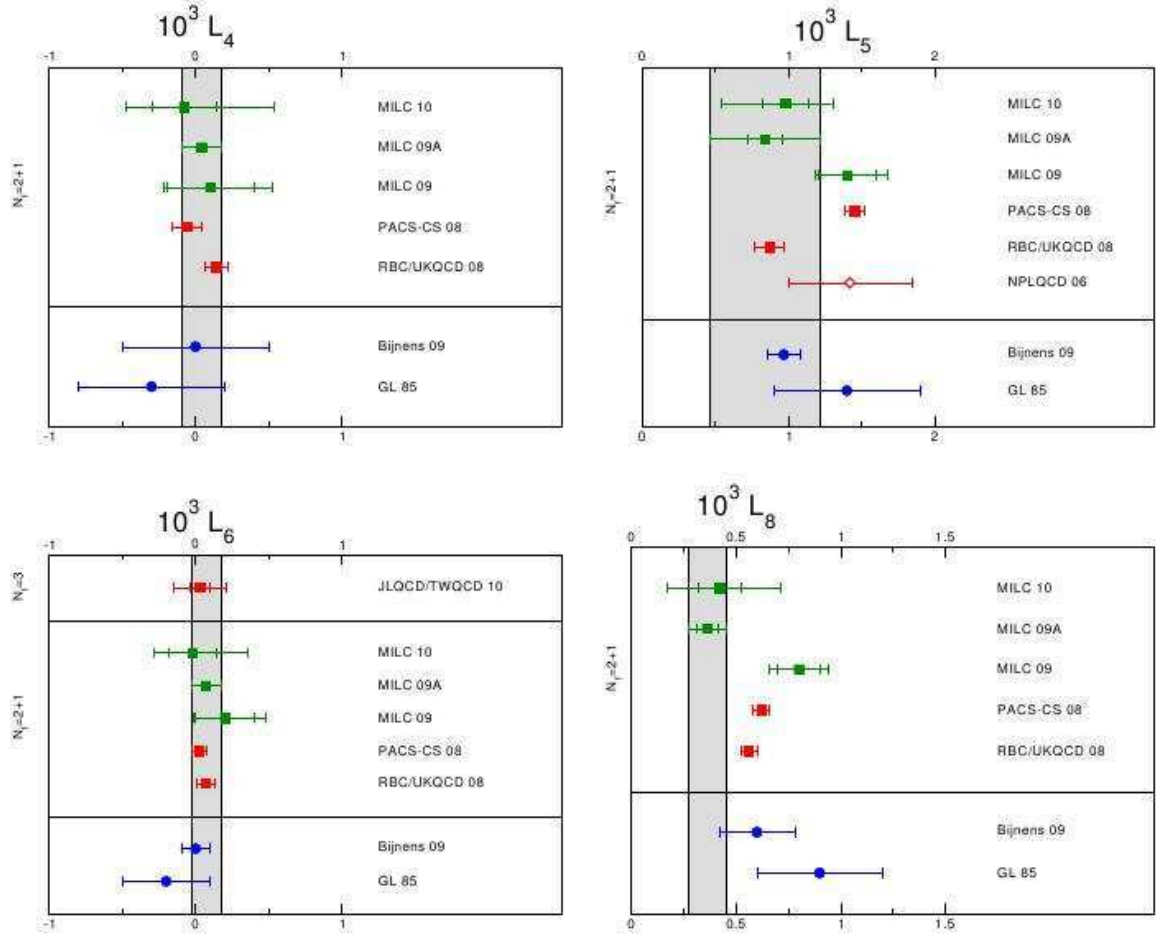

Figure 2.4: Summary of lattice determinations for $L^r_{4,5,6,8}(M_\rho)$ from [69].

the exact form of the chiral extrapolations used and the assumptions concerning the physical point. A recent summary of the different determinations for the low-energy constants $L^r_{4,5,6,8}$ can be found in [69], and the associated figures are recalled in table 2.4. We observe that positive values are favoured for $L^r_{4,6}$, as was the case for ref. [40] discussed above.

2.7.2 $N_f = 2$

The $SU(2)$ next-to-leading order low-energy constants l^r_i can be determined much the same way as for the L^r_i. Again, we can separate them into two groups: the ones involving operators containing derivatives only, (l_1, l_2, l_5, l_6), and the others involving operators with quark masses (l_3, l_4, l_7). Their values were obtained by combining estimates of $SU(3)$ χPT with information on pion observables, and by matching the $N_f = 2$ theory only using the outcome of NNLO fits [40]. A summary is given in table 2.3.

It is also possible to get information from Lattice QCD, even if the simulated masses are above the physical ones (see sec. 2.2). A summary for the different determinations of the values of $l^r_{3,4}$ can be found in [69].

Also, recent results from NA48/2 [62] as well as lattice simulations have indicated that $\pi\pi$ scattering confirmed the picture of a large two-flavour quark condensate, as summarized in figure 2.6 the two $\pi\pi$ scattering lengths.

l_i	Source (in [1])	[1]	[40] All
l_1	D-wave $\pi\pi$ scattering lengths	-2.3 ± 3.7	-1.9
l_2	D-wave $\pi\pi$ scattering lengths	6.0 ± 1.3	5.3
l_3	$M^2_{K^0} - M^2_{K^+}$, $\frac{2m_s - m_u - m_d}{m_d - m_u}$	2.9 ± 2.4	4.2
l_4	$\langle r^2 \rangle^S_\pi$	4.6 ± 0.9	4.8
l_5	Sum rule for vector and axial mesons	14	-
l_6	$\langle r^2 \rangle^V_\pi$	16.5 ± 1.1	-

Table 2.3: Table of $N_f = 2$ LECs l_i

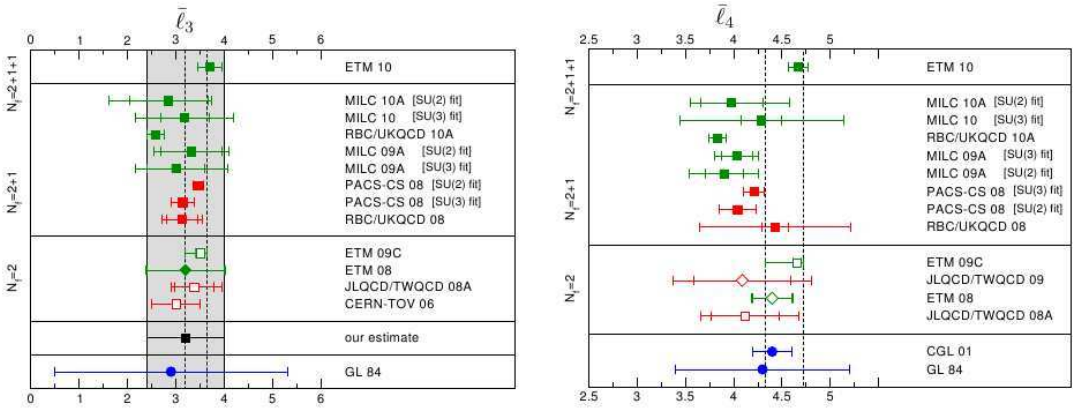

Figure 2.5: Summary of lattice determinations for $\bar{l}_{3,4}$ from [69], where $\bar{l}_i = 32\pi^2(l^r_i/\gamma_i) - log(M^2_\pi/\mu^2)$, $\gamma_{3,4} = -1/2,\ 2$, see ref. [1].

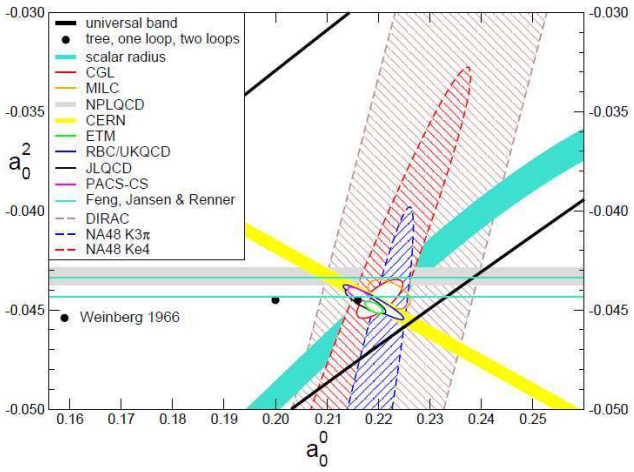

Figure 2.6: Plot of the experimental and theoretical results for the S-wave $\pi\pi$ scattering lengths, from [64].

2.7.3 Some issues concerning the $SU(3)$ theory

Some lattice collaborations performing simulations with 2+1 dynamical quarks found difficulties in fitting their data with some of $N_f = 3$ chiral expansions [96, 99, 100, 101, 102, 103]: masses, decay constants and $K_{\ell 3}$ form factors. Putting aside the different issues concerning lattice systematics (see sec. 2.2), and assuming that the lattice data does not suffer intrinsic problems, it may be a sign that the chiral series for $N_f = 3$ do not meet the expected convergence behaviour. In fact, it happens that the $SU(2)$ and $SU(3)$ theories do not show the same pattern of chiral symmetry breaking when compared to some specific lattice data: it

has been observed that the two main order parameters, the quark condensate and the decay constant, decreased significantly when one moved from the $N_f = 2$ to the $N_f = 3$ chiral limit. We can quote the following results from PACS-CS [96] and MILC [102, 103]:

$$\text{PACS-CS: } \frac{F}{F_0} = 1.089 \pm 0.045, \qquad \frac{\Sigma(2)}{\Sigma(3)} = 1.245 \pm 0.010 \tag{2.87}$$

$$\text{MILC: } \frac{F}{F_0} = 1.15 \pm 0.05 \begin{pmatrix} +0.10 \\ -0.03 \end{pmatrix}, \ \frac{\Sigma(2)}{\Sigma(3)} = 1.52 \pm 0.17 \begin{pmatrix} +0.38 \\ -0.15 \end{pmatrix} \tag{2.88}$$

Moreover, the MILC collaboration [103] observed from fits with staggered chiral perturbation theory that M_π^2 received NNLO corrections of the same size as next-to-leading order contributions, canceling each other to a large extent, with small NNNLO corrections (the latter being taken as analytic in quark masses and lattice spacings), whereas F_π exhibited no problems of convergence. On the other hand, the RBC/UKQCD collaboration [99] experienced difficulties in fitting F_π both in $N_f = 2$ and $N_f = 3$ theories. They also noticed that fits to M_K^2 and F_K using the $N_f = 3$ chiral expansion led to very significant next-to-leading order contributions (of order 50%) when data up to the kaon mass scale was included, and they conclude that higher-order corrections could be very significant (up to 30%).

We also notice that a joint lattice study from the collaborations JLQCD and TWQCD of the distribution of low-lying Dirac eigenvalues obtained [117]: $\Sigma(2)/\Sigma(3) = 1.30 \pm 0.54$ (see sec. 1.4.4).

Furthermore, experimental results on $\pi\pi$ and πK scattering indicate a good convergence for $N_f = 2$ chiral expansions for pion observables, but difficulties appear for $N_f = 3$, even when next-to-next-to-leading order terms are taken into account [51, 52, 53, 54, 55, 56, 62, 63]. We can interpret these results by the fact that the $SU(3)$ chiral series do not converge quickly, in the sense that their leading order terms in the chiral counting are no longer numerically dominant and compete with higher order ones, at least with the next-to-leading order. Therefore, one ends up with a weak convergence situation where the leading and next-to-leading order numerically compete, instead of the usually expected situation where the leading order is dominant. All their observations are in favor of a significant paramagnetic suppression when one moves from the $N_f = 2$ to the $N_f = 3$ chiral limit. A pessimistic way of considering the problem would be to dismiss chiral perturbation theory when dealing with issues of "bad" convergence. A less restrictive point of view, adopted in [79], has been proposed to allow for a numerical competition between leading and next-to-leading order in $N_f = 3$ chiral expansions. This will be the topic of the next chapter.

2.8 Summary

In this chapter, we first presented a general overview of Lattice QCD and Effective Field Theories, two alternative methods that can be used to probe QCD at low energies. Lattice QCD consists in discretizing the $3 + 1$-dimensional Minkowskian space-time into a 4-dimensional pseudo-euclidean space and performing numerical computations of hadronic observables using Monte-Carlo techniques. This process allows in particular to study the dependence of these various observables on the quark masses. The extraction of physical observables from these simulations go through several steps (and in particular extrapolation) that are sources of systematic uncertainties. On the other side, Effective Field Theories consist in analytical methods where the degrees of freedom describing the physics at high energies are replaced by *effective* degrees of freedom that are adapted to the low-energy scales under consideration.

For QCD at low energies, such an effective theory consists in "integrating" out the quarks and gluons degrees of freedom to "replace" them by fields that are identified to the eight

pseudo-scalar mesons of the QCD spectrum at low energy, below the scale of chiral symmetry breaking. This is Chiral Perturbation Theory, which is build from the spontaneous breaking of chiral symmetry, with degrees of freedom corresponding to the pions, kaons and η. As an Effective Field Theory, χPT contains a certain number of unknown parameters, that must be evaluated using data from experiment or lattice simulations. A small review of those evaluations was made in the last section of the chapter, indicating that the saturation is settled for $N_f = 2$ chiral symmetry breaking, but remains unclear for $N_f = 3$.

In particular, we have mentioned that some lattice collaborations [96, 99, 100, 101, 102, 103] performing simulations with 2+1 dynamical quarks found difficulties in fitting their data with some of chiral expansions calculated in three-flavours χPT. This could be a hint that for three flavours, chiral series in fact suffer some problems of convergence, since the leading order would be numerically competing with the next-to-leading order − this prompted the creation of a new framework, called Resummed χPT, in order to deal with such a numerical competition. The next chapter is devoted to introduce ReχPT in details.

Chapter 3

Resummed Chiral Perturbation Theory

3.1 Introduction

As we presented in sec. 1.4.4 and sec. 2.7.1, there might be some significant differences between the patterns of $N_f = 3$ and $N_f = 2$ chiral symmetry breaking - in particular, one would witness the suppression of the LO order parameters $\Sigma(3)$ and $F(3)$, along with large values of the low-energy constants L_4 and L_6. In sec. 2.7.3, we also mentioned that some $N_f = 3$ chiral expansions could then be subjected to numerical instabilities: their leading order in the chiral counting may not be numerically dominant, and may compete (at least) with the next-to-leading order. The usual assumption that the leading order is substantially larger than next-to-leading order should then be dropped, and it is the sum $LO + NLO$ that is to be compared to the higher orders (HO). It would then be important to take into account the possibility of this numerical competition in the analysis of experiment and lattice data, before abandoning the idea of building an effective theory around the three-flavour chiral limit. To cope with this issue, a framework called Resummed Chiral Perturbation Theory was proposed in [79]. It corresponds to a re-shuffling of the chiral series that starts from specific assumptions concerning the convergence.

In section 3.2 we will discuss in detail the problem of numerical competition between leading and next-to-leading order in the chiral series. In section 3.3, we will make an overall presentation of Resummed Chiral Perturbation Theory. Finally, we shall apply this framework to several low-energy observables: pseudo-scalar meson decay constants and masses (section 3.4), pion and kaon electromagnetic form factors (section 3.5), and $K_{\ell 3}$ form factors (section 3.6). The very last section consists in a discussion of the different treatment that can be applied to unitarity contributions in this framework.

3.2 The problem of weak convergence

When we drop the usual hypothesis stating that leading order saturates the series, we have to be very careful on how to handle its expansion. Let us consider any observable A computable in χPT. It has the most general expression:

$$A = A_{LO} + A_{NLO} + A\delta A \tag{3.1}$$

A_{LO} corresponds to the leading order of the correlator's expansion, A_{NLO} gathers all the next-to-leading order terms, and $A\delta A$ collects all the higher orders starting from next-to-next-to-leading order. δA is a notation for the relative remainder of the series, expected

to be small for the chiral series to make sense. We define good global convergence as the condition that δA is much smaller than one. But this condition does not tell anything about the relative size of A_{LO} compared to the rest of the series. Without further information, we consider an unspecific situation for which only higher orders are small, i.e. $A_{LO} + A_{NLO}$ being much larger than $A\delta A$, then we ask the question: what is the convergence for another observable $F = f(A)$?

We can always write the formal expansion:

$$F = F_{LO} + F_{NLO} + F\delta F \tag{3.2}$$

By expanding $F(A)$ with respect to the expansion of A, we get :

$$F_{LO} = f(A_{LO}), \qquad F_{NLO} = A_{NLO} f'(A_{LO}) \tag{3.3}$$

$$\delta F = 1 - \frac{f(A_{LO})}{f(A)} - \frac{f'(A_{LO})}{f(A)}[A - A_{LO} - A\delta A] \tag{3.4}$$

We define $X_A = A_{LO}/A$, the saturation of the chiral expansion of A by its leading order. The two limits $X_A \to 0$ and $X_A \to 1$ are of particular importance, since we expect δF to behave differentely with respect to those limits:

$$X_A = \frac{A_{LO}}{A} \to 1, \quad \delta F \to -\frac{f'(A)}{f(A)} A\delta A \tag{3.5}$$

$$X_A = \frac{A_{LO}}{A} \to 0, \quad \delta F \to 1 - \frac{f(0)}{f(A)} - \frac{f'(0)}{f(A)} A + \frac{f'(0)}{f(A)} A\delta A \tag{3.6}$$

So we see that according to whether the leading order does saturate or not the expansion, δF is not necessarily small. In the case of saturation (3.5), the size of δA controls that of δF. But, if there is no saturation (eq. (3.6)) then its numerical behavior is no more driven by the behavior of δA, therefore there can be no guarantee that $F(A)$ is converging well. As practical examples, we take $F(A) = 1/A$ and $G(A) = \sqrt{A}$:

$$F_{LO} = 1/A_{LO}, \qquad F_{NLO} = -A_{NLO}/A_{LO}^2 \tag{3.7}$$

$$\delta F = \frac{(1 - A_{LO}/A)^2}{(A_{LO}/A)^2} - \frac{\delta A}{(A_{LO}/A)^2} \tag{3.8}$$

$$G_{LO} = \sqrt{A_{LO}}, \qquad G_{NLO} = A_{NLO} \frac{1}{2\sqrt{A_{LO}}} \tag{3.9}$$

$$\delta G = 1 - \frac{1}{2}\sqrt{A/A_{LO}} - \frac{1}{2}\sqrt{A_{LO}/A} + \frac{1}{2}\sqrt{A\ A_{LO}}\delta A \tag{3.10}$$

We take as a numerical criterion for a good global convergence that the higher orders are to be at most of order 10%, so even in the case where δA would be 0, A_{LO}/A should be above 76% for $|\delta F| \leq 10\%$, and 41% for $|\delta G| \leq 10\%$. Thus, if the chiral expansion of some correlators is not saturated by its leading order term, we can not assume that any arbitrary function of these correlators will converge. The right set of observables having a convergent expansion must therefore be chosen carefully.

3.3 Resumming chiral series

3.3.1 Procedure

First, we recall how the chiral series are treated in the standard framework of χPT:

- We first compute the bare expansion of the correlators, in powers of momenta and quark masses. "Bare expansion" means that the series is expressed in terms of the parameters of the chiral lagrangian, i.e. F_0, B_0, L_i, $m_{u,d,s}$... No supposition is made at that point about the convergence properties of the expansion.

- The "bare" leading order parameters F_0, B_0 and the quark masses are eliminated order by order in favour of the physical pseudo-Goldstone observables like $M_{\pi,K,\eta}$ and $F_{\pi,K,\eta}$. This means that their chiral expansions [2] are inverted to re-express F_0, B_0... in terms of physical quantities:

$$2mB_0 = M_\pi^2\Big[1 + \frac{1}{32\pi^2F_0^2}\Big(- M_\pi^2 \log\frac{M_\pi^2}{\mu^2} + \frac{1}{3}M_\eta^2 \log\frac{M_\eta^2}{\mu^2}\Big) - \frac{B_0}{F_0^2}\Big(16m(2L_8 - L_5) + 16(2m + m_s)(2L_6 - L_4)\Big) + \ ...\Big] \tag{3.11}$$

$$F_0^2 = F_\pi^2\Big[1 + \frac{1}{32\pi^2F_0^2}\Big(2M_\pi^2 \log\frac{M_\pi^2}{\mu^2} + M_K^2 \log\frac{M_K^2}{\mu^2}\Big) - \frac{B_0}{F_0^2}\Big(8mL_5 + 8(2m + m_s)L_4\Big) + \ ...\Big] \tag{3.12}$$

- No remainders are taken into account: at a given order, we assume that the observables are fully described by their chiral expansions neglecting the contributions from higher orders. At the end of the computation, an additional uncertainty can be added to results to take into account these HO remainders.

All of the observables different from masses and decay constants are re-expressed as expansions in powers of M_P^2 and $\log(M_P^2)$. It is at the level of the second step that large vacuum fluctuations of $\bar{s}s$ pairs, i.e. large values of L_4 and L_6, would hinder the perturbative re-expression of leading order quantities like the above examples, $2mB_0$ and F_0^2. The Resummed framework, devised to circumvent this obstacle, consists of the following alternative steps in the treatment of chiral expansions:

- Assume a subset of observables, whose correlators possess "good" global convergence, i.e. the sum $LO + NLO$ numerically dominates the higher orders. We take the QCD correlators built from scalar/pseudoscalar densities and vector/axial currents which generate the standard low-energy observables like decay constants, pseudo-Goldstone boson masses and form factors, as they form a linear space.

- Exactly as in standard χPT, take their chiral expansion in terms of the parameters of the effective lagrangian.

- Express chiral order parameters in terms of physical masses *only* to restore the non-analytical structures of the correlators: poles at the physical masses M_P^2, cuts at the thresholds of channel openings... This is necessary to ensure that unitarity is fully satisfied and that higher-order contributions are small.

- Keep track of the higher orders contributions by defining them as the remainders of the expansion. They are assumed to be small for the global convergence hypothesis (first step) to hold.
- The resulting expressions are exploited algebraically, without further expansions (in order to avoid the pitfall explained in section 3.2)

During this procedure the leading-order chiral order parameters F_0 and $\Sigma(3)$ are expressed in terms of the following parameters:

$$X(3) = \frac{2m\Sigma(3)}{F_\pi^2 M_\pi^2}, \qquad Z(3) = \frac{F_0^2}{F_\pi^2} \tag{3.13}$$

$X(3)$ and $Z(3)$ are of particular interest since they assess the saturation of the chiral series of $F_\pi^2 M_\pi^2$ and F_π^2, two basic low-energy quantities that are expected to converge well. We will also use r, the quark mass ratio, which measures the relative size of the quark masses, and also use the following quantity $Y(3)$:

$$r = \frac{m_s}{m}, \quad Y(3) = \frac{X(3)}{Z(3)} = \frac{2mB_0}{M_\pi^2} \tag{3.14}$$

which assesses the saturation of the chiral expansion of the pion mass by its leading order, eq. (2.51). For instance, the leading order masses $\overset{\circ}{M}{}_P^2$ in the isospin limit (2.56) are written in the Resummed framework, in terms of $Y(3)$ and r:

$$\overset{\circ}{M}{}_\pi^2 = M_\pi^2 Y(3), \quad \overset{\circ}{M}{}_K^2 = M_\pi^2 \frac{r+1}{2} Y(3), \quad \overset{\circ}{M}{}_\eta^2 = M_\pi^2 \frac{1}{3}(2r+1) Y(3) \tag{3.15}$$

The important point of the Resummed χPT is *not to trade* leading-order terms for physical ones (for example $2mB_0$ is not traded for M_π^2), as is usually done in the standard expansions. We point out that this framework is compatible with the usual treatment of chiral series in the limit where they are satured by their leading order term, but it allows for a consistent treatment of the series even if there is a significant competition of leading and next-to-leading orders contributions for some of the observables.

Under the hypothesis that some quantities describing the dynamics of pseudoscalar mesons are well measured, and possess good convergence properties, we can invert the relationships between these observables and the $O(p^4)$ LEC's to express the latter in terms of:

- physical observables like masses, decay constants, form factors...
- the leading order parameters $X(3)$ and $Z(3)$, and the quark mass ratio r, defined in eq. (3.14).
- the higher-order remainders associated to each observable, assumed to be small (for global convergence)

The resulting expressions can then be exploited in the chiral expansions of other (good) observables, in order to express them in terms of the leading order parameters, r, and remainders. This will be illustrated in the following sections with the examples of decay constants, masses and form factors. A particular attention will be drawn upon the $O(p^4)$ LEC's L_4 and L_6, since they account for the effect of $\bar{s}s$ sea pairs on the chiral structure of the QCD vacuum, as mentioned in sec. 2.7.3.

3.3.2 Issue of unitarity

In the set of observables that we will investigate, some, like form factors, display a dependence on variables involving external momenta. As introduced in sec. 2.5.4, at next-to-leading order in the chiral expansion the non-analytic dependence on quark masses and momenta arises through the unitary function $\bar{J}_{PQ}$, i.e. one-loop scalar bubble with a cut. Following our prescription of sec. 3.3, we compute the functions $\bar{J}$ and $\bar{\bar{J}}$ (see Appendix A.1) with the physical values of the masses $M^2_{\pi,K,\eta}$ rather than their leading-order expansion $\overset{\circ}{M}{}^2_{\pi,K,\eta}$ (eq. (2.51)), i.e. in the Resummed framework they appear in the chiral expansion as (for reasons of clarity we show here the simplified case $P = Q$):

$$\bar{J}_{PP}(s) = \frac{s}{16\pi^2}\int_{4M_P^2}^{\infty} dx \frac{1}{x(x-s)}\sqrt{1-\frac{4M_P^2}{x}} = \frac{1}{16\pi^2}\left(\sigma \log\frac{\sigma-1}{\sigma+1} + 2\right) \tag{3.16}$$

$$\sigma = \sqrt{1-\frac{4M_P^2}{s}}, \quad (s \text{ is any Mandelstam variable.})$$

where the notations make clear that the masses M_P^2 are taken at their physical values. Chiral series involving the $\bar{J}$ functions therefore feature a unitarity cut from the two-particle channel, starting at $t = (M_P + M_Q)^2$. The position of the cut at leading order is given by $(\overset{\circ}{M}_P + \overset{\circ}{M}_Q)^2$. From general arguments of unitarity, we know that the higher-order corrections will shift the start of the right-hand cut from $(\overset{\circ}{M}_P + \overset{\circ}{M}_Q)^2$ to $(M_P + M_Q)^2$. However, unitarity does not provide us more information on the structure of the cut (in particular the coefficients multipliying the $\bar{J}$) due to the perturbative nature of the chiral expansion. Naturally, the same replacement is made when the $\bar{J}_{PQ}$ and $\bar{\bar{J}}_{PQ}$ occur through the one-loop integrals K_{PQ}, L_{PQ} and M^r_{PQ} introduced in sec. 2.5.4. However, we will not perform any further replacement neither in the unitary functions nor in the rest of the chiral expansions: for instance, the coefficients multiplying the $\bar{J}$ and the chiral logarithms are not modified, since we have no way of determining if the modification $\overset{\circ}{M}{}^2_P \to M^2_P$ would improve, or spoil, the convergence of the series.

This is a slightly different procedure than the previous approach taken in [83], where the modification was performed everywhere in the J, K, L and M functions and in the chiral logarithms. It turns out that the difference is usually very small: the unitarity functions yield only a small contribution below the first threshhold, and there is only a logarithmic difference of higher order in the case of the chiral logarithm. We will come back to this discussion at the end of the chapter in sec. 3.7.

3.4 Masses and decay constants

The first observables we investigate in the case of Resummed χPT are the pseudoscalar decay constants and masses. Pions and Kaons will be used to introduce in details the resummed procedure outlined in the previous section 3.3. The case of the η, involving the GMO relation and the specific low energy constant L_7, will be discussed in a separate section 3.4.4.

3.4.1 Pions and Kaons

Masses and decay constants for pions and kaons are experimentally well-known quantities. The masses are experimentally very well measured, and their decay constants F_π and F_K are accessible at high precision through leptonic decays (respectively π_{l2} and K_{l2} [68]). In the framework of the Standard Model, it provides [66, 67]:

$$|\frac{V_{us}}{V_{ud}}| \times \frac{F_K}{F_\pi} = 0.2758 \pm 0.0005 \tag{3.17}$$

The very accurate determination of V_{ud} from super-allowed $0^+ \to 0^+$ nuclear beta decays:

$$|V_{ud}| = 0.97425 \pm 0.0002 \tag{3.18}$$

can be used to extract value for F_π (see for example [65]):

$$F_\pi|_{SM} = 92.2 \pm 0.3 \text{ MeV} \tag{3.19}$$

From the unitarity of the CKM matrix and the smallness of $|V_{ub}|$ so that $V_{us} \simeq \sqrt{1-|V_{ud}|^2}$, we get the following numerical estimate for the ratio F_K/F_π:

$$F_K/F_\pi|_{SM} = 1.192 \pm 0.006 \tag{3.20}$$

We derive the expressions for decay constants F_P^2 and masses $F_P^2 M_P^2$ from the axial/axial correlators $\langle A_\mu A_\nu \rangle$ and the derivative $\langle \partial_\mu A^\mu \partial_\nu A^\nu \rangle$ up to next-to-leading order. We begin with the two-point axial correlator, expecting to have the necessary good convergence properties:

$$\begin{aligned} \Pi^{ab}_{AA,\mu\nu}(p^2) &= i \int d^4x e^{ipx} \langle \Omega | T\{A^a_\mu(x) A^b_\nu(0)\} | \Omega \rangle \\ &= \delta^{ab} \left[\frac{p^\mu p^\nu F_P^2}{M_P^2 - p^2} + g_{\mu\nu} F_P^2 + (p^\mu p^\nu - g_{\mu\nu}) \Pi^T_{AA}(p^2) + p^\mu p^\nu \Pi^L_{AA}(p^2) \right] \end{aligned} \tag{3.21}$$

where a, b are flavour indices corresponding to any meson P and $\Pi^T_{AA}(p^2)$ and $\Pi^L_{AA}(p^2)$ are the transverse and longitudinal parts respectively. The observables corresponding to decay constants and masses can be obtained from $\Pi^{ab}_{AA,\mu\nu}(p^2)$:

$$F_P^2 \delta^{ab} = \frac{1}{4} \Pi^{ab}_{AA,\mu\mu}(0) \tag{3.22}$$

$$F_P^2 M_P^2 \delta^{ab} = \lim_{p^2 \to M_P^2} (M_P^2 - p^2) \Pi^{ab}_{AA,\mu\mu}(p^2) \tag{3.23}$$

Computing the correlator in χPT, and expressing them in terms of $X(3)$, $Z(3)$, r, the next-to-leading order low-energy constants $L^r_{4,5,6,8}$ and remainders, we get for the pion and the kaon:

$$F_\pi^2 = F_\pi^2 Z(3) + M_\pi^2 Y(3)[8(r+2)L_4^r + 8L_5^r] \tag{3.24}$$
$$- \frac{1}{32\pi^2} M_\pi^2 Y(3)\Big[4\log\frac{\overset{\circ}{M}{}_\pi^2}{\mu^2} + (r+1)\log\frac{\overset{\circ}{M}{}_K^2}{\mu^2}\Big] + F_\pi^2 e_\pi$$

$$F_K^2 = F_\pi^2 Z(3) + M_\pi^2 Y(3)[8(r+2)L_4^r + 4(r+1)L_5^r] \tag{3.25}$$
$$- \frac{1}{32\pi^2} M_\pi^2 Y(3)\Big[\frac{3}{2}\log\frac{\overset{\circ}{M}{}_\pi^2}{\mu^2} + \frac{3}{2}(r+1)\log\frac{\overset{\circ}{M}{}_K^2}{\mu^2} + \frac{1}{2}(2r+1)\log\frac{\overset{\circ}{M}{}_\eta^2}{\mu^2}\Big] + F_K^2 e_K$$

$$F_\pi^2 M_\pi^2 = F_\pi^2 M_\pi^2 X(3) + M_\pi^4 Y(3)^2[16(r+2)L_6^r + 16L_8^r] \tag{3.26}$$
$$- \frac{1}{32\pi^2} M_\pi^4 Y(3)^2\Big[3\log\frac{\overset{\circ}{M}{}_\pi^2}{\mu^2} + (r+1)\log\frac{\overset{\circ}{M}{}_K^2}{\mu^2} + \frac{1}{9}(2r+1)\log\frac{\overset{\circ}{M}{}_\eta^2}{\mu^2}\Big] + F_\pi^2 M_\pi^2 d_\pi$$

$$F_K^2 M_K^2 = \frac{1}{2}(r+1)\Big[F_\pi^2 M_\pi^2 X(3) + M_\pi^4 Y(3)^2[16(r+2)L_6^r + 8(r+1)L_8^r] \tag{3.27}$$
$$- \frac{1}{32\pi^2} M_\pi^4 Y(3)^2\Big(\frac{3}{2}\log\frac{\overset{\circ}{M}{}_\pi^2}{\mu^2} + \frac{3}{2}(r+1)\log\frac{\overset{\circ}{M}{}_K^2}{\mu^2}\frac{5}{18}(2r+1)\log\frac{\overset{\circ}{M}{}_\eta^2}{\mu^2}\Big)\Big] + F_K^2 M_K^2 d_K$$

$e_\pi,\ e_K,\ d_\pi,\ d_K$ are the relative highers order remainders. The leading order masses $\overset{\circ}{M}{}_P^2$ are given by eq. (3.15).

One can express eqs. (3.24)-(3.27) in terms of scale-independent combinations of next-to-leading order low-energy constants and chiral logarithms $\Delta L_i = L_i^r(\mu) - \hat{L}_i(\mu)$:

$$F_\pi^2 = F_\pi^2 Z(3) + 8M_\pi^2 Y(3)[(r+2)\Delta L_4 + \Delta L_5] + F_\pi^2 e_\pi \tag{3.28}$$

$$F_K^2 = F_\pi^2 Z(3) + 8M_\pi^2 Y(3)[(r+2)\Delta L_4 + \frac{1}{2}(r+1)\Delta L_5] + F_K^2 e_K \tag{3.29}$$

$$F_\pi^2 M_\pi^2 = F_\pi^2 M_\pi^2 X(3) + 16M_\pi^4 Y(3)^2[(r+2)\Delta L_6 + \Delta L_8] + F_\pi^2 M_\pi^2 d_\pi \tag{3.30}$$

$$F_K^2 M_K^2 = \frac{1}{2}(r+1)\Big[F_\pi^2 M_\pi^2 X(3) + 16M_\pi^4 Y(3)^2\big((r+2)\Delta L_6 + \frac{1}{2}(r+1)\Delta L_8\big)\Big] + F_K^2 M_K^2 d_K \tag{3.31}$$

By inverting the system of equations (3.28)-(3.31), we can re-express the ΔL_i in terms of $X(3)$, $Z(3)$, r, pion and kaon masses, decay constants and remainders:

$$\Delta L_4 = \frac{1}{8Y(3)(r+2)}\frac{F_\pi^2}{M_\pi^2}[1 - \eta(r) - Z(3) - e] \tag{3.32}$$

$$\Delta L_5 = \frac{1}{8Y(3)}\frac{F_\pi^2}{M_\pi^2}[\eta(r) + e'] \tag{3.33}$$

$$\Delta L_6 = \frac{1}{16Y(3)^2(r+2)}\frac{F_\pi^2}{M_\pi^2}[1 - \epsilon(r) - X(3) - d] \tag{3.34}$$

$$\Delta L_8 = \frac{1}{16Y(3)^2}\frac{F_\pi^2}{M_\pi^2}[\epsilon(r) + d'] \tag{3.35}$$

with the terms $\hat{L}_i$ gathering the chiral logarithms:

$$32\pi^2\hat{L}_4 = \frac{1}{8}\left[\log\frac{\overset{\circ}{M}{}_K^2}{\mu^2} - \frac{1}{(r-1)(r+2)}\left((4r+1)\log\frac{\overset{\circ}{M}{}_K^2}{\overset{\circ}{M}{}_\pi^2} + (2r+1)\log\frac{\overset{\circ}{M}{}_\eta^2}{\overset{\circ}{M}{}_K^2}\right)\right] \tag{3.36}$$

$$32\pi^2\hat{L}_5 = \frac{1}{8}\left[\log\frac{\overset{\circ}{M}{}_K^2}{\mu^2} + 2\log\frac{\overset{\circ}{M}{}_\eta^2}{\mu^2} - \frac{1}{(r-1)}\left(5\log\frac{\overset{\circ}{M}{}_K^2}{\overset{\circ}{M}{}_\pi^2} + 3\log\frac{\overset{\circ}{M}{}_\eta^2}{\overset{\circ}{M}{}_K^2}\right)\right] \tag{3.37}$$

$$32\pi^2\hat{L}_6 = \frac{1}{16}\left[\log\frac{\overset{\circ}{M}{}_K^2}{\mu^2} + \frac{2}{9}\log\frac{\overset{\circ}{M}{}_\eta^2}{\mu^2} - \frac{r}{(r-1)(r+2)}\left(3\log\frac{\overset{\circ}{M}{}_K^2}{\overset{\circ}{M}{}_\pi^2} + \log\frac{\overset{\circ}{M}{}_\eta^2}{\overset{\circ}{M}{}_K^2}\right)\right] \tag{3.38}$$

$$32\pi^2\hat{L}_8 = \frac{1}{16}\left[\log\frac{\overset{\circ}{M}{}_K^2}{\mu^2} + \frac{2}{3}\log\frac{\overset{\circ}{M}{}_\eta^2}{\mu^2} + \frac{1}{r-1}\left(3\log\frac{\overset{\circ}{M}{}_K^2}{\overset{\circ}{M}{}_\pi^2} + \log\frac{\overset{\circ}{M}{}_\eta^2}{\overset{\circ}{M}{}_K^2}\right)\right] \tag{3.39}$$

where we have defined the following quantities:

$$\epsilon(r) = 2\frac{r_2 - r}{r^2-1}, \qquad \eta(r) = \frac{2}{r-1}\left(\frac{F_K^2}{F_\pi^2} - 1\right), \qquad r_2 = 2\frac{F_K^2 M_K^2}{F_\pi^2 M_\pi^2} - 1 \sim 36 \tag{3.40}$$

The definition of the various ΔL_i combines the renormalized and quark mass-independent constants $L_{4,5,6,8}$ and the chiral logarithms $\frac{1}{32\pi^2}\log\frac{\overset{\circ}{M}{}_P^2}{\mu^2}$, so as to display explicitly the independence of the renormalization scale μ of (3.24)-(3.27). We stress that the equalities (3.28) to (3.31) are exact: they are simply a re-expression of the bare chiral series of F_π^2, F_K^2, $F_\pi^2 M_\pi^2$, $F_K^2 M_K^2$. The quantities e, $e^{'}$, d, $d^{'}$ appearing in (3.32)-(3.35) are linear combinations of the higher-order remainders e_P and d_P:

$$d = \frac{r+1}{r-1}d_\pi - \left(\epsilon(r) + \frac{2}{r-1}\right)d_K, \qquad d^{'} = d - d_\pi \tag{3.41}$$

$$e = \frac{r+1}{r-1}e_\pi - \left(\eta(r) + \frac{2}{r-1}\right)e_K, \qquad e^{'} = e - e_\pi \tag{3.42}$$

3.4.2 Handling Higher-Order remainders

In the generic chiral expansion of an observable $A = A_{LO} + A_{NLO} + A\delta A$, $A\delta A$ stands for all the higher order contributions starting with next-to-next-to-leading order (NNLO). Nonetheless, we can try to make some reasonable assumptions on the size of the higher order remainders using simple models.

We begin by re-stating that the higher order remainders are expected to be sufficiently small (δA much smaller than one) to ensure that the series are well-converging for the number of observables considered. In the most general manner, we suppose that δA is of order $O(m_q^2)$ (q either u/d or s), with the rule that, in principle, next-to-next-to-leading order corrections dominate the higher orders. As order of magnitude for the different quark masses, we take $O(m_{u,d}) \sim 10\%$ and $O(m_s) \sim 30\%$. This stems respectively from the overall size of violation for $SU(2)$ and $SU(3)$ breaking effects. In $N_f = 3$ χPT, we consider that the dominant contribution is given by the strange quark mass, so δA is either $O(m_s^2)$ or $O(m_s m)$. Thus, the size of the higher order remainders should not exceed $(30\%)^2 \simeq 10\%$ for $O(m_s^2)$, while for $O(m_s m)$ it would not be above $30\% \times 10\% \simeq 3\%$.

Another way of adressing this issue is to use resonance saturation [41], involving an hadronic scale Λ_H only mildly affected by the actual value of the quark masses (mass of the ρ, K^*...). In order to keep track of the scaling of the remainders containing quark masses, we use next-to-next-to-leading order estimate which involve the hadronic scale Λ_H at fourth power. It suggests that each order in the chiral series should be suppressed by M_P^2/Λ_H^2, where P is any light meson, and Λ_H is taken as the mass of the lighest resonance state (for instance, it would correspond to the ρ mass).

The identities 3.41 concerning remainders are algebraically exact, but meaningful as long as the higher-order remainders defined above are small. We can apply the criterion given in sec. 3.4.2 to get an estimate:

$$d, e = O(m_s^2) \sim 10\%, \qquad d^{'}, e^{'} = O(mm_s) \sim 3\% \tag{3.43}$$

Following the dimensional arguments stemming from resonance saturation as discussed in sec. 3.4.2, we take the following estimates (e_π^V is to be defined in eq. 3.71):

$$d, e, d_K, e_K, d_+ = O\left(\frac{M_K^4}{\Lambda_H^4}\right), \quad e_+ = O\left(\frac{F_\pi^2 M_K^2}{\Lambda_H^4}\right), \quad e_\pi^V = O\left(\frac{6}{\langle r^2\rangle_V^\pi}\frac{M_K^2}{\Lambda_H^4}\right) \tag{3.44}$$

$$d', e', d_- = O\left(\frac{2M_\pi^2 M_K^2}{\Lambda_H^4}\right), \quad e_- = O\left(\frac{2F_\pi^2 M_\pi^2}{\Lambda_H^4}\right) \tag{3.45}$$

where M_π^2 and M_K^2 follow the known dependence of the remainders on m and m_s, whereas F_π^2 is inserted when a dimensionful constant with no dependence on m_q is required.

Therefore, they are constrained in the following range:

Remainder	size
d, e, d_+	0.148
d', e', d_-	0.024
e_+	0.005
e_-	0.001
e_π^V	0.318

Table 3.1: Allowed size of the higher-orders remainders, based on a dimensional estimate. The remainder e_π^V stands for the remainder the pion electromagnetic square radius introduced in sec. 3.5.2.

3.4.3 Resumming vacuum fluctuations

We combine equations (3.32) and (3.34) in order to obtain two relations between the leading order quantities $X(3)$, $Z(3)$ and $Y(3)$:

$$\begin{aligned} X(3) &= 1 - \epsilon(r) - Y(3)^2\frac{\rho}{4} - d \\ Z(3) &= 1 - \eta(r) - Y(3)\frac{\lambda}{4} - e \end{aligned} \tag{3.46}$$

where we have introduced the two parameters ρ and λ containing the dependence on L_4 and L_6:

$$\rho = 64\frac{M_\pi^2}{F_\pi^2}(r+2)\Delta L_6, \quad \lambda = 32\frac{M_\pi^2}{F_\pi^2}(r+2)\Delta L_4 \tag{3.47}$$

We proceed in a similar way for the quantities $\epsilon(r)$ and $\eta(r)$, defined in (3.40):

$$\begin{aligned}\epsilon(r) &= 16\frac{M_\pi^2}{F_\pi^2}Y(3)^2\Delta L_8 - d^{'} \\ \eta(r) &= 8\frac{M_\pi^2}{F_\pi^2}Y(3)\Delta L_5 - e^{'}\end{aligned} \tag{3.48}$$

We can now use the relations (3.46) and (3.48) to illustrate how the instabilities manifest themselves in the perturbative development of X and Z in powers of the meson masses M_P^2, eqs. (3.11) and (3.12). Using the usual "standard" treatment of chiral series, we set $Y(3) = 1 + O(M_P^2)$ and neglect all the higher orders, so $Y(3)$ can be replaced by 1 in expressions (3.46) and (3.48). From the previous relations (3.48) we express the ratios F_K^2/F_π^2 and $r = m_s/m$ in terms of ΔL_5 and ΔL_8, always neglecting the higher orders.

Then inverting eqs. (3.40) we obtain the next-to-leading order expressions:

$$\begin{aligned}\frac{F_K^2}{F_\pi^2} &= 1 + 8\frac{M_K^2 - M_\pi^2}{F_\pi^2}\Delta L_5 + ... \\ r + 1 &= 2\frac{M_K^2}{M_\pi^2}\Big(1 + 8\frac{M_K^2 - M_\pi^2}{F_\pi^2}(\Delta L_5 - 2\Delta L_8) + ...\Big)\end{aligned} \tag{3.49}$$

We observe that expressions (3.49) do not contain any direct dependence on L_4 and L_6 that keep track of the Zweig rule violation (sec. 2.7.1) by the vacuum fluctuations of the $\bar{s}s$ sea quark pairs. However, they do appear in the series for $X(3)$ and $Z(3)$. Inserting r from (3.49) in eqs. (3.46) we get:

$$\begin{aligned}X(3) &= 1 - 16\frac{M_\pi^2}{F_\pi^2}\Delta L_8 - 16\frac{2M_K^2 + M_\pi^2}{F_\pi^2}\Delta L_6 + ... \\ Z(3) &= 1 - 8\frac{M_\pi^2}{F_\pi^2}\Delta L_5 - \frac{2M_K^2 + M_\pi^2}{F_\pi^2}\Delta L_4 + ...\end{aligned} \tag{3.50}$$

The perturbative re-expression of $1/(F_\pi^2 M_\pi^2)$ and $1/F_\pi^2$ in the definition of $X(3)$ and $Z(3)$ leads therefore to large numerical coefficients for ΔL_4 and ΔL_6 in eq.(3.50):

$$X(3) = 1 - 37\Delta L_8 - 950\Delta L_6 + ..., \quad Z(3) = 1 - 18\Delta L_5 - 475\Delta L_4 + ... \tag{3.51}$$

In eqs. (3.50), we observe that the main next-to-leading order contribution comes from an M_K^2-enhanced term proportional to the low-energy constants L_4 and L_6 encoding Zweig rule violation in the scalar sector. If those low-energy constants are close to critical values defined as $L_{i,crit}^r = \hat{L}_i$, i.e. $\Delta L_i = 0$, leading to $\Delta L_{4,6} \sim 0$ and $L_4^r(M_\rho) \simeq -0.50 \times 10^{-3}$, $L_6^r(M_\rho) \simeq -0.25 \times 10^{-3}$ for $r = 25$ and $Y(3) = 1$, we see that their contribution remains small.

However, if the Zweig rule is not verified, i.e. if the contributions from L_4 and L_6 are large, the perturbative treatment is hindered by the vacuum fluctuations of the sea-pairs. The expressions (3.46) should not be linearized: (3.46) must be treated without any kind of approximation. As explained in [77], the non-linear system (3.46) can be inverted to obtain an expression for $Y(3) = X(3)/Z(3)$. In fact, since it reduces to a second order polynomial in $Y(3)$, it yields two solutions:

$$Y(3)_{\pm} = \frac{2(1-\epsilon(r)-d)}{1-\eta(r)-e \pm \sqrt{(1-\eta(r)-e)^2 + [\rho-\lambda](1-\epsilon(r)-d)}} \tag{3.52}$$

The square root in the denominator of (3.52) accounts for the non-linearity of (3.46). The factor $\rho - \lambda$, or, in terms of the NLO low-energy constants, $2L_6 - L_4$ (from 3.47), regulates the behaviour of $Y(3)$. Moreover, the first solution $Y(3)_+$ corresponds to $0 < Y(3)_+ < 2$ and the second one to $Y(3)_- \geq 2$ (the properties of those solutions are discussed in ref. [77]). For the remainder of the discussion, we will center on the physical case $0 < Y(3)_+ < 2$: the perturbative treatment leading to expressions (3.49) and (3.50) corresponds in fact to the linearization of (3.52) in the case $\rho - \lambda \ll 1$:

$$Y(3) \simeq \frac{1-\epsilon(r)-d}{1-\eta(r)-e}\left(1 - \frac{\rho-\lambda}{4}\frac{1-\epsilon(r)-d}{(1-\eta(r)-e)^2} + \frac{(\rho-\lambda)^2}{16}\frac{(1-\epsilon(r)-d)^2}{(1-\eta(r)-e)^4} + ...\right), \tag{3.53}$$

(for the solution $Y(3)_+$)

Therefore, we observe that the (non-perturbative) solution (3.52) resums a series of terms corresponding to the fluctuation parameters ρ and λ. We see that if those fluctuations are large, i.e. if ρ and λ are of order 1 then the linearization (3.53) can not be justified (the series does not converge). Expression (3.52) would thus lead to a suppression of $Y(3)$, which in turn would reduce the contribution of ρ and λ in eqs. (3.46). Indeed this can be seen in figure 3.1, where the value $Y(3) = 1$ corresponds to the line $\rho = \lambda$, or from eq. (3.47), $2\Delta L_6 = \Delta L_4$.

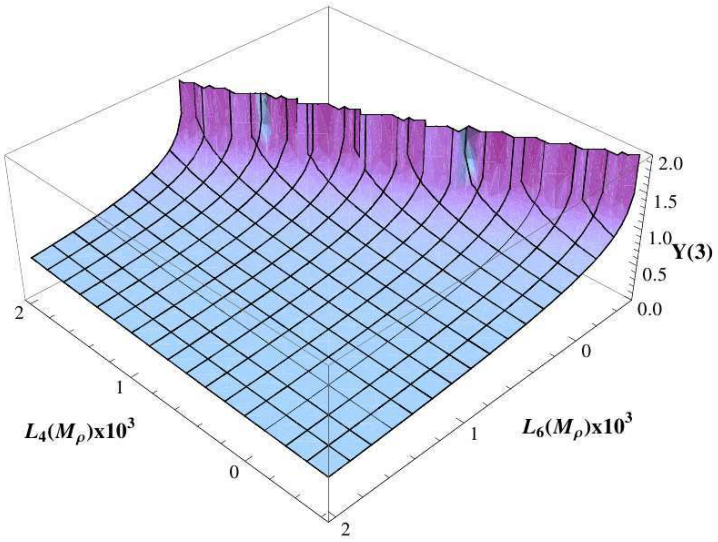

Figure 3.1: The leading order parameter $Y(3)$ as a function of L_4^r and L_6^r (eq. 3.52), with $r = 25$, and the remainders e and d set to 0. The upper frontier marks the region for which ρ and λ do not give solutions for eq. (3.52). Taken from ref. [84].

In this sense, the approach described in sec. 3.3 allows a resummation of the effects of $\bar{s}s$ pairs encoded in L_4 and L_6, assuming that they capture the main effect of vacuum fluctuations, and that the higher orders are not affected − thus the name of *Resummed* Chiral Perturbation Theory.

A similar discussion can be made for $X(3)$, ρ and L_6, and $Z(3)$, λ and L_4: in both cases, values of the Zweig rule violating low-energy constants L_6 and L_4 shifted a bit from their critical values $\hat{L}_{4,6}$ towards positive values are sufficient to provide a significant supression of

the leading order parameters $X(3)$ and $Z(3)$, in way that the LECs could not reach "large" values without suppressing them strongly, as shown in figure 3.2. We see that in the case $N_f = 3$, the LO parameters suffer a significant decrease while for $N_f = 2$ their values stay close to 1 − as can be seen by re-expressing the low energy constants L_4 and L_6 in eqs. (2.78) and 2.79:

$$Z(2) = \frac{r}{r+2}(1-\eta(r)) + \frac{2}{r+2}Z(3) - \frac{r}{r+2}Y(3)g_1 + ... \tag{3.54}$$

$$X(2) = \frac{r}{r+2}(1-\epsilon(r)) + \frac{2}{r+2}X(3) - \frac{r}{r+2}Y(3)^2 f_1 + ... \tag{3.55}$$

where g_1 and f_1 are small combinations of chiral logarithms, and the ellipsis ... denotes higher order terms [79]. This shows that $Z(2)$ and $X(2)$ are eventually independent of $Z(3)$ and $X(3)$ (i.e. L_4 and L_6) but strongly sensitive to the quark mass ratio r.

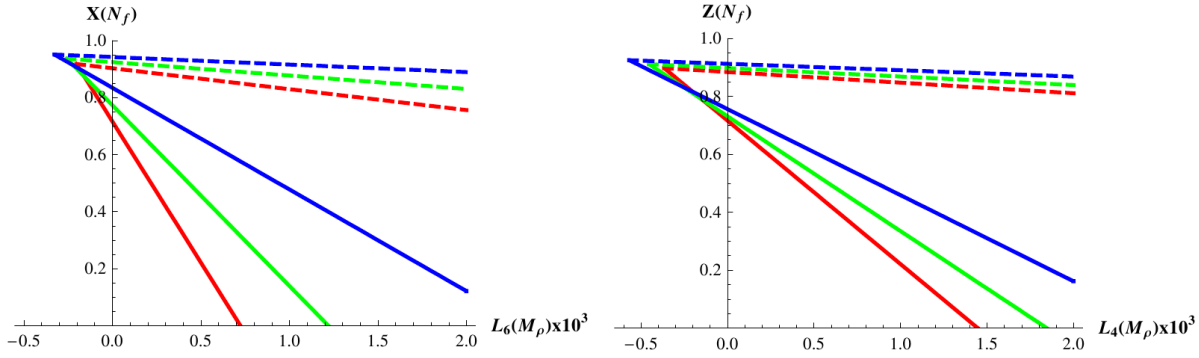

Figure 3.2: $X(N_f)$ and $Z(N_f)$ as functions of L_6^r and L_4^r respectively, evaluated for different values of $Y(3)$: blue → 0.6, green → 0.8, red → 1. The dashed lines correspond to $N_f = 2$ and the solid lines to $N_f = 3$. The value for r is 25 and the remainders have been neglected. Values of $X(2)$ and $Z(2)$ we computed from eqs. (2.78) and (2.79). Taken from ref. [84].

3.4.4 The η

The mass and decay constant of the η meson involves also the next-to-leading order low-energy constant L_7 and two extra remainders e_η and d_η:

$$\begin{aligned} F_\eta^2 &= F_\pi^2 Z(3) \\ &+ Y(3)M_\pi^2\left(8(r+2)L_4^r + \frac{8}{3}(2r+1)L_5^r\right) - \frac{1}{32\pi^2}M_\pi^2 Y(3)\log\frac{\overset{\circ}{M}_K^2}{\mu^2} + F_\eta^2 e_\eta \end{aligned} \tag{3.56}$$

$$\begin{aligned} F_\eta^2 M_\eta^2 &= \frac{2r+1}{3}F_\pi^2 M_\pi^2 X(3) \\ &+ \frac{16}{3}(2r+1)(r+2)Y(3)^2 M_\pi^4 L_6^r + \frac{32}{3}(r-1)^2 Y(3)^2 M_\pi^4 L_7 + \frac{16}{3}(2r^2+1)Y(3)^2 M_\pi^4 L_8^r \\ &- \frac{1}{32\pi^2}Y(3)^2 M_\pi^4\left[\frac{1}{3}(2r+1)\left(2(r+1)\log\frac{\overset{\circ}{M}_K^2}{\mu^2} + \frac{4}{9}(2r+1)\log\frac{\overset{\circ}{M}_\eta^2}{\mu^2}\right)\right. \\ &\left. + \left(\log\frac{\overset{\circ}{M}_\pi^2}{\mu^2} - \frac{1}{3}(r+1)\log\frac{\overset{\circ}{M}_K^2}{\mu^2} - \frac{1}{9}(2r+1)\log\frac{\overset{\circ}{M}_\eta^2}{\mu^2}\right)\right] + F_\eta^2 M_\eta^2 d_\eta \end{aligned} \tag{3.57}$$

F_η itself is not accessible experimentally, but we can compute it using its expression (3.56). We introduce the Gell-Mann Okubo (GMO) mass difference Δ_{GMO} and the remainder combination d_{GMO}:

$$\Delta_{GMO} = \frac{3F_\eta^2 M_\eta^2 - 4F_K^2 M_K^2 + F_\pi^2 M_\pi^2}{F_\pi^2 M_\pi^2}, \qquad d_{GMO} = \frac{3F_\eta^2 M_\eta^2}{F_\pi^2 M_\pi^2} d_\eta - \frac{4F_K^2 M_K^2}{F_\pi^2 M_\pi^2} d_K + d_\pi \quad (3.58)$$

By using the expressions (3.26)-(3.27) and (3.57), we can write Δ_{GMO} in terms of the low-energy constants and the remainders. We get:

$$\Delta_{GMO} = 16\frac{M_\pi^2}{F_\pi^2}(r-1)^2 Y(3)^2 (2L_7 + \Delta L_8) + d_{GMO} \quad (3.59)$$

As in the previous section, we use the above identities to re-express L_7 in terms of the parameters (3.13) and decay constants and masses:

$$L_7 = \frac{1}{32Y(3)^2(r-1)^2}\frac{F_\pi^2}{M_\pi^2}\left[\frac{3F_\eta^2 M_\eta^2 - 4F_K^2 M_K^2 + F_\pi^2 M_\pi^2}{F_\pi^2 M_\pi^2} - d_{GMO} - (r-1)^2(\epsilon(r) + d')\right] \quad (3.60)$$

In a similar manner, we have for F_η^2:

$$\frac{F_\eta^2}{F_\pi^2} = 1 + \frac{4}{3}\left(\frac{F_K^2}{F_\pi^2} - 1\right) + \frac{1}{48\pi^2}\frac{M_\pi^2}{F_\pi^2}\left[(2r+1)\log\frac{\overset{\circ}{M}{}_\eta^2}{\overset{\circ}{M}{}_K^2} + \log\frac{\overset{\circ}{M}{}_K^2}{\overset{\circ}{M}{}_\pi^2}\right] + e_{GMO} \quad (3.61)$$

with e_{GMO} a combination of remainders, similarly to d_{GMO}:

$$e_{GMO} = \frac{F_\eta^2}{F_\pi^2} e_\eta + \frac{4}{3}\frac{F_K^2}{F_\pi^2} e_K - \frac{1}{3} e_\pi \quad (3.62)$$

Multiplying (3.61) by F_π^2, and taking the expansions (3.24) and (3.25), one can easily check that expression (3.56) is properly recovered. As for π and K, all those expressions are exact as long as the remainders are taken into account. We estimate their order of magnitude: $e_\eta,\ d_\eta \sim O(m_s^2) \sim O(10\%)$ by the criterion discussed in sec. 3.4.2.

So far we have been able to write the GMO relation eq. (3.59) directly in terms of low-energy constant L_7, the parameters $Y(3)$ and r and higher order remainders. Neglecting d_{GMO} and e_{GMO} for the purpose of the discussion, one can give a numerical estimate, with $F_\eta^2/F_\pi^2 = 1.565$ (for $Y(3) = 1$, $r = 25$, from eq. (3.61)):

$$\Delta_{GMO} = 72.34 - 71.45 + 1 = 1.89 \quad (3.63)$$

where the three contributions corresponding respectively to η, K and π have been split. The numerical value for the kaon mass is the mean between the $K^{+,-}$ and $\bar{K}^0$, K^0 masses. It is customary to use the fact that the GMO relation (2.59) is well satisfied to justify that the leading order condensate term should dominate the chiral expansion of the pseudoscalar masses. From those grounds, the values of L_7 and L_8 would need no fine-tuning when one

tries to recover the above estimate with the right-hand side of (3.59). However, using (3.35) for $r = r_0 \sim 24$ (to be defined in terms of M_K and M_π), and neglecting $d^{'}$, we obtain:

$$16\frac{M_\pi^2}{F_\pi^2}(r-1)^2 Y(3)^2 \Delta L_8 = (r-1)^2(\epsilon(r)+d') = 19.3 \tag{3.64}$$

This number is one order of magnitude higher than the evaluation (3.63) of Δ_{GMO} which contains L_7 and L_8 eq. (3.59). To recover correctly (3.63) one would have to fine-tune[1] L_7 (using $Y(3) = 1$ and $r = r_0$): $L_7 \sim -0.05 \times 10^{-4}$. This means that the GMO formula is satisfied too well compared to the expectation from next-to-leading order χPT and that it is not a very compelling argument for a saturation of the chiral expansions by the quark condensate.

3.5 Electromagnetic form factors

3.5.1 Definition and discussion

We can further illustrate the resummed procedure with the example of form factors, and in particular the pion electromagnetic form factor:

$$\langle \pi^+(p^{'})|j^\mu|\pi^+(p)\rangle = (p+p^{'})^\mu F_V^\pi(t) \tag{3.65}$$

where j_μ is the electromagnetic current for the light quarks[2]: $j_\mu = \frac{2}{3}\bar{u}\gamma^\mu u - \frac{1}{3}\bar{d}\gamma^\mu d - \frac{1}{3}\bar{s}\gamma^\mu s$, where p and $p^{'}$ are the momenta of the incoming and outgoing pion, and t is the momentum transfer $t = (p^{'}-p)^2$. This form factor is obtained from the correlator $\langle (A^\mu_{\pi^+})^\dagger j_\nu A^\sigma_{\pi^+}\rangle$ ($A^\mu_{\pi^+}$ being the interpolating fields for the π^+), which leads to the product $F_\pi^2 F_V^\pi$ through the LSZ reduction formula, where the factor F_π^2 stems from the pion's wave function renormalization. This observable will permit to get an insight about another low energy constant, tied to processes involving the coupling to vector and axial sources: L_9. We get the expansion (in accordance with [43]-[45]):

$$F_\pi^2 F_V^\pi(t) = F_\pi^2 Z(3) + M_\pi^2 Y(3)[8(r+2)L_4^r + 8L_5^r] - \frac{1}{32\pi^2}M_\pi^2 Y(3)\Big[4\log\frac{\overset{\circ}{M}{}_\pi^2}{\mu^2} + (r+1)\log\frac{\overset{\circ}{M}{}_K^2}{\mu^2}\Big] \tag{3.66}$$

$$+ t\Big[2L_9^r - \frac{1}{32\pi^2}M_\pi^2 Y(3)\Big(\frac{1}{3}\log\frac{\overset{\circ}{M}{}_\pi^2}{\mu^2} + \frac{1}{6}\log\frac{\overset{\circ}{M}{}_K^2}{\mu^2} + \frac{1}{6}\Big)\Big]$$
$$+ \frac{1}{6}(t - 4M_\pi^2 Y(3))\bar{J}_{\pi\pi}(t) + \frac{1}{12}(t - 2(r+1)M_\pi^2 Y(3))\bar{J}_{KK}(t) + \mathcal{R}F_\pi^2 F_V^\pi(t)$$

The $\bar{J}_{PP}$ functions encode the non-analytic pieces from the opening of the two-meson channel (cf. secs. 2.5.4 and 3.3.2). $\mathcal{R}F_\pi^2 F_V^\pi(t)$ is a polynomial function in t collecting the higher order remainders:

$$\mathcal{R}F_\pi^2 F_V^\pi(t) = (\mathcal{R}F_\pi^2 F_V^\pi)_0 + \frac{t}{F_\pi^2}(\mathcal{R}F_\pi^2 F_V^\pi)_1 + O(t^2) \tag{3.67}$$

with the following orders of magnitude $(\mathcal{R}F_\pi^2 F_V^\pi)_0 = O(m_q^2)$ and $(\mathcal{R}F_\pi^2 F_V^\pi)_1 = O(m_q)$. In the case where the series is saturated by its leading order, it is possible to recover the standard NLO chiral expansion of the electromagnetic form factor as in [43]:

[1] We take $F_\pi = 92.2$ MeV, $M_\pi = 139$ MeV, $F_K/F_\pi = 1.192$.

[2] Concerning the pion, only the u and d currents contribute.

$$F_V^\pi(t) = 1 + 2H_{\pi\pi}(t) + H_{KK}(t) + O(p^4) \tag{3.68}$$

with the $H_{PQ}(t)$ function:

$$H_{PQ}(t) = \frac{1}{F_0^2}\Big[\frac{1}{12}\Big(t - 2\Sigma_{PQ} + \frac{\Delta_{PQ}^2}{t}\Big)\bar{J}_{PQ}(t) - \frac{\Delta_{PQ}^2}{3t}\bar{\bar{J}}_{PQ}(t) - \frac{t}{6}k_{PQ} + \frac{t}{228\pi^2}\Big] + \frac{2t}{3F_0^2} \tag{3.69}$$

using the following notations: $\Sigma_{PQ} = M_P^2 + M_Q^2$, $\Delta_{PQ} = M_P^2 - M_Q^2$ where P and Q is any light meson. (See Appendix A.1 for the expressions of k_{PQ} and $\bar{\bar{J}}$). This is achieved by expanding the product $F_\pi^2 F_V^\pi(t)$ at next-to-leading order using expression (3.24) for F_π^2, replacing the leading order masses $\overset{\circ}{M}{}_P^2$ by the physical ones M_P^2, and neglecting all the higher orders terms and remainders.

3.5.2 Pion electromagnetic square radius

The pion electromagnetic square radius $\langle r^2\rangle_V^\pi$ is one of the main low-energy observables associated to the pion electromagnetic form factor F_V^π. It is defined by the relation:

$$F_\pi^2\langle r^2\rangle_V^\pi = 6F_\pi^2\frac{d}{dt}F_V^\pi(t)_{|t=0} \tag{3.70}$$

An expression for $\langle r^2\rangle_V^\pi$ follows immediately from eq. (3.66):

$$\langle r^2\rangle_V^\pi = \frac{6}{F_\pi^2}\Big[2\Delta L_9 - \frac{1}{32\pi^2}\Big(\frac{1}{6} + \frac{2}{9}Y(3) + \frac{M_\pi^2}{18M_K^2}(r+1)Y(3)\Big)\Big] + \langle r^2\rangle_V^\pi e_V^\pi \tag{3.71}$$

where we have introduced, as in sec. (3.4.1), the scale-independent combination for the low-energy constants: $\Delta L_9 = L_9^r(\mu) - \hat{L}_9^r(\mu)$, with the following relation for the chiral logarithms:

$$\hat{L}_9^r(\mu) = \frac{1}{32\pi^2}\left[\frac{1}{6}\log\frac{\overset{\circ}{M}{}_\pi^2}{\mu^2} + \frac{1}{12}\log\frac{\overset{\circ}{M}{}_K^2}{\mu^2}\right] \tag{3.72}$$

and the relative remainder e_V^π:

$$e_V^\pi = \frac{6}{F_\pi^4}\frac{(\mathcal{R}F_\pi^2F_V^\pi)_1}{\langle r^2\rangle_V^\pi} \tag{3.73}$$

whose size, estimated through resonance saturation discussed in sec. 3.4.2, is of order $e_V^\pi = O((6M_K^2)/(\langle r^2\rangle_V^\pi\Lambda_H^4))$.

$\langle r^2\rangle_V^\pi$ is a well-determined quantity experimentally. Therefore, this is the observable we will use to re-express L_9 as a function of $Y(3)$, r, the physical quantity $\langle r^2\rangle_V^\pi$, π and K masses, and the remainders:

$$\Delta L_9 = \frac{F_\pi^2}{12}\langle r^2\rangle_V^\pi(1 - e_V^\pi) + \frac{1}{32\pi^2}\Big[\frac{1}{12} + \frac{1}{9}Y(3) + \frac{M_\pi^2}{36M_K^2}(r+1)Y(3)\Big] \tag{3.74}$$

For all the numerical calculations that will follow, we shall use the following value for $\langle r^2\rangle_V^\pi$ [68]:

$$\langle r^2\rangle_V^\pi = 0.452 \pm 0.011 \quad \text{fm}^2 \tag{3.75}$$

3.5.3 Kaon electromagnetic form factor

Now that we have been able to re-express the various low energy constants $L_{4,5,6,7,8,9}$ in terms of the parameters $X(3)$, $Z(3)$, r, the physical quantities and the higher-order remainders, we can apply the same framework to other observables, like the form factors. In this section, we therefore proceed with a similar discussion for the kaon electromagnetic form factors:

$$\langle K^{+,0}(p^{'})|j^{\mu}|K^{+,0}(p)\rangle = (p+p^{'})^{\mu}F_V^{K^{+,0}}(t) \tag{3.76}$$

We have the expansions of $F^{K^{+,0}}$, following from the correlators $\langle (A^{\mu}_{K^{+,0}})^{\dagger} j_{\nu} A^{\sigma}_{K^{+,0}}\rangle$ (with F_K^2 stemming from the kaon wave-function renormalization):

$$\begin{aligned} F_K^2 F_V^{K^+}(t) = F_\pi^2 \Bigg[& Z(3) + \frac{M_\pi^2}{F_\pi^2} Y(3)(8(r+2)L_4^r + 4(r+1)L_5^r) \\ & - \frac{1}{32\pi^2}\frac{M_\pi^2}{F_\pi^2} Y(3)\left[\frac{3}{2}\log\frac{\overset{\circ}{M}{}_\pi^2}{\mu^2} + \frac{3}{2}(r+1)\log\frac{\overset{\circ}{M}{}_K^2}{\mu^2} + \frac{1}{2}(2r+1)\log\frac{\overset{\circ}{M}{}_\eta^2}{\mu^2}\right] \\ & + \frac{t}{F_\pi^2}\left[2L_9^r - \frac{1}{32\pi^2}\left(\frac{1}{6}\log\frac{\overset{\circ}{M}{}_\pi^2}{\mu^2} + \frac{1}{3}\log\frac{\overset{\circ}{M}{}_K^2}{\mu^2} + \frac{1}{6}\right)\right] \\ & + \frac{1}{12F_\pi^2}[t - 4M_\pi^2 Y(3)]\bar{J}_{\pi\pi}(t) + \frac{1}{6F_\pi^2}[t - 2(r+1)M_\pi^2 Y(3)]\bar{J}_{KK}(t) \\ & + \frac{1}{F_\pi^2}\mathcal{R}F_K^2 F_V^{K^+}(t)\Bigg] \end{aligned} \tag{3.77}$$

$$\begin{aligned} F_K^2 F_V^{K^0}(t) = F_\pi^2 \Bigg[& - \frac{t}{192\pi^2 F_\pi^2}\log\frac{\overset{\circ}{M}{}_K^2}{\overset{\circ}{M}{}_\pi^2} - \frac{1}{12F_\pi^2}[t - 4M_\pi^2 Y(3)]\bar{J}_{\pi\pi}(t) \\ & + \frac{1}{12F_\pi^2}[t - 2(r+1)M_\pi^2 Y(3)]\bar{J}_{KK}(t) + \frac{1}{F_\pi^2}\mathcal{R}F_K^2 F_V^{K^0}(t)\Bigg] \end{aligned} \tag{3.78}$$

Exactly as in sec. 3.5.1, $\mathcal{R}F_K^2 F_V^{K^0}(t)$ and $\mathcal{R}F_K^2 F_V^{K^+}(t)$ are the polynomial functions of t collecting the remainders:

$$\mathcal{R}F_K^2 F_V^{K^+}(t) = (\Re F_K^2 F_V^{K^+})_0 + \frac{t}{F_K^2}(\mathcal{R}F_K^2 F_V^{K^+})_1 + O(t^2) \tag{3.79}$$

$$\mathcal{R}F_K^2 F_V^{K^0}(t) = \frac{t}{F_K^2}(\Re F_K^2 F_V^{K^0})_1 + O(t^2) \tag{3.80}$$

with the following orders of magnitude: $(\mathcal{R}F_V^K)_1 = O(m_q)$ and $(\mathcal{R}F_V^K)_0 = O(m_q^2)$.

Standard next-to-leading order expansions are recovered using the same procedure as before [43, 45]:

$$F_V^{K^+}(t) = F_V^{\pi}(t) + F_V^{K^0}(t) + O(p^4), \quad F_V^{K^0}(t) = -H_{\pi\pi}(t) + H_{KK}(t) + O(p^4) \tag{3.81}$$

3.5.4 Kaon electromagnetic square radius

We finally turn to the K electromagnetic radii - first, for the K^+:

$$\langle r^2\rangle_V^{K^+} = \frac{6}{F_K^2}\left[2\Delta L_9 - \frac{1}{32\pi^2}\left(\frac{1}{6}\log\frac{\overset{\circ}{M}{}_K^2}{\overset{\circ}{M}{}_\pi^2} + \frac{1}{6} + \frac{1}{9}Y(3) + \frac{M_\pi^2}{9M_K^2}(r+1)Y(3)\right)\right] + \langle r^2\rangle_V^{K^+} e_V^{K^+} \tag{3.82}$$

with the remainder:

$$e_V^{K^+} = \frac{6}{F_K^4}\frac{(\mathcal{R}F_K^2 F_{K^+}^V)_1}{\langle r^2\rangle_V^{K^+}} \tag{3.83}$$

Re-expressing L_9 in terms of the pion radius $\langle r^2\rangle_V^\pi$ using eq. (3.74), we obtain the following relation:

$$F_K^2\langle r^2\rangle_V^{K^+}(1-e_V^{K^+}) - F_\pi^2\langle r^2\rangle_V^\pi(1-e_V^\pi) = \frac{1}{32\pi^2}\left(-\log\frac{\overset{\circ}{M}{}_K^2}{\overset{\circ}{M}{}_\pi^2} + \frac{2}{3}Y(3) - \frac{M_\pi^2}{3M_K^2}(r+1)Y(3)\right) \tag{3.84}$$

The right-hand side of eq. (3.84) is very small for reasonable values of $Y(3)$ and r, so we get that the electromagnetic radius of the K^+ is essentially predicted by the pion's radius: $\langle r^2\rangle_V^{K^+} \simeq \frac{F_\pi^2}{F_K^2}\langle r^2\rangle_V^\pi \simeq 0.32$ fm^2. We have the following experimental value [68]:

$$\langle r^2\rangle_V^{K^+} = 0.314 \pm 0.035 \text{ fm}^2 \tag{3.85}$$

For the neutral kaon we have:

$$F_K^2\langle r^2\rangle_V^{K^0}(1-e_V^{K^0}) = \frac{1}{32\pi^2}\left(-\log\frac{\overset{\circ}{M}{}_K^2}{\overset{\circ}{M}{}_\pi^2} + \frac{2}{3}Y(3) - \frac{M_\pi^2}{3M_K^2}(r+1)Y(3)\right) \tag{3.86}$$

with the remainder:

$$e_V^{K^0} = \frac{6}{F_K^2}\frac{(\mathcal{R}F_{K^0}^V)_1}{\langle r^2\rangle_V^{K^0}} \tag{3.87}$$

The experimental value is [68]:

$$\langle r^2\rangle_V^{K^+} = -0.077 \pm 0.010 \text{ fm}^2 \tag{3.88}$$

From eqs. (3.84) and (3.86) one obtains the following relation between the K^+ and K^0 electromagnetic radii:

$$\langle r^2\rangle_V^\pi(1-e_V^\pi) = \frac{F_K^2}{F_\pi^2}\left(\langle r^2\rangle_V^{K^+}(1-e_V^{K^+}) - \langle r^2\rangle_V^{K^0}(1-e_V^{K^0})\right) \tag{3.89}$$

This equation is verified for the experimental values (3.75), (3.85), (3.88) and the value of F_K/F_π in the Standard Model (3.20), with the remainders being on the large side of their allowed value according to the discussion of sec. 3.4.2. In principle, one could invert the problem and use the measurements for the radii combined with knowledge about the higher-order remainders to obtain an accurate estimate of F_K/F_π.

3.6 $K\ell_3$ form factors

3.6.1 Definition and discussion

Now we apply our framework to the $K_{\ell 3}$ form factors. We begin by recalling the two decay channels giving rise to $K\pi$ form factors:

$$K^0 \to \pi^- + \ell^+ + \nu \tag{3.90}$$
$$K^+ \to \pi^0 + \ell^+ + \nu \tag{3.91}$$

with the corresponding S-matrix element:

$$S_{if} = \frac{G_F}{\sqrt{2}} V_{us} \left\langle \ell\nu\pi^{+,0}(p') \right| \bar{l}\gamma^\mu(1-\gamma^5)\nu\overline{u}\gamma_\mu s \left| \bar{K}^{0,+}(p) \right\rangle \tag{3.92}$$

where G_F is the Fermi constant and V_{us} is the relevant CKM matrix element. Since the leptonic part is independent from the hadronic part, we factorize the S-matrix element in order to isolate the latter:

$$F_\mu^{0,+} = \left\langle \pi^{+,0}(p') \right| \overline{u}\gamma_\mu s \left| \bar{K}^{0,+}(p) \right\rangle \tag{3.93}$$

Exploiting Lorentz covariance, we define the two form factors $f_+(t)$ and $f_-(t)$:

$$F_\mu^{0,+} = \mathcal{C}[(p'+p)_\mu f_+(t) + (p'-p)_\mu f_-(t)] \tag{3.94}$$

where t is the momentum transfer $t = (p^{'} - p)^2$, and $\mathcal{C}$ is a constant which is either 1 or $1/\sqrt{2}$ for F_μ^0 or F_μ^+ respectively. $f_+(t)$ is the vector form factor: it corresponds to the P-wave projection of $F_\mu^{0,+}$. We can further define a scalar form factor $f_0(t)$, associated to S-wave projection:

$$f_0(t) = f_+(t) + \frac{t}{\Delta_{K\pi}} f_-(t) \tag{3.95}$$

with the squared-mass difference $\Delta_{K\pi} = M_K^2 - M_\pi^2$.

The $f_+(t)$ vector form factor at zero momentum transfer is a quantity of interest, since the measurement of $K_{\ell 3}$ decays can be analysed in the framework of the Standard Model to determine the product $|V_{us} f_+(0)|$, and thus the CKM matrix element $|V_{us}|$. A recent fit to $|V_{ud}|$ from the super-allowed $0^+ \to 0^+$ nuclear decays, $|V_{us}| f_+(0)$ from $K_{\ell 3}$ and $|V_{us}/V_{ud}| F_K/F_\pi$ from $\pi_{\ell 2}$ and $K_{\ell 2}$ together with the unitarity of the CKM matrix led to [67, 68]:

$$f_+(0)|_{SM} = 0.959 \pm 0.005 \tag{3.96}$$

and a value of $F_K/F_\pi|_{SM}$ in full agreement with the value (3.20), with a strong correlation between these two quantities. Deviation of $f_+(0)$ from this value would be an indication of new physics, so that this quantity plays an important role to test the Standard Model in the light quark sector (see figure 3.3).

Always following the discussion in sec. (3.3), we expect that $F_\pi F_K f_+$ and $F_\pi F_K f_0$ are the quantities to exhibit good convergence properties, away from singularities (opening thresholds at $t = (M_K + M_\pi)^2$...). They stem from the axial/vector/axial correlators $\langle A^\mu V_\nu A^\sigma \rangle$ (F_π

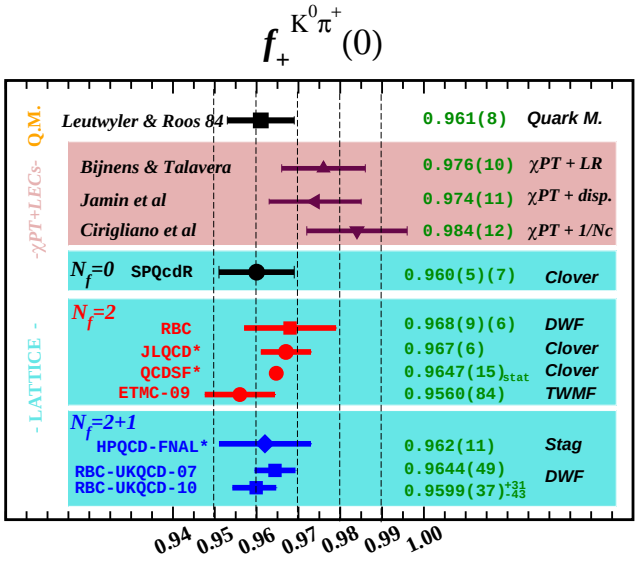

Figure 3.3: Determination of $f_+^{K^0\pi^-}(0)$ taken from [67].

and F_K account respectively for the pion and the kaon). We therefore express their chiral series in terms of the parameters (3.13), the relevant low energy constants ($L_{4,5,9}$) and higher order remainders. By re-expressing L_4 and L_5 in terms of $F_\pi F_K$ with eqs. (3.32)-(3.33), we obtain the following expansions:

$$F_\pi F_K f_+(t) = \frac{F_K^2 + F_\pi^2}{2} + \frac{3}{2}[t(M_{K\pi}^r(t) + M_{K\eta}^r(t)) - L_{K\pi}(t) - L_{K\eta}(t)] \qquad (3.97)$$
$$2tL_9^r + F_\pi F_K d_+ + te_+$$

$$F_\pi F_K f_-(t) = \frac{F_K^2 - F_\pi^2}{2} - \frac{3}{2}(M_K^2 - M_\pi^2)(M_{K\pi}^r(t) + M_{K\eta}^r(t)) \qquad (3.98)$$
$$+ \frac{1}{4}K_{K\pi}(t)\Big[5(t - M_\pi^2 - M_K^2) + \frac{3}{2}(r+3)M_\pi^2 Y(3)\Big]$$
$$- \frac{1}{4}K_{K\eta}(t)\Big[3(t - M_\pi^2 - M_K^2) + \frac{1}{2}(r+3)M_\pi^2 Y(3)\Big]$$
$$- 2(M_K^2 - M_\pi^2)L_9^r + F_\pi F_K(d_- - d_+) + t(e_- - e_+)$$

with $d_\pm$ and $e_\pm$ combining the remainders $\mathcal{R}F_\pi F_K f_\pm(t)$ from the form factors, and the remainders $e_{\pi,K}$ from the decay constants (eqs. (3.24) and (3.25)):

$$F_\pi F_K d_+ = (\mathcal{R}F_\pi F_K f_+)_0 - \frac{F_\pi^2 e_\pi + F_K^2 e_K}{2} \qquad (3.99)$$

$$F_\pi F_K (d_- - d_+) = (\mathcal{R}F_\pi F_K f_-)_0 + \frac{F_\pi^2 e_\pi - F_K^2 e_K}{2} \qquad (3.100)$$

$$F_\pi F_K e_+ = (\mathcal{R}F_\pi F_K f_+)_1 \qquad (3.101)$$

$$F_\pi F_K (e_- - e_+) = (\mathcal{R}F_\pi F_K f_-)_1 \qquad (3.102)$$

where the pre-factor $F_K F_\pi$ come from the re-expression of L_4 and L_5 in eqs. (3.24) and (3.25). Expressions of $M_{PQ}(t)$, $L_{PQ}(t)$ and $K_{PQ}(t)$ are recalled in Appendix A.1. We have also used the polynomial expansion:

$$\mathcal{R}F_\pi F_K f_\pm(t) = (\mathcal{R}F_\pi F_K f_\pm)_{(0)} + t/(F_\pi F_K)(\mathcal{R}F_\pi F_K f_\pm)_{(1)} + O(t^2) \qquad (3.103)$$

.

By inserting (3.97) and (3.98) in (3.95) we get for the scalar form factor:

$$\begin{aligned} F_\pi F_K f_0(t) &= \frac{F_K^2+F_\pi^2}{2} + \frac{t}{\Delta_{K\pi}}\frac{F_K^2-F_\pi^2}{2} - \frac{3}{2}(L_{K\pi}(t)+L_{K\eta}(t)) \\ &+ \frac{t}{4\Delta_{K\pi}}K_{K\pi}(t)\Big[5(t-M_\pi^2-M_K^2)+\frac{3}{2}(r+3)M_\pi^2 Y(3)\Big] \\ &- \frac{t}{4\Delta_{K\pi}}K_{K\eta}(t)\Big[3(t-M_\pi^2-M_K^2)+\frac{1}{2}(r+3)M_\pi^2 Y(3)\Big] \\ &+ (F_\pi F_K d_+ + te_+)\Big(1-\frac{t}{\Delta_{K\pi}}\Big) + (F_\pi F_K d_- + te_-)\Big(1-\frac{t}{\Delta_{K\pi}}\Big) \end{aligned} \tag{3.104}$$

As always, we recover the standard expressions in the case of a saturation by the leading order [43]:

$$f_+^{K\pi}(t) = 1 + \frac{3}{2}H_{K\pi}(t) + \frac{3}{2}H_{K\pi}(t) + O(p^4) \tag{3.105}$$

$$\begin{aligned} f_0^{K\pi}(t) &= 1 + \frac{1}{8F_0^2}\Big(5t - 2\Sigma_{K\pi} - 3\frac{\Delta_{K\pi}^2}{t}\Big)\bar{J}_{K\pi}(t) + \frac{1}{24F_0^2}\Big(3t - 2\Sigma_{K\pi} - \frac{\Delta_{K\pi}^2}{t}\Big)\bar{J}_{K\eta}(t) \\ &+ \frac{t}{4\Delta_{K\pi}^2}\frac{1}{32\pi^2F_0^2}\Big(5\log\frac{M_\pi^2}{\mu^2} - 2\log\frac{M_K^2}{\mu^2} - 3\log\frac{M_\eta^2}{\mu^2}\Big) + \frac{4}{F_0^2}L_5^r t + O(p^4) \end{aligned} \tag{3.106}$$

with the function $H_{PQ}(t)$ defined in eq.(3.69).

3.6.2 The Callan-Treiman points

The Callan-Treiman theorem [46] states that in the soft-pion limit ($p'^2 = M_\pi^2 = 0$), the scalar form factor at the Callan-Treiman point $t = \Delta_{K\pi} = M_K^2 - M_\pi^2$ sould be equal to F_K/F_π. This in turn implies that $F_K F_\pi f_0(\Delta_{K\pi}) - F_K^2$ is expected to vanish in the $N_f = 2$ chiral limit ($m \to 0$). A soft kaon analog of the theorem holds at $t = \tilde{\Delta}_{K\pi} \equiv -\Delta_{K\pi}$, asserting that $F_K F_\pi f_0(\tilde{\Delta}_{K\pi}) - F_\pi^2$ vanishes in the $N_f = 3$ chiral limit ($m, m_s \to 0$). We have the expressions of $F_K F_\pi f_0(t)$ at the two Callan-Treiman points:

$$\begin{aligned} F_K F_\pi f_0(\Delta_{K\pi}) &= F_K^2 + \frac{3}{2}L_{K\pi}(\Delta_{K\pi}) - \frac{3}{2}L_{K\eta}(\Delta_{K\pi}) \\ &+ \frac{1}{4}K_{K\pi}(\Delta_{K\pi})\Big(-10M_\pi^2 + \frac{3}{2}(r+3)M_\pi^2 Y(3)\Big) \\ &- \frac{1}{4}K_{K\eta}(\Delta_{K\pi})\Big(-5M_\pi^2 + \frac{1}{2}(r+3)M_\pi^2 Y(3)\Big) + F_K F_\pi d_- + \Delta_{K\pi}e_- \end{aligned} \tag{3.107}$$

$$\begin{aligned} F_K F_\pi f_0(-\Delta_{K\pi}) &= F_\pi^2 - \frac{3}{2}L_{K\pi}(-\Delta_{K\pi}) - \frac{3}{2}L_{K\eta}(-\Delta_{K\pi}) \\ &+ \frac{1}{4}K_{K\pi}(-\Delta_{K\pi})\Big(-10M_K^2 + \frac{3}{2}(r+3)M_\pi^2 Y(3)\Big) \\ &- \frac{1}{4}K_{K\eta}(-\Delta_{K\pi})\Big(-6M_K^2 + \frac{1}{2}(r+3)M_\pi^2 Y(3)\Big) + F_K F_\pi(2d_+ - d_-) - \Delta_{K\pi}(2e_+ - e_-) \end{aligned} \tag{3.108}$$

Those expressions fulfill the Callan-Treiman theorem and the soft-kaon analog (with K and L contributions canceling each other in the two chiral limits). This imposes a tighter constraint on the size of the higher-order remainders:

$$d_- = O(mm_s), \quad e_- = O(m) \tag{3.109}$$

so that d_- and e_- and supressed compared to d_+ and e_+. This ensures that the Callan-Treiman theorem will be numerically well satisfied even in the case of a small quark condensate in the Resummed χPT framework. Finally, we define the discrepancies from the two Callan-Treiman theorems:

$$\Delta_{CT} = f_0(\Delta_{K\pi}) - \frac{F_K}{F_\pi}, \quad \tilde{\Delta}_{CT} = f_0(\Delta_{K\pi}) - \frac{F_\pi}{F_K} \tag{3.110}$$

These quantities have been calculated in standard χPT (see eq. (3.108) in the standard framework) at one-loop order, in the isospin limit [43]:

$$\Delta_{CT} = -3.5.10^{-3}, \quad \tilde{\Delta}_{CT} = 0.03 \tag{3.111}$$

Further computations have been performed at two loops [47], and including isospin breaking effects [48]. It has been shown in refs. [49, 50] that a precise assessment of the scalar form factor f_0 at the Callan-Treiman points could provide a probe to physics beyond the Standard Model in the strange quark sector, in particular the right-handed coupling of quarks to W bosons. The pioneering work [49] led to re-analysis of $K_{\ell 3}$ data by several collaborations [59, 60, 61] which at present show a good/marginal agreement with the Standard Model.

3.7 Alternative treatments of the unitarity part

As we have indicated before in sec. 3.3.2, we modify the position of the singularities in the unitarity part of the chiral expansions expressed using the low energy constants of the chiral lagrangian, in order to satisfy the requirement that the known singularities (poles and cuts) are located at the physical position. The substitution $\overset{\circ}{M}{}^2_P \to M_P^2$ in the next-to-leading order expansions is performed in order to diminish the size of higher-order remainders, as we expect higher and higher-order contributions to contribute to this shift in the location of the non-analytic contribution. If the operation is non-ambiguous for the poles, the status of the cuts is less clear. One can indeed design several different ways of performing this change.

In the present thesis, following the work in ref. [92], we have decided to perform the substitution only at the level of the masses involved in the scalar-bubble function $\bar{J}_{PQ}$ recalled in Appendix A.1. At one-loop order in the effective theory, this function generates all the nonanalytic cuts stemming from the propagation of the mesons P and Q above threshold, with:

$$\text{Im } \bar{J}_{PQ}(s) = \frac{1}{16\pi} \frac{\sqrt{\delta_{PQ}(s)}}{s} \theta(s - (M_P + M_Q)^2) \tag{3.112}$$

with

$$\delta_{PQ}(s) = (s - (M_P + M_Q)^2)(s - (M_P - M_Q)^2) \tag{3.113}$$

Indeed one can check in eqs. (3.97) and (3.98) that the form factors exhibit non-analytic structures corresponding to polynomial terms multiplied by $\bar{J}_{PQ}$. These polynomial terms can be determined from unitarity. For instance, if we consider the pion electromagnetic

form factor, one can easily derive the following unitarity relation, by inserting all the possible intermediate states in the matrix element eq. (3.65) defining the electromagnetic form factor [3]:

$$\begin{aligned}\text{Im } F_V^\pi(t) &= \sqrt{1-\frac{4M_\pi^2}{t}}F_V^\pi(t)f_1^{\pi\pi}(t) + \frac{\sqrt{2}}{8}\sqrt{1-\frac{4M_K^2}{t}}(s-4M_K^2)F_V^K(t)g_1^{KK}(t) \qquad (3.114)\\ &= \text{Im}\left[\bar{J}_{\pi\pi}(t)\times 16\pi F_V^\pi(t)f_1^{\pi\pi}(t) + \bar{J}_{KK}(t)\times 16\pi\frac{\sqrt{2}}{8}(t-4M_K^2)F_V^K(t)g_1^{KK}(t)\right]\end{aligned}$$

where $f_1^{\pi\pi}(s)$ and $g_1^{KK}(s)$ are the P-wave partial wave amplitudes for $\pi\pi\to\pi\pi$ and $\pi\pi\to K\bar{K}$ defined for instance as in refs. [52] and [90] respectively. In terms of chiral counting, we need only these amplitudes and the form factors at leading order in order to determine Im F_V^π at next-to-leading order.

Indeed, with our prescription, detailed in ref. [92] and recalled in sec. 3.3.2, we have obtained the following expression:

$$\begin{aligned}F_\pi^2 F^\pi_{V;\text{prescr }1}(t) &= F_\pi^2 Z(3) + M_\pi^2 Y(3)[8(r+2)L_4^r + 8L_5^r] \qquad (3.115)\\ &\quad - \frac{1}{32\pi^2}M_\pi^2 Y(3)\left[4\log\frac{\overset{\circ}{M}{}_\pi^2}{\mu^2} + (r+1)\log\frac{\overset{\circ}{M}{}_K^2}{\mu^2}\right]\\ &\quad + t\left[2L_9^r - \frac{1}{32\pi^2}\left[\frac{1}{3}\log\frac{\overset{\circ}{M}{}_\pi^2}{\mu^2} + \frac{1}{6}\log\frac{\overset{\circ}{M}{}_K^2}{\mu^2}\right]\right] + \frac{1}{6}[t-4\overset{\circ}{M}{}_\pi^2]\bar{J}_{\pi\pi}(t)\\ &\quad + \frac{1}{12}[t-4\overset{\circ}{M}{}_K^2]\bar{J}_{KK}(t)\end{aligned}$$

where $\bar{J}_{PP}$ is expressed in terms of the physical mass M_P^2, and one can check easily that the polynomials multiplying $\bar{J}_{\pi\pi}(t)$ and $\bar{J}_{KK}(t)$ correspond to the products of partial-wave amplitudes and form factors in eq. (3.114), expanded at leading order in terms of the couplings arising in the chiral Lagrangian:

$$F^\pi_{V;\text{unit prescr }1} = 1 \qquad f^{\pi\pi}_{1;\text{unit prescr }1} = \frac{1}{3F_0^2}(t-4\overset{\circ}{M}{}_\pi^2) \qquad (3.116)$$

$$F^K_{V;\text{unit prescr }1} = 1 \qquad [g_1^{KK}\times(t-4M_K^2)]_{\text{unit prescr }1} = \frac{4}{3\sqrt{2}F_0^2}(t-4\overset{\circ}{M}{}_K^2) \qquad (3.117)$$

As said before, we expect the position of the cuts to move from $(\overset{\circ}{M}_P+\overset{\circ}{M}_Q)^2$ to $(M_P+M_Q)^2$ once higher orders are included: we thus performed the shift preventively, in order to reduce the size of higher-order remainders. However, we have no further information on the analytic structure of the amplitude (in particular that of the polynomials multiplying $\bar{J}_{PQ}$ or the logarithms), and we decided in ref. [92] not to perform any further modification.

One could also consider two alternative ways of treating the unitarity parts:

- In ref. [81], physical masses were used not only inside $\bar{J}$ but also in the functions J^r, K, L, M^r in the unitarity contribution to the one-loop generating functional Z_u (see sec. 2.5.4), as well as in the argument of the logarithms in the tadpole contribution Z_t.

[3] We consider here only terms that contribute at one loop in chiral perturbation theory. This selects only two-pseudo Goldstone boson intermediate states with the same quantum numbers as the original $\pi\pi$ pair. There is no contribution to the electromagnetic form factor from the $\pi\eta$ and $\eta\eta$ intermediate states as they are produced only in the S-wave from $\pi\pi$.

- In ref. [85], it was claimed that one could improve the convergence of the series by redefining the (NLO) unitary contributions, replacing their expression in terms of chiral couplings by another one derived from the application of unitarity relations, together with the replacement of $\overset{\circ}{M}{}_P^2$ by M_P^2 in the logarithms stemming from $J^r(0)$.

We will illustrate these two procedures in the following. Obviously, the differences induced by the choice of one prescription or another would correspond to an equivalent shift in the higher-order remainders: all of them are equivalent as long as we do not set a bound on the size of these higher-order remainders. Since it is however what we want to do in the following, it is useful to compare these prescriptions in a specific case, i.e., the electromagnetic pion form factor.

If we follow the prescription of ref. [81] and use physical masses in Z_t as well as in all the functions occurring in Z_u (while keeping the couplings of the chiral Lagrangian for the prefactors), the argument of the logarithms coming from the reexpression of J^r in term of $\bar{J}$ is modified, yielding:

$$\begin{aligned} F_\pi^2 F_{V;\text{prescr }2}^\pi(t) &= F_\pi^2 Z(3) + M_\pi^2 Y(3)[8(r+2)L_4^r + 8L_5^r] \\ &- \frac{1}{32\pi^2} M_\pi^2 Y(3)\left[4\log\frac{M_\pi^2}{\mu^2} + (r+1)\log\frac{M_K^2}{\mu^2}\right] \\ &+ t\left[2L_9^r - \frac{1}{32\pi^2}\left[\frac{1}{3}\log\frac{M_\pi^2}{\mu^2} + \frac{1}{6}\log\frac{M_K^2}{\mu^2}\right]\right] + \frac{1}{6}[t - 4\,\overset{\circ}{M}{}_\pi^2]\bar{J}_{\pi\pi}(t) \\ &+ \frac{1}{12}[t - 4\,\overset{\circ}{M}{}_K^2]\bar{J}_{KK}(t) \end{aligned} \tag{3.118}$$

Comparing with eq. (3.115), we notice that the argument of all the logarithms have been changed form the leading order masses to the physical ones.

If we follow the prescription of ref. [85], we should replace the unitarity part of eq. (3.115) by the one reconstructed from eq. (3.114) considered at next-to-leading order, inserting the leading order expression of the form factors and partial-waves amplitudes derived from the related good observables:

$$F_{V;\text{unit prescr }3}^\pi = \frac{F_0^2}{F_\pi^2} \qquad f_{1;\text{unit prescr }3}^{\pi\pi} = \frac{F_0^2}{3F_\pi^4}(t - 4M_\pi^2) \tag{3.119}$$

$$F_{V;\text{unit prescr }3}^K = \frac{F_0^2}{F_K^2} \qquad g_{1;\text{unit prescr }3}^{KK} = \frac{4F_0^2}{3\sqrt{2}F_\pi^2 F_K^2} \tag{3.120}$$

where, as before, the extra factors of F_π and F_K come from the expression of form factors and scattering amplitudes in terms of the correlators of vector/axial currents and scalar/pseudoscalar densities. Inserting these expressions in eq. (3.114), we obtain the unitarity piece according to the prescription of ref. [85]:

$$F_\pi^2\, F_V^\pi(t)|_{\text{unit part;prescr }3} = \frac{F_0^4}{F_\pi^4}\frac{1}{6}(t - 4M_\pi^2)\bar{J}_{\pi\pi}(t) + \frac{F_0^4}{F_K^4}\frac{1}{12}(t - 4M_K^2)\bar{J}_{\pi\pi}(t) \tag{3.121}$$

Moreover, one has to change the argument of the logarithms coming from $J^r(0)$ from leading order to physical masses. We obtain thus the expansion of the chiral form factor following the prescription of ref. [85]:

$$
\begin{aligned}
F_\pi^2 F^\pi_{V;\text{prescr }3}(t) = {} & F_\pi^2 Z(3) + M_\pi^2 Y(3)[8(r+2)L_4^r + 8L_5^r] \\
& - \frac{1}{32\pi^2} M_\pi^2 Y(3) \left[4 \log \frac{\overset{\circ}{M}{}_\pi^2}{\mu^2} + (r+1) \log \frac{\overset{\circ}{M}{}_K^2}{\mu^2} \right] \\
& + t \left[2L_9^r - \frac{1}{32\pi^2} \left[\frac{1}{3} \log \frac{M_\pi^2}{\mu^2} + \frac{1}{6} \log \frac{M_K^2}{\mu^2} \right] \right] + \frac{F_0^4}{F_\pi^4} \frac{1}{6} [t - 4M_\pi^2] \bar{J}_{\pi\pi}(t) \\
& + \frac{F_0^4}{F_K^4} \frac{1}{12} [t - 4M_K^2] \bar{J}_{KK}(t)
\end{aligned}
\tag{3.122}
$$

We see that eq. (3.122), i.e., the prescription of ref. [85], comes close to the usual chiral expansion presented in eq. (3.66), differing through extra F_0/F_P factors for the unitarity contribution, and the mass term involved the tadpole logarithms. Eq. (3.115) from ref. [92] is the closest to the expression in terms of the couplings arising in the chiral Lagrangian, whereas eq. (3.115) in ref. [81] corresponds to an intermediate situation.

Having presented the three prescriptions, we can now discuss the impact of changing the structure of the unitarity part, as well as the argument of the logarithms. If $Y(3)$ tends to zero, we see that the chiral logarithms coming from $J^r_{PQ}(0)$ in the unitarity part will diverge in eq. (3.118) from ref. [92]. Such divergences are expected in the limit where the whole Goldstone boson masses vanish, but not when only their leading-order term is set to zero. This unwelcome feature is not present in the two other prescriptions, where these logarithms have a physical mass for argument [4]. Let us however emphasise that such an effect, present in the mathematical limit where $Y(3) \to 0$, has little impact as soon as $Y(3)$ is different from zero. Indeed, in the case of the electromagnetic form factor, the difference between eqs. (3.115) and (3.118), i.e., refs. [92] and [81], is of order:

$$
\frac{t}{F_\pi^2} \frac{1}{32\pi^2} \log \frac{\overset{\circ}{M}{}_P^2}{M_P^2} \tag{3.123}
$$

For $r = 25$ and $P = \pi, K, \eta$, such a term would remain smaller than 6% at the first threshold $t = 4M_\pi^2$ for $Y(3) \geq 0.1$. One would thus expect the prescription of ref. [92] to be acceptable in the subthreshold region as long as $Y(3)$ is not very close to 0.

If $Z(3) = F_0^2/F_\pi^2$ is small, the prescription of ref. [85] yields a very significant (quartic) suppression of all the unitarity contributions as can be seen in eq. (3.122). This suppression is rather surprising, since the unitary part is expected to be sensitive to the couplings of the Goldstone bosons (i.e., F_π and F_K) but not particularly to their leading order. This unexpected result relies on the ad-hoc assumption that good observables should have an improved convergence once their unitarity parts satisfy perturbative unitarity expressed in terms of good observables themselves. However, the next-to-leading order unitarity relation eq. (3.114) involves the product of good observables taken at leading order *only*, whereas the definition of good observables is a global statement on the size of higher order terms compared to leading order and next-to-leading order ones. Therefore, using the leading order term of good observables in the unitarity contribution does not guarantee that the most significant contribution of the unitarity part is captured by the treatment of ref. [85],

[4] The problem does not arise for the logarithms involve in the tadpole contributions Z_t, which are of the form $\overset{\circ}{M}{}_P^2 \log \overset{\circ}{M}{}_P^2 / \mu^2$. As discussed in refs. [81, 92], the replacement of the argument of the logarithm by the physical mass for these tapdole diagrams induces a change that is numerically small in the chiral expansions (at the level of a few percent) over the whole range of $Y(3)$ from 0 to 1. In particular, the difference vanishes in the two limiting cases $Y(3) \to 0$ (as the whole tadpole contribution vanishes) and $Y(3) \simeq 1$ (where the chiral expansion of M_P^2 is saturated by its leading order).

nor that this prescription reduces the size of higher-order remainders compared to that of ref. [81, 92].

This discussion should invite us to discard the prescription of ref. [85] (eq. (3.122)) and to prefer that of ref. [81] (eq. (3.118)), or that of ref. [92] (eq. (3.115)). In the latter case, the modification of the argument of the logarithms coming from $J^r(0)$ in Z_u should also be performed in order to prevent the divergences pointed out in ref. [85]. In practice, we will see that our results, quoted from ref. [92], yield $Y(3)$ not very small, so that the problem outlined before in the case of a vanishing $Y(3)$ does not affect the outcome of our fits significantly. For completeness, in sec. 4.3.3, we will also briefly discuss the results obtained once the argument of the logarithms coming from $J^r_{PQ}(0)$ in Z_u is changed from $\mathring{M}_P^2$ to M_P^2.

3.8 Summary

In this chapter, we have made a presentation of an alternative framework of $N_f = 3$ Chiral Perturbation Theory called Resummed Chiral Perturbation Theory. It consists into a re-ordering of the chiral series that allows one to take into account the possible numerical competition between leading and next-to-leading orders that was hinted at in sec. 2.7.3 and developped in sec. 3.2 and sec. 3.3. It differs from the standard treatment of chiral series in the following way (see sec. 3.3.1):

- Only some "good" observables possess convergent expansions, when expressed in terms of the chiral lagrangian parameters (F_0, B_0, L_is...).
- A series is considered as convergent when the sum of its leading and next-to-leading order $LO + NLO$ is large compared to all the remaining higher orders.
- The resulting formula must be treated analytically, without neglecting corrections from the higher orders (treated as an overall remainder) when re-expressing the low energy constants in terms of observables.
- The order parameters F_0 and $\Sigma(3)$ are expressed in terms of the leading order parameters $X(3) = 2m\Sigma(3)/(F_\pi^2 M_\pi^2)$ and $Z(3) = F_0^2/F_\pi^2$ (equivalently $Y(3) = 2mB_0/M_\pi^2$). The quark mass ratio $r = m_s/m$ introduced.
- The next-to-leading order low-energy constants L_i^r are re-expressed in terms of the physical observables, the parameters $X(3)$, $Z(3)$, $Y(3)$ and r, and (small) higher-order remainders.

This procedure then provides a re-expression of the chiral series that can be used for the analysis of experimental and lattice data in the possible case that the leading order would not saturate the chiral series as it is usually expected in the standard treatement. This general approach is of course fully compatible with the case of a saturation scenario, since it only allows the LO/NLO numerical competition, but does not enforce it. We have then applied it to the decay constants and masses of pseudoscalar mesons (sec. 3.4.1), as well as to pion and kaon electromagnetic form factors (sec. 3.5) and $K_{\ell 3}$ form factors (sec. 3.6). We have also discussed alternative treatment of the unitarity part, and exploited our preferred choice to deal with these contributions. A fully similar approach can be applied to scattering amplitudes, see for example [81, 85], and also to other processes like $K \to 3\pi$ and $\eta \to 3\pi$ [87].

In the following chapters, we will apply it to the $N_f = 2+1$ data provided by some lattice collaborations [96, 99, 100, 101] which encountered some problems when fitting the outcome of their simulations using chiral expansions in the standard case. We will observe that the Resummed framework indeed provides a good description of the lattice results when the

leading order is no more numerically dominant in the chiral expansions of some low-energy QCD observables: the decay constants and masses, the $K_{\ell 3}$ form factors (Chapter 4) and the topological quantities (Chapters 5 and 6).

Chapter 4

Analysis of $N_f = 2 + 1$ lattice data using Resummed Chiral Perturbation Theory

4.1 Introduction

As was hinted at in sec. 2.7.3, various analyses of lattice results [96, 99, 100, 101, 102, 103] suggest an overall good agreement between lattice simulations and Chiral Perturbation Theory concerning chiral series obtained as an expansion in m_u and m_d only ($N_f = 2$ χPT), but difficulties with the chiral expansions in powers of m_u, m_d, m_s ($N_f = 3$ χPT). In some cases, one observes small values of the $N_f = 3$ quark condensate and pseudoscalar decay constant failing to saturate the chiral expansions, the convergence of the three-flavour chiral series exhibiting therefore a numerical competition between the leading and next-to-leading order. Resummed Chiral Perturbation Theory, discussed in the previous chapter, provides an alternative framework to the usual treatment of chiral expansions that allows for this competition.

The work presented in this chapter is the object of the article [92]. We fit data provided by the collaborations PACS-CS and RBC/UKQCD [96, 99, 100, 101], to the relevant expressions of light mesons decay constants, masses (sec. 3.4) and $K_{\ell 3}$ form factors (sec. 3.6) written in the resummed framework introduced in sec. 3.3. This will enable us to extract information about the pattern of chiral symmetry breaking, and also to check the consistency of the picture concerning the numerical competition between leading order and next-to-leading order.

4.2 Lattice inputs

In principle, our analysis in the Resummed framework would require lattice data performed with several u, d and s quark masses (whose renormalized values are known) and transferred momenta (in the case of form factors), but where the continuum and infinite-volume limit have already been performed ($a \to 0$, $V \to \infty$). The situation is however not so favorable. Some collaborations (MILC [102, 103]) provide numbers directly in the physical limit, performing the chiral extrapolation at the same time as the continuum limit. This prevents one from testing different alternatives concerning chiral extrapolations, even though the results sometimes contradict the standard treatment of χPT (for instance concerning the size of the quark condensate and the decay constant in the three-flavours chiral limit). Others (BMW [104, 105], ETMC [106] and TWQCD-JLQCD [107]) do not provide

the decay constants and the renormalized quark masses mandatory for our study. Two collaborations, RBC/UKQCD [99, 100, 101] and PACS-CS [96], have performed their analysis only at particular lattice spacings and/or particular volumes, without estimating the systematics associated with the continuum and infinite-volume limits fully. The fact that only statistical errors are quoted in both cases prevents us from using a fully-fledged statistical treatment [81], but they can still be used for this exploratory study.

For the specific data sets studied here, we consider the quantities given by these collaborations corresponding to light quark masses and small momenta (i.e. we fit over a "subset" of the whole data) where at least a version of Chiral Perturbation Theory is assumed to be valid.

RBC/UKQCD Collaboration

The RBC/UKQCD collaboration performed simulations for $2+1$ dynamical flavours [99, 100, 101][1] using domain-wall fermions at one lattice spacing: $a^{-1} = 1.729(28)$ GeV, at two different volumes $16^3 \times 32$ and $24^3 \times 64$ (2.74^3 fm^3), with a fifth dimension of length 16. The simulations were done at each quark mass for the two volumes, except the lightest mass which was only simulated for the larger volume. A non-perturbative renormalization was performed to relate the lattice quark masses to those in the RI-MOM scheme. We only use the points for which valence and sea quark masses are identical (i.e. this corresponds to the unitary situation presented in Chapter 2.2). For decay constants and masses, there are four sets corresponding to such a situation (ref. [99]). We consider only the lightest ones to ensure that the chiral series will converge well.

The quark masses are given in the RI-MOM scheme, but they can be related to the $\bar{M}S$ scheme through a multiplicative factor Z_m, which is mass-independent: $\bar{m}(2GeV) = Z_m a^{-1}(a\tilde{m}^{lat})$. It drops in all the input quantities, since quark masses are involved only through ratios of the parameters p and q (eq. (4.2)). The values for the decay constants and masses [99, 108], expressed in units of 10^{-3} GeV^2, are given in table 4.1.

$(\tilde{m}, \tilde{m}_s)$	(p, q)	F_π^2 (GeV^2)	$F_\pi^2 M_\pi^2$ (GeV^4)	F_K^2 (GeV^2)	$F_K^2 M_K^2$ (GeV^4)
$(0.005, 0.040)$	$(1.15, 0.189)$	10.98 ± 0.16	1.196 ± 0.022	14.11 ± 0.19	4.644 ± 0.076
$(0.010, 0.040)$	$(1.15, 0.304)$	12.85 ± 0.16	2.249 ± 0.036	15.59 ± 0.18	5.730 ± 0.082

Table 4.1: Values for masses and decay constants from refs. [99, 108] for points with identical valence and sea quark masses. $\tilde{m}_q$ is the simulated quark mass $\tilde{m}_q = a(\tilde{m}_q^{lat} - m_{res})$ where $am_{res} = 0.00315(2)$. The uncertainties here are purely statistical and do not include those induced by the uncertainty on the value of the lattice spacing a^{-1}.

In the papers [100, 101], the RBC/UKQCD collaboration investigated the $K_{\ell 3}$ form factors f_0 and f_+ (eqs. (3.97) and (3.98) using twisted boundary conditions to obtain a sample of momentum transfer, with the same two sets of values corresponding to the non-degenerate masses: $(a(\tilde{m}^{lat} - m_{res}), a(\tilde{m}_s^{lat} - m_{res})) = (0.005, 0.040), (0.010, 0.040)$. The set with the lighter u and d quark masses yields the values gathered in table 4.2.

t (GeV^2)	60.7	59.87	38.1	21.6	0.30
$F_\pi F_K f_0(t)$	12.68 ± 0.17	12.73 ± 0.17	12.49 ± 0.17	12.32 ± 0.17	12.15 ± 0.16
$F_\pi F_K f_+(t)$	$\times$	$\times$	12.71 ± 0.176	12.42 ± 0.175	12.15 ± 0.17

The set for the scalar form factor with the heavier masses values is given in table 4.3.

[1] We only follow the last reference [101].

t (GeV^2)	-44.00	-129.3
$F_\pi F_K f_0(t)$	11.68 ± 0.21	10.95 ± 0.32
$F_\pi F_K f_+(t)$	$\times$	$\times$

Table 4.2: Values of the vector and scalar form factors $F_\pi F_K f_{+,0}(t)$ for different values of the momentum transfer t from refs. [100, 101], for the light set of quark masses u and d.

t (GeV^2)	35.42	-90.51	-195.3
$F_\pi F_K f_0(t)$	14.28 ± 0.17	13.05 ± 0.21	11.64 ± 0.38

Table 4.3: Values of the scalar form factors $F_\pi F_K f_0(t)$ for different values of the momentum transfer t from refs. [100, 101], for the heavier set of quark masses u and d

We drop the points for $t \leq -0.2$ GeV^{-2} where χPT is likely to lose its relevance (in ref. [100], it corresponds to the two points of f_0 with the lowest values of the momentum transfer). The values of the physical quark masses m and m_s and the lattice spacing a are obtained by studying the dependence of the π, K and Ω hadrons on these three parameters and tuning them to reproduce the physical hadron masses. If $\tilde{m}_{s,ref}$ is the value of the simulated strange quark mass corresponding to the set $(0.005, 0.040)$, the RBC/UKQCD collaboration obtained $\tilde{m}_{s,ref}/m_s = 1.150$. Also, in the present chapter and in the case of both collaborations, we will assume that the determination of the lattice spacing is not affected by the issue of convergence of the chiral series described here − we will therefore use the values obtained by the collaboration. This will be reconsidered in the next chapter.

PACS-CS Collaboration

The PACS-CS collaboration [96] investigated the pseudoscalar masses and decay constants for a large sample of light quark masses for one value of lattice spacing $a^{-1} = 2.176(31)$ GeV, on a $32^3 \times 64$ volume, using a non-perturbatively $O(a)$-improved Wilson quark action and performing the renormalization of quark masses perturbatively at one loop (with tadpole improvement). They obtained the following results, in units of 10^{-3} GeV^2:

$(am_{ud}^{MS}, am_s^{MS})$	(p, q)	F_π^2	$F_\pi^2 M_\pi^2$	F_K^2	$F_K^2 M_K^2$
$(0.001, 0.040)$	$(1.410, 0.040)$	10.19 ± 1.09	0.247 ± 0.035	14.29 ± 0.48	4.385 ± 0.151
$(0.006, 0.041)$	$(1.456, 0.138)$	11.51 ± 0.26	1.007 ± 0.031	15.49 ± 0.22	5.459 ± 0.088
$(0.010, 0.036)$	$(1.256, 0.271)$	12.48 ± 0.21	1.846 ± 0.041	15.37 ± 0.16	5.200 ± 0.067

Table 4.4: Values of decay constants and masses from ref. [96]. $am_q^{\bar{M}S}$ are the bare lattice quark masses. The uncertainties are of purely statistical origin and do not include the one coming from the determination of the lattice spacing.

As was the case for the RBC/UKQCD collaboration, the values of the physical quark masses m and m_s, and the lattice spacing a, are obtained by studying the dependence of the masses of the K, π and Ω hadrons on these three parameters and tuning them to reproduce the physical hadron masses. If $\tilde{m}_{s,ref}$ denotes the value of the strange quark mass corresponding to the set with the lightest u and d masses, the PACS-CS collaboration obtained $\tilde{m}_{s,ref}/m_s = 1.19$.

Results from the two collaborations:

For RBC-UKQCD fits to the $N_f = 2$ and $N_f = 3$ next-to-leading order chiral series for pseudoscalar masses and decay constants were performed by the collaboration in ref. [99]. It turned out that the $N_f = 3$ chiral expansions led to rather poor fits (large χ^2 per d.o.f), in particular for decay constants, unless they put stringent cuts on the values of quark masses where such expansions should hold. This led the authors in ref. [99] to perform fits to $N_f = 2$ next-to-leading order chiral expansions. In ref. [109], next-to-next-to-leading $SU(2)$ chiral expansions were shown to have only a limited utility to extrapolate the data: many more data points would be needed to fix the size of the combinations of $O(p^6)$ counterterms involved. The results obtained in ref. [99] that are relevant for our discussion are summarised in table 4.5.

r	$28.8 \pm 0.4 \pm 1.6$
$\tilde{m}_{s,ref}/m_s$	1.150
F_K/F_π	$1.205 \pm 0.018 \pm 0.062$
$m_s(2\text{ GeV})$[MeV]	$107.3 \pm 4.4 \pm 9.7 \pm 4.9$
$m(2\text{ GeV})$[MeV]	$3.72 \pm 0.16 \pm 0.33 \pm 0.18$
$B(2\text{ GeV})$[GeV]	$2.52 \pm 0.11 \pm 0.23 \pm 0.12$
F[MeV]	$81.2 \pm 2.9 \pm 5.7$
$\bar{\ell}_3$	$3.13 \pm 0.33 \pm 0.24$
$\bar{\ell}_4$	$4.43 \pm 0.14 \pm 0.77$

Table 4.5: Results obtained by the RBC/UKQCD collaboration in ref. [99]. No values for the $SU(3)$ parameters F_0 and B_0 and the LEC's L_i could be provided because of the convergence problems the collaboration encountered with $N_f = 3$ chiral expansions.

In addition, two different values for $f_+(0)$ were obtained in refs. [100, 101] from the same gauge configurations, using either data for the scalar form factor or data for both form factors, and applying a pole ansatz based on either $N_f = 3$ or $N_f = 2$ chiral perturbation theory for $K_{\ell 3}$ form factors [110]:

$$f_+(0) = 0.964 \pm 0.033 \pm 0.0034 \pm 0.0014 \text{ [100]}, \quad f_+(0) = 0.960(^{+5}_{-6}) \text{ [101]} \qquad (4.1)$$

The situation for PACS-CS is similar: fits to the $N_f = 2$ and $N_f = 3$ next-to-leading order chiral series for pseudoscalar masses and decay constants were performed in ref. [96]. It turned out that the $N_f = 3$ chiral expansions led to rather poor fits, related to very significant next-to-leading order contributions compared to leading order terms, in particular for the decay constants, related to large contributions from kaon loops. In other words, the dependence of these quantities on the strange quark mass seen in these simulations is not accounted for properly by next-to-leading order $SU(3)$ chiral perturbation theory. This led the authors in ref. [96] to perform fits to $N_f = 2$ chiral expansions. The results obtained in ref. [96] that are relevant for our discussion are summarised in table 4.6.

We will compare these results with the outcome of our fits (sec. 4.3.2), which will illustrate the impact of the choice of the chiral series.

r	28.8 ± 0.4
$Y(3)$	0.88 ± 0.01
$Z(3)$	0.76 ± 0.04
F_K/F_π	1.189 ± 0.020
$\tilde{m}_{s,ref}/m_s$	1.19
m_s(2 GeV)[MeV]	72.72 ± 0.78
m(2 GeV)[MeV]	2.527 ± 0.047
B_0(2 GeV)[GeV]	3.869 ± 0.092
F_0[MeV]	83.8 ± 6.4
$L_4(\mu) \cdot 10^3$	-0.06 ± 0.10
$L_5(\mu) \cdot 10^3$	1.45 ± 0.07
$L_6(\mu) \cdot 10^3$	0.03 ± 0.05
$L_8(\mu) \cdot 10^3$	0.61 ± 0.04
$Y(2)$	0.96 ± 0.01
$Z(2)$	0.88 ± 0.01
B(2 GeV)[GeV]	0.96 ± 0.01
F[MeV]	88.2 ± 3.4
$\bar{\ell}_3$	3.14 ± 0.23
$\bar{\ell}_4$	4.04 ± 0.19
Σ/Σ_0	1.205 ± 0.014
B/B_0	1.073 ± 0.055
F/F_0	1.065 ± 0.058

Table 4.6: Results obtained by the PACS-CS collaboration with one-loop perturbative renormalisation and extrapolation to the physical limit [96]. The values for the quantities in the $N_f = 2$ chiral limit correspond to $N_f = 2$ fits to the so-called Range I with finite-size effects included. The renormalization scale μ is set at M_ρ. We have evaluated from their results the values the parameters Y and Z.

4.3 Fits to lattice data

4.3.1 Observables and Parameters

For the observables under consideration, we turn to the decay constants, masses and $K_{\ell 3}$ form factors described in secs. 3.4 and 3.6: We will consider these observables for $N_f = 3$ simulated dynamical flavours in the isospin limit: $\tilde{m}$, $\tilde{m}$ and $\tilde{m}_s$. $\tilde{X}$ denotes the values for the lattice quantities (whereas the tildeless notation X is the corresponding value for the physical ones). In addition to the ratio $r = m_s/m$ of the physical quark masses, the leading order chiral parameters $X(3)$ and $Z(3)$ (eq. (3.13)), and the higher-order parameters, we introduce the following ratios for the masses on the lattice:

$$p = \frac{\tilde{m}_s}{m_s}, \quad q = \frac{\tilde{m}}{\tilde{m}_s} \tag{4.2}$$

The relevant lattice observables $\tilde{X}$ are now functions of p and q as well as $X(3)$, $Z(3)$, r and the miscellaneous remainders, which will have to be estimated to take into account the fact that the simulated quark masses are different from the physical ones as explained in sec. 4.3.1.

Following the same approach as in sec. 3.4.1, we get the following expansions for the decay constants on the lattice:

$$\tilde{F}_\pi^2 = F_\pi^2 Z(3) + M_\pi^2 pqr Y(3)\left[8\left(\frac{1}{q}+2\right)L_4^r + 8L_5^r\right] - M_\pi^2 \frac{1}{32\pi^2} pqr Y(3)\left[4\log\frac{\overset{\circ}{\tilde{M}}_\pi^2}{\mu^2} + \left(\frac{1}{q}+1\right)\log\frac{\overset{\circ}{\tilde{M}}_K^2}{\mu^2}\right] + \tilde{F}_\pi^2\tilde{e}_\pi \tag{4.3}$$

$$\tilde{F}_K^2 = F_\pi^2 Z(3) + M_\pi^2 pqr Y(3)\left[8\left(\frac{1}{q}+2\right)L_4^r + 4\left(\frac{1}{q}+1\right)L_5^r\right] - M_\pi^2 \frac{1}{32\pi^2} pqr Y(3)\left[\frac{3}{2}\log\frac{\overset{\circ}{\tilde{M}}_\pi^2}{\mu^2} + \frac{3}{2}\left(\frac{1}{q}+1\right)\log\frac{\overset{\circ}{\tilde{M}}_K^2}{\mu^2} + \frac{1}{2}\left(\frac{2}{q}+1\right)\log\frac{\overset{\circ}{\tilde{M}}_\eta^2}{\mu^2}\right] + \tilde{F}_K^2\tilde{e}_K \tag{4.4}$$

where $\overset{\circ}{\tilde{M}}_P^2$ is the leading-order contribution to the simulated pseudoscalar masses:

$$\overset{\circ}{\tilde{M}}_\pi^2 = pqr M_\pi^2 Y(3), \quad \overset{\circ}{\tilde{M}}_K^2 = \frac{pqr}{2}\left(\frac{1}{q}+1\right)M_\pi^2 Y(3), \quad \overset{\circ}{\tilde{M}}_\eta^2 = \frac{pqr}{3}\left(\frac{2}{q}+1\right)M_\pi^2 Y(3) \tag{4.5}$$

$\tilde{e}_P$ are the relative remainders of order $O(\tilde{m}_q^2)$ (with $\tilde{m}_q$ denoting either $\tilde{m}_s$ or $\tilde{m}$). Similarly, the chiral expansions for the masses on the lattice reads:

$$\tilde{F}_\pi^2\tilde{M}_\pi^2 = pqr\Bigg\{F_\pi^2 M_\pi^2 X(3) + M_\pi^4 pqr[Y(3)]^2\left[16\left(\frac{1}{q}+2\right)L_6^r + 16L_8^r\right] - M_\pi^4\frac{1}{32\pi^2}pqr[Y(3)]^2\left[3\log\frac{\overset{\circ}{\tilde{M}}_\pi^2}{\mu^2} + \left(\frac{1}{q}+1\right)\log\frac{\overset{\circ}{\tilde{M}}_K^2}{\mu^2} + \frac{1}{9}\left(\frac{2}{q}+1\right)\log\frac{\overset{\circ}{\tilde{M}}_\eta^2}{\mu^2}\right]\Bigg\} + \tilde{F}_\pi^2\tilde{M}_\pi^2\tilde{d}_\pi \tag{4.6}$$

$$\tilde{F}_K^2\tilde{M}_K^2 = \frac{pqr}{2}\left(\frac{1}{q}+1\right)\Bigg\{F_\pi^2 M_\pi^2 X(3) + M_\pi^4 pqr[Y(3)]^2\left[16\left(\frac{1}{q}+2\right)L_6^r + 8\left(\frac{1}{q}+1\right)L_8^r\right] - M_\pi^4\frac{1}{32\pi^2}pqr[Y(3)]^2\left[\frac{3}{2}\log\frac{\overset{\circ}{\tilde{M}}_\pi^2}{\mu^2} + \frac{3}{2}\left(\frac{1}{q}+1\right)\log\frac{\overset{\circ}{\tilde{M}}_K^2}{\mu^2} + \frac{5}{18}\left(\frac{2}{q}+1\right)\log\frac{\overset{\circ}{\tilde{M}}_\eta^2}{\mu^2}\right]\Bigg\} + \tilde{F}_K^2\tilde{M}_K^2\tilde{d}_K \tag{4.7}$$

$\tilde{d}_P$ are the relative remainders of order $O(\tilde{m}_q^2)$. The low-energy constants L_i^r, being quark mass independent, are identical for the chiral expansions of X and $\tilde{X}$. Following the discussion of Chapter 3, they can be re-expressed in terms of the parameters $X(3)$, $Z(3)$, r, the physical decay constant and mass F_π^2, M_π^2, F_K^2, M_K^2, and the higher-order remainders at the physical point as in equations (3.24)-(3.27).

We proceed in a similar fashion for the vector and scalar form factors:

$$\begin{aligned}\tilde{F}_\pi\tilde{F}_K\tilde{f}_+(t) = &\frac{\tilde{F}_\pi^2+\tilde{F}_K^2}{2} + \frac{3}{2}[t\tilde{M}^r_{K\pi}(t) + t\tilde{M}^r_{K\eta}(t) - \tilde{L}_{K\pi}(t) - \tilde{L}_{K\eta}(t)] \\ &+ 2tL_9^r + \tilde{F}_\pi\tilde{F}_K\tilde{d}_+ + \tilde{t}e_+\end{aligned} \tag{4.8}$$

$$\begin{aligned}\tilde{F}_\pi\tilde{F}_K\tilde{f}_0(t) = &\frac{\tilde{F}_K^2+\tilde{F}_\pi^2}{2} + \frac{t}{\tilde{\Delta}_{K\pi}}\frac{\tilde{F}_K^2-\tilde{F}_\pi^2}{2} - \frac{3}{2}\tilde{L}_{K\pi}(t) - \frac{3}{2}\tilde{L}_{K\eta}(t) \\ &+ \frac{t}{4\tilde{\Delta}_{K\pi}}\tilde{K}_{K\pi}(t)\left[5(t-\tilde{M}_\pi^2-\tilde{M}_K^2) + \frac{3}{2}\left(\frac{1}{q}+3\right)pqrM_\pi^2Y(3)\right] \\ &- \frac{t}{4\tilde{\Delta}_{K\pi}}\tilde{K}_{K\eta}(t)\left[3(t-\tilde{M}_\pi^2-\tilde{M}_K^2) + \frac{1}{2}\left(\frac{1}{q}+3\right)pqrM_\pi^2Y(3)\right] \\ &+ (\tilde{F}_\pi\tilde{F}_K\tilde{d}_+ + t\tilde{e}_+)\left(1-\frac{t}{\tilde{\Delta}_{K\pi}}\right) + (\tilde{F}_\pi\tilde{F}_K\tilde{d}_- + t\tilde{e}_-)\frac{t}{\tilde{\Delta}_{K\pi}}\end{aligned} \tag{4.9}$$

Following the prescription discussed in sec. 3.3.2, the functions $\tilde{L}_{PQ}(t)$, $\tilde{K}_{PQ}(t)$, $\tilde{M}_{PQ}(t)$ are evaluated with the leading-order pseudoscalar masses at the simulated quark masses using eq. (4.5), apart from the $\bar{J}_{PQ}$ function which is evaluated at the simulated pion and kaon masses using eqs. (4.3)-(4.4) and (4.6)-(4.7). In the formulae (4.8) and (4.9), the decay constants on the right-hand side arise from the reexpression of L_4 and L_5, and should be understood as a short-hand notation of the full expressions in eqs. (4.3)-(4.4). For the vector form factor, we can trade L_9 for the pion electromagnetic square radius using eq. (3.74).

We will then use the following inputs for the evaluation of the various observables:

- $\tilde{F}_\pi^2$, $\tilde{F}_K^2$, $\tilde{F}_\pi^2\tilde{M}_\pi^2$, $\tilde{F}_K^2\tilde{M}_K^2$ (eqs. (4.3)-(4.4) and eqs. (4.6)-(4.7) respectively) for different values of the quark masses $\tilde{m}$ and $\tilde{m}_s$, for the collaborations PACS-CS and RBC/UKQCD
- $\tilde{F}_\pi\tilde{F}_K\tilde{f}_+$, $\tilde{F}_\pi\tilde{F}_K\tilde{f}_0$ (eqs. (4.8)-(4.9)) for different values of the quark mass $\tilde{m}$ (and identical $\tilde{m}_s$) and for several transfer momenta t for RBC/UKQCD.

There are several parameters entering the fits:

- The leading-order parameters of Resummed χPT, $X(3)$ and $Z(3)$, and the quark mass ratio r (eqs. (3.13) and (3.14)).
- The value of p_{ref}, which is defined as $p_{ref} = \tilde{m}_{s,ref}/m_s$, for a data set of reference. It provides the equivalence between the lattice and the physical quark masses.
- The ratio of the pion and kaon decay constants, F_K/F_π, left in our fit as a free parameter.
- The higher-order remainders d, d', e, e' (for all the fits), and also d_+, e_+, d_-, e_-, e_π^V when the data for the $K_{\ell 3}$ form factors is involved.

The expressions for the simulated observables involve the higher order remainders whose precise value is unknown (see sec. 3.4.2 and sec. 3.4.1). We can use the expected scaling of the remainders in simulations where $\tilde{m}_s$ is significantly larger than $\tilde{m}$ to perform their extrapolation to the simulated quark masses. From the discussion of sec. 3.4.2, we have $\tilde{d}' = O(\tilde{m}, \tilde{m}_s) \simeq p^2qrd'$, $\tilde{d} = O(\tilde{m}_s^2) = p^2d$, the same holds for e' and e respectively. Therefore we obtain the scaling:

$$\tilde{d}_\pi = p^2 d - p^2 qrd', \quad \tilde{d}_K = \left(\frac{F_K M_K}{F_\pi M_\pi}\right)^2 p^2 \frac{r+1}{2}\left(d - \frac{r+1}{2} qrd'\right) \tag{4.10}$$

$$\tilde{e}_\pi = p^2 e - p^2 qre', \quad \tilde{e}_K = \left(\frac{F_K}{F_\pi}\right)^2 p^2 \left(e - \frac{r+1}{2} qre'\right) \tag{4.11}$$

The input values for the remainders e, d, $e^{'}$, $d^{'}$, e_+, d_+, e_-, d_- can be found in table 3.4.2.

The quantity p_{ref} is estimated for both collaborations, but in order to take partially into account systematic effects related to the determination of lattice spacing and quark masses, we keep this parameter free in our fits. Since the quark masses are expressed in a mass-independent scheme involving only multiplicative renormalization, we can determine the value of p for any data set once we know p for a given reference set using $\tilde{m}_s = (\tilde{m}_s/\tilde{m}_{s,ref}) \times p_{ref}$.

When computing the values of the observables from the chiral series eqs. (4.3)-(4.4), (4.6)-(4.7), and (4.8)-(4.9), we need the value of the decay constants and masses on the lattice, $\tilde{F}_P^2$, $\tilde{M}_P^2$, for the simulated quark masses (for instance the unitarity functions $\bar{J}$). Therefore, we computed systematically the values of the decay constants and masses from the lattice counterparts of their chiral expansions, eqs. (4.3)-(4.4) and eqs. (4.6)-(4.7), rather than plugging their values obtained from the lattice simulations. This distinction may have some importance for the $K_{\ell 3}$ form factors, eqs. (3.97) and (3.104), where we have re-expressed L_4 and L_5 in terms of $\tilde{F}_\pi^2$ and $\tilde{F}_K^2$.

Moreover, the mass $\tilde{M}_\eta$ and decay constant $\tilde{F}_\eta$ of the η are needed for the evaluation of the one-loop integral $\bar{J}_{PQ}$ (and the other unitary functions K, L, M, see Appendix A.1). They are obtained at sufficient accuracy for such purposes using the two following leading-order formulae reminiscent of the Gell-Mann-Okubo formula (see eqs. (6.6) and (6.7) in Chapter 5):

$$\tilde{F}_\eta^2 = \frac{4}{3}\tilde{F}_K^2 - \frac{1}{3}\tilde{F}_\pi^2, \quad \tilde{F}_\eta^2 \tilde{M}_\eta^2 = \frac{4}{3}\tilde{F}_K^2 \tilde{M}_K^2 - \frac{1}{3}\tilde{F}_\pi^2 \tilde{M}_\pi^2 \tag{4.12}$$

To perform the fit we minimize a standard χ^2 function built from the observables considered, using the "MINUIT" routine from the CERN program library. The uncertainties on the simulated quantities are obtained by combining the uncertainties in quadrature; no correlation between the different observables is provided in the articles of both collaborations. Only the statistical errors are available, there is no estimate for the systematic uncertainties for any of the relevant quantities. Furthermore, we propagate the errors exploiting the covariance matrix provided by the "MINOS" subroutine of the MINUIT package, assuming a gaussian distribution for all the uncertainties calculated by MINUIT.

4.3.2 Results and discussion

Our results are summarized in table 4.7. The first seven rows correspond to the outcome of the fit, whereas the lower rows are quantities derived from the results of the fit (leading and next-to-leading order low-energy constants, quantities in the $N_f = 2$ chiral limit, $K_{\ell 3}$ quantities, and the relative fraction of LO/NLO/remainders contributions at the minimum of the χ^2 for decay constants and masses), and the last row is the χ^2 per degree of freedom.

	PACS − CS Without $K_{\ell 3}$	RBC/UKQCD With $K_{\ell 3}$
r	26.5 ± 2.3	23.2 ± 1.5
$X(3)$	0.59 ± 0.21	0.20 ± 0.14
$Y(3)$	0.90 ± 0.22	0.43 ± 0.30
$Z(3)$	0.66 ± 0.09	0.46 ± 0.04
F_K/F_π	1.237 ± 0.025	1.148 ± 0.015
Rem. at limit	none	d, e
$\tilde{m}_{s,ref}/m_s$	1.24 ± 0.08	$1.15^\star$
$m_s(2\text{ GeV})$[MeV]	70 ± 4	107
$m(2\text{ GeV})$[MeV]	2.6 ± 0.3	4.6 ± 0.3
$B_0(2\text{ GeV})$[GeV]	3.34 ± 1.18	0.92 ± 0.67
F_0[MeV]	74.8 ± 4.9	62.2 ± 2.5
$L_4(\mu) \cdot 10^3$	-0.1 ± 0.2	2.4 ± 2.0
$L_5(\mu) \cdot 10^3$	1.8 ± 0.4	1.8 ± 1.6
$L_6(\mu) \cdot 10^3$	0.1 ± 0.4	4.7 ± 7.1
$L_8(\mu) \cdot 10^3$	0.8 ± 0.7	4.4 ± 7.1
$L_9(\mu) \cdot 10^3$	$\times$	4.4 ± 2.8
$X(2)$	0.90 ± 0.01	0.90 ± 0.02
$Y(2)$	1.04 ± 0.02	1.00 ± 0.03
$Z(2)$	0.87 ± 0.02	0.90 ± 0.02
$B(2\text{ GeV})$[GeV]	3.83 ± 0.50	2.09 ± 0.19
F[MeV]	85.8 ± 0.7	87.7 ± 0.8
$\bar{\ell}_3$	5.0 ± 2.1	-0.6 ± 3.7
$\bar{\ell}_4$	4.5 ± 0.5	3.3 ± 0.5
Σ/Σ_0	1.51 ± 0.51	4.52 ± 2.83
B/B_0	1.15 ± 0.26	2.28 ± 1.39
F/F_0	1.15 ± 0.08	1.41 ± 0.06
$f_+(0)$	1.004 ± 0.149	0.985 ± 0.008
$\Delta_{CT} \cdot 10^3$	$\times$	-0.2 ± 12.1
$\Delta'_{CT} \cdot 10^3$	$\times$	-126 ± 104
$\langle r^2 \rangle_V^{K^+}$[fm^2]	$\times$	0.248 ± 0.156
$\langle r^2 \rangle_V^{K^0}$[fm^2]	$\times$	-0.027 ± 0.106
F_π^2	$0.66 + 0.22 + 0.12$	$0.45 + 0.69 - 0.14$
F_K^2	$0.44 + 0.48 + 0.08$	$0.34 + 0.76 - 0.10$
$F_\pi^2 M_\pi^2$	$0.60 + 0.30 + 0.10$	$0.20 + 0.95 - 0.15$
$F_K^2 M_K^2$	$0.42 + 0.50 + 0.08$	$0.14 + 0.97 - 0.11$
$F_\pi F_K f_+(0)$	$\times$	$0.40 + 0.75 - 0.15$
χ^2/N	0.9/3	4.4/8

Table 4.7: Results of fits performed on the data from the PACS-CS [96] and RBC/UKQCD [99, 100, 101] collaborations on pseudoscalar masses and decay constants, and $K_{\ell 3}$ form factors in the case of RBC/UKQCD. In all cases, only statistical errors are shown. In the RBC/UKQCD case, we fixed the lattice strange quark mass (marked with a star). The LECs are given at the scale $\mu = m_\rho$. In the PACS-CS case, the $K_{\ell 3}$ form factor at zero momentum transfer is a prediction of the fit (with an error combining those obtained from the fit and the maximal contribution allowed for the remainder from dimensional estimation). The penultimate set of rows collects the relative fractions of LO/NLO/remainders for decay constants, masses and $K_{\ell 3}$ form factor at vanishing transfer momentum (for RBC/UKQCD) at the minimum.

General remarks

The fit of RBC/UKQCD results includes only a limited number of data points for the decay constants and masses, which forces us to fix one of the parameters of the fit − the simulated strange quark mass. Letting all parameters free gives comparable results for the central values, but some parameters get very large uncertainties, larger than their allowed range. Therefore, propagating the errors in such a situation would be meaningless, and reporting the results of this fit would not provide much information than the constrained fit presented here.

It is also necessary to impose some bounds on the size of the higher-order remainders, based on an estimate from resonance saturation as explained in sec. 4.3.1. Indeed, some of these remainders are pushed to the limits of their range when the set of data is too small, because there is not enough information for MINUIT to choose a particular value for these remainders, while keeping them free would lead to a larger contribution from higher orders and a further decrease of the leading-order contribution. Nonetheless, the situation improves when data points for higher masses and momenta are included, so that remainders remains small, within the rescaled window estimated in sec. 4.3.1 − the corresponding table is provided in Appendix C.

From a qualitative point of view, it is interesting to notice that the results from RBC/UKQCD are consistent with the fits to the PACS-CS data: r is close to 25, i.e., close to the ratio $2M_K^2/M_\pi^2 - 1$, even though its value is left free in our framework. Also, we observe in both cases a suppression of the two order parameters: the quark condensate remains around $X(3) \sim 0.5$, and the squared decay constant is $Z(3) \sim 0.6$, leading to a value for the leading-order term of the squared pion mass $Y(3) \sim 0.8$.

Furthermore, the ratio of decay constants F_K/F_π, left free in our fit, comes out slightly larger (respectively smaller) for PACS-CS (respectively for RBC/UKQCD) than its Standard Model value, eq. 3.20, in the fit for the decay constants and masses, illustrating the impact of the chiral extrapolation for the extraction of F_K/F_π. We obtain also values of simulated strange quark masses and the physical mass in good agreement with the results obtained by the two collaborations, the discrepancy between the two collaboration coming from the different choice of renormalization procedure (which explains the low value obtained from the PACS-CS data [97]). A later article of the same collaboration [97] considered simulations directly performed at the physical point including non-perturbative renormalization. This has induced a significant modification for the quark mass renormalisation factor, becoming $Z_m = 1.441(15)$ (non-perturbative) instead of $Z_m = 1.114$ (one-loop perturbation theory) leading to an increase (decrease) in the values of quark masses (condensates) by a factor 1.30.

r	31.2 ± 2.7
F_K/F_π	1.333 ± 0.072
$m_s(2\text{ GeV})$[MeV]	$92.75 \pm 0.58 \pm 0.95$
$m(2\text{ GeV})$[MeV]	$2.97 \pm 0.28 \pm 0.03$

Table 4.8: Results obtained from the PACS-CS collaboration [97] with non-perturbative renormalization and simulation at the physical point.

This should be taken into account when comparing the results obtained from the PACS-CS and RBC/UKQCD sets in this thesis. The results obtained in ref. [97] that are relevant for our discussion are summarised in table 4.8, and can be compared with table 4.6. Since the simulation was performed at the physical point, there is no further information on low-energy constants describing the pattern of $N_f = 2$ and $N_f = 3$ chiral symmetry breakings.

Order parameters

The decay constant in the $N_f = 3$ chiral limit (central values of F_0 at 74.8 and 62.2 MeV for PACS-CS and RBC/UKQCD respectively) is found to be rather low, in agreement with other recent works [111, 112]. The pattern of $N_f = 3$ chiral symmetry breaking (with low quark condensate and decay constant) is reflected by the values obtained for the low energy constants L_4 and L_6, which are both positive and do not show any sign of Zweig rule violation (see sec. 2.7.1). As discussed in sec. 3.4.3, positive values of L_4 and L_6 are known to induce a significant dependence of the LO chiral order parameters on the strange quark mass, and therefore it is not surprising to witness a strong supression from the $N_f = 2$ chiral limit to the $N_f = 3$ one.

Let us notice that we obtain values for $N_f = 2$ chiral order parameters which are in agreement with the hypothesis of standard χPT, confirming that this framework is appropriate for the $N_f = 2$ sector as shown by the recent data on $K_{\ell 4}$ decays [62, 63], though this does not seem to be the case for $N_f = 3$. The other low energy constants $L_{5,8,9}$ have values in agreement with conventional estimates − this was expected in particular for L_9 since the resummed framework induces only minor modifications compared to the usual treatment of chiral expansions for vector quantities such as the pion electromagnetic form factor.

In chiral expansions, tadpole diagrams generate chiral logarithms of the form $M_P^2 \log(M_P^2/\mu^2)$ which can prove troublesome to fit. For instance, the RBC/UKQCD collaboration [99, 100, 101] finds a better agreement of their data on decay constants with polynomial fits than with chiral series. In our treatment, these chiral logarithms always involve the leading-order mass $\overset{\circ}{M}{}_P^2$. Therefore, a small value of $Y(3)$ tames the chiral logarithms of the form $\overset{\circ}{M}{}_P^2 \log(\overset{\circ}{M}{}_P^2/\mu^2)$ in our expansions, so that they become hard to distinguish from a polynomial at the numerical level on the range of masses where Chiral Perturbation Theory could be valid.

Furthermore, large contributions from next-to-leading order low energy constants, and in particular L_4 and L_6 as just discussed, will enhance the quadratic dependance on the quark masses, and thus the chiral expressions in the resummed framework shall mimic a polynomial dependence on the quark masses that can not be reproduced in the more usual treatment of chiral expansions. These mechanisms could explain why chiral logarithms are often difficult to identify in lattice data, in addition to other effects like a heavy strange quark mass or lattice systematics.

$K_{\ell 3}$ form factors

The $K_{\ell 3}$ form factor at zero momentum transfer, $f_+(0) = f_0(0)$, involves only the low energy constants $L_{4,5,6,8}$, related to decay constants and masses (eq. 3.97). In principle, it can be predicted from a fit of the latter quantities up to the determination of the remainder d_+. We quote the corresponding results in table 4.7, where the central value for $f_+(0)$ corresponds to the remainders set to zero. The uncertainty on this quantity includes the maximal size allowed for the remainder d_+ based on the dimensional estimate presented in table 3.4.2, as well as the uncertainties coming from the parameters of the fit. Indeed, the higher-order remainder d_+ hinders any accurate determination of $f_+(0)$, unless its value is also precisely determined from the fit, which is possible once data on $K_{\ell 3}$ form factors themselves is included (second column of table 4.7).

The obtained values for $f_+(0)$ are somewhat larger than the Standard Model value, eq. (3.96), as well as those obtained from the RBC/UKQCD collaboration using different forms for the extrapolation in quark masses [100, 101]. This illustrates the importance of the mass extrapolation for lattice simulations at the level of accuracy which is currently aimed. A particular attention was paid in ref. [101] to the structure of the chiral expansion of $f_+(0) = 1 + f_2 + f_4$, where f_2 is the next-to-leading order contribution and f_4 all the higher orders. It only involves a combination of chiral logarithms, divided by F_0^2:

$$f_2 = -\frac{3}{256\pi^2 F_0^2}\left[(M_K^2 + M_\pi^2)h\Big(\frac{M_\pi^2}{M_K^2}\Big) + (M_K^2 + M_\eta^2)h\Big(\frac{M_\eta^2}{M_K^2}\Big)\right], \quad h(x) = 1 + \frac{2x}{1-x^2}\log x \tag{4.13}$$

f_2 is free from low energy constants, and thus is said to be known precisely from Chiral Perturbation Theory. This statement is not totally correct for the following reasons: one assumes that the value of F_0 is close to that of F_π, so it can be replaced in actual calculations by the physical value of the pion decay constant, leading to the estimate $f_2 \simeq -0.023$. Since the difference between the two quantities is a higher-order effect, one can always perform this replacement. However, using such a prescription, one has to determine how large the higher-order term f_4 can be − and consequently how well the chiral series for f_+ converges. If F_0 is significantly lower than F_π, this forces us to treat the next-to-leading order contribution to $f_+(0)$ more carefully. Besides, we advocated that correlators of vector and axial currents yield observables with good convergence properties, selecting $F_\pi F_K f_0(0)$. In this case, we shou ld replace F_0^2 by $F_\pi F_K$ in the evaluation of eq. (4.13), as can be checked in our expression for f_+, eq. (3.97).

Finally, once the $K_{\ell 3}$ form factors are included in our fits, L_9 can be determined from the pion electromagnetic radius $\langle r^2\rangle_V^\pi$ even though the fit does not constrain tightly this particular low-energy constant. In table 4.7, the deviations from the Callan-Treiman relation at $t = \Delta_{K\pi}$ and its soft-kaon analog at $-\Delta_{K\pi}$ are given. Their values are of the expected size for chiral-symmetry breaking quantities for $N_f = 2$ or 3 flavours respectively, and thus with the ones obtained in standard Chiral Perturbation Theory, eq. (3.111). The value of the square radii of the charged and neutral kaons, also shown, have rather large uncertainties and thus within experimental errors bars, eqs. (3.85-3.88).

Convergence of chiral series

In the last lines of table 4.7 (the five rows before the last), we have indicated for each fit the contribution from leading, next-to-leading, and higher order remainders, to decay constants and masses for values of the parameters at the minimum of the fit. We can see that the series converge well on overall (the HO remainders being much smaller than the sum $LO + NLO$), but that the leading order term is far from saturating the series. The values of $Y(3)$ obtained is smaller than 1, reducing the contribution from chiral logarithms compared to that from the next-to-leading order low energy constants. We see that the results are different from the results obtained by the collaborations.

Now does the choice of the chiral series (resummed or standard) have any specific impacts on the results of the fit ? We can compare the results obtained from the resummed framework (table 4.7) with those from a fit of the same observables, where the next-to-leading and higher-order contributions (chiral logarithms μ_P, low energy constants L_i, and the remainders) are computed replacing $2mB_0$, $(m + m_s)B_0$ and F_0 by the physical pion and kaon masses and the pion decay constant. This is equivalent to performing the same fit as before with the following replacements in the next-to-leading order and higher-order contributions:

$$r \to 2\frac{M_K^2}{M_\pi^2} - 1, \quad q \to \frac{\tilde{M}_\pi^2}{2\tilde{M}_K^2 - \tilde{M}_\pi^2}, \quad p \to \frac{2\tilde{M}_K^2 - \tilde{M}_\pi^2}{2M_K^2 - M_\pi^2}, \quad Y(3) \to 1 \tag{4.14}$$

$$\eta(r) \to \eta(r_0), \qquad \epsilon(r) \to \epsilon(r_0) - 2X(3)\frac{r - r_0}{r_0^2 - 1}, \quad \log\frac{\overset{\circ}{M}{}_P^2}{\mu^2} \to \log\frac{M_P^2}{\mu^2} \tag{4.15}$$

both for the observables that we consider, eqs. (4.3)-(4.4), (4.6)-(4.7) and eqs. (4.8-4.9); and the equations allowing the determination of $L_{4,5,6,8,9}$, eqs. (3.74) and (3.36)-(3.39). For PACS-CS collaboration, this leads to a χ^2 over degrees of freedom N: $\chi^2/N = 1.1/3$ - compared to our result 0.9/3, with very similar values for the fundamental parameters $r, X(3), Y(3), Z(3)$. For RBC/UKQCD, the fitting procedure yields $\chi^2/N = 9.5/8$ (compared to our result 4.4/8), with much more uncertain values of the fundamental parameters (i.e. $r = 14.9 \pm 12.1$, $X(3) = 0.30 \pm 0.26$, $Y(3) = 0.68 \pm 0.60$). This is not particularly surprising since our fits to the PACS-CS data led to values of r and $Y(3)$ in good agreement with eq. (4.14), but not the RBC/UKQCD ones. The corresponding convergence of the pseudoscalar masses and decay constants is then, with the relative contribution for leading, next-to-leading and higher orders:

Observable	PACS-CS	RBC/UKQCD
F_π^2	$0.64 + 0.26 + 0.10$	$0.45 + 0.70 - 0.15$
F_K^2	$0.42 + 0.51 + 0.07$	$0.34 + 0.76 - 0.10$
$F_\pi^2 M_\pi^2$	$0.67 + 0.24 + 0.09$	$0.31 + 0.81 - 0.12$
$F_K^2 M_K^2$	$0.50 + 0.44 + 0.06$	$0.15 + 0.94 - 0.11$

Table 4.9: Sum of the relative contributions $LO + NLO + HO$ in the case of physical masses and pion decay constant.

There is no saturation of the series by their leading order. We see that our formulae yields results that are in good agreement with those obtained after reexpressing the next-to-leading order contributions in terms of F_π, M_π, M_K in the PACS-CS case, where $Y(3)$ is close to 1. On the other hand, when $Y(3)$ is not close to 1 (for instance, in the RBC/UKQCD case), our formulae provide more efficient and accurate fits (lower χ^2 and smaller error bars). From a more methodological point of view, we avoid a perturbative reexpression of low energy constants in terms of F_π, M_π, M_K, in a regime where it is not justified.

Our results confirm the difficulties reported by the two collaborations to fit $N_f = 3$ next-to-leading order chiral expressions usually used, and highlights the improvement provided by our ReχPT formulae for the extrapolations in quark masses of these quantities. As a further check, we have performed fits where we have taken that the physical masses (and not the leading-order ones) in the unitarity functions J, K, L, M and the argument of the chiral logarithms (similarly to what was done in ref. [83]). The quality and parameters of the fits are almost unchanged, and the outcome for the derived quantities is also very similar, meaning that the relevant issue is the proper choice of the "good observables" whose chiral series converge well.

4.3.3 Impact of alternative treatments of unitarity contributions

As discussed in sec. 3.7, there exist alternative prescriptions concerning the replacement of leading order masses $\overset{\circ}{M}{}_P^2$ by their physical values in the unitarity contributions. We have indicated that the prescription adopted in ref. [92] and in the present thesis exhibits a logarithmic divergence when $Y(3) \to 0$. As pointed out in ref. [85], one can avoid this

unwelcome divergence by replacing the leading order masses by the physical ones in $J^r_{PQ}(0)$ in Z_u. This induces very limited changes in our analyses, i.e. the following change in the expressions of the form factors:

$$t \log \frac{\overset{\circ}{M}{}^2_P}{\mu^2} \to t \log \frac{M_P^2}{\mu^2} \tag{4.16}$$

whereas masses and decay constants remain unaffected. leading order masses should then be replaced by physical masses in the arguments of the logarithms for $F_\pi^2 F_V^\pi$, eq. (3.66), and $\langle r^2 \rangle_V^\pi$, eq. (3.71), the definition of L_9^r in eq. (3.74), $F_K^2 F_V^{K^+}$, eq. (3.77) and $F_K^2 F_V^{K^0}$, eq. (3.78), as well as $\langle r^2 \rangle_{K^+}^\pi$, eq. (3.82). We have performed the RBC/UKQCD fit with this new prescription [2]. As could be expected from the outcome of the fit with $Y(3)$ not extremely close to 1, there is almost no change with respect to the previous fit, with a $\chi^2 = 4.4/8$ and values of the fundamental parameters almost unchanged:

$$r = 23.2 \pm 1.7, \quad X(3) = 0.20 \pm 0.16, \quad Y(3) = 0.44 \pm 0.34, \quad Z(3) = 0.46 \pm 0.04 \tag{4.17}$$

L_9 is unaffected, but the predictions for the kaon radii are slightly modified:

$$\langle r^2 \rangle_V^{K^+} = 0.220 \pm 0.155 \text{ fm}^2, \quad \langle r^2 \rangle_V^{K^0} = -0.028 \pm 0.106 \text{ fm}^2 \tag{4.18}$$

We see that even in this case where $Y(3)$ can be rather small (but not strictly zero), the overall picture is not modified by different prescriptions concerning the logarithms coming from $J^r_{PQ}(0)$ in Z_u and affecting (in principle) the chiral expansion of the form factors.

As described in sec. 3.7, other prescriptions have been proposed to modifiy the unitarity part of the chiral expansions in order to ensure that higher-order remainders will be small. In order to check the stability of our results, we have also performed a fit of the RBC/UKQCD data with the prescription of ref. [81]. We obtain a slightly better fit $\chi^2 = 4.0/8$, with essentially the same fundamental parameters:

$$r = 23.1 \pm 1.4, \quad X(3) = 0.19 \pm 0.13, \quad Y(3) = 0.43 \pm 0.30, \quad Z(3) = 0.44 \pm 0.03 \tag{4.19}$$

A few quantities are slightly modified:

$$\frac{F_K}{F_\pi} = 1.152 \pm 0.013, \quad F_0 = 61.4 \pm 2.2 \text{ MeV}, \quad L_5(M_\rho) \cdot 10^3 = 3.0 \pm 2.4, \quad \langle r^2 \rangle_V^{K^+} = 0.220 \pm 0.155 \text{ fm}^2 \tag{4.20}$$

whereas the rest of the outcome is essentially unchanged. We see therefore that the prescriptions of refs. [81] and [92], though different in principle, yield very similar results in practice, which gives us further confidence in the stability of our results with respect to the prescriptions adopted for the unitarity and tadpole contributions.

4.4 Summary

In this chapter, we presented the methods and results found in ref. [92]. We used the $2+1$ lattice data provided by the RBC/UKQCD [99, 100, 101] and PACS-CS [96] collaborations, in order to fit the expressions of decay constants, masses and $K_{\ell 3}$ form factors obtained in the framework of Resummed χPT. After a presentation of our fitting method, we shown our results and discussed their various issues. We pinpoint here the main tendencies:

[2] The fit of PACS-CS involves masses and decay constants only and is not affected by the change of prescription.

- The decay constant and the quark condensate in the $N_f = 3$ limit ($m_u = m_d = m_s = 0$) are both small and suppressed compared to the $N_f = 2$ case ($m_u = m_d = 0$ and m_s physical).
- The low-energy constants L_4 and L_6 do not follow the Zweig rule suppression generally advocated to set them to zero at the η-mass scale.
- The other low-energy constants L_5, L_8 and L_9 have values in good agreement with usual estimates.
- The ratio of quark masses r remains quite close to the most simple estimate from pseudoscalar masses.
- $N_f = 2$ chiral order parameters are in good agreement with the values extracted from $K_{\ell 4}$ decays.
- When the sets of data are large enough, the NNLO remainders remain in the expected range from a naive dimensional estimate.
- The expected numerical competition between leading and next-to-leading order chiral expansions indeed occurs for F_π^2, F_K^2, $F_\pi^2 M_\pi^2$ and $F_K^2 M_K^2$.

Beyond this description of the pattern of $N_f = 3$ chiral symmetry breaking and its implication for the convergence of chiral expansions, we point out that the values obtained for the kaon electromagnetic radii are in good agreement with experimental data. In the case of RBC/UKQCD, the value obtained for the $K_{\ell 3}$ form factor $f_+(0)$ with our fits is slightly larger than the ones quoted by the collaboration, relying on alternative formulae for the chiral expansion of the $K_{\ell 3}$ form factors. This has naturally an impact on the determination of $|V_{us}|$, considering the level of accuracy achieved in $K_{\ell 3}$ decays [66, 67].

We should also emphasize that the framework of Resummed χPT used in those fits *does not* contain any bias concerning the size of $X(3)$, $Y(3)$ and $Z(3)$ or on the relative size of the leading and next-to-leading orders contributions. It is compatible with the usual assumptions that chiral series of decay constants, squared masses and $K_{\ell 3}$ form factors are saturated by their leading order contribution, but it also accommodates situations where there is a numerical competition between leading order and next-to-leading order terms. It turns out that the lattice data set from the RBC/UKQCD and PACS-CS collaborations favour values for the three quantities $X(3), Y(3), Z(3)$ smaller than 1, with a χ^2/d.o.f. which ranges from fairly good to excellent.

Finally, lattice simulations could provide a valuable tool to investigate some issues related to the structure of QCD vacuum. In the two last chapters of this thesis, we shall turn to the study of the two topological quantities introduced in Chapter 1: the topological susceptibility and the fourth cumulant of the winding number, which will be studied in the light of Resummed χPT (Chapter 5). We will also include the topological susceptibility in the fits presented here and discuss further uses concerning lattice data (Chapter 6).

Chapter 5

Topological observables

5.1 Introduction

We have seen in the previous chapter that one can use the dependence of the spectrum of pseudoscalar mesons on the light quark masses to extract information on the quark condensate and the decay constant in the $N_f = 3$ chiral limit. Two alternative strategies are often used in lattice simulations to determine the three-flavour quark condensate, both being related to the topological properties of QCD on the lattice: the first one consists in studying the infrared end of the spectrum of the Dirac operator directly, as the accumulation of its eigenvalues around zero provides information on the value of the quark condensate [74, 113] (see sec. 1.4.4). We will not address this type of determination in this thesis, even though we notice that lattice determinations of the condensate by this method found a suppression for the three-flavour case ($\Sigma(2)/\Sigma(3) = 1.30 \pm 0.54$ in [117]). Another possibility consists in studying the topological susceptibility χ_t and the fourth cumulant c_4 of the winding number ν defined in the last paragraph of sec. 1.4.5, which will be the main focus of the present chapter.

The work presented in this chapter is the object of the articles [93, 94]. After having re-stated the definitions of χ_t and c_4, we will obtain their expressions up to next-to-leading order in $N_f = 3$ χPT, in the standard and in the Resummed frameworks. In particular, we will discuss the importance of identifying the η-pole in these results in order to minimize the size of higher order remainders. We will analyse briefly the potential of the topological suceptibility and the fourth cumulant to extract the pattern of three-flavour chiral symmetry breaking before drawing some first few conclusions.

5.2 Derivation through the effective potential

5.2.1 Structure of the one-loop generating functional

In the case of large volumes and small quark masses, the partition function is dominated by the lightest states of the theory, i.e. the pseudoscalar Goldstone bosons, and therefore it is possible to rely on Chiral Perturbation Theory to extract information concerning χ_t and c_4 through (1.83). Dealing with constant source terms, we can focus on modes with vanishing momentum, i.e. the matrix collecting the Goldstone bosons becomes independent of the space-time coordinates x:

$$Z[\theta_0, M] = \int [\mathcal{D}U] e^{-V\mathcal{L}_{eff}[U,\theta_0,M]} = e^{-VW[\theta_0,M]} \tag{5.1}$$

$\mathcal{L}_{eff}$ being the χPT lagrangian, and $\mathcal{W}$ is the Euclidean effective potential, which can

be derived at one-loop from the expression found in [2] in the Minkowskian metric. As shown in [3], in the case of finite-volume simulations with periodic boundary conditions, the effective theory is described by the same lagrangian as in the infinite volume. The properties of this partition function have been extensively studied in refs. [74, 113], and in particular the distribution of the winding number ν according to the leading-order chiral lagrangian.

The source $\theta(x)$ in the generating functional (see sec. 2.4.2) is only affected by axial flavour-singlet transformations, and thus connected to that of the (pseudo)scalar source term through (from (2.22) and (2.42)):

$$[s(x) + ip(x) = M,\ \theta(x) = \theta_0] \leftrightarrow [s(x) + ip(x) = g_L M g_R^\dagger,\ \theta(x) = \theta_0 + \arg(\det[M])] \quad (5.2)$$

with M being the general quark-mass matrix. If one of the quark masses is equal to zero, this transformation can also be used to shift the vacuum angle θ_0 by an arbitrary amount without modifying the theory: the χPT effective potential becomes independent of θ_0, and its derivatives, i.e., χ_t and c_4, should vanish in this limit.

In refs. [93, 119, 133], the same approach was carried out using the next-to-leading order chiral lagrangian in order to compute the chiral expansion of the topological susceptibility χ_t, using either the generic approach from the effective potential or diagrammatic analysis, and to assess its potential in extracting the three-flavour chiral condensate from lattice computations. In a similar way, the fourth cumulant c_4 can be computed at next-to-leading order χPT using the same methods.

We can follow the arguments of ref. [119] to derive the expression of the topological susceptibility and c_4 in an elegant way using the effective potential of the theory. The latter can be obtained from the one-loop generating functional Z discussed in sec. 2.5.4, but in the absence of a source term for the vacuum angle. This is however sufficient for our purposes, as a constant source term θ can be introduced in the effective potential via an anomalous $U_A(1)$ rotation which leaves the generating functional invariant: $Z(s + ip = s_0 + ip_0, \theta = \theta_0) = Z((s_0 + ip_0)e^{i\theta_0/N}, 0)$ (see eq. (2.43)).

The one-loop generating functional Z computed in [2] is thus enough for our purposes since we want to determine the contribution of order $O(\theta^4)$ in the effective potential. We set the sources

$$v_\mu = a_\mu = 0, (s + ip) = \mathcal{M}e^{i\theta/N} \qquad \mathcal{M} = \mathrm{diag}(m_1, \dots m_N) \quad (5.3)$$

where N denotes the number of light flavours considered (we use here the notation N instead of N_f to simplify the writing). It is easy to determine the classical solution to the leading order equation of motion under the form:

$$\bar{U} = (e^{i\alpha_1} \dots e^{i\alpha_N}) \qquad \sum_j \alpha_j = 0 \quad (5.4)$$

which should minimize the leading order lagrangian (eq. (2.46), extended to the case of an arbitrary number of flavours [115]):

$$\mathcal{L}_{eff}^{(2)} = F_N^2 B_N \sum_j m_j \cos(\phi_j) \quad (5.5)$$

with $\phi_j = \theta/N - \alpha_j$ under the condition that $\sum_j \phi_j = \theta$. This lagrangian involves the pseudoscalar decay constant F_N and the chiral condensate $\Sigma(N) = -F_N^2 B_N$ in the chiral limit of N massless flavours.

Using a Lagrange parameter, we can determine the minimum as an expansion in powers of θ [119]:

$$\phi_i = \frac{\bar{m}}{m_i}\theta + \left[\left(\frac{\bar{m}}{m_i}\right)^3 - \left(\frac{\bar{m}}{m_i}\right)\frac{\bar{m}^3}{\bar{m}^{[3]}}\right]\frac{\theta^3}{6} + O(\theta^5) \tag{5.6}$$

where we have introduced the notation for the various sums and harmonic means:

$$\bar{m}^{[k]} \equiv \frac{1}{\sum_j \frac{1}{m_j^k}}\,, \qquad s^{[k]} \equiv \sum_j m_j^k\,, \qquad \bar{m} \equiv \bar{m}^{[1]}\,, \qquad s \equiv s^{[1]} \tag{5.7}$$

We can then plug this expression into the one-loop generating functional Z (eq. (2.65)) evaluated at the point eq. (5.3) (there is no contribution from the anomalous part Z_A).

$$\begin{aligned} Z_t/V \to \sum_P &\left[\frac{N}{2(N^2-1)}F_N^2 - \frac{\overset{\circ}{M}{}_P^2}{32\pi^2}\log\frac{\overset{\circ}{M}{}_P^2}{\mu^2}\right]\sigma^\chi_{PP} \\ &+ 16B_N^2 L^r_{6;N}(\mu)\left(\sum_j m_j\cos\phi_j\right)^2 - 16B_N^2 L^r_{7;N}(\mu)\left(\sum_j m_j\sin\phi_j\right)^2 \\ &+ 8B_N^2 L^r_{8;N}(\mu)\sum_j m_j^2\cos 2\phi_j \end{aligned} \tag{5.8}$$

$$Z_u/V \to \frac{1}{4}\sum_{P,Q}\int dx\ J^r_{PQ}(x)\sigma^\chi_{PQ}\sigma^\chi_{QP} \tag{5.9}$$

with:

$$\begin{aligned} \sigma^\chi_{PQ} &= \frac{B_N}{4}\langle\{\lambda_P,\lambda_Q^\dagger\}(uMue^{-i\theta/N} + u^\dagger Mu^\dagger e^{i\theta/N})\rangle - \delta_{PQ}\ \overset{\circ}{M}{}_P^2 \\ &= \frac{B_N}{2}\langle\{\lambda_P,\lambda_Q^\dagger\}A\rangle \end{aligned} \tag{5.10}$$

$$u = (e^{i\alpha_1/2}\dots e^{i\alpha_n/2})\,, \qquad A = (m_1(\cos\phi_1 - 1),\dots m_N(\cos\phi_N - 1)) \tag{5.11}$$

$\overset{\circ}{M}{}_P^2$ denotes the leading-order contribution to the masses of the N^2-1 pseudoscalar mesons, J^r corresponds to the one-loop scalar integral with two mesons P and Q, and $\mathcal{L}^{(2)}_{eff}$ is the next-to-leading order chiral lagrangian (eq. (2.62)) collecting low-energy constants, in particular those denoted L_6, L_7, L_8 in the basis of operators in eq. (2.62) for $N = 3$ χPT.

Using eq. (5.6), we have the expansion of the trigonometric functions:

$$\sum_j m_j\cos\phi_j = s - \bar{m}\frac{\theta^2}{2} + \frac{\bar{m}^4}{\bar{m}^{[3]}}\frac{\theta^4}{24} + O(\theta^6) \tag{5.12}$$

$$\sum_j m_j\sin\phi_j = N\bar{m}\theta - N\frac{\bar{m}^4}{\bar{m}^{[3]}}\frac{\theta^3}{6} + O(\theta^6) \tag{5.13}$$

$$\sum_j m_j^2\cos 2\phi_j = s^{[2]} - 2N\bar{m}^2\theta^2 + \frac{2}{3}N\frac{\bar{m}^5}{\bar{m}^{[3]}}\theta^4 + O(\theta^6) \tag{5.14}$$

as well as the expansion of σ^χ:

$$\sigma^{\chi}_{PQ} = \frac{B_N}{2}\sum_i \{\lambda_P, \lambda_Q^\dagger\}_{ii} m_i \left[-\left(\frac{\bar{m}}{m_i}\right)^2 \frac{\theta^2}{2} + \left(\frac{\bar{m}}{m_i}\right)^2 \left[4\frac{\bar{m}^3}{\bar{m}^{[3]}} - 3\left(\frac{\bar{m}}{m_i}\right)^2 \right] \frac{\theta^4}{24} + O(\theta^6) \right] \tag{5.15}$$

and the scalar integral at vanishing transfer momentum (see Appendices A.1 and A.2 for a detailed account of $\bar{J}_{PQ}$ and σ^{χ}_{PQ}):

$$\int dx\, J^r_{PQ}(x) = -2k_{PQ} = -\frac{1}{16\pi^2} \frac{\overset{\circ}{M}{}^2_P \log \frac{\overset{\circ}{M}{}^2_P}{\mu^2} - \overset{\circ}{M}{}^2_Q \log \frac{\overset{\circ}{M}{}^2_Q}{\mu^2}}{\overset{\circ}{M}{}^2_P - \overset{\circ}{M}{}^2_Q} \tag{5.16}$$

so that all the elements in Z_t and Z_u are simple functions of the quark masses and the low-energy constants.

5.2.2 NLO expression of the topological susceptibility and the fourth cumulant

• **Topological susceptibility:**

We are now in a position to determine the one-loop expression of the first two cumulants of the winding number. At the order $O(\theta^2)$, needed for the topological susceptibility χ_t, one has the following contribution:

$$\begin{aligned} Z_t/V \;\to\; \frac{\theta^2}{2}\Bigg[& -B_N F_N^2 \bar{m} + B_0 \sum_{P,i} \frac{\overset{\circ}{M}{}^2_P}{64\pi^2} \log \frac{\overset{\circ}{M}{}^2_P}{\mu^2} \frac{\bar{m}^2}{m_i} \{\lambda_P, \lambda_P^\dagger\}_{ii} \qquad (5.17) \\ & -32B_N^2 L^r_{6;N}(\mu) s\bar{m} - 32B_0^2 L^r_{7;N}(\mu) N^2 \bar{m}^2 - 32B_0^2 L^r_{8;N}(\mu) N \bar{m}^2 \Bigg] \\ Z_u/V \;\to\; & 0 \qquad (5.18) \end{aligned}$$

Using the summation formula:

$$\sum_P \{\lambda_P, \lambda_P^\dagger\}_{ij} = \frac{4(N^2-1)}{N}\delta_{ij} \tag{5.19}$$

the expression of the topological susceptibility at one loop given in refs. [93, 119, 133] is recovered in a straightforward way:

$$\begin{aligned} \chi_t = {} & B_N F_N^2 \bar{m} - B_N \sum_{P,i} \frac{\overset{\circ}{M}{}^2_P}{64\pi^2} \log \frac{\overset{\circ}{M}{}^2_P}{\mu^2} \frac{\bar{m}^2}{m_i} \{\lambda_P, \lambda_P^\dagger\}_{ii} \qquad (5.20) \\ & + 32B_N^2 L^r_{6;N}(\mu) s\bar{m} + 32B_N^2 N[N L^r_{7;N}(\mu) + L^r_{8;N}(\mu)]\bar{m}^2 \end{aligned}$$

Let us notice that ref. [119] obtained this result by determining the classical solution eq. (5.6) corresponding to the minimum of the chiral Lagrangian up to next-to-leading order. This is actually an unnecessary complication, since the expression of the one-loop effective potential given in ref. [2] is precisely designed to require the classical solution from the leading-order Lagrangian only. Indeed we recover the expression of the topological susceptibility without performing the same elaborate minimization of ref. [119].

In the case of $N_f = 3$, we have performed the calculation keeping all orders in strong isospin-breaking and obtained (the meaning of the notation "no pole" will be explained in the following section when we perform the same calculations using diagrammatic methods):

$$\begin{aligned}\chi_t^{\text{no pole}} &= \bar{m}F_0^2B_0 + 32\bar{m}(m_u+m_d+m_s)B_0^2L_6^r(\mu) + 96\bar{m}^2B_0^2(3L_7+L_8^r(\mu)) \\ &- \frac{\bar{m}^2B_0}{32\pi^2}\times\Bigg[\sum_{i\neq j}\frac{(m_i+m_j)^2B_0}{m_im_j}\log\frac{B_0(m_i+m_j)}{\mu^2} \\ &+ \Big(\frac{m_u+m_d}{m_um_d}+\frac{2\sin\epsilon\cos\epsilon}{\sqrt{3}}\frac{m_d-m_u}{m_um_d} \\ &+ \frac{2}{3}\sin^2\epsilon\frac{2m_um_d-m_s(m_u+m_d)}{m_um_dm_s}\Big)\overset{\circ}{M}{}^2_{\pi^0}\log\frac{\overset{\circ}{M}{}^2_{\pi^0}}{\mu^2} \\ &+ \Big(\frac{4m_um_d+m_s(m_u+m_d)}{3m_um_dm_s}-\frac{2\sin\epsilon\cos\epsilon}{\sqrt{3}}\frac{m_d-m_u}{m_um_d} \\ &- \frac{2}{3}\sin^2\epsilon\frac{2m_um_d-m_s(m_u+m_d)}{m_um_dm_s}\Big)\overset{\circ}{M}{}^2_{\eta}\log\frac{\overset{\circ}{M}{}^2_{\eta}}{\mu^2}\Bigg] + O(m_q^3)\end{aligned} \tag{5.21}$$

This expression is indeed independent of the renormalization scale μ and agrees with ref. [119] in the isospin limit, as expected. In the isospin limit $m = m_u = m_d$ for $N = 3$ flavours, one has [93, 119, 133]:

$$\begin{aligned}\chi_t^{\text{no pole}} &= \frac{B_0F_0^2mm_s}{m+2m_s} \\ &+ \frac{32mm_sB_0^2L_6^r(\mu)(2m^2+5mm_s+2m_s^2)}{(m+2m_s)^2} + \frac{96m^2m_s^2B_0^2[3L_7+L_8^r(\mu)]}{(m+2m_s)^2} \\ &- \frac{3B_0^2m^2m_s^2}{8\pi^2(m+2m_s)^2}\log\frac{\overset{\circ}{M}{}^2_{\pi}}{\mu^2} - \frac{mm_sB_0^2(m+m_s)^2}{8\pi^2(m+2m_s)^2}\log\frac{\overset{\circ}{M}{}^2_{K}}{\mu^2} \\ &- \frac{mm_sB_0^2(2m+m_s)}{72\pi^2(m+2m_s)}\log\frac{\overset{\circ}{M}{}^2_{\eta}}{\mu^2} + \chi_t^{\text{no pole}}d_{\chi_t^{\text{no pole}}}\end{aligned} \tag{5.22}$$

where $d_{\chi_t^{\text{no pole}}}$ is a remainder collecting higher-order contributions, which starts at $O(m^2)$.

The leading order formula for the topological susceptibility was exploited by the TWQCD collaboration to extract the value of the three-flavour quark condensate [120] from RBC/UKQCD configurations with 2+1 domain-wall fermions [98]: $\Sigma(3, 2\text{ GeV}) = [259(6)(9)\text{ MeV}]^3$ (in the $\overline{MS}$ scheme). Another study was performed by the RBC and UKQCD collaborations based on data at larger volumes using the NLO formula [122], but it was not fully exploited as only a consistency check with the dependence on $m_{u,d}$ was performed and the three-flavour quark condensate was not determined by this method. It seems obvious that an accurate determination of the quark condensate from the topological susceptibility requires to go beyond a leading-order analysis, the same remark also applies for the fourth cumulant c_4.

• **Fourth cumulant:**

At the order $O(\theta^4)$ leading to the fourth cumulant c_4, the one-loop generating functional reads:

$$
\begin{aligned}
Z_t/V \;\to\; \frac{\theta^4}{24}\Bigg[& B_N F_N^2 \frac{\bar{m}^4}{\bar{m}^{[3]}} && (5.23)\\
& -B_N \sum_{P,i} \frac{\overset{\circ}{M}{}_P^{\,2}}{64\pi^2} \log \frac{\overset{\circ}{M}{}_P^{\,2}}{\mu^2} \{\lambda_P, \lambda_P^\dagger\}_{ii} \frac{\bar{m}^2}{m_i} \left[4\frac{\bar{m}^3}{\bar{m}^{[3]}} - 3\left(\frac{\bar{m}}{m_i}\right)^2 \right] \\
& +32 B_N^2 L^r_{6;N}(\mu) \left(\frac{s\bar{m}^4}{\bar{m}^{[3]}} + 3\bar{m}^2 \right) + 128 B_N^2 L^r_{7;N}(\mu) N^2 \frac{\bar{m}^5}{\bar{m}^{[3]}} && (5.24)\\
& +128 B_N^2 L^r_{8;N}(\mu) N \frac{\bar{m}^5}{\bar{m}^{[3]}} \Bigg] \\
Z_u/V \;\to\; & -\frac{\theta^4}{24} \frac{3B_N^2}{4} \bar{m}^4 \sum_{PQ} k_{PQ} \left(\sum_i \{\lambda_P, \lambda_Q^\dagger\}_{ii} \frac{1}{m_i} \right) \left(\sum_j \{\lambda_Q, \lambda_P^\dagger\}_{jj} \frac{1}{m_j} \right) && (5.25)
\end{aligned}
$$

which yields the one-loop expression of the fourth cumulant:

$$
\begin{aligned}
c_4 \;=\; & -B_N F_N^2 \frac{\bar{m}^4}{\bar{m}^{[3]}} + B_N \sum_{P,i} \frac{\overset{\circ}{M}{}_P^{\,2}}{64\pi^2} \log \frac{\overset{\circ}{M}{}_P^{\,2}}{\mu^2} \{\lambda_P, \lambda_P^\dagger\}_{ii} \frac{\bar{m}^2}{m_i} \left[4\frac{\bar{m}^3}{\bar{m}^{[3]}} - 3\left(\frac{\bar{m}}{m_i}\right)^2 \right] && (5.26)\\
& -32 B_N^2 L^r_{6;N}(\mu) \left(\frac{s\bar{m}^4}{\bar{m}^{[3]}} + 3\bar{m}^2 \right) - 128 B_N^2 N [N L^r_{7;N}(\mu) + L^r_{8;N}(\mu)] \frac{\bar{m}^5}{\bar{m}^{[3]}} \\
& + \frac{3B_N^2}{4} \bar{m}^4 \sum_{PQ} k_{PQ} \left(\sum_i \{\lambda_P, \lambda_Q^\dagger\}_{ii} \frac{1}{m_i} \right) \left(\sum_j \{\lambda_Q, \lambda_P^\dagger\}_{jj} \frac{1}{m_j} \right)
\end{aligned}
$$

To our knowledge, eq. (5.26) is the first next-to-leading order computation of the fourth cumulant in χPT. Let us add that this formula agrees with the leading-order result presented in ref. [119]. Equations (5.20) and (5.26) could be used in principle to derive the expression of χ_t and c_4 for an arbitrary number of flavours N. However, one should emphasise that the notation and definitions of the low-energy constants in these equations are derived from the three-flavour case which will be our main focus. In sec. 5.5, we will discuss how these formulae must be adapted in the case of $N = 2$ Chiral Perturbation Theory.

Coming back to three flavours, it is straightforward to check that our next-to-leading expression for c_4 is indeed scale independent, even in the presence of strong isospin. In the isospin limit $m = m_u = m_d$, one can find easily the expression for c_4 (the meaning of the notation "no pole" will be explained in the following section when we will perform the same calculations using diagrammatic methods):

$$
\begin{aligned}
c_4^{\text{no pole}} = & -\frac{B_0 F_0^2 m m_s (m^3+2m_s^3)}{(m+2m_s)^4} \\
& - \frac{64 B_0^2 m m_s L_6^r(\mu)\left(m^4+2m^3 m_s+6m^2 m_s^2+8 m m_s^3+m_s^4\right)}{(m+2m_s)^4} \\
& - \frac{384 B_0^2 m^2 m_s^2 (3L_7+L_8^r(\mu))\left(m^3+2m_s^3\right)}{(m+2m_s)^5} + \frac{3m^2 m_s^2 B_0^2\left(m^3+2m_s^3\right)}{2\pi^2 (m+2m_s)^5}\log\frac{\overset{\circ}{M}_\pi^{\,2}}{\mu^2} \\
& + \frac{m m_s B_0^2\left(m^3+9 m m_s^2+2m_s^3\right)(m+m_s)^2}{8\pi^2(m+2m_s)^5}\log\frac{\overset{\circ}{M}_K^{\,2}}{\mu^2} \\
& + \frac{B_0^2 m m_s\left(m^4+2m^3 m_s+6m^2 m_s^2+8 m m_s^3+m_s^4\right)}{36\pi^2(m+2m_s)^4}\log\frac{\overset{\circ}{M}_\eta^{\,2}}{\mu^2} \\
& + \frac{B_0^2 m^2 m_s^2\left(13m^2+22 m m_s+37 m_s^2\right)}{24\pi^2(m+2m_s)^4} + c_4^{\text{no pole}} d_{c_4}^{\text{no pole}}
\end{aligned}
\tag{5.27}
$$

where $d_{c_4}^{\text{no pole}}$ is a remainder collecting higher order contributions, starting at $O(m_q^2)$.

The above formula features chiral logarithms of different origins. Some of them come from tadpole contributions (Z_t), whereas others stem from the loop function J_{PQ}^r taken at vanishing momentum transfer as indicated in eq. (5.16) (Z_u). At this order, one could in principle redefine the argument of (some of) the logarithms in order to have physical masses instead of leading order masses. This change would not affect the rest of next-to-leading order expansion, apart from a redefinition of higher order remainders. Following the discussion in refs. [81, 85, 92], we will consider either the above prescription where all the logarithms have leading order masses as their arguments, or the one where we take physical masses for the unitary logarithms but leading order ones for the tadpole logarithms (for a discussion about this topic see secs. 3.3.2 and 3.7). If we perform this separation, we obtain:

$$
\begin{aligned}
c_4^{\text{no pole}} = & -\frac{B_0 F_0^2 m m_s (m^3+2m_s^3)}{(m+2m_s)^4} \\
& - \frac{384 B_0^2 m^2 m_s^2 [3L_7+L_8^r(\mu)]\left(m^3+2m_s^3\right)}{(m+2m_s)^5} \\
& - \frac{64 B_0^2 L_6^r(\mu) m m_s\left(m^4+2m^3 m_s+6m^2 m_s^2+8 m m_s^3+m_s^4\right)}{(m+2m_s)^4} \\
& + \frac{B_0^2 m^2 m_s^2\left(13m^2+22 m m_s+37 m_s^2\right)}{24\pi^2(m+2m_s)^4} + \frac{3B_0^2 m^2 m_s^2\left(4m^3-3 m m_s^2+2m_s^3\right)}{8\pi^2(m+2m_s)^5}\log\frac{\overset{\circ}{M}_\pi^{\,2}}{\mu^2} \\
& + \frac{B_0^2 m m_s (m+m_s)^2\left(m^3-3m^2 m_s+3 m m_s^2+2m_s^3\right)}{8\pi^2(m+2m_s)^5}\log\frac{\overset{\circ}{M}_K^{\,2}}{\mu^2} \\
& + \frac{B_0^2 m m_s\left(2m^4-8m^3 m_s+13 m m_s^3+2m_s^4\right)}{72\pi^2(m+2m_s)^4}\log\frac{\overset{\circ}{M}_\eta^{\,2}}{\mu^2} \\
& + \frac{9B_0^2 m^2 m_s^4}{8\pi^2(m+2m_s)^4}\log\frac{M_\pi^2}{\mu^2} + \frac{3B_0^2 m^2 m_s^2 (m+m_s)^2}{8\pi^2(m+2m_s)^4}\log\frac{M_K^2}{\mu^2} \\
& + \frac{B_0^2 m^2 m_s^2 (2m+m_s)^2}{24\pi^2(m+2m_s)^4}\log\frac{M_\eta^2}{\mu^2} + c_4^{\text{no pole}} d'^{\text{ no pole}}_{c_4}
\end{aligned}
\tag{5.28}
$$

It is obvious that the higher order remainder $d'^{\text{ no pole}}_{c_4}$ has absorbed this redefinition of the argument of the logarithms. In the following section, we will show the computation

for c_4 using Feynman diagrams and performing this distinction, keeping in mind that we can always revert to the prescription in eq. (5.27) by setting leading order masses in the argument of all the logarithms. For both prescriptions eqs. (5.27) and (5.28), we see that c_4 vanishes in the limit where $m = 0$ or $m_s = 0$. This is expected since the effective potential becomes independent of θ in the limit where at least one of the quark masses vanishes, as the vacuum angle can be rotated away through an anomalous $U_A(1)$ rotation.

5.3 Derivation using diagrammatic analysis

5.3.1 Combinatorics

It is also possible to derive the value of χ_t and c_4 using the formalism of Feynman diagrams in $N_f = 3$ χPT. It is obviously completely equivalent to the previous approach in terms of the one-loop generating functional, but it allows one to separate the contributions coming from the propagation of the different meson fields. Computing the second and fourth derivatives of the generating functional with respect to θ, we obtain:

$$\begin{aligned}\left.\frac{\delta^2 Z}{\delta\theta^2}\right|_{\theta=0} &= \int [dU] e^{iL}\left[i\frac{\delta^2 L}{\delta\theta^2} + \left(\frac{\delta L}{\delta\theta}\right)^2\right]_{\theta=0} \\ \left.\frac{\delta^4 Z}{\delta\theta^4}\right|_{\theta=0} &= \int [dU] e^{iL}\left[i\frac{\delta^4 L}{\delta\theta^4} - 4\frac{\delta^3 L}{\delta\theta^3}\frac{\delta L}{\delta\theta} - 3\left(\frac{\delta^2 L}{\delta\theta^2}\right)^2 - 6i\left(\frac{\delta^2 L}{\delta\theta^2}\right)\left(\frac{\delta L}{\delta\theta}\right)^2 + \left(\frac{\delta L}{\delta\theta}\right)^4\right]_{\theta=0}\end{aligned} \tag{5.29}$$

with $L = \int \mathcal{L}_{eff}$. At leading order, only the leading-order chiral Lagrangian $\mathcal{L}^{(2)}_{eff}$ (eq. 5.5) is needed, and more precisely, as all incoming momenta vanish, the mass term with $Me^{i\theta/N}$. The tree diagrams generated for both quantities χ_t and c_4 are indicated in figures 5.1 and 5.2 respectively, in the same order as the derivatives in eq. (5.29). χ_t and c_4 are derived from $W[\theta]$ with $\theta = Cst$ meaning that all mesons lines have vanishing momentum. Using the expression (2.46) of $\mathcal{L}^{(2)}_{eff}$, we obtain for the first two derivatives in terms of U, M and θ, for $N_f = 3$:

$$\begin{aligned}\frac{\delta\mathcal{L}^{(2)}_{eff}}{\delta\theta} &= -\frac{i}{3}\frac{F_0^2}{4}\langle Ue^{-i\theta/3}\chi^\dagger - U^\dagger e^{i\theta/3}\chi\rangle \\ \frac{\delta^2\mathcal{L}^{(2)}_{eff}}{\delta\theta^2} &= -\frac{1}{9}\frac{F_0^2}{4}\langle Ue^{-i\theta/3}\chi^\dagger + U^\dagger e^{i\theta/3}\chi\rangle\end{aligned} \tag{5.30}$$

We now proceed to the expansion in Φ as in eq. (2.48) to illustrate the coupling between the light mesons and the θ induced vertices. Setting θ to 0, we get, with Φ defined in sec. 2.4.3:

$$\begin{aligned}\frac{\delta\mathcal{L}^{(2)}_{eff}}{\delta\theta}|_{\theta=0} &= -\frac{i}{3}\frac{F_0^2}{4}\langle 2i\chi(-\frac{\sqrt{2}}{F_0}\Phi + \frac{\sqrt{2}}{3F_0^3}\Phi^3 + O(\Phi^5))\rangle \\ \frac{\delta^2\mathcal{L}^{(2)}_{eff}}{\delta\theta^2}|_{\theta=0} &= -\frac{1}{9}\frac{F_0^2}{4}\langle 2\chi(1 - \frac{1}{F_0^2}\Phi^2 + \frac{1}{6F_0^4}\Phi^4 + O(\Phi^6))\rangle\end{aligned} \tag{5.31}$$

We see that a θ induced vertex from an even(odd) number of derivatives can only couple to an even (odd) number of vertices. Moreover, since $\chi = 2mB_0$, we see that a single meson coupling to $\delta\mathcal{L}^{(2)}_{eff}/\delta\theta$ is necessarily an η meson in the isospin limit.

Now it is easy to compute these diagrams, with the respective contributions in the isospin limit:

$$\begin{aligned}\chi_{t,LO}^{\text{no pole}} = (a) + (b) &= -\frac{F_0^2 B_0}{9}(2m + m_s) + \frac{2}{9}F_0^2 B_0 \frac{(m - m_s)^2}{m + 2m_s} \\ &= \Sigma(3)\bar{m} + O(m_q^2)\end{aligned} \tag{5.32}$$

$$\begin{aligned}c_{4,LO}^{\text{no pole}} &= (1) + (2) + (3) + (4) + (5) \\ &= F_0^2 B_0 \Bigg[-\frac{1}{81}(2m + m_s) + \frac{8}{81}\frac{(m - m_s)^2}{m + 2m_s} - \frac{4}{27}\frac{(m - m_s)^2}{m + 2m_s} \\ &+ \frac{8}{81}\frac{(m - 4m_s)(m - m_s)^3}{(m + 2m_s)^3} - \frac{2}{81}\frac{(m - m_s)^4(m + 8m_s)}{81(m + 2m_s)^4}\Bigg] \\ &= -\frac{B_0 F_0^2 m m_s (m^3 + 2m_s^3)}{(m + 2m_s)^4} + O(m_q^2)\end{aligned} \tag{5.33}$$

corresponding, as expected, to the leading order results obtained in the previous section. In eqs. (5.32) and (5.33), the terms are indicated in the same order as the derivatives in eqs. (5.29). The third term in eq. (5.29) cannot yield any contribution to c_4 at tree level, whereas the fifth term yields both diagrams 4 and 5. In figures 5.1 and 5.2, the number inside each circle indicates the number of derivatives with respect to θ applied to $\mathcal{L}_1$ to obtain the corresponding θ-induced vertex, whereas the four-leg central vertex in diagram 5 is obtained directly from $\mathcal{L}_1$ (taking the term proportional to B_0, which has no derivatives).

Moving to next-to-leading order, we can dress the tree diagrams by *a)* inserting a vertex from the next-to-leading order lagrangian $\mathcal{L}_{eff}^{(4)}$ eq. (2.62) inside one of the propagators, *b)* replacing a θ-induced vertex from $\mathcal{L}_{eff}^{(2)}$ by its counterpart from $\mathcal{L}_{eff}^{(4)}$, *c)* adding a loop on one of the θ-induced vertices from $\mathcal{L}_{eff}^{(2)}$, *d)* adding a vertex from $\mathcal{L}_{eff}^{(2)}$ to build a loop either as a rescattering diagram or a tadpole on one of the propagators. These operations are illustrated in figures 5.1, 5.3 and 5.4. The number inside each circle (respectively square) indicates the number of derivatives with respect to θ applied to $\mathcal{L}_{eff}^{(2)}$ (respectively $\mathcal{L}_{eff}^{(4)}$ to obtain the corresponding θ-induced vertex. In addition to dressing the diagrams in figure 5.2, one can also take more legs out of the θ-induced vertices from $\mathcal{L}_{eff}^{(2)}$ and draw new diagrams, given in figure 5.4.

We provide the contributions of the different diagrams in Appendices D.1 and D.2 (in the isospin limit), and one can check explicitly that the sum of all these diagrams yields indeed eqs. (5.22) and (5.28) as expected.

5.3.2 Isolating the η propagator

According to the analysis of the previous section, the powers of $(m + 2m_s)$ in the denominator of eqs. (5.22) and (5.28) are related to the propagation of η mesons with vanishing momentum, which are the only states coupling to the θ-induced vertices in the isospin limit. Since we used next-to-leading order χPT, it is normal that the η-mass involved in the propagator is the leading order value $\overset{\circ}{M}{}_\eta^2 = 2(2m_s + m)/3$. However, if we go to higher and higher orders in Chiral Perturbation Theory, there would be tadpole and counterterm contributions to the propagator which would shift the propagator masses from leading order to physical value. This is already the case with some of the contributions in the different tree diagrams,

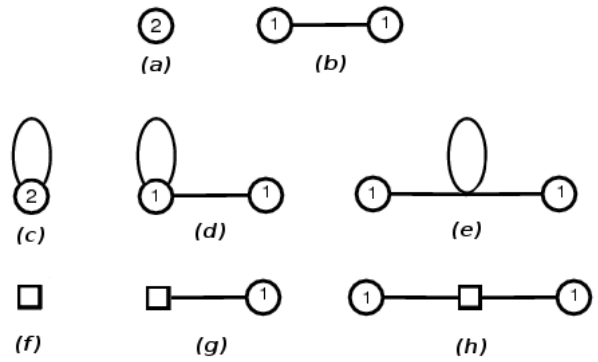

Figure 5.1: Diagrams involved in the evaluation of the correlator χ_t at LO (a and b) and NLO (c, d, e, f, g and h). The θ induced vertices are represented by the circles, containing the number of derivatives with respect to θ. The propagating η and π^0 mesons are represented by the solid lines attached to the sources, whereas the loops contain any of the eight Goldstone bosons. Any line crossing corresponds to the four-point vertex from $\mathcal{L}_{eff}^{(2)}$, and the white square in diagrams (f), (g) and (h) to the NLO counter-terms from $\mathcal{L}_{eff}^{(4)}$.

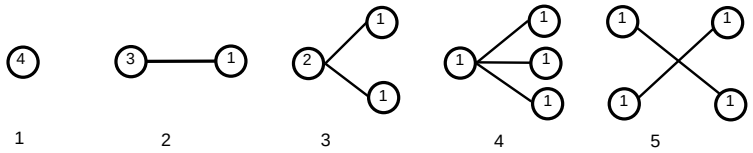

Figure 5.2: Tree diagrams contributing to c_4. The θ-induced vertices are denoted by circles containing the number of derivatives with respect to θ applied to the mass term from the LO Lagrangian in order to obtain the corresponding vertex.

which arise when one inserts a tadpole or a next-to-leading order low energy constant in the propagator. These "double-propagator" contributions should actually be reabsorbed inside the mass of the η propagator to shift its pole from $\overset{\circ}{M}{}_\eta^2$ to M_η^2.

This problem is all the more acute if we do not assume that three-flavour chiral symmetry breaking is triggered by large values of the chiral condensate and the pseudoscalar decay constant. In this case, the leading order contribution to the η mass might be significantly different from its physical value, due to large contributions from next-to-leading order terms in its chiral expansion. In view of the large powers of $\overset{\circ}{M}{}_\eta^2$ or M_η^2 involved (up to the fourth order for diagram 5 in the case of c_4), this distinction might be quite important, and suggests that one should identify the contributions due to η propagation in the previous computation and replace the leading order η mass by its physical value. This point of view is in agreement with the philosophy of Resummed χPT (see Chapter 3), which is built to accommodate such patterns of chiral symmetry breaking and where physically-motivated redefinitions of the chiral expansions are performed in order to limit the size of higher-order remainders.

Let us notice that a similar discussion takes place when one considers the two-point correlators of the axial current and/or pseudoscalar density, where the propagation of a single Goldstone boson occurs also at leading order. Indeed, in refs. [75, 76, 77, 78, 79, 80, 81, 92], it was considered that the decay constants and masses as they could be obtained from the next-to-leading order expression of $\langle A_\mu A_\nu \rangle$ (see sec. 3.4.1), where the propagators are explicitly expressed in terms of the physical masses, considering either the correlator at 0 (for F_π^2) or

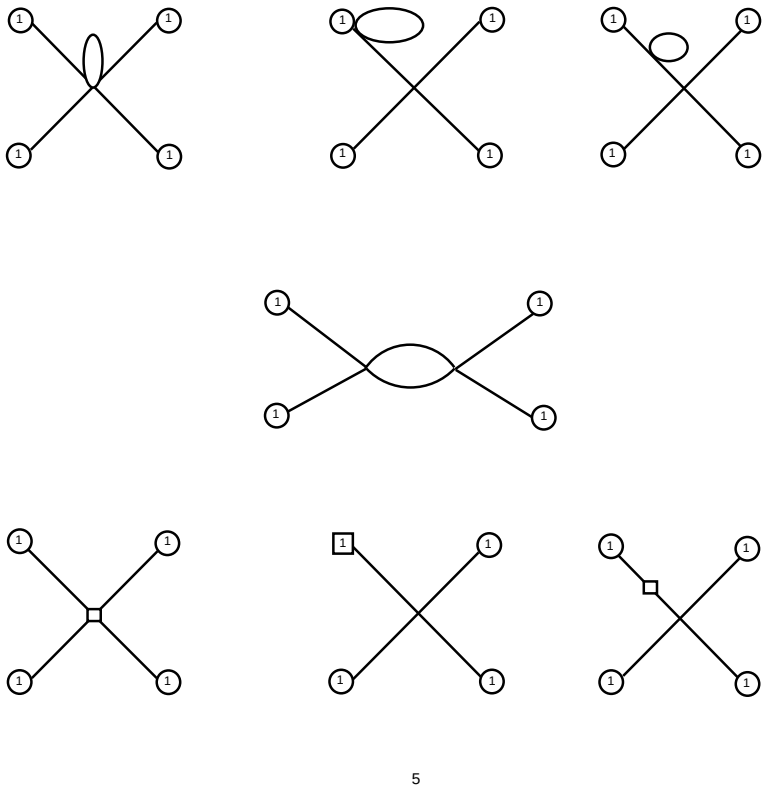

Figure 5.3: Scattering diagrams contributing to c_4 at one loop and obtained by dressing the tree diagram 5, either by adding a tadpole loop (first two lines) or by replacing a LO vertex by its NLO counterpart (denoted by a square). The θ-induced vertices are denoted by circles (squares respectively) containing the number of derivatives with respect to θ applied to the mass term from the LO (NLO respectively) Lagrangian in order to obtain the corresponding vertex.

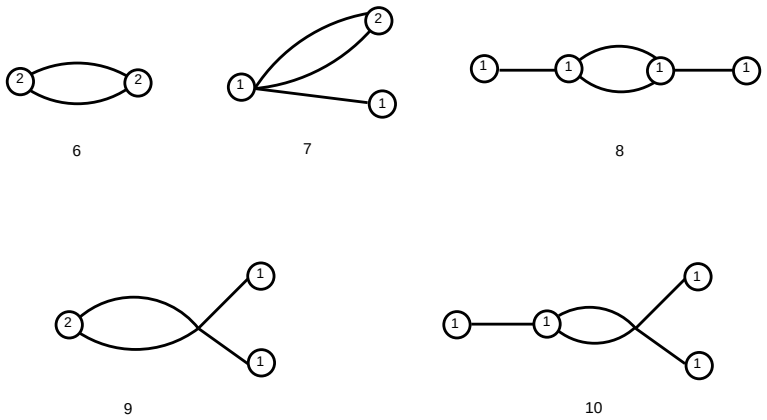

Figure 5.4: Additional diagrams involving local terms contributing to c_4 at one loop and not derived by dressing tree diagrams.

its residue at the pseudoscalar pole (for $F_\pi^2 M_\pi^2$). In the case of χ_t it yields:

$$\chi(q^2) = \sum_{P=\pi^0,\eta} \frac{R_P}{M_P^2 - p^2} + S(q^2) \tag{5.34}$$

where $R_P \equiv |\langle\Omega|\omega|P\rangle|^2$ is the relevant coupling to Goldstone bosons, and S is analytic up to the next thresholds (the first singularities being the cut from $s \geq 9M_\pi^2$ and pole at $M_{\eta'}^2$). One obtains the separation:

$$\chi^{\text{pole}} = \frac{R}{M_\eta^2} + S\,, \qquad R \equiv R_\eta = |\langle\Omega|\omega|\eta\rangle|^2\,, \qquad S \equiv S(0) \tag{5.35}$$

The π^0 meson does not couple to the winding number density in the isospin limit $m_u = m_d$, due to G-parity. Using the expression of $\chi_t^{\text{no pole}}$ eq. (5.22), we get up to next-to-leading order the pole residue R and the analytical piece S:

$$\begin{aligned} R = &-\frac{4}{27}B_0^2F_0^2(m-m_s)^2\left[1+\frac{1}{F_0^2}\left(\frac{\overset{\circ}{M}{}_K^2}{16\pi^2}\log\frac{\overset{\circ}{M}{}_K^2}{\mu^2} - 16B_0\Big(L_4^r(\mu)(2m+m_s)\right.\right. \\ &\left.\left.+\frac{1}{3}L_5^r(\mu)(m+2m_s)\Big)\right)\right] \\ &+\frac{4}{27}B_0^2\frac{(m-m_s)}{16\pi^2}\left[3m\ \overset{\circ}{M}{}_\pi^2\log\frac{\overset{\circ}{M}{}_\pi^2}{\mu^2} - 2m_s\ \overset{\circ}{M}{}_K^2\log\frac{\overset{\circ}{M}{}_K^2}{\mu^2} + \frac{1}{3}(m-4m_s)\ \overset{\circ}{M}{}_\eta^2\log\frac{\overset{\circ}{M}{}_\eta^2}{\mu^2}\right] \\ &-\frac{256}{27}B_0^3(m-m_s)\left[(L_6^r(\mu)+L_7^r(\mu))(m-m_s)(2m+m_s)+L_8^r(\mu)(m^2-m_s^2)\right] \end{aligned} \tag{5.36}$$

$$\begin{aligned} S = &\frac{1}{9}B_0F_0^2(2m+m_s) \\ &-\frac{B_0}{144\pi^2}\left[3m\ \overset{\circ}{M}{}_\pi^2\log\frac{\overset{\circ}{M}{}_\pi^2}{\mu^2} + 2(m+m_s)\ \overset{\circ}{M}{}_K^2\log\frac{\overset{\circ}{M}{}_K^2}{\mu^2} + \frac{1}{3}(2m_s+m)\ \overset{\circ}{M}{}_\eta^2\log\frac{\overset{\circ}{M}{}_\eta^2}{\mu^2})\right] \\ &+\frac{32}{9}B_0^2\left[(2m+m_s)^2(L_6^r(\mu)+L_7^r(\mu))+(2m^2+m_s^2)L_8^r(\mu)\right] \end{aligned} \tag{5.37}$$

It is easy to check that eq. (5.35) coincides with eq. (5.21) in the isospin limit, up to higher-order terms in the chiral expansion: one simply re-expand the pole $1/M_\eta^2$ by taking the chiral series of M_η^2 up to next-to-leading order, and truncate all the higher order terms that may appear.

In the same manner, the leading expression for c_4 eq. (5.33) could be understood as:

$$\begin{aligned} c_4 \;=\; &-\frac{1}{81}B_0F_0^2(2m+ms) + \frac{16B_0^2F_0^2(m-m_s)^2}{243M_\eta^2} - \frac{16B_0^2(m-m_s)^2(m+2m_s)}{243M_\eta^4} \\ &+\frac{64B_0^4F_0^2(m-4m_s)(m-m_s)^3}{2187M_\eta^6} - \frac{32B_0^5F_0^2(m-m_s)^4(m+8m_s)}{6561M_\eta^8} + O(m_q^2) \end{aligned} \tag{5.38}$$

In the present case, it is quite straightforward for each diagram to identify the NLO contributions that should be absorbed in the shift since the structure of the η mass up to NLO is well known [2]. It yields the following expressions for the different diagrams, which should be added to obtain the next-to-leading order expression of c_4 with a physical η propagator:

- Diagrams 1

$$-\frac{1}{81}B_0F_0^2(2m+ms) + \frac{B_0^2m^2}{216\pi^2}\ln\frac{\overset{\circ}{M}{}_\pi^2}{\mu^2}$$

$$
\begin{aligned}
&+\frac{B_0^2\left(m+m_s\right)^2}{648\pi^2}\ln\frac{\overset{\circ}{M}_K^2}{\mu^2}+\frac{B_0^2\left(m+2m_s\right)^2}{5832\pi^2}\ln\frac{\overset{\circ}{M}_\eta^2}{\mu^2}\\
&-\frac{128}{81}B_0^2\left(m_s+2m\right)^2L_6^r(\mu)-\frac{128}{81}B_0^2\left(m_s+2m\right)^2L_7\\
&-\frac{128}{81}B_0^2\left(2m^2+m_s^2\right)L_8^r(\mu)
\end{aligned}
\tag{5.39}
$$

- Diagrams 2

$$
\begin{aligned}
&\frac{16B_0^2F_0^2(m-m_s)^2}{243M_\eta^2}-\frac{2B_0^3m^2\left(m-m_s\right)}{81\pi^2M_\eta^2}\ln\frac{\overset{\circ}{M}_\pi^2}{\mu^2}+\frac{2B_0^3\left(m-m_s\right)\left(m+m_s\right)^2}{243\pi^2M_\eta^2}\ln\frac{\overset{\circ}{M}_K^2}{\mu^2}\\
&-\frac{2B_0^3\left(m-m_s\right)\left(m-4m_s\right)\left(m+2m_s\right)}{2187\pi^2M_\eta^2}\ln\frac{\overset{\circ}{M}_\eta^2}{\mu^2}\\
&-\frac{256B_0^3\left(m-m_s\right)^2\left(2m+m_s\right)}{243M_\eta^2}L_4^r(\mu)-\frac{256B_0^3\left(m-m_s\right)^2\left(m+2m_s\right)}{729M_\eta^2}L_5^r(\mu)\\
&+\frac{2560B_0^3\left(m-m_s\right)^2\left(2m+m_s\right)}{243M_\eta^2}L_6^r(\mu)+\frac{2560B_0^3\left(m-m_s\right)^2\left(2m+m_s\right)}{243M_\eta^2}L_7\\
&+\frac{2560B_0^3\left(m-m_s\right)^2\left(m+m_s\right)}{243M_\eta^2}L_8^r(\mu)
\end{aligned}
\tag{5.40}
$$

- Diagrams 3

$$
\begin{aligned}
&-\frac{16B_0^2(m-m_s)^2(m+2m_s)}{243M_\eta^4}\\
&+\frac{B_0^4m^2\left(m-m_s\right)\left(m+m_s\right)}{27\pi^2M_\eta^4}\ln\frac{\overset{\circ}{M}_\pi^2}{\mu^2}-\frac{B_0^4\left(m-m_s\right)\left(m+m_s\right)^3}{162\pi^2M_\eta^4}\ln\frac{\overset{\circ}{M}_K^2}{\mu^2}\\
&+\frac{B_0^4\left(m-m_s\right)\left(m+2m_s\right)\left(m^2+mm_s-8m_s^2\right)}{729\pi^2M_\eta^4}\ln\frac{\overset{\circ}{M}_\eta^2}{\mu^2}\\
&+\frac{512B_0^4\left(m-m_s\right)^2\left(2m+m_s\right)\left(m+2m_s\right)}{243M_\eta^4}L_4^r(\mu)+\frac{512B_0^4\left(m-m_s\right)^2\left(m+2m_s\right)^2}{243M_\eta^2}L_5^r(\mu)\\
&-\frac{2040B_0^4\left(m-m_s\right)^2\left(m^2+mm_s+m_s^2\right)}{81M_\eta^4}L_6^r(\mu)-\frac{2040B_0^4\left(m-m_s\right)^2\left(m^2+mm_s+m_s^2\right)}{81M_\eta^4}L_7\\
&-\frac{1024B_0^4\left(m-m_s\right)^2\left(m^2+mm_s+2m_s^2\right)}{81M_\eta^4}L_8^r(\mu)
\end{aligned}
\tag{5.41}
$$

- Diagrams 4

$$
\begin{aligned}
&\frac{64B_0^4F_0^2(m-4m_s)(m-m_s)^3}{2187M_\eta^6}-\frac{4B_0^5m^2\left(4m-13m_s\right)\left(m-m_s\right)^2}{729\pi^2M_\eta^6}\ln\frac{\overset{\circ}{M}_\pi^2}{\mu^2}\\
&+\frac{2B_0^5\left(m+m_s\right)\left(m-m_s\right)^2\left(32m^2-99mm_s-23m_s^2\right)}{10935\pi^2M_\eta^6}\ln\frac{\overset{\circ}{M}_K^2}{\mu^2}\\
&-\frac{4B_0^5\left(m+m_s\right)\left(m-m_s\right)^2\left(4m^2-41mm_s+64m_s^2\right)}{19683\pi^2M_\eta^6}\ln\frac{\overset{\circ}{M}_\eta^2}{\mu^2}\\
&-\frac{1024B_0^5\left(m-m_s\right)^3\left(m-4m_s\right)\left(2m+m_s\right)}{729M_\eta^6}L_4^r(\mu)\\
&-\frac{1024B_0^5\left(m-m_s\right)^3\left(m-4m_s\right)\left(m+2m_s\right)}{2187M_\eta^2}L_5^r(\mu)
\end{aligned}
$$

$$
\begin{aligned}
&+\frac{4096B_0^5\left(m-m_s\right)^3\left(7m^2-11mm_s-14m_s^2\right)}{2187M_\eta^6}L_6^r(\mu)\\
&+\frac{4096B_0^5\left(m-m_s\right)^3\left(7m^2-11mm_s-14m_s^2\right)}{2187M_\eta^6}L_7\\
&+\frac{2048B_0^5\left(m-m_s\right)^3\left(7m^2-9mm_s-28m_s^2\right)}{2187M_\eta^6}L_8^r(\mu)
\end{aligned}
\tag{5.42}
$$

- Diagrams 5

$$
\begin{aligned}
&-\frac{32B_0^5F_0^2(m-m_s)^4(m+8m_s)}{6561M_\eta^8}+\frac{2B_0^6m^2\left(m-m_s\right)^3\left(5m+31m_s\right)}{2187\pi^2M_\eta^8}\ln\frac{\overset{\circ}{M}{}_\pi^2}{\mu^2}\\
&+\frac{2B_0^6\left(m-m_s\right)^3\left(m+m_s\right)\left(m^2-189mm_s+8m_s^2\right)}{32805\pi^2M_\eta^8}\ln\frac{\overset{\circ}{M}{}_K^2}{\mu^2}\\
&+\frac{2B_0^6\left(m-m_s\right)^3\left(m+2m_s\right)\left(5m^2+47mm_s-160m_s^2\right)}{59049\pi^2M_\eta^8}\ln\frac{\overset{\circ}{M}{}_\eta^2}{\mu^2}\\
&+\frac{2B_0^6m^2\left(m-m_s\right)^4}{729\pi^2M_\eta^8}\ln\frac{M_\pi^2}{\mu^2}+\frac{2B_0^6m^2\left(m-m_s\right)^4}{2187\pi^2M_\eta^8}\ln\frac{M_K^2}{\mu^2}\\
&+\frac{2B_0^6\left(m-m_s\right)^4\left(m+8m_s\right)^2}{19683\pi^2M_\eta^8}\ln\frac{M_\eta^2}{\mu^2}\\
&+\frac{2048B_0^6\left(m-m_s\right)^4\left(m+8m_s\right)\left(2m+m_s\right)}{6561M_\eta^8}L_4^r(\mu)\\
&+\frac{2048B_0^6\left(m-m_s\right)^4\left(m+8m_s\right)\left(m+2m_s\right)}{19683M_\eta^8}L_5^r(\mu)\\
&-\frac{1024B_0^2\left(m-m_s\right)^4\left(16m^2+109mm_s+64m_s^2\right)}{6561M_\eta^8}L_6^r(\mu)\\
&-\frac{4096B_0^2\left(m-m_s\right)^4\left(4m^2+7mm_s+16m_s^2\right)}{6561M_\eta^8}L_7\\
&-\frac{4096B_0^2\left(m-m_s\right)^4\left(2m^2+9mm_s+16m_s^2\right)}{6561M_\eta^8}L_8\\
&+\frac{2B_0^6\left(m-m_s\right)^4\left(37m^2+16mm_s+64m_s^2\right)}{19683\pi^2M_\eta^8}
\end{aligned}
\tag{5.43}
$$

- Diagrams 6

$$
\begin{aligned}
&\frac{B_0^2}{72\pi^2}m^2\ln\frac{M_\pi^2}{\mu^2}+\frac{B_0^2}{216\pi^2}\left(m+m_s\right)^2\ln\frac{M_K^2}{\mu^2}+\frac{B_0^2}{1944\pi^2}\left(m+2m_s\right)^2\ln\frac{M_\eta^2}{\mu^2}\\
&+\frac{B_0^2}{1944\pi^2}\left(37m^2+22mm_s+13m_s^2\right)
\end{aligned}
\tag{5.44}
$$

- Diagrams 7

$$
\begin{aligned}
&-\frac{B_0^3m^2\left(m-m_s\right)}{27\pi^2M_\eta^2}\ln\frac{M_\pi^2}{\mu^2}-\frac{B_0^3m_s\left(m_s^2-m^2\right)}{81\pi^2M_\eta^2}\ln\frac{M_K^2}{\mu^2}\\
&-\frac{B_0^3\left(m-4m_s\right)\left(m-m_s\right)\left(m+2m_s\right)}{729M_\eta^2\pi^2}\ln\frac{M_\eta^2}{\mu^2}\\
&-\frac{B_0^2\left(m-m_s\right)^2\left(17m_s+28m\right)}{729\pi^2M_\eta^2}
\end{aligned}
\tag{5.45}
$$

- Diagrams 8

$$\begin{aligned}&\frac{2B_0^4m^2\left(m-m_s\right)^2}{81\pi^2M_\eta^4}\ln\frac{M_\pi^2}{\mu^2}+\frac{2B_0^2m_s^2\left(m-m_s\right)^2}{243\pi^2M_\eta^4}\ln\frac{M_K^2}{\mu^2}\\&+\frac{2B_0^2\left(m-4m_s\right)^2\left(m-m_s\right)^2}{2187\pi^2M_\eta^4}\ln\frac{M_\eta^2}{\mu^2}\\&+\frac{2B_0^2\left(m-m_s\right)^2\left(28m^2-8mm_s+25m_s^2\right)}{2187\pi^2M_\eta^4}\end{aligned}\tag{5.46}$$

- Diagrams 9

$$\begin{aligned}&\frac{B_0^4m^2\left(m-m_s\right)^2}{81\pi^2M_\eta^4}\ln\frac{M_\pi^2}{\mu^2}-\frac{B_0^2m\left(m-m_s\right)^2\left(m+m_s\right)}{243\pi^2M_\eta^4}\ln\frac{M_K^2}{\mu^2}\\&+\frac{B_0^4\left(m+8m_s\right)\left(m-m_s\right)^2\left(m+2m_s\right)}{2187\pi^2M_\eta^4}\ln\frac{M_\eta^2}{\mu^2}-\frac{B_0^4\left(m-m_s\right)^2\left(m+m_s\right)^2}{162\pi^2M_\eta^4}\ln\frac{\overset{\circ}{M}{}_K^2}{\mu^2}\\&+\frac{B_0^4\left(m-m_s\right)^2\left(19m^2+mm_s+16m_s^2\right)}{2187\pi^2M_\eta^4}\end{aligned}\tag{5.47}$$

- Diagrams 10

$$\begin{aligned}&-\frac{4B_0^5m^2\left(m-m_s\right)^3}{243\pi^2M_\eta^6}\ln\frac{M_\pi^2}{\mu^2}-\frac{4B_0^2mm_s\left(m-m_s\right)^3}{729\pi^2M_\eta^6}\ln\frac{M_K^2}{\mu^2}\\&-\frac{4B_0^5\left(m-4m_s\right)\left(m+8m_s\right)\left(m-m_s\right)^3}{6561\pi^2M_\eta^6}\ln\frac{M_\eta^2}{\mu^2}-\frac{2B_0^5(m+m_s)m_s\left(m-m_s\right)^3}{243\pi^2M_\eta^6}\ln\frac{\overset{\circ}{M}{}_K^2}{\mu^2}\\&-\frac{4B_0^5\left(m-m_s\right)^3\left(28m^2+13mm_s-32m_s^2\right)}{6561\pi^2M_\eta^6}\end{aligned}\tag{5.48}$$

(Having isolated the η propagator in the expressions of χ_t and c_4, we will postpone the discussion of HO remainders to sec. 5.6.2).

5.4 Expected sensitivity to the three-flavour chiral condensate

Now we discuss the sensitivity of the cumulants of the winding number to the pattern of chiral symmetry breaking in the limit of three massless quarks. We see that the topological susceptibility eq. (5.20) involves the three-flavour quark condensate $\Sigma(3)$ together with the Zweig-rule violating next-to-leading order low-energy constants L_6 in the combination (see sec. 5.6):

$$\chi \leftrightarrow F_0^2B_0+32B_0^2L_6^rs\tag{5.49}$$

As discussed in [78], for physical quark masses, this combination is actually very close to the quark condensate defined in the two-flavour chiral limit $m_u, m_d \to 0$, but m_s kept at its physical value (eq. (2.79)):

$$\Sigma(2)=-\lim_{m_u,m_d\to0}\langle0|\bar uu|0\rangle=F_0^2B_0+32m_sB_0^2L_6^r(\mu)-\frac{m_sB_0^2}{16\pi^2}\log\frac{m_sB_0}{\mu^2}-\frac{m_sB_0^2}{72\pi^2}\log\frac{4m_sB_0}{3\mu^2}+\ldots\tag{5.50}$$

where the ellipsis denotes higher order contributions starting at $O(m_s^2)$. For simulations close to the physical case where m is much smaller than m_s, the topological susceptibility

essentially probes the two-flavour quark condensate (as the two quantities differ only by a contribution suppressed by a factor m/m_s), and consequently, χ_t does not *not* probe the three-flavour quark condensate (defined in the corresponding chiral limit $m_u, m_d, m_s \to 0$), contrary to what is often asserted.

The situation becomes more interesting when turning to the fourth cumulant c_4, which involves L_6 in two different combinations:

$$c_4 \leftrightarrow F_0^2 B_0 + 32 B_0^2 L_6^r s \ , \ -96 B_0^2 L_6^r \frac{\bar{m}^{[3]}}{\bar{m}^2} \tag{5.51}$$

For simulations close to the physical quark mass hierarchy, the first term corresponds to the two-flavour condensate (like for the topological susceptibility), but the second term opens the possibility to disentangle L_6^r and $\Sigma(3)$ by considering the dependence of c_4 on the light-quark mass m. Therefore, contrary to χ_t, the fourth cumulant c_4 may provide a probe of the pattern of three-flavour chiral symmetry breaking even for simulations close to the physical case.

Before turning to lattice settings close to the physical quark mass hierarchy, let us emphasise that simulations with degenerate quarks could be much more interesting to extract the three-flavour condensate from topological quantities. Indeed, in the limit where the N quarks in Eqs (5.20) and (5.26) are degenerate with mass $\hat{m}$ (leading to pseudoscalar mesons with a common physical mass M), the following combination

$$\chi^{\text{no pole}} + \frac{N^2}{4} c_4^{\text{no pole}} = \frac{3\hat{m}^2 F_N^2 B_N}{4N} + \frac{N^2-1}{N^2}\frac{3\hat{m}^2 B_N^2}{32\pi^2} - \frac{N^2-1}{N^2}\frac{3\hat{m}^2 B_N^2}{32\pi^2}\log\frac{2\hat{m}B_N}{M^2} + O(\hat{m}^3) \tag{5.52}$$

does not involve next-to-leading order low-energy constants, and would thus be particularly suited to determine the quark condensate $\Sigma(N) = F_N^2 B_N$ in the chiral limit of N massless flavours from simulations with N degenerate light quarks.

5.5 The two-flavour case

As indicated after eq. (5.26), it is possible to compute the topological susceptibility or the fourth cumulant in $N = 2$ χPT [1] (see sec. 2.6 for the presentation of $N_f = 2$ χPT) built around the two-flavour chiral limit $m_u = m_d = 0$ (but m_s kept physical).

It is straightforward to repeat the same arguments as in sec. 5.2.1 with the generating functional of $N_f = 2$ χPT given in ref. [1], in order to obtain the two-flavour expressions in the isospin limit:

$$\chi^{\text{no pole}} = \frac{mBF^2}{2} + 2m^2B^2[\ell_3^r(\mu) + h_1^r(\mu) - \ell_7 - h_3] - \frac{3B^2m^2}{32\pi^2}\log\frac{2mB}{\mu^2} + O(m^3) \tag{5.53}$$

$$\begin{aligned} c_4^{\text{no pole}} &= -\frac{mBF^2}{8} + \frac{9m^2B^2}{128\pi^2} - 2m^2B^2[\ell_3^r(\mu) + h_1^r(\mu) - \ell_7 - h_3] \\ &\quad + \frac{3m^2B^2}{128\pi^2}\left[\log\frac{2mB}{\mu^2} + 3\log\frac{M_\pi^2}{\mu^2}\right] + O(m^3) \end{aligned}$$

where we have performed the same separation between unitarity and tadpole contributions for c_4 as in the $N = 3$ case. These formulae should be used to extract the two-flavour chiral condensate from simulations performed at $\tilde{m}_s = m_s$ and various values of the light quark mass $\tilde{m}$.

Let us emphasize the ambiguity of the alternative expression used in the literature [119, 122] and derived from eqs. (5.20) and (5.26) by setting $N = 2$. The resulting expressions

have the same structure as eqs. (5.53), but they involve low-energy constants usually labelled L_6, L_7, L_8 which are very easy to misunderstand. Their names allude the three-flavour case, but they are actually defined in the two-flavour chiral limit. In our notation, we would denote them as $L_{6,7,8;N=2}$ which have definitions and values that differ from those in three-flavour χPT (which we would denote $L_{6,7,8;N=3}$). Moreover the connection between these low-energy constants $L_{6,7,8;N=2}$ and the usual ℓ_i and h_i is not straightforward. In order to avoid any confusion and make a direct connection with $N = 2$ χPT [1], one should always use the expressions Eqs. (5.53) to deal with the two-flavour chiral expansions of the topological susceptibility and the fourth cumulant.

One can go further and actually match $N = 2$ and $N = 3$ chiral theories in order to exhibit the m_s-dependence of $N = 2$ low-energy constants [1, 135, 136, 137], yielding the next-to-leading order matching formulae for the quark condensates and pseudoscalar decay constants (eqs. (2.78) and (2.79)):

$$F^2 = F_0^2 + 16 m_s B_0 L_4^r(\mu) - \frac{m_s B_0}{16\pi^2} \log \frac{m_s B_0}{\mu^2} \tag{5.54}$$

$$F^2 B^2 = F_0^2 B_0 + 32 m_s B_0 L_6^r(\mu) - \frac{m_s B_0^2}{16\pi^2} \log \frac{m_s B_0}{\mu^2} - \frac{m_s B_0^2}{72\pi^2} \log \frac{4 m_s B_0}{3\mu^2} \tag{5.55}$$

as well as for the relevant next-to-leading order low-energy constants:

$$\begin{aligned} 2m^2 B^2 [\ell_3^r(\mu) + h_1^r(\mu) - \ell_7 - h_3] = 24 m^2 B_0^2 [L_6^r + 3L_7^r + L_8^r] - \frac{m^2 B_0^2}{32\pi^2} \log \frac{m_s B_0}{\mu^2} \\ - \frac{m^2 B_0^2}{96\pi^2} \log \frac{4 m_s B_0}{3\mu^2} - \frac{5 m^2 B_0^2}{144\pi^2} - \frac{F_0^2 B_0 m^2}{4 m_s} \end{aligned} \tag{5.56}$$

It is then easy to check that eqs. (5.53) correspond indeed to the second-order expansion in m of the three-flavour results eqs. (5.22) and (5.28), providing a further cross-check of these equations.

One more comment is in order concerning the low-energy constants involved in eqs. (5.53). First, one might be surprised that two high-energy counter-terms h_1 and h_3 arise in these expansions. Indeed, these high-energy counterterms encode physics of higher energy scales that are not included dynamically in the theory and their value is dependent on its ultraviolet regularisation. This seems to contradict the fact that χ_t and c_4 are topological quantities related to chiral symmetry breaking arising in QCD at low energies. This paradox can be solved thanks to the matching with three-flavour χPT. The two-flavour chiral expansions of χ_t and c_4 involve only the difference of high energy counterterms $h_1 - h_3$, which can be matched with three-flavour χPT as in eq. (5.56). The next-to-leading order expansion of $h_1 - h_3$ in powers of m_s involves only $N = 3$ low-energy constants, but none of the high-energy counterterms H_i. It means that $h_1 - h_3$ is a combination of $N = 2$ high-energy counterterms which is characterised by the dynamics of K and η mesons but is independent of the ultraviolet regularisation of the theory in relation with more massive (non-Goldstone) degrees of freedom. Indeed we have seen that our three-flavour results for χ_t and c_4 rely crucially on the propagation of the η-meson, which is not a dynamical degree of freedom of two-flavour χPT. Therefore, all the diagrams in $N = 3$ χPT involving the propagation of K and η mesons (such as figure 5.2) must be absorbed into high-energy counterterms once the computation is performed in $N = 2$ χPT. The presence of $h_1 - h_3$ in eq. (5.54) is thus normal and can be easily explained by the role of the η meson when computing the next-to-leading order expansions of χ_t and c_4.

5.6 Topological observables on the lattice

In this section, we will now study the behavior of the topological susceptibility on the lattice, as we have done in the preceeding chapter regarding decay constants, masses, and form factors. Two cases will be taken into account separately: a first case corresponding to the "no pole" expression eq. (5.22), and a second case for which the physical η pole has been isolated, eq. (5.35).

5.6.1 Resummed framework (1): no η pole

In Chapter 3, we have argued that the pattern of $N_f = 3$ chiral symmetry breaking could be affected significantly by vacuum fluctuations of $s\bar{s}$ pairs, leading to the suppression of the quark condensate, the enhancement of L_4 and L_6, and finally a numerical competition between leading order and next-to-leading order contributions in $N_f = 3$ chiral expansions. As indicated in sec. 3.4.3, such a problem would occur for χ_t and c_4, which explains why we want to analyse these quantities in the Resummed χPT framework.

We consider now a lattice simulation with dynamical quarks of unphysical masses $(\tilde{m}, \tilde{m}, \tilde{m}_s)$, and we use again the notation of Chapter 4: $p = \tilde{m}_s/m_s,\ q = \tilde{m}/\tilde{m}_s$. If we do not isolate the contribution from the η pole and simply re-express eq. (5.21) using eqs. (3.13) and (4.2), we obtain the expression for the topological susceptibility on the lattice $\tilde{\chi}_t$ (following the $\tilde{X}$ notation of sec. 2.2):

$$\tilde{\chi}_t^{\text{no pole}} = \frac{F_\pi^2 M_\pi^2}{2}\frac{pqr}{q+2}\left[X(3) + 16[Y(3)]^2\frac{M_\pi^2}{F_\pi^2}pr\left[L_6^r(\mu)(2q+1) + 3(3L_7 + L_8^r(\mu))\frac{q}{q+2}\right]\right. \tag{5.57}$$

$$\left. - \frac{1}{16\pi^2}[Y(3)]^2\frac{M_\pi^2}{F_\pi^2}pr\left[\frac{3q}{q+2}\log\frac{\overset{\circ}{\tilde{M}}_\pi^2}{\mu^2} + \frac{(1+q)^2}{q+2}\log\frac{\overset{\circ}{\tilde{M}}_K^2}{\mu^2} + \frac{2q+1}{9}\log\frac{\overset{\circ}{\tilde{M}}_\eta^2}{\mu^2}\right]\right]$$

$$+ \tilde{\chi}^{\text{no pole}}\tilde{d}_{\chi^{\text{no pole}}}$$

If we replace $L_{6,7,8}$ by their expressions in terms of leading order quantities and physical observables (eq. (3.60) and eqs. (3.32)-(3.39), and if we consider a simulation at the physical point $(q = 1/r, p = 1)$, the topological susceptibility boils down to:

$$\chi_t^{\text{no pole}} = \frac{F_\pi^2 M_\pi^2}{2}\frac{r}{2r+1}\left[1 - \epsilon(r)\frac{7r+2}{2r(2r+1)} + \frac{9}{2}\frac{r}{(r-1)^2(r+2)}\Delta_{GMO}\right] + ... \tag{5.58}$$

where the ellipsis denotes higher-order remainders. Eq. (5.58) shows that in the physical case, the topological susceptibility has no sensitivity to the three-flavour condensate $X(3)$ (as was seen before in sec 5.4).

Therefore, the topological susceptibility close to the physical point ($p = 1$, $r = 1/q$ large) exhibits a rather poor sensitivity to the three-flavour condensate $X(3)$. In a similar way to pseudoscalar masses and decay constants, simulations aiming at disentangling the pattern of three-flavour chiral symmetry breaking should be performed not only for quark masses with a hierarchy similar to the physical case, but also light (almost) degenerate masses with values between the physical m_u, m_d and m_s. The (unphysical) region where simulations probe $X(3)$ efficiently can be determined by expanding eq. (5.57) in powers of $1/r$:

$$\tilde{\chi}_t^{\text{no pole}} = \frac{F_\pi^2 M_\pi^2}{2}\frac{pqr}{q+2}\left[X(3)[1 - p(2q+1)] + p(2q+1) - \frac{3pq}{2(q+2)}\frac{r_2 - r}{r}\right] + \dots \tag{5.59}$$

where the ellipsis denotes chiral logarithms and higher order remainders. It is clear from this expression that we need $q = O(1)$ rather than $O(1/r)$ to get a reasonable sensitivity to $X(3)$: for instance, $q = 1$ (i.e., $\tilde{m} = \tilde{m}_s$ yields $[1 - 3p]X(3) + p[3 - (r_2 - r)/(2r)]$, so that the coefficient of $X(3)$ has a similar size to that of the constant term. This is sketched in a more quantitative way in fig. 5.5 which compares the topological susceptibility at $X(3) = 0$ and $X(3) = 1$ in some illustrative cases [1]. The comparison between the two values indicates the sensitivity to the size of the three-flavour quark condensate, which tends to decrease the value of the topological susceptibility. We see that the contributions from $X(3)$ are at least twice as small as the remaining contributions, and they in particular might be hidden in the uncertainties if q is small (e.g., of $O(1/r)$ if the simulated quark masses are tuned to be close to the physical ones).

Another way of escaping the poor sensitivity of the topological susceptibility to the three-flavour quark condensate consists in simulations involving significant isospin breaking, which can be easily implemented in particular for twisted-mass fermion actions [124, 127]. An expression for the topological susceptibility on the lattice similar eq. (5.57) can be written, involving the two quantities $q_u = \tilde{m}_u/\tilde{m}_s$ and $q_d = \tilde{m}_d/\tilde{m}_s$ instead of q:

$$\begin{aligned}\tilde{\chi}_t^{\text{no pole}} &= \frac{F_\pi^2 M_\pi^2}{2} \frac{pq_u q_d r}{q_u + q_d + q_u q_d} \\ &\times \left[X(3) \left\{ 1 - \frac{pr(1 + q_u + q_d)}{r + 2} \right\} - \epsilon(r) pr \left\{ \frac{3q_u q_d}{2(q_u + q_d + q_u q_d)} + \frac{1 + q_u + q_d}{r + 2} \right\} \right. \\ &\left. + \frac{pr(1 + q_u + q_d)}{r + 2} + \frac{9pq_u q_d r}{2(r - 1)^2 (q_u + q_d + q_u q_d)} \Delta_{GO} \right] + \dots \end{aligned} \tag{5.60}$$

where we expressed the next-to-leading order low energy constants $L_{6,7,8}$ using, as always, eqs. (3.32)-(3.39) (we have checked that including the $m_d - m_u$ difference in the expressions of eqs. (3.32)-(3.39) would not modify our conclusions). The ellipsis denotes chiral logarithms and higher order remainders. The dependence of χ_t on the two quantities q_u and q_d is illustrated in figure 5.6. As expected, $\tilde{\chi}_t(q_u, q_d) = \tilde{\chi}_t(q_d, q_u)$ vanishes for $q_u = 0$ or $q_d = 0$ (either mass m_u or m_d being zero) since the theory becomes independent of θ when one of the quark masses vanishes. The value of the topological susceptibility increases when one of the two quark masses increases, the other one being kept fixed. As clearly seen in figure 5.6, the contribution to the topological susceptibility independent of $X(3)$ increases faster than the one proportional to $X(3)$, so that a scan through values of $(\tilde{m}_u, \tilde{m}_d)$ at fixed $\tilde{m}_s$ could help to determine unambiguously the contribution (and thus the value) of the three-flavour quark condensate.

[1] For this comparison, we assume that the physical value of F_η is known in order to compute the Gell-Mann-Okubo contribution Δ_{GMO} to L_7 (eq. (3.59)). In the following sections, we will not make this assumption and we will use eq. (3.56) to determine F_η.

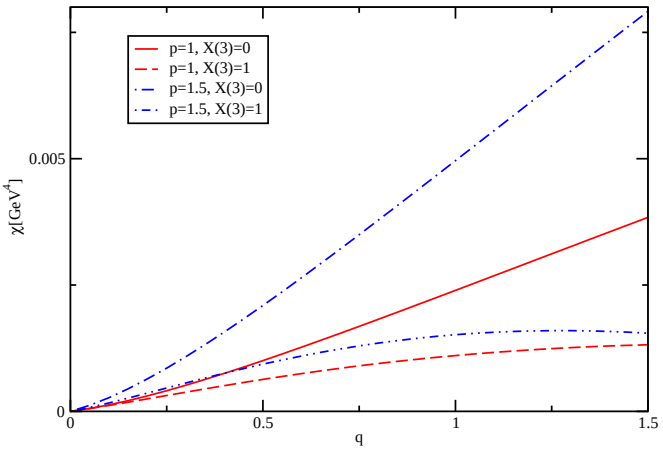

Figure 5.5: The topological susceptibility $\tilde{\chi}_t^{\text{no pole}}$ as a function of the ratio of simulated quark masses q for $X(3) = 0$ (solid lines) and $X(3) = 1$ (dashed lines) for two different values of p (related to the simulated strange quark mass). For illustration, the remainders are set to be zero, $Y(3) = 0.8$, $r = 26$, $F_K/F_\pi = 1.19$ and F_η =130 MeV.

Furthermore, we obtain for the fourth cumulant on the lattice:

$$
\begin{aligned}
\tilde{c}_4^{\text{no pole}} = & -\frac{F_\pi^2 M_\pi^2 pq\left(q^3+2\right) rX(3)}{2(q+2)^4} + \frac{M_\pi^4 p^2 q^2((13q^2+22q+37)r^2Y(3)^2}{96\pi^2(q+2)^4} \\
& - \frac{16L_6^r(\mu)M_\pi^4 p^2 q\left(q^4+2q^3+6q^2+8q+1\right) r^2Y(3)^2}{(q+2)^4} \\
& - \frac{96(3L_7+L_8^r(\mu))M_\pi^4 p^2q^2\left(q^3+2\right) r^2Y(3)^2}{(q+2)^5} \\
& + \frac{9M_\pi^4 p^2q^2r^2Y(3)^2}{32\pi^2(q+2)^4}\ln\frac{\tilde{M}_\pi^2}{\mu^2} + \frac{3M_\pi^4 p^2q^2\left(4q^3-3q+2\right) r^2Y(3)^2}{32\pi^2(q+2)^5}\ln\frac{\mathring{\tilde{M}}_\pi^2}{\mu^2} \\
& - \frac{M_\pi^4 3p^2q^2(q+1)^2r^2Y(3)^2}{32\pi^2(q+2)^4}\ln\frac{\tilde{M}_K^2}{\mu^2} + \frac{M_\pi^4 p^2q(q+1)^2\left(q^3-3q^2+3q+2\right) r^2Y(3)^2}{32\pi^2(q+2)^5}\ln\frac{\mathring{\tilde{M}}_K^2}{\mu^2} \\
& + \frac{M_\pi^4 p^2q^2(2q+1)^2r^2Y(3)^2}{96\pi^2(q+2)^4}\ln\frac{\tilde{M}_\eta^2}{\mu^2} + \frac{M_\pi^4 p^2q\left(2q^4-8q^3+13q+2\right) r^2Y(3)^2}{288\pi^2(q+2)^4}\ln\frac{\mathring{\tilde{M}}_\eta^2}{\mu^2} \\
& + \tilde{c}_4^{\text{no pole}}\tilde{d}_{c_4}^{\text{no pole}}
\end{aligned}
\tag{5.61}
$$

$L_{6,7,8}^r(\mu)$ must be replaced by their expressions eqs. (3.34)-(3.35), (3.38)-(3.39) and (3.60) to evaluate c_4. $\tilde{d}_{c_4}$ is the higher order remainder which is set to zero in the present analysis (it is expected to be of order $O(\tilde{m}_s^2)$ and thus with the scaling $\tilde{d}_{c_4} \simeq p^2 d_{c_4}$ for simulations where $q = \tilde{m}/\tilde{m}_s$ is small).

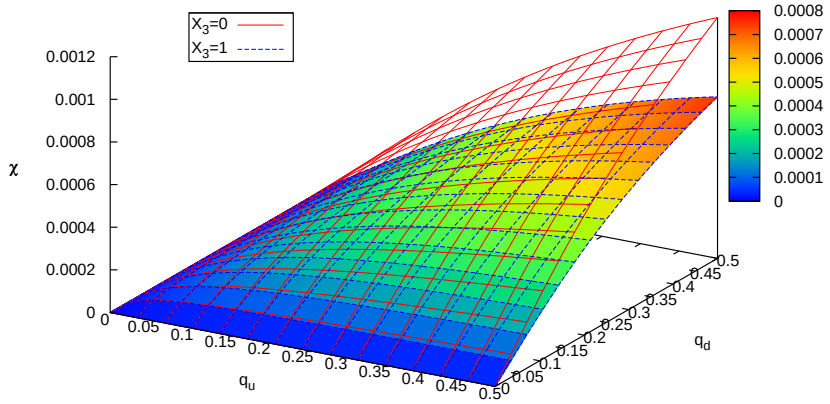

Figure 5.6: The topological susceptibility $\tilde{\chi}_t^{\text{no pole}}$ (in units of GeV^4) as a function of $q_u = \tilde{m}_u/\tilde{m}_s$ and $q_d = \tilde{m}_d/\tilde{m}_s$ for $X(3) = 0$ (solid) and $X_3 = 1$ (dashed with colour levels). For illustration, the remainders are set to be zero, $p = 1$, $Y(3) = 0.8$, $r = 26$, $F_K/F_\pi = 1.19$ and F_η =130 MeV.

The lattice counterpart of eq. (5.27) can be obtained by replacing all masses in the logarithms by their leading order values, yielding:

$$\begin{aligned}
\tilde{c}_4^{\text{no pole}} &= -\frac{F_\pi^2 M_\pi^2 pq\left(q^3+2\right) rX(3)}{2(q+2)^4} + \frac{M_\pi^4 p^2 q^2((13q^2+22q+37)r^2Y(3)^2}{96\pi^2(q+2)^4} \\
&- \frac{16L_6^r(\mu)M_\pi^4 p^2 q\left(q^4+2q^3+6q^2+8q+1\right) r^2Y(3)^2}{(q+2)^4} \\
&- \frac{96(3L_7+L_8^r(\mu))M_\pi^4 p^2 q^2\left(q^3+2\right) r^2Y(3)^2}{(q+2)^5} \\
&+ \frac{3M_\pi^4 p^2 q^2\left(2+q^2\right) r^2Y(3)^2}{8\pi^2(q+2)^5} \ln\frac{\overset{\circ}{\tilde{M}}_\pi^2}{\mu^2} + \frac{M_\pi^4 p^2 q(q+1)^2\left(q^3+9q+2\right) r^2Y(3)^2}{32\pi^2(q+2)^5} \ln\frac{\overset{\circ}{\tilde{M}}_K^2}{\mu^2} \\
&+ \frac{M_\pi^4 p^2 q\left(q^4+2q^3+6q^2+8q+1\right) r^2Y(3)^2}{144\pi^2(q+2)^4} \ln\frac{\overset{\circ}{\tilde{M}}_\eta^2}{\mu^2} + \tilde{c}_4^{\text{no pole}}\tilde{d}_{c_4}^{\text{no pole}}
\end{aligned} \tag{5.62}$$

We will use eq. (5.62) to determine the potentiality of the fourth cumulant c_4 to extract the three-flavour quark condensate from simulations performed with a mass hierarchy similar to the physical situation.

Let us first consider the physical case where $p = 1, q = 1/r$. In figure. 5.7, the dependence of c_4 on $X(3)$ and $Y(3)$ is plotted in the case where $r = 25$, indicating a noticeable sensitivity to $X(3)$ and a weak sensitivity to $Y(3)$, as expected from the discussion in sec. 5.4. We can now consider simulations with a near physical strange quark mass and light quark masses larger than the physical one (i.e., p close to 1 and $q \geq 1/r$). The variation of c_4 with respect to p and q, $X(3)$ and $Y(3)$ is shown in figure. 5.8. One notices that the slope of the curve is very dependent on $X(3)$, and more weakly on $Y(3)$, providing an efficient probe of the three-flavour quark condensate $X(3)$.

As expected from the qualitative discussion of the previous section, the topological susceptibility χ has a much weaker sensitivity to $X(3)$, which arises only for values of q closer

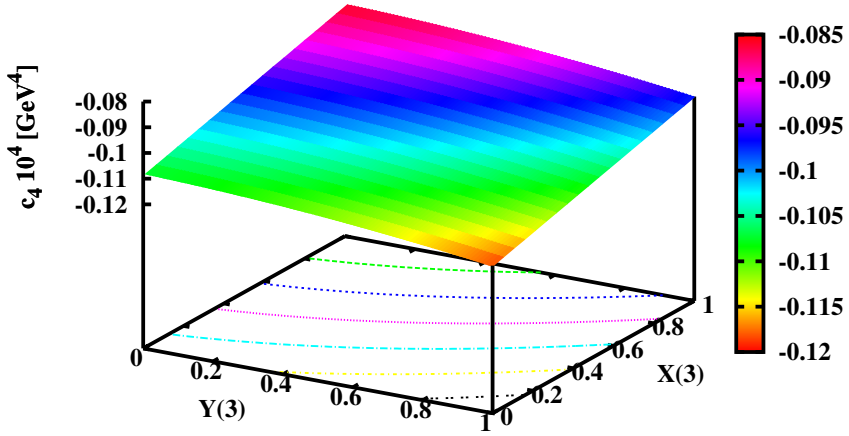

Figure 5.7: c_4 (in units of 10^4 GeV^4) as a function of $X(3)$ and $Y(3)$ for $p = 1, r = 1/q = 25$, and all HO remainders set to zero.

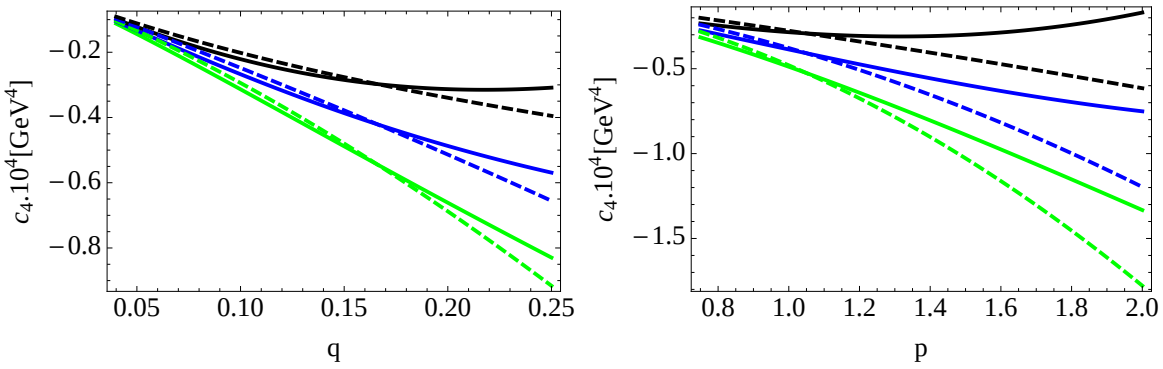

Figure 5.8: c_4 as a function of $q = \tilde{m}/\tilde{m}_s$ for $p = 1$ (left panel) and as a function of $p = \tilde{m}_s/m_s$ for $q = 0.15$ (right panel). Light (green), dark (blue) and black curves correspond to $X(3) = 0.2, 0.5, 0.8$ respectively, whereas solid and dashed curves correspond to $Y(3) = 0.9, 0.2$ respectively. We take $r = 25$ and all HO remainders are set to zero.

to 1, i.e., light quark masses away from the physical situation. This can be seen from the left-hand side of figure 5.9 (we plot here eq. (5.22) obtained without singling out the η-pole). We also display the normalised fourth cumulant $b_2 = c_4/(12\chi)$ on the right hand-side of figure 5.9, which exhibits the same interesting features as c_4 for the extraction of the three-flavour quark condensate. We notice that its dependence on the simulated light quark mass is modified compared to the leading order result [119]:

$$\tilde{b}_{2;LO} = -\frac{2+q^3}{12(2+q)^3} = -\frac{1}{48} + \frac{q}{32} + O(q^2) \tag{5.63}$$

both for the value at the origin and the slope, when the quark condensate does not saturate the thee-flavour expansions of quark masses. Different patterns of three-flavour chiral symmetry breaking, and in particular, different values of the three-flavour quark condensate,

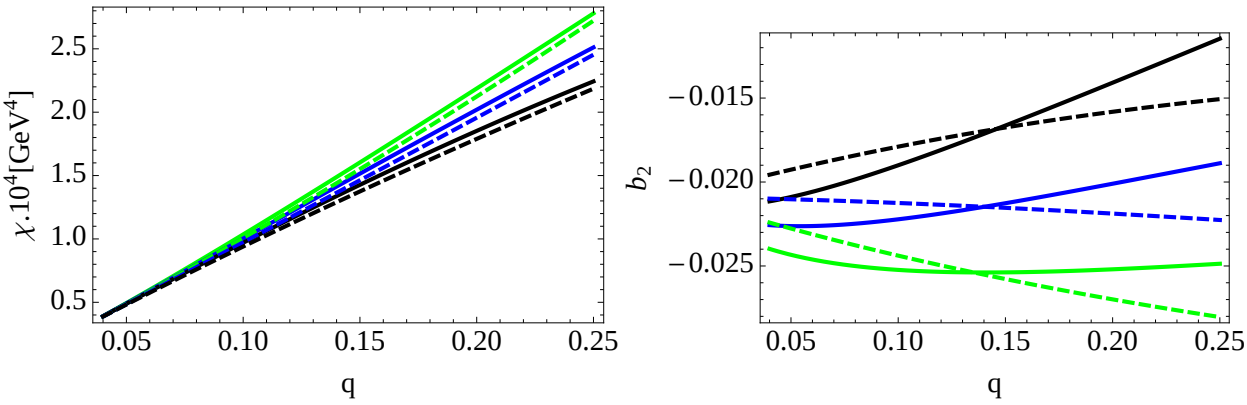

Figure 5.9: χ_t (left panel) and $b_2 = c_4/(12\chi)$ (right panel) as a function of $q = \tilde{m}/\tilde{m}_s$ for $p = 1, r = 25$. Light (green), dark (blue) and black curves correspond to $X(3) = 0.2, 0.5, 0.8$ respectively, whereas solid and dashed curves correspond to $Y(3) = 0.9, 0.2$ respectively. All HO remainders are set to zero.

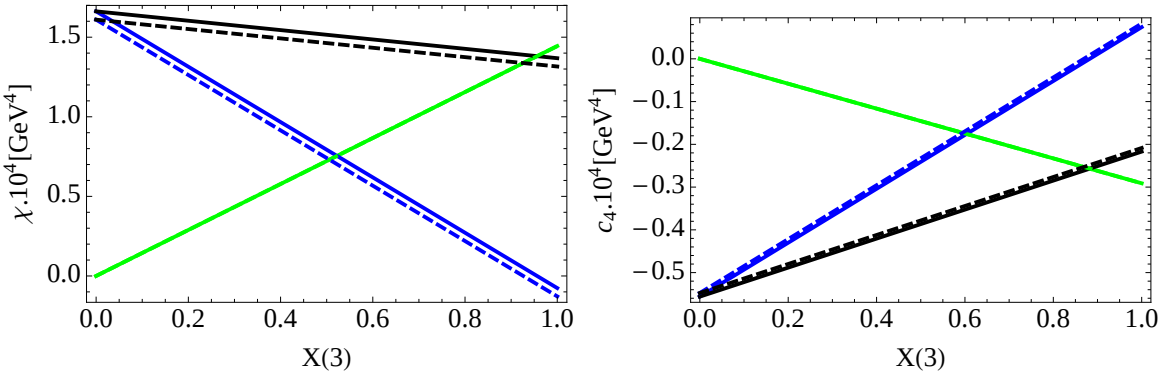

Figure 5.10: Order-by-order contributions to χ (left panel) and c_4 (right panel) as a function of $X(3)$ in the case $p = 1, q = 0.15, r = 25$. Light (green), dark (blue) and black curves correspond to LO contributions, NLO ones and their sum respectively. Solid and dashed curves correspond to $Y(3) = 0.9, 0.2$ respectively (they are identical for the LO contribution which depends on $X(3)$ and quark masses only). All HO remainders are set to zero.

can modify the dependence of this cumulant on the simulated light quark mass in a striking way.

In figure 5.10, we indicate the leading and next-to-leading order contributions to χ_t and c_4 for a simulation with $p = 1, q = 0.15$. One observes a significant cancellation of the two contributions in the case of c_4, emphasising the need to perform the analysis of this quantity up to one loop, no matter the pattern of chiral symmetry breaking. Moreover, one notices that the partial cancellation does not prevent the sum of leading and next-to-leading order contributions for c_4 to exhibit a strong dependence on $X(3)$, contrary to the topological susceptibility χ_t which again shows a very mild dependence on $X(3)$ (as expected since $q = \tilde{m}/\tilde{m}_s$ is small).

5.6.2 Resummed framework (2): with η pole

Identifying the poles corresponding to the propagation of the pseudoscalar mesons is of particular relevance within Resummed χPT. In this framework, smaller higher order remainders are expected when singularities of the expansion (and in particular, poles) are correctly lo-

cated at the physical positions. Thanks to our diagrammatical analysis of the two-point correlator χ in χPT, we can easily identify the contribution from the propagation of the η meson in eq. (5.57), and we obtain the expressions for the pole residue and the analytical piece arising in eq. (5.35), $\tilde{R}$:

$$\tilde{R} = -\frac{(pr(q-1))^2}{27}F_\pi^2 M_\pi^4 X(3)Y(3) + \frac{8}{27}(pr)^3(1-q)^2 M_\pi^6 Y(3)^3\left[(2q+1)L_4^r + \frac{q+2}{3}L_5^r\right] \tag{5.64}$$
$$- \frac{32}{27}(pr)^3 Y(3)^3 M_\pi^6[(L_6^r+L_7)(q-1)^2(2q+1) + L_8^r(q^2-1)(q-1)]$$
$$+ \frac{(pr)^3(q-1)}{864\pi^2}M_\pi^6 Y(3)^3\left[6q^2\log\frac{\overset{\circ}{\tilde{M}}_\pi^2}{\mu^2} - (1+q)^2\log\frac{\overset{\circ}{\tilde{M}}_K^2}{\mu^2} + \frac{2}{9}(q-4)(q+2)\log\frac{\overset{\circ}{\tilde{M}}_\eta^2}{\mu^2}\right]$$

and $\tilde{S}$:

$$\tilde{S} = \frac{pr(2q+1)}{18}F_\pi^2 M_\pi^2 X(3) + \frac{8}{9}(pr)^2 Y(3)^2 M_\pi^4[(2q+1)^2(L_6^r+L_7) + (2q^2+1)L_8^r] \tag{5.65}$$
$$- \frac{(pr)^2}{576\pi^2}Y(3)^2 M_\pi^4\left[6q^2\log\frac{\overset{\circ}{\tilde{M}}_\pi^2}{\mu^2} + 2(q+1)^2\log\frac{\overset{\circ}{\tilde{M}}_K^2}{\mu^2} + \frac{2}{9}(2+q)^2\log\frac{\overset{\circ}{\tilde{M}}_\eta^2}{\mu^2}\right]$$

where the counterterms can be expressed in terms of $r, X(3), Z(3)$ and the remainders. The topological susceptibility then reads:

$$\tilde{\chi}_t^{\text{pole}} = \frac{\tilde{R}}{\tilde{M}_\eta^2} + \tilde{S} + \tilde{\chi}^{\text{pole}}\tilde{d}_{\chi^{\text{pole}}} \tag{5.66}$$

where the η mass on the lattice, $\tilde{M}_\eta^2$, is given by the ratio $(\tilde{F}_\eta^2\tilde{M}_\eta^2)/\tilde{F}_\eta^2$, from equations (6.6)-(6.7) given in sec. 6.2.3. At this stage, one has still to discuss the direct remainder $\chi_t d_{\chi_t}$ which corresponds to higher-order terms, and has been added in eq. (5.66) as well as in eq. (5.57). One wants d_{χ_t} to start at next-to-next-to-leading order, and thus to be of order $O(m_q^2)$. This expectation can be checked by considering various chiral limits sending $\tilde{m}$ and/or $\tilde{m}_s$ to zero. As already explained previously, the topological susceptibility χ should vanish in the limit where one of the quark masses goes to zero. In our framework, this can be translated as $\chi_t \to 0$ for the three chiral limits:

- $\tilde{m}_s \to 0$, $\tilde{m}$ fixed: $p \to 0$, pq fixed,
- $\tilde{m} \to 0$, $\tilde{m}_s$ fixed: $q \to 0$, p fixed,
- $\tilde{m}, \tilde{m}_s \to 0$, $\tilde{m}/\tilde{m}_s$ fixed: $p \to 0$, q fixed.

By inspection, one can check that the sum of leading and next-to-leading order in eq. (5.57) does vanish in these three limits, whereas eqs. (5.64)-(5.65) vanish in these limits only up to nonzero higher-order corrections. Therefore, if we consider the expression for the topological susceptibility not singling out the η-pole, eq. (5.57), we can add a higher-order remainder of the form $\tilde{\chi}_t^{\text{no pole}}\tilde{d}_{\chi_t^{\text{no pole}}}$ with $\tilde{d}_{\chi_t^{\text{no pole}}} = O(\tilde{m}_q^2)$ that has no singularities when any $\tilde{m}_q \to 0$. In the situations that we consider (one of the masses much larger than the other ones), we expect $\tilde{d}_{\chi_t^{\text{no pole}}}$ to be dominated by $\tilde{m}_s^2$ contributions.

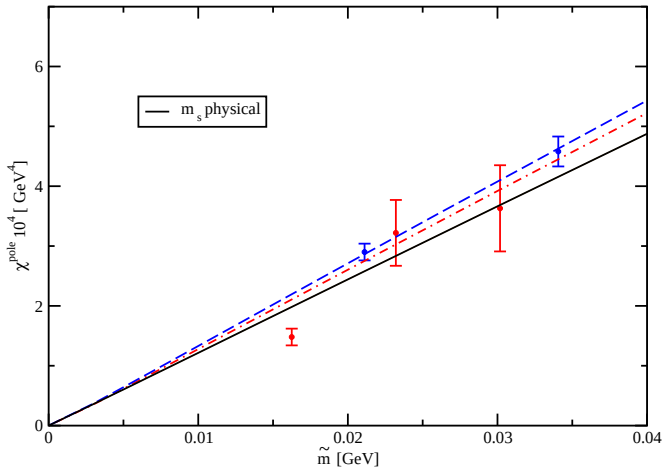

Figure 5.11: The topological susceptibility $\tilde{\chi}_t^{\rm pole}$ as a function of the light quark mass. The black [red] points correspond to the $(24)^3 \times 64$ volume [$(32)^3 \times 64$], using the estimates of lattice spacings quoted in ref. [122]. The dashed curves correspond to the best fit using $\chi_t^{\rm pole}$ with finite-volume effects, as indicated in the last column of table 6.4 (removing finite-volume effects would lead to almost identical curves). We have not included the lightest point in our analysis, as discussed in the text. As a reference, we have also indicated the same variation when the strange quark mass is set to its physical value.

On the other hand, if we single out the η-pole contributions following eq. (5.57), we would need $\tilde{d}_{\chi_t^{\rm pole}}$ to become singular in the chiral limits considered before, so that $\tilde{\chi}_t^{\rm pole}\tilde{d}_{\chi_t^{\rm pole}}$ does not vanish and cancels the non-vanishing value of eqs. (5.64)-(5.65) coming from higher-order terms. A more satisfying solution consists in subtracting these higher-order pieces from the higher order remainders, so that d_{χ_t} does not exhibit singularities in any of the chiral limits. In other words, using eqs. (5.64)-(5.65), we write the topological susceptibility as:

$$C(\tilde{m},\tilde{m}_s) = \frac{\tilde{R}}{\tilde{M}_\eta^2} + \tilde{S}\,, \qquad \tilde{\chi}_t^{\rm pole} = C(\tilde{m},\tilde{m}_s) - C(0,\tilde{m}_s) - C(\tilde{m},0) + \tilde{\chi}_t^{\rm pole}\tilde{d}_{\chi_t^{\rm pole}} \qquad (5.67)$$

One can check that the subtracted terms $C(0,\tilde{m}_s) = O(\tilde{m}_s^2)$ and $C(\tilde{m},0) = O(\tilde{m}^2)$ are indeed higher order terms. With the definition eq. (5.67), which will be used in the following, $\tilde{d}_\chi^{\rm pole}$ is regular in the chiral limits described above, and can be considered as $O(\tilde{m}_s^2)$ for the simulations considered here. Finally, one should notice that $\tilde{R}$ and $\tilde{S}$ involve again not only the three-flavour condensate $X(3)$ but also next-to-leading order low energy constants, and in particular L_6. This dependence is equivalent to that of eq. (5.57) up to higher orders in the expansion of the quark masses. It is therefore of no surprise that we find only small numerical differences between eq. (5.57) and eqs. (5.64)-(5.65) in the range of quark masses of physical interest, and that the previous conclusion concerning the potentiality of the topological susceptibility to determine the three-flavour quark condensate still applies in this setting.

We stress that the fourth cumulant c_4 can undergo the same treatment. We will not display the corresponding equations, but they can be easily recorded from the physical case shown in sec. 5.3.2. If we call C the sum of all the diagrams with the η propagator being identified (from sec. 5.3.2), one could naively think that we just have to add to the leading and next-to-leading order terms a higher order remainder $d_{c_4}^{\rm pole}$ of the form:

$$c_4^{\text{pole}} = C + c_4^{\text{pole}} d_{c_4}^{\text{pole}} \tag{5.68}$$

However, like in the case of the topological susceptibility, one notices that C does not vanish in the limit $m \to 0$ and/or $m_s \to 0$, contrary to the expectation that $c_4^{\text{pole}} \to 0$ then, since the effective potential becomes independent of θ in these limits. This definition of $d_{c_4}^{\text{pole}}$ must thus exhibit a divergent contribution in these chiral limits, so that $c_4^{\text{pole}} d_{c_4}^{\text{pole}}$ can compensate the non-vanishing value of C to fulfill $c_4^{\text{pole}} \to 0$.

Such a behaviour of $d_{c_4}^{\text{pole}}$ is not very satisfying, as we would like higher-order remainders to become smaller and smaller in the limits of vanishing quark masses. This can be resolved by defining the remainder as

$$c_4^{\text{pole}}(m, m_s) = C(m, m_s) - C(m, 0) - C(0, m_s) + c_4^{\text{pole}} d_{c_4}^{\text{pole}} \tag{5.69}$$

This corresponds formally to a redefinition of the higher-order remainder, but has the important consequence that $d_{c_4}^{\text{pole}}$ exhibits no divergence in the two massless limits, should be small even in the chiral limit(s) and can be approximated by a polynomial. In the physical setting where m_s is much larger than m, we expect $d_{c_4}^{\text{pole}} = O(m_s^2)$.

The difference between the two expressions eqs. (5.28) and (5.69) corresponds to a reshuffling between the sum of leading order and next-to-leading order contributions and higher-order remainders. Since we hope to achieve a formulation with small higher order remainders, the numerical differences between these expressions may become important to extract information on the pattern of $N = 3$ chiral symmetry breaking from precise lattice values of c_4.

5.7 Summary

This chapter was devoted to the detailed introduction of two topological quantities, the topological susceptibility χ_t and the fourth cumulant c_4, in the framework of Chiral Perturbation Theory. They were first derived using the method of effective potential minimization, up to next-to-leading order, in the case of an arbitrary number of quark flavours. The subsequent expressions for $N_f = 3$ were straighforwardly obtained. We then performed the same calculations but this time using diagrammatic methods (in the isospin limit). This helped in particular to isolate the propagator of the η in order to shift the pole of the two observables from $\overset{\circ}{M}{}_\eta^2$ to M_η^2.

From this basis, we discussed the expected sensitivity of the two quantities to the three-flavour quark condensate. We saw in particular that for simulations close to the physical point, the topological susceptibility would be sensitive to the two-flavour quark condensate and could not probe the three-flavour quark condensate, contrarily to the fourth cumulant. We also gave their expressions in the case $N_f = 2$, and discussed the matching of these expressions with those obtained in the case $N_f = 3$ χPT.

In the last section, we studied in more detail the behavior of χ_t and c_4 on the lattice, separating the cases where the η pole was not identified and where it was singled out. We showed more precisely how χ_t exhibited a poor sensitivity to the three-flavour quark condensate close to the physical point. The same was carried out for c_4, which indeed showed a strong dependence on the quark condensate, as opposed to the topological susceptibility. We also discussed the treatment of higher order remainders in the two ways of dealing with the η pole, highlighting that unphysical divergences could affect these remainders if they are not defined properly. In the final chapter, we will be studying a series of fits to decay constants, masses and the topological susceptibility using data from $2+1$ lattice simulations in the same spirit as in Chapter 4.

Chapter 6

Fits to lattice data on topological susceptibility

6.1 Introduction

We want now to exploit the topological susceptibility to improve our determination of the pattern of three-flavour chiral symmetry breaking. We have however seen in sec. 5.6.1 that the usual setting of lattice simulations is not appropriate, as the topological susceptibility is then driven by the two-flavour condensate. If we want to extract information on the three-flavour pattern, we need either to make simulations away from the physical case (as discussed in sec. 5.6.1), or to supplement the topological susceptibility with other sources of information. We will now take this second option, which is also required due to the number of parameters involved in the next-to-leading order expression of the topological susceptibility (in particular the parameters of the leading order chiral Lagrangian and higher order remainders). We shall therefore include pseudoscalar masses and decay constants in our considerations, and test the compatibility of the topological susceptibility with the pattern of three-flavour chiral symmetry breaking obtained from the lattice data.

The material presented in this chapter is the object of [93]. There are several lattice calculations of the topological susceptibility in the literature, e.g. refs. [120, 122]. As an illustration of our approach, we will focus on the ones from RBC/UKQCD following the work presented in chapter 4, as this collaboration provides all the details (masses, decay constants and topological susceptibility) necessary for our analysis. Since the work presented in Chapter 4, new data from this collaboration have been issued with a new volume and different quark masses, given in ref. [122], and we will use them as a reference in the coming sections. We follow the approach of Chapter 4 and perform a fit to the two sets of data in the $24^3 \times 64$ ($a^{-1} = 1.73(3)$ GeV) and $32^3 \times 64$ volumes ($a^{-1} = 2.28(3)$ GeV) with and without including finite volume effects. In this chapter, the determination of the lattice spacings will be discussed.

6.2 Fits to lattice data

6.2.1 Lattice inputs

We take our data points for pseudoscalar decay constants and masses as well as for the topological susceptibility from the recent work of the RBC/UKQCD collaboration [122]. They considered $2 + 1$ dynamical flavours of domain wall fermions for two different lattice volumes $24^3 \times 64 \times 16$ and $32^3 \times 64 \times 16$ (where the 16 corresponds to the extent of the fifth dimension inherent in the domain-wall fermion formulation of QCD). We consider only unitary sets where the masses of the sea and valence quarks are identical, with parameters

L	a^{-1}	Δ_q	Δ_s	Z_m^q	Z_m^s	$\tilde{m}_q$	$\tilde{m}_s$	m_s	p	q
24	1.73	0.005	0.04	1.4980	1.4707	0.0211	0.1098	0.0962	1.1420	0.1924
		0.010				0.0342				0.3111
32	2.28	0.004	0.03	1.527	1.510	0.0163	0.1056	0.0962	1.0976	0.1539
		0.006				0.0232				0.2196
		0.008				0.0302				0.2859

Table 6.1: Parameters of the unitary lattice sets taken from ref. [122].

L	p	q	$\chi_t \cdot 10^{-4}$	F_π^2	F_K^2	$F_\pi^2 M_\pi^2$	$F_K^2 M_K^2$
24	1.1420	0.1924	2.90(14)	10.41(13)	13.47(14)	1.129(16)	4.459(50)
		0.3111	4.58(25)	12.26(14)	14.85(18)	2.152(25)	5.471(68)
32	1.0976	0.1539	[1.48(14)]	9.799(96)	12.99(11)	0.820(10)	3.988(36)
		0.2196	3.22(55)	10.65(10)	13.51(11)	1.265(13)	4.390(38)
		0.2859	3.63(72)	11.53(10)	14.16(12)	1.788(18)	4.895(42)

Table 6.2: Lattice data for the pseudoscalar masses and decay constants as well as topological susceptibility taken from ref. [122].

recalled in table 6.1 and observables in table 6.2. For the masses and decay constants they correspond to the data used in Chapter 4, without the data on the $K_{\ell 3}$ form factors, but adding the ones on the topological susceptibility from [122] corresponding to the same pairs of quark masses.

We denote $\Delta_q = a(\tilde{m}_q - m_{res})$ the combination corresponding to bare masses (before addition of the residual mass m_{res} and the conversion into the $\bar{M}S$ scheme by a multiplication by Z^m). We give a^{-1} and quark masses in units of GeV, χ_t in units of 10^{-4} GeV^4, F_P^2 in units of 10^{-3} GeV^2, $F_P^2 M_P^2$ in units of 10^{-3} GeV^4. The dimensionful quantities have been converted from the lattice results by multiplying by the appropriate power of the lattice spacing, assuming for the latter the values quoted in the table. When the lattice spacings are allowed to vary and included in the parameters of the fits in sec. 6.3.1, these quantities are naturally rescaled by the appropriate power of the relevant lattice spacing.

In table 6.2, we do not include uncertainties coming from the determination of the lattice spacings, as these uncertainties would be completely correlated. Moreover, as explained at the end of sec. 6.2.4, we do not include the value of the topological susceptibility at a lighter quark mass given in ref. [122], since it is likely to be affected by large systematics of unknown origin. In sec. 6.2.4, we discuss the determination of the lattice spacings performed in ref. [122] using the mass of the Ω baryon, gathered in table 6.3.

L	a^{-1}	Δ_q	Δ_s	aM_Ω
24	1.73	0.005	0.04	1.013(3)
		0.010		1.028(4)
32	2.28	0.004	0.03	0.760(2)
		0.006		0.765(2)
		0.008		0.766(3)

Table 6.3: Lattice data for the Ω baryon taken from ref. [122].

A last comment is in order concerning the determination of the topological susceptibility in ref. [120], based on gauge configurations for a smaller volume $(16)^3 \times 32$ in refs. [98, 134].

In principle, this work could provide valuable additional information, but we have not been able to obtain consistent fits of the masses and decay constants of pions and kaons with the three ensembles $(16)^3 \times 32$, $(24)^3 \times 64$, $(32)^3 \times 64$, leading us to suspect an underestimation of the errors attached to the data for $(16)^3 \times 32$. We have thus decided to keep only data for $(24)^3 \times 64$, $(32)^3 \times 64$, which were obtained for larger volumes and lighter quark masses, and thus less likely to be affected by sizable systematics.

Concerning c_4, several lattice computations of the (normalized) fourth cumulant have been performed in pure gauge theory for different number of colours [138, 139, 140]. Even though their values for 3 colours are rather close to those that we will obtain in the following, they cannot be used to investigate the role of sea quark-pairs in chiral symmetry breaking (see ref. [141] for more details and references on these simulations). There exist also computations with 2 and (2+1) dynamical fermions from the TWQCD collaboration [120, 123], whose central values are in the same ball park as our results, but with so large uncertainties that any practical comparison with our figures is meaningless at the current stage. So, no data concerning c_4 were included in our fits.

6.2.2 Finite-volume effects

Before delving into the heart of the matter, it is necessary to introduce the issue of finite-volume effects, and how the next-to-leading order expressions for decay constants, masses and topological susceptibility are to be modified. Two different lattice artefacts can affect the results of simulations before considering the continuum limit: the first corresponds to the finite size of the lattice spacing, which can be included, in principle, in the chiral expansion through spurions that depends on the implementation of the fermion action (see ref. [128] and references therein). We will not include this effect in the first step of our analysis, but we will include it (partially) in our final fits.

A second effect comes from the finiteness of the volume used for lattice simulations, which induces finite-volume modifications of the chiral expansions. As discussed in refs. [113, 129, 130, 131, 132], the finite-volume effects for next-to-leading order chiral perturbation theory amount to a modification of the chiral logarithms:

$$\frac{\overset{\circ}{M}{}_P^2}{16\pi^2} \log \frac{\overset{\circ}{M}{}_P^2}{\mu^2} \to \frac{1}{2L^3} \sum_\ell \frac{1}{\omega_P} = \frac{1}{2L^3} \sigma_P \tag{6.1}$$

where $\ell \in 2\pi/L \times Z^3$ and $\omega_P = \sqrt{\ell^2 + \overset{\circ}{M}{}_P^2}$ is the quantized momentum. The summation over the three spatial directions comes from the quantization of momenta due to the periodic boundary conditions on the lattice box (making it a torus in practice). We consider simulations where the time component is significantly larger than the spatial components, and therefore consider only the finite-volume effects related to the latter [130, 131, 132]. One can relate the finite-volume chiral "logarithm" with its infinite-volume counterpart through the function:

$$\frac{\sigma_P}{L^3} = \frac{\overset{\circ}{M}{}_P^2}{8\pi^2} \log \frac{\overset{\circ}{M}{}_P^2}{\mu^2} + \Xi_P \tag{6.2}$$

where the function $\Xi_P = \xi_{1/2}(L, \overset{\circ}{M}{}_P^2)$ was introduced in ref. [130]. An alternative definition of Ξ_P was proposed in ref. [80] and is rediscussed in Appendix B. So, in practice, one has to make the (very simple) shift (6.1) in order to take finite-volume effects into account in next-to-leading order chiral expressions. We will take into account these corrections in the following analysis for all the quantities of interest: for masses and decay constants, the

corrections can be read directly from the expressions in ref. [92] (one has simply to make the shift (6.1) to recover the expansions at finite volume). In the same manner, we have for the topological susceptibility the following correction from finite-volume effects to the expression without singling out the η-pole:

$$\chi_t^{\text{no pole}}(L) = \chi_t^{\text{no pole}}(\infty) - \frac{1}{8}Y(3)M_\pi^2 \frac{pqr}{(q+2)^2}\left[6\Xi_\pi + 4(q+1)\Xi_K + \frac{2}{3}(2q+1)\Xi_\eta\right] \quad (6.3)$$

and when one singles out the η-pole:

$$\tilde{R}(L) = \tilde{R}(\infty) + \frac{(pr)^2(q-1)}{54}Y(3)^2 M_\pi^4\left[3q\Xi_\pi - (1+q)\Xi_K + \frac{1}{3}(q-4)\Xi_\eta\right] \quad (6.4)$$

$$\tilde{S}(L) = \tilde{S}(\infty) - \frac{pr}{72}Y(3)M_\pi^2\left[6q\Xi_\pi + 4(q+1)\Xi_K + \frac{2}{3}(2+q)\Xi_\eta\right] \quad (6.5)$$

where the quantities labeled at infinity are taken in the infinite volume limit. We neglect any dependence of the higher-order remainders on finite-volume effects, effectively identifying the higher-order remainders at finite and infinite volumes.

6.2.3 Parameters and data

The fits include the data collected in sec. 6.2.1, i.e. pion and kaon masses and decay constants as well as the topological susceptibility. Similarly as in Chapter 4, we build a χ^2 depending on the following parameters:

- the three leading-order parameters $r, X(3), Z(3)$ (eq. 3.13)
- a reference ratio between a simulated strange quark (chosen conventionally to be for the 24^3 simulations) and the physical strange quark mass,
- the higher order remainders associated with the pion and kaon masses and decay constants (denoted d, e, d', e'),
- the ratio F_K/F_π (on the other hand, we set $F_\pi = 92.2$ MeV),
- if the topological susceptibility is included, the corresponding higher-order remainders for the η mass and decay constant (d_η, e_η) as well as the one for the topological susceptibility (d_{χ_t}).

Higher order remainders are restricted to remain within a range based on a naive dimensional analysis, as was described in sec. 3.4.2. At this step, we will include no discretization error effects in our three-flavour chiral expansions, and we shall come back to that issue in sec. 6.3.1.

We also need the following expressions for the η mass and decay constant for lattice simulations:

$$\tilde{F}_\eta^2 = F_\pi^2 Z(3) + 8pqr\left(\frac{1}{q}+2\right)Y(3)M_\pi^2 L_4^r(\mu) + \frac{8}{3}pqr\left(\frac{2}{q}+1\right)Y(3)M_\pi^2 L_5^r(\mu) \quad (6.6)$$
$$- \frac{M_\pi^2}{32\pi^2}pqrY(3)\log\frac{\overset{\circ}{\tilde{M}}{}_K^2}{\mu} + \tilde{F}_\eta^2\tilde{e}_\eta$$

$$\tilde{F}_\eta^2\tilde{M}_\eta^2 = \frac{pqr}{3}\left(\frac{2}{q}+1\right)F_\pi^2 M_\pi^2 X(3) + \frac{16}{3}(pqr)^2\left(\frac{2}{q}+1\right)\left(\frac{1}{q}+2\right)Y^2(3)M_\pi^4 L_6^r(\mu) \tag{6.7}$$
$$+ \frac{32}{3}(pqr)^2\left(\frac{1}{q}-1\right)^2 Y^2(3)M_\pi^4 L_7 + \frac{16}{3}\left(\frac{2}{q^2}+1\right)(pqr)^2 Y^2(3)M_\pi^4 L_8^r(\mu)$$
$$- \frac{M_\pi^4}{32\pi^2}[pqrY(3)]^2\left(\frac{1}{3}\left(\frac{2}{q}+1\right)\left[2\left(\frac{1}{q}+1\right)\log\frac{\overset{\circ}{\tilde{M}}_K^2}{\mu^2} + \frac{4}{9}\left(\frac{2}{q}+1\right)\log\frac{\overset{\circ}{\tilde{M}}_\eta^2}{\mu^2}\right]\right.$$
$$\left. + \left[\log\frac{\overset{\circ}{\tilde{M}}_\pi^2}{\mu^2} - \frac{1}{3}\left(\frac{1}{q}+1\right)\log\frac{\overset{\circ}{\tilde{M}}_K^2}{\mu^2} - \frac{1}{9}\left(\frac{2}{q}+1\right)\log\frac{\overset{\circ}{\tilde{M}}_\eta^2}{\mu^2}\right]\right) + \tilde{F}_\eta^2\tilde{M}_\eta^2\tilde{d}_\eta$$

where L_7 is given by eq. (3.60), and equivalent expressions for $L^r_{4,5,6,8}$ can be found from eqs. (3.32) to (3.39) in terms of $r, X(3), Z(3)$, higher order remainders, masses and decay constants). The higher order remainders $\tilde{d}_\eta, \tilde{e}_\eta$ are supposed to scale like $\tilde{m}_s^2$ for simulations where the simulated strange quark is much heavier than the other ones.

6.2.4 Results and discussion

In this section, we discuss a first series of fits, including or not the topological susceptibility as well as finite volume effects. As shown in table 6.4, the pattern of $N_f = 3$ chiral symmetry breaking with low quark condensate and decay constant observed in [122] is confirmed by our analysis, whether we include or not the topological susceptibility in our fit. The outcome of the fit is thus mainly driven by the spectrum of pseudoscalar mesons, but the quality of the agreement is not modified by the inclusion of the topological susceptibility, which thus exhibits a good compatibility with the rest of the fit and is consistent with the pattern of chiral symmetry breaking described in Chapter 4. As in our previous work, L_4 and L_6 do not show any sign of Zweig suppression and the competition between leading and next-to-leading orders in three-flavour chiral expansions is clearly seen. We obtain values for the $N_f = 2$ chiral order parameters in agreement with expectations from two-flavour χPT [1] as well as experimental information on $\pi\pi$ scattering, such as that from K_{l4} decays [53, 54, 56, 57, 58, 62, 63]. The values of $\bar{\ell}_3$ and $\bar{\ell}_4$ given there can be compared to the one obtained from the RBC/UKQCD collaboration, ref. [122]: $\bar{\ell}_3 = 2.82(16), \bar{\ell}_4 = 3.76(9)$ in infinite-volume χPT and $\bar{\ell}_3 = 2.57(18), \bar{\ell}_4 = 3.83(9)$ in finite-volume χPT. One can also recall the value quoted by the Flavour Lattice Averaging Group [95] for $\bar{\ell}_3 = 3.2(8)$ (no value was quoted for $\bar{\ell}_4$ in this reference). Finally, one notices that singling out the η-pole or not in the expression of the topological susceptibility does not modify significantly the analysis: the values obtained with eqs. (5.57) and (5.64)-(5.65) are very close numerically for the ranges of parameters considered here.

Fit name	$A1$	$A2$	$A3$	$A4$	$A5$
χ_t	No	No	χ_t^{nopole}	χ_t^{pole}	χ_t^{pole}
Finite volume	No	Yes	No	No	Yes
r	23.0 ± 0.7	23.4 ± 0.7	23.0 ± 0.7	23.0 ± 0.7	23.4 ± 0.7
$X(3)$	0.33 ± 0.10	0.34 ± 0.05	0.33 ± 0.06	0.33 ± 0.06	0.34 ± 0.05
$Y(3)$	0.49 ± 0.15	0.53 ± 0.07	0.49 ± 0.08	0.49 ± 0.08	0.53 ± 0.07
$Z(3)$	0.68 ± 0.03	0.65 ± 0.03	0.68 ± 0.03	0.68 ± 0.03	0.65 ± 0.03
F_K/F_π	1.17 ± 0.01	1.17 ± 0.01	1.17 ± 0.01	1.17 ± 0.01	1.17 ± 0.01
Rem. at limit	d	d	$d, e, d_{\chi t}$	$d, e, d_{\chi t}$	$d, e_\eta, d_{\chi t}$
$\tilde{m}_s(24^3)/m_s$	1.12 ± 0.02	1.12 ± 0.02	1.12 ± 0.02	1.12 ± 0.02	1.12 ± 0.02
$m_s(2\text{ GeV})$[MeV]	98.1 ± 1.7	98.4 ± 1.8	98.0 ± 1.7	98.0 ± 1.7	98.4 ± 1.8
$m(2\text{ GeV})$[MeV]	4.3 ± 0.1	4.2 ± 0.1	4.3 ± 0.1	4.3 ± 0.1	4.2 ± 0.1
$\Sigma_0^{1/3}(2\text{ GeV})$[MeV]	186 ± 19	211 ± 7	186 ± 11	186 ± 12	189 ± 10
$B_0(2\text{ GeV})$[GeV]	1.12 ± 0.34	1.22 ± 0.17	1.11 ± 0.21	1.12 ± 0.21	1.22 ± 0.17
F_0[MeV]	75.9 ± 1.3	74.4 ± 1.4	75.9 ± 1.3	75.9 ± 1.3	74.5 ± 1.4
F_η[MeV]	–	–	117 ± 16	128 ± 10	124 ± 6
$\chi_t \cdot 10^4[\text{GeV}^4]$	–	–	0.51 ± 0.01	0.49 ± 0.02	0.50 ± 0.02
$\tilde{m}_s(32^3)/m_s$	1.08 ± 0.02	1.09 ± 0.02	1.07 ± 0.02	1.08 ± 0.02	1.07 ± 0.02
$L_4(\mu) \cdot 10^3$	1.12 ± 0.46	0.65 ± 0.45	1.13 ± 0.30	1.12 ± 0.30	0.60 ± 0.43
$L_5(\mu) \cdot 10^3$	2.13 ± 0.78	2.05 ± 0.40	2.14 ± 0.53	2.13 ± 0.53	2.04 ± 0.39
$L_6(\mu) \cdot 10^3$	3.00 ± 3.05	2.55 ± 0.89	3.13 ± 1.44	3.10 ± 1.42	2.52 ± 0.88
$L_7(\mu) \cdot 10^3$	–	–	-2.60 ± 1.02	-1.82 ± 0.47	-1.70 ± 0.40
$L_8(\mu) \cdot 10^3$	4.12 ± 2.74	3.39 ± 1.13	4.17 ± 1.79	4.12 ± 1.77	3.35 ± 1.11
$X(2)$	0.90 ± 0.01	0.90 ± 0.01	0.90 ± 0.01	0.90 ± 0.01	0.90 ± 0.01
$Y(2)$	0.99 ± 0.01	1.00 ± 0.01	0.99 ± 0.01	0.99 ± 0.01	1.00 ± 0.01
$Z(2)$	0.91 ± 0.01	0.91 ± 0.01	0.91 ± 0.01	0.91 ± 0.01	0.90 ± 0.01
$\Sigma^{1/3}(2\text{ GeV})$[MeV]	260 ± 3	261 ± 3	260 ± 2	260 ± 3	261 ± 2
$B(2\text{ GeV})$[GeV]	2.26 ± 0.07	2.31 ± 0.06	2.26 ± 0.07	2.26 ± 0.07	2.31 ± 0.06
F[MeV]	88.0 ± 0.4	87.8 ± 0.2	88.1 ± 0.2	88.0 ± 0.22	87.8 ± 0.14
$\bar{\ell}_3$	-1.6 ± 1.4	-0.5 ± 0.9	-1.6 ± 1.2	-1.6 ± 1.2	-0.5 ± 0.9
$\bar{\ell}_4$	3.0 ± 0.3	3.2 ± 0.1	3.0 ± 0.1	3.0 ± 0.2	3.2 ± 0.1
$\Sigma/\Sigma_0 = \Sigma(2)/\Sigma(3)$	2.72 ± 0.78	2.64 ± 0.35	2.74 ± 0.46	2.72 ± 0.46	2.62 ± 0.35
$B/B_0 = B(2)/B(3)$	2.02 ± 0.56	1.89 ± 0.23	2.03 ± 0.32	2.02 ± 0.33	1.89 ± 0.22
$F/F_0 = F(2)/F(3)$	1.16 ± 0.02	1.18 ± 0.02	1.16 ± 0.02	1.16 ± 0.02	1.18 ± 0.02
χ^2/N	28.7/11	18.7/11	29.2/12	29.4/12	19.2/12
Gaussian equiv.	3.0σ	1.8σ	2.9σ	2.9σ	1.7σ

Table 6.4: Results of fits performed on the data from RBC/UKQCD collaboration on pseudoscalar masses and decay constants, including or not the topological susceptibility [122]. In two cases, finite-volume effects are taken into account. In all cases, we considered only data with light pions and only statistical errors are shown. The LECs are given at the scale $\mu = M_\rho$.

Focusing on the results including $\chi_t^{\rm pole}$ with finite-volume effects, we obtain the following convergence at $\chi^2_{\rm min}$ with the relative leading order, next-to-leading and higher order contributions:

$$\begin{array}{rcl@{\qquad}rcl} F_\pi^2 & : & 0.65 + 0.40 - 0.05\,, & F_\pi^2 M_\pi^2 & : & 0.35 + 0.79 - 0.14 \\ F_K^2 & : & 0.47 + 0.56 - 0.03\,, & F_K^2 M_K^2 & : & 0.24 + 0.86 - 0.10 \\ F_\eta^2 & : & 0.40 + 0.57 + 0.03\,, & F_\eta^2 M_\eta^2 & : & 0.23 + 0.80 - 0.03 \\ \chi_t^{\rm pole} & : & 0.22 + 0.63 + 0.15\,, & & & \end{array} \tag{6.8}$$

showing that the global convergence is good (small higher order remainders), but the leading and next-to-leading order contributions are indeed competing numerically, confirming the results obtained in the previous chapter. However, fitting the RBC/UKQCD data in the two volumes, we obtain a rather poor fit of χ^2/d.o.f.=29.4/12 without finite-volume effects, which can be seen as a 2.9σ discrepancy in a naive (purely Gaussian) statistical interpretation. The fit improves when one includes finite-volume effects, getting down to a 1.7σ effect, as can be seen by comparing the fits $A1$ and $A2$ (or $A4$ and $A5$) in table 6.4. Indeed, even though these effects are rather small in the ranges of quark masses considered here, they tend to bring the various quantities in better agreement with the lattice data (cf. sec. 6.2.1). The main contribution to the minimum chi square $\chi^2_{\rm min}$ comes from F_π (we will come back to this issue in the next section) whereas the topological susceptibility contributes only marginally.

In figure 5.11 are illustrated the results of the fit for the topological susceptibility as a function of the simulated light-quark mass. Finite-volume effects have little impact, since at large $\tilde{m}$, the product of $\tilde{M}_\pi L$ is much larger than 1 and thus finite-volume effects are small, whereas at small $\tilde{m}$, the topological susceptibility (with or without finite volume effects) goes to 0 linearly. One notices also the linearity of the three curves, related to the fact that q remains small (≤ 0.4) in this range of $\tilde{m}$, so that the topological susceptibility in eq. (5.57) or (5.64)-(5.65) can be expanded in powers of q with only small $O(q^2)$ corrections. As is clear from eq. (5.57), the slopes of these curves at zero are not directly related to the three-flavour quark condensate, as it involves also the next-to-leading order low energy constant L_6^r as well as chiral logarithms.

6.3 Improved fits to pseudoscalar spectrum and topological susceptibility

6.3.1 The dependence of F_π on the lightest quarks

Our approach, allowing for a numerical competition between leading order and next-to-leading order contributions to three-flavour chiral series, has provided a good, but not completely satisfying, fit of masses, decay constants and topological susceptibility from the RBC/UKQCD data. This is illustrated in the lower part of figure 6.1, where we plot $\tilde{F}_\pi$ as a function of $\tilde{m}$ (as given by the equivalent of eqs. (6.6)-(6.7) for $\tilde{F}_\pi^2$ and $\tilde{F}_\pi^2\tilde{M}_\pi^2$, see sec. 2.2 in the previous chapter). The (dashed) curves correspond to our best fit (last column in table 6.4) and the solid line indicates the dependence of F_π for a physical m_s in an infinite volume. Indeed, in spite of this broad agreement, we notice that we get a large contribution to $\chi^2_{\rm min}$ from the $\tilde{F}_\pi$ data points. This is a reminder of the problem encountered in [122], where neither a chiral nor an analytic extrapolation formula was able to accommodate the observed dependence of $\tilde{F}_\pi$ on $\tilde{m}$ with the physical point $(m_{\rm phys}, F_\pi)$. Our formalism can include both pieces of information with a reasonable $\chi^2_{\rm min}$, but we can improve the latter by letting the physical value of F_π vary as a free parameter. We obtain the results indicated as fit $B1$ in the first column of table 6.5 with a very low value of $F_\pi = 86.4$ MeV, in agreement with the results in ref. [122].

Fit name	$B1$	$B2$	$B3$	$B4$	$B5$
χ_t	No	No	No	No	χ_t^{pole}
Finite volume	Yes	Yes	Yes	Yes	Yes
Lattice spacing	Fixed	From M_Ω	Fixed	From M_Ω	From M_Ω
$O(a^2)$ corr	No	No	Yes	Yes	Yes
F_π[MeV]	86.5 ± 2.2	$92.2^\star$	$92.2^\star$	$92.2^\star$	$92.2^\star$
r	25.6 ± 1.1	26.1 ± 1.1	23.3 ± 0.8	25.6 ± 1.1	25.6 ± 1.0
$X(3)$	0.40 ± 0.04	0.54 ± 0.05	0.35 ± 0.07	0.55 ± 0.04	0.55 ± 0.04
$Y(3)$	0.79 ± 0.10	0.86 ± 0.08	0.52 ± 0.05	0.91 ± 0.06	0.91 ± 0.07
$Z(3)$	0.50 ± 0.07	0.62 ± 0.05	0.68 ± 0.07	0.60 ± 0.05	0.60 ± 0.04
F_K/F_π	1.23 ± 0.03	1.25 ± 0.03	1.17 ± 0.02	1.25 ± 0.02	1.25 ± 0.02
Rem. at limit	–	d	e	d, e	$d, e, d_\eta, e_\eta, d_{\chi_t}$
$\tilde{m}_s(24^3)/m_s$	1.14 ± 0.03	1.62 ± 0.16	1.12 ± 0.03	1.71 ± 0.13	1.71 ± 0.13
$a^{-1}(24^3)$[GeV]	$1.73^\star$	2.14 ± 0.12	$1.73^\star$	2.02 ± 0.08	2.19 ± 0.08
$a^{-1}(32^3)$[GeV]	$2.28^\star$	2.76 ± 0.13	$2.28^\star$	2.82 ± 0.09	2.81 ± 0.09
c_1	–	9.08 ± 0.44	–	8.98 ± 0.37	8.98 ± 0.37
c_2	–	1.42 ± 0.43	–	1.44 ± 0.44	1.44 ± 0.43
c_{F_π} [GeV^2]	–	–	0.13 ± 0.14	-1.09 ± 1.19	-1.09 ± 1.19
c_{F_K} [GeV^2]	–	–	0.13 ± 0.17	0.09 ± 0.48	0.09 ± 0.48
m_s(2 GeV)[MeV]	96.5 ± 2.2	83.9 ± 8.1	97.9 ± 2.2	81.2 ± 6.0	81.2 ± 6.0
m(2 GeV)[MeV]	3.8 ± 0.2	3.2 ± 0.4	4.2 ± 0.1	3.2 ± 0.3	3.2 ± 0.3
$\Sigma_0^{1/3}$(2 MeV)[GeV]	197 ± 7	240 ± 16	191 ± 2	243 ± 12	243 ± 12
B_0(2 GeV)[GeV]	2.03 ± 0.32	2.60 ± 0.52	1.21 ± 0.12	2.81 ± 0.39	2.81 ± 0.38
F_0[MeV]	61.5 ± 5.2	72.8 ± 2.8	76.0 ± 3.7	71.3 ± 2.4	71.3 ± 2.4
F_η[MeV]	–	–	–	–	123 ± 3
$\chi_t^{\text{pole}} \cdot 10^4$[GeV^4]	–	0.33 ± 0.03	0.41 ± 0.03	0.33 ± 0.03	0.43 ± 0.03
$\tilde{m}_s(32^3)/m_s$	1.09 ± 0.03	1.52 ± 0.15	1.08 ± 0.03	1.61 ± 0.12	1.61 ± 0.12
$L_4(\mu) \cdot 10^3$	0.28 ± 0.29	-0.11 ± 0.14	0.99 ± 0.17	-0.08 ± 0.09	-0.08 ± 0.09
$L_5(\mu) \cdot 10^3$	1.62 ± 0.19	2.13 ± 0.21	2.03 ± 0.43	2.00 ± 0.20	2.01 ± 0.20
$L_6(\mu) \cdot 10^3$	0.47 ± 0.35	0.09 ± 0.10	2.53 ± 0.79	0.05 ± 0.07	0.04 ± 0.07
$L_7(\mu) \cdot 10^3$	–	–	–	–	-0.25 ± 0.14
$L_8(\mu) \cdot 10^3$	1.08 ± 0.38	1.13 ± 0.20	3.42 ± 0.88	1.04 ± 0.14	1.04 ± 0.09
$X(2)$	0.89 ± 0.02	0.89 ± 0.01	0.90 ± 0.01	0.88 ± 0.01	0.88 ± 0.01
$Y(2)$	1.03 ± 0.02	1.03 ± 0.01	0.99 ± 0.01	1.04 ± 0.01	1.04 ± 0.01
$Z(2)$	0.86 ± 0.02	0.86 ± 0.01	0.91 ± 0.01	0.86 ± 0.01	0.85 ± 0.01
$\Sigma^{1/3}$(2 GeV)[MeV]	258 ± 4	248 ± 2	261 ± 3	285 ± 7	285 ± 8
B(2 GeV)[GeV]	2.68 ± 0.16	3.13 ± 0.42	1.90 ± 0.18	3.18 ± 0.28	3.18 ± 0.27
F[MeV]	80.2 ± 2.9	85.5 ± 0.50	88.0 ± 0.4	85.2 ± 0.4	85.2 ± 0.4
$\bar{\ell}_3$	4.0 ± 1.5	4.5 ± 0.9	-1.0 ± 0.9	4.6 ± 0.7	4.6 ± 0.7
$\bar{\ell}_4$	4.2 ± 0.4	4.7 ± 0.3	3.1 ± 0.3	4.9 ± 0.3	4.9 ± 0.3
$\Sigma/\Sigma_0 = \Sigma(2)/\Sigma(3)$	2.24 ± 0.22	1.66 ± 0.14	2.54 ± 0.02	1.61 ± 0.11	1.61 ± 0.11
$B/B_0 = B(2)/B(3)$	1.32 ± 0.17	1.20 ± 0.10	1.90 ± 0.18	1.13 ± 0.09	1.13 ± 0.08
$F/F_0 = F(2)/F(3)$	1.30 ± 0.08	1.17 ± 0.05	1.15 ± 0.06	1.19 ± 0.04	1.19 ± 0.04
χ^2/N	12.1/10	17.3/12	18.1/9	16.0/10	16.2/11
Gaussian equiv.	1.1σ	1.5σ	2.1σ	1.6σ	1.5σ

Table 6.5: Results of fits performed on the data from RBC/UKQCD collaboration on pseudoscalar masses, decay constants and topological susceptibility [122]. The first fit lets F_π vary freely. The other columns either a determination of the lattice spacings using the Ω mass or $O(a^2)$ discretisation effects for the decay constants. The star superscript indicates a quantity set to a fixed value (no uncertainty). These results should be compared with fits $A2$ and $A5$ of table 6.4.

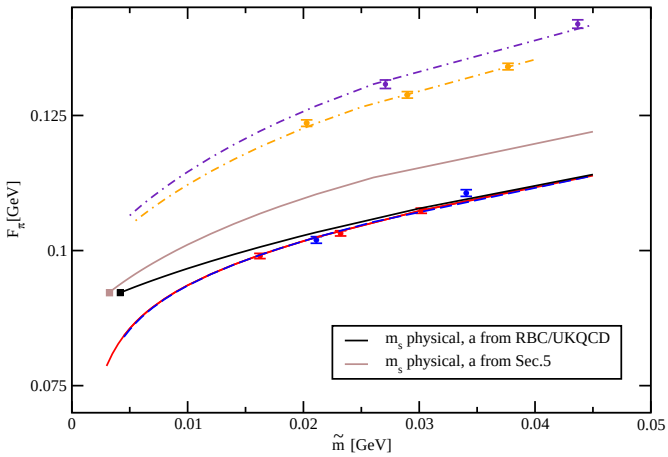

Figure 6.1: The pion decay constant as a function of the light-quark mass. Blue/ [red] points correspond to the data for the $(24)^3 \times 64$ volume [$(32)^3 \times 64$], using the estimates of lattice spacing given in ref. [122]. Purple [orange] points correspond to the same points, using our own estimates of lattice spacing discussed in sec. 6.2.4. The dashed curves indicate our best fit in each case ($A5$ and $B5$), as given in the last columns of tables 6.4 and 6.5 respectively. They are interrupted for $\tilde{M}_\pi L \leq 2$ where our description of finite-volume effects becomes unreliable. The solid curves indicate the corresponding variations for the physical value of the strange quark mass, without finite-volume effects. In both cases (estimate of the lattice spacings from ref. [122] or sec. 6.3.1), the position of the physical point $(m_{\rm phys}, F_\pi)$ is indicated with a square.

This discrepancy between lattice and physical values of F_π hints at a more general issue concerning the determination of the absolute scale of lattice quantities, which is obtained by converting the lattice spacing into physical units. In [122], it was determined by identifying "scaling trajectories" corresponding to lines in the $(a, \tilde{m}, \tilde{m}_s)$ space with fixed $\tilde{M}_\pi/\tilde{M}_\Omega$ and $\tilde{M}_K/\tilde{M}_\Omega$ ratios. An iterative interpolation method was used to reach values of M_π, M_K, M_Ω corresponding to physical values of their ratios, which was identified as the physical point for the quark masses. The lattice spacings were then determined by requiring that $1/a = 1.672/(a\tilde{M}_\Omega)$ GeV where 1.672 GeV is the physical mass of this baryon and $a\tilde{M}_\Omega$ is the mass of the Ω as measured in lattice units. The actual interpolation was performed through two kinds of interpolating formulae for the hadron masses in terms of quark masses, either based on next-to-leading two-flavour χPT or an analytic (polynomial) ansatz, fitted to partially-quenched data. This led to values of the lattice spacing that were compatible and quoted with an accuracy at the level of a few percents.

However, such determinations based on the quark-mass dependence of light-meson quantities might be affected significantly if one takes into account the numerical competition between leading and next-to-leading order contributions to three-flavour chiral series. This means that one should consider at the same time the chiral expansions of $F_P^2 M_P^2$ and F_P^2 and include higher order remainders, to determine the dependence of M_π and M_K on the quark masses. But, as far as the Ω mass is concerned, we will follow ref. [122] and take a linear dependence on the quark masses

$$\tilde{M}_\Omega = M_\Omega + c_1(\tilde{m}_s - m_s) + c_2(\tilde{m} - m) \tag{6.9}$$

inspired by the analysis of RBC/UKQCD. A fully consistent treatment should include a treatment of the baryon masses in the resummed framework, extending eq. (6.9) to chiral

logarithms and higher order remainders. Such an analysis is however beyond the scope of this thesis (in the present case, we have checked that adding a quartic term in eq. (6.9) does not change the results discussed below).

In addition, since we are interested in effects related to lattice spacing, we should also consider discretization errors, which could reach 10 to 15% in the analysis of [122]. We follow the latter analysis and include only leading-order discretization effects affecting the decay constants [1]:

$$\begin{aligned} \tilde{F}_\pi^2(a,V,\tilde{m},\tilde{m_s}) &= \tilde{F}_\pi^2(0,V,\tilde{m},\tilde{m_s}) + F_\pi^2 Z(3) c_{F_\pi} a^2 \\ \tilde{F}_K^2(a,V,\tilde{m},\tilde{m_s}) &= \tilde{F}_K^2(0,V,\tilde{m},\tilde{m_s}) + F_\pi^2 Z(3) c_{F_K} a^2 \end{aligned} \tag{6.10}$$

where the correction term is defined with respect to the leading-order term in the chiral expansion. The errors are $O(a^2)$, and not $O(a)$, due to the good chiral properties of domain-wall fermions (see sec. 2.2).

6.3.2 Including the lattice spacings in the fits

We are not in a position to perform the same joint determination of lattice spacings and quark masses as the RBC/UKQCD collaboration to include the dependence of the pion and kaon masses on the light-quark mass inferred from Resummed χPT from scratch. However, we can perform a combined fit of the pion and kaon masses and decay constants, as well as the Ω mass (see sec. 6.2.1), with the parameters from sec. 6.2.3 and the parameters corresponding to the Ω mass formula eq. (6.9):

- the three leading-order parameters $r, X(3), Z(3)$
- a reference ratio between a simulated strange quark (chosen conventionally to be for the 24^3 simulations) and the physical strange quark mass
- the higher order remainders associated with the pion and kaon masses and decay constants (denoted d, e, d', e')
- the ratio F_K/F_π (on the other hand, we set $F_\pi = 92.2$ MeV)
- if the topological susceptibility is included, the corresponding higher order remainders for the η mass and decay constant (d_η, e_η) as well as the one for the topological susceptibility (d_{χ_t}).
- if the lattice spacings are left free, the two effective constants c_1, c_2 for the Ω mass (eq. (6.9)).
- if discretisation errors are included, the two effective constants c_{F_π}, c_{F_K} for the decay constants (eqs. (6.10)).

Our approach is not very different in its spirit from the "combined scaling and chiral fitting" performed in ref. [122], up to the following modifications: we include information on the values of the masses and decay constants at the physical point, we consider $F_P^2 M_P^2$ and F_P^2 rather than M_P^2 and F_P, we use three-flavour resummed χPT rather than two-flavour expansions to perform the interpolation of the data, we include the presence of higher order

[1] In principle, one should consider all the terms coming from discretisation effects and due to the breaking of chiral symmetry, and also add correction terms for the masses. This would however increase the number of free parameters and lead to fits with a poor stability, due to flat directions in the subspace of correction terms and the limited number of data points.

remainders, we do not include partially-quenched data and we fix at the same time m, m_s and the lattice spacings in contrast with the two-step procedure in [122] (physical masses first, lattice spacing afterwards).

6.3.3 Results and discussion

The results are given in table. 6.5 including finite-volume effects. First we consider fits $B2, 3, 4$ without the topological susceptibility, including or not discretization errors and lattice spacing determined from M_Ω. Discretization errors remain generally small (at most 5%) apart for F_π^2 in fit $B4$ (20% effect, in good agreement with the results of ref. [122]), but lead to enlarged uncertainties on the other parameters. We notice that these discretisation effects are compatible with zero within error bars, which explains that the fits $A2$ and $B3$ (differing only through the effect of discretisation errors) yield very similar results. The re-determination of lattice spacing through M_Ω performed in $B2$ and $B4$ has a much more significant impact, as it tends to decrease the lattice spacings significantly (20-30%) as well as the value of the physical quark masses, and to increase F_π/F_K noticeably. In these fits, the simulated quark masses stand much further away from the physical value than quoted in ref. [122], implying that higher order remainders at the simulated quark masses (scaling generically as p^2 with respect to the higher order at the physical point) play a significant role in the chiral expansion of observables (up to 40% for the heaviest $\tilde{m}_s$). The large error bars for dimensionful quantities is a reflection of the uncertainty on the lattice spacings determined from M_Ω.

The topological susceptibility is introduced among the inputs in the fit $B5$. As in sec. 6.2.4, the role of this input in the fit is marginal compared to the other data, and the outcome of fits $B4$ and $B5$ is very similar. Indeed, the chi-square obtained from fit $B5$ gets similar contributions from F_π, $F_\pi M_\pi$, $F_K M_K$ and M_Ω, whereas the contribution from the topological susceptibility is small. The rest of the analysis is unchanged, with a competition between leading and next-to-leading order contributions for the observables of interest ($\hat{\mathcal{O}} = LO + NLO + HO$):

$$\begin{array}{rcl@{\qquad}rcl} F_\pi^2 & : & 0.60 + 0.25 + 0.15\,, & F_\pi^2 M_\pi^2 & : & 0.55 + 0.30 + 0.15 \\ F_K^2 & : & 0.38 + 0.52 + 0.10\,, & F_K^2 M_K^2 & : & 0.37 + 0.52 + 0.11 \\ F_\eta^2 & : & 0.33 + 0.58 + 0.09\,, & F_\eta^2 M_\eta^2 & : & 0.35 + 0.66 - 0.01 \\ \chi_t^{\rm pole} & : & 0.50 + 0.35 + 0.15 & & & \end{array} \tag{6.11}$$

The competition between leading and next-to-leading order terms of the chiral expansions observed in the previous fits remains though a bit less pronounced: $Y(3)$ is closer to one, and the value of L_6 is closer to zero, but there is still an enhancement of next-to-leading contributions to observables. Indeed, this enhancement is parametrised by $m_s B_0 \Delta L_4$ and $m_s B_0 \Delta L_6$ (see sec. 3.4.3) rather than L_4 and L_6 themselves, as can be seen for instance in eqs. (3.56)-(3.57) (see also figure 3.2).

Furthermore, the fit $B5$ features a fairly good $\chi^2_{\rm min}/N$ compared to the results in ref. [122], taking into account that our fit reproduces the physical values of the pseudoscalar masses and F_π by construction. We agree with ref. [122] on the size of discretisation errors, but obtain different results concerning the determination of the lattice spacings from M_Ω. The main difference stems from our use of Resummed χPT in the fit, as can be illustrated by performing the same fit as B_5 but constraining $X(3)$ and $Z(3)$ to remain between 0.9 and 1.05. This last constraint mimics the usual assumption made in three-flavour χPT that both F_π and M_π are nearly saturated by their leading order term. The minimum of the fit may look satisfying with $r = 26.1$, $X(3) = 0.9$, $Y(3) = 0.97$, $Z(3) = 0.93$, $F_K/F_\pi = 1.18$ and values of the lattice spacings compatible at the 5% level with ref. [122], but the value

at the minimum is rather awful with $\chi^2_{\rm min} = 151/11$. This shows clearly that allowing for a numerical competition between leading and next-to-leading order is mandatory to reach decent fits to the whole set of data considered here.

Finally, the results from $B5$ can be illustrated through the upper part of figure 6.1. The change in the value of the lattice spacings rescales all lattice data points, which fall on the dashed curves corresponding to the best ReχPT fit including finite-volume effects (responsible for most of the curvature at small $\tilde{m}$) more easily than in sec. 6.2.4. The values of $p = \tilde{m}_s/m_s$ and $Y(3)$ are larger than in fit $A5$: from eq. (3.56) (which has a similar structure to the Resummed χPT expression for $\tilde{F}_\pi$), we see that the next-to-leading order contributions are proportional to the product $p \times Y(3)$ and tend thus to drive the dashed curves corresponding to the two volumes further apart than in the previous section. We also display the solid curve corresponding to the physical value of m_s in an infinite volume, which by construction passes through the physical point $F_\pi = 92.2$ MeV (this point corresponds to a slightly different value of $\tilde{m}$ from sec. 6.2.4). The curvature is then essentially tied to the value at the origin, i.e., $Z(2)$: a lower value of $Z(2)$ will yield a steeper increase of $\tilde{F}_\pi$ when $\tilde{m}$ increases. The dependence of $Z(2)$ on the various parameters can be read from the three-flavour expansion of F_π^2 in the chiral limit $m_u = m_d = 0$ [79]:

$$Z(2) = \frac{r}{r+2}[1-\eta(r)] + \frac{2}{r+2}Z(3) - \frac{r}{r+2}Y(3)g_1 + \dots \tag{6.12}$$

where g_1 denotes a small positive combination of chiral logarithms (around 7% near the physical point) and the ellipsis indicate higher order remainders (see sec. 3.4.3). Therefore, a dependence with a stronger curvature around the physical point and a flatter behavior above can be achieved by taking a larger value $Y(3)$ or a smaller value of $Z(3)$, as illustrated in figure 6.2 and observed in fit $B5$ compared to $A5$. As an illustration, we indicate on the same figure the curves obtained with the same inputs as the best values for fit $B5$ of table 6.5, but setting $Y(3) = 1$ and/or $Z(3) = 1$. The case of a complete saturation of the chiral series for F_π^2 and $F_\pi^2 M_\pi^2$ by their leading order contribution ($X(3) = Z(3) = 1$) yields a higher $Z(2)$ and a flatter curve than our best fit.

At last, we notice that an increase of r (at fixed p) yields a slight increase of $Z(2)$, but more importantly an upward shift of the physical value of $\tilde{m}$, so that the corresponding line remains above the best-fit curve over a larger range of $\tilde{m}$. The combination of these effects allows our formulae to reproduce a diversity of behaviours for the dependence of $\tilde{F}_\pi$ on $\tilde{m}$, including the one exhibited by the RBC/UKQCD data.

Finally, we can illustrate typical values for the fourth cumulant c_4 and b_2 for current lattice simulations. We consider the results of fit B5 from table 6.5: one notices the rather low values for the quark condensate and the pseudoscalar decay constant in the three-flavour chiral limit: $X(3) = 0.55 \pm 0.04$ and $Z(3) = 0.60 \pm 0.04$. Using the outcome of this fit (including the correlations among the leading order parameters and the higher order remainders), we obtain the predictions for $\chi_t^{no\ pole}$, $c_4^{no\ pole}$ and b_2 collected in table 6.6 for the different sets considered in sec. 6.2.1 as well as in the physical case. The values for $p = \tilde{m}_s/m_s$ are different from those quoted in ref. [122], since we have reassessed the determination of the lattice spacing and quark mass based on the mass of the Ω baryon (see sec. 6.3.1). Finite-volume effects are not included, whereas the effect of higher order remainders is taken into account (including an estimate of $\tilde{d}_{c_4}$ that enlarges the corresponding uncertainty of $\tilde{c}_4$). As in the case of the topological susceptibility illustrated in the previous sections, the impact of $\tilde{d}_{c_4}$ can be easily modeled and determined from a fit once a sufficiently large set of values at different simulated quark masses is available. It would be very interesting to compare these predictions for c_4 and b_2 with data from lattice simulations.

To conclude, since the results presented in table 6.4 do not include effects related to

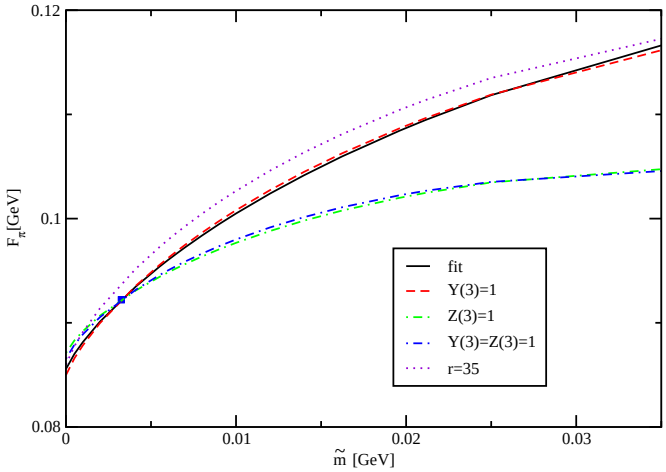

Figure 6.2: The pion decay constant as a function of the light-quark mass, according to the best fit in the last column of table 6.5 (solid), with the same inputs but setting $Y(3) = 1$ and/or $Z(3) = 1$ (dashed and dashed-dotted curves), and with the same inputs but setting $r = 35$ (dotted curve). The physical point according to the fit result is indicated with a square.

Case	p	q	$\chi_t \cdot 10^4$ [GeV^4]	$c_4 \cdot 10^4$ [GeV^4]	b_2
$L_s = 24$	1.71	0.192	5.66 ± 1.54	-0.81 ± 0.47	-0.012 ± 0.009
	1.71	0.311	8.98 ± 2.61	-0.87 ± 0.75	-0.008 ± 0.010
$L_s = 32$	1.61	0.154	3.88 ± 0.83	-0.67 ± 0.32	-0.014 ± 0.007
	1.61	0.220	5.60 ± 1.26	-0.84 ± 0.47	-0.013 ± 0.008
	1.61	0.286	7.23 ± 1.71	-0.89 ± 0.61	-0.010 ± 0.009
Physical	1	$1/r$	0.40 ± 0.02	-0.10 ± 0.01	-0.021 ± 0.004

Table 6.6: Predictions for the topological susceptibility and the fourth cumulant (without identifying the η pole) for different lattice data sets presented in sec. 6.2.1 and in the physical case, following the analysis performed in sec. 6.3.1 leading to the results of table 6.5.

lattice spacings and since the determination of the lattice spacings involves assumptions on the form of chiral extrapolation, we consider the most complete fit $B5$ in table 6.5 as the final result of our analysis, featuring a satisfying $\chi^2_{\rm min}/N$. Interestingly, these results show a good compatibility with what was obtained in ref. [92] for the parameters of the leading order chiral lagrangian according to the results of the PACS-CS collaboration [96]. The value of the condensate in the $N_f = 3$ chiral limit is:

$$(\Sigma(3; 2\,\mathrm{GeV}))^{1/3} = 243 \pm 12\,\mathrm{MeV} \tag{6.13}$$

on the lower side of was obtained by the RBC/UKQCD collaboration (i.e., 256 ± 6 MeV) [122], while the condensate in the two-flavour limit is

$$(\Sigma(2; 2\,\mathrm{GeV}))^{1/3} = 285 \pm 8\,\mathrm{MeV}\,, \qquad \Sigma(2; 2\mathrm{GeV})/\Sigma(3; 2\mathrm{GeV}) = 1.51 \pm 0.11 \tag{6.14}$$

which illustrates the paramagnetic suppression of the $N_f = 3$ condensate with respect to the $N_f = 2$ one (a similar statement holds for the pseudoscalar decay constant).

6.4 Summary

In this chapter, we have presented the fits that we have performed on decay constants, masses and topological susceptibility (excluding here the $K_{\ell 3}$ form factors). This work was the object of [93]. The fitting method we used is the same as in Chapter 4, with the difference that in some of the fits, we performed a determination of lattice spacings from the Ω mass, we included discretization effects partially and we took into account finite-volume effects. We used the $2+1$ lattice data provided by the RBC/UKQCD [122] collaboration. The parameters upon which ours fits were performed are the same as in Chapter 4, adding the higher-order remainders related to topological susceptiblity (d_η, e_η, and d_{χ_t}). In our "Improved series" of fits in sec. 6.3, we also added to those parameters the lattice spacings a and the quantities c_1 and c_2 related to the dependence of the Ω mass on the light quarks masses, as well as c_{F_π} and c_{F_K} stemming from the dicretization effects of order $O(a^2)$ for the π and K decay constants.

From our first series of fits (sec. 6.2.4), we have confirmed that these data do suggest a suppression of the leading order $N_f = 3$ chiral order parameters (quark condensate and pseudoscalar decay constant) and the enhancement of next-to-leading order contributions related to the violation of the Zweig rule in the scalar sector (L_4 and L_6 contributions). This outcome is mainly driven by the input from pseudoscalar masses and decay constants. The data on topological susceptibility shows a good compatibility with the pattern of three-flavour chiral symmetry breaking already discussed in Chapter 4. In addition, we confirm the difficulties (though at a lesser degree) encountered by the RBC/UKQCD collaboration to accommodate the dependence of F_π on the light-quark mass $m = m_u = m_d$ given by their data and the physical value of F_π at the same time.

This problem has led us to reconsider the procedure used to determine the lattice spacing using our expressions to describe the dependence of the pseudoscalar observables on the quark masses, in our second series of fits in sec. 6.3: we performed a joint fit of pion/kaon observables and the Ω mass to fix the lattice spacings at the same time as the parameters of the chiral lagrangian. We also considered leading-order discretization errors that may affect the kaon and pion decay constants, and that are expected to be the most important effects among discretization errors. We finally performed a fit combining these two effects and adding data on the topological susceptibility (fit $B5$). We noticed a significant enhancement (20%-30%) of the inverse of lattice spacings compared to the values quoted in ref. [122], as well as small discretization errors (5% or less, and compatible with zero). Like in the previous analysis, the data on the topological susceptibility play a marginal role, but show a good compatibility with the rest of the data, yielding a satisfying $\chi^2_{\rm min}/N$. Since they include the largest sets of data and use ReχPT consistently for the fit of the data and the determination of the lattice spacings, the results of fit $B5$ should thus be considered as the actual outcome of our analysis.

This confirms the suppression of the three-flavour quark condensate and decay constant, while pointing at interesting new sources of systematics uncertainties (determination of the lattice spacings, extrapolation to light quark masses). Obviously, our result does not include properly all the correlations, and it would be very interesting that lattice collaborations include Resummed χPT formulae as an alternative to the standard chiral expansion to assess more precisely these uncertainties.

Conclusion

"Et lorsque Sophia découvrit la conséquence de son désir, celle-ci prit la forme d'un serpent à face de lion, et ses yeux étaient comme les feux flamboyants des éclairs. Elle le chassa hors de sa portée, hors de ce royaume, afin qu'aucun des immortels ne le voit, car elle l'avait engendré dans l'ignorance."

Le livre secret de Jean, Bibliothèque de Nag-Hammadi

In this thesis, we studied some aspects of low-energy QCD below the scale of chiral symmetry breaking (Λ_χ), where the usual perturbative methods consisting in the expansion in terms of powers of the strong coupling constant is no more relevant. We have seen that the spontaneous breaking of chiral symmetry generates an octet of Goldstone bosons that are identified with the eight pseudo-scalar light mesons π, K and η once light quark masses are included. Because of the light quark mass hierarchy $m_u \sim m_d \ll m_s$, we can consider two different chiral limits: the $N_f = 3$ chiral limit, for which all of the light flavours are sent to zero: $m_{u,d,s} \to 0$, and the $N_f = 2$ chiral limit, for which the u and d quark masses are sent to 0, but with m_s kept at his physical value: $m_{u,d} \to 0$, m_s *physical*. One fundamental question is then: are the patterns of chiral symmetry breaking stemming from the $N_f = 3$ and $N_f = 2$ chiral limits identical, or do they differ, and how ?

We have seen that the two main order parameters of chiral symmetry breaking, the quark consensate Σ, and the decay constant F, should decrease when one goes from the $N_f = 2$ to the $N_f = 3$ chiral limits, due to the presence of massive strange quark sea-pairs in the vacuum. This in turn would impact the convergence of the series expansions calculated within the framework of the effective theory of low-energy QCD, Chiral Perturbation Theory. The leading order contributions, which involve both Σ and F, would be suppressed in this situation. On the other hand, the Zweig rule suppressed, next-to-leading order low-energy constants L_4 and L_6 of the three-flavour theory would be enhanced, as they account for the dependence on the strange quark mass m_s of the order parameters (eqs. (2.78) and (2.79)). The combination of these two effects could lead to a numerical competition between the leading and next-to-leading order in the $N_f = 3$ chiral expansions.

Indeed, many problems of convergence have been experienced both in phenomenological analysis (interpretation of experimental data on $\pi\pi$ scattering, fits to NNLO chiral expansions) and in the extrapolation of results obtained in Lattice QCD (incompatibility between lattice results, values at the physical point and curvature from the chiral expansions). One could obviously choose to dismiss the whole idea of an expansion around the chiral limit $m_u = m_d = m_s = 0$, arguing that strange quark is too massive for such an expansion. However, one would also hope that this could only be an accident involving LO and NLO contributions, and that the problem of convergence would be tamed at higher orders in the chiral expansion (as suggested by simple models of correlator saturation by resonances).

We have decided to take the second approach, and assumed that the convergence problems in three-flavour chiral expansions would be restricted to LO and NLO, and that an appropriate treatment of chiral series could be designed to cope with a numerical competition between their two first orders.

This framework, called Resummed χPT, has already been applied to some physical observables (pseudoscalar masses, decay constants, $\pi\pi$ and πK scatterings). The purpose of this thesis was to apply it to settings and observables closer to Lattice QCD simulations. We considered observables related to pseudoscalar mesons (masses, decay constants, electromagnetic and $K_{\ell 3}$ form factors) for values of quark masses different from the physical masses. We also discussed topological observables describing the distribution of the gluonic winding number, namely the topological susceptibility and the fourth cumulant of the winding number. In both cases, we performed fits to available lattice data to extract information on the pattern of chiral symmetry breaking, with an outcome in agreement with our expectation: the three-flavour quark condensate and decay constant are significantly suppressed compared to the two-flavour case, whereas the low energy constants L_4 and L_6 are larger than assumed on the basis of the Zweig rule. There is no indication of large higher order remainders, indicating that the problems of convergence are indeed limited to leading and next-to-leading orders. Moreover, there are significant differences in the results of our extrapolations of pseudoscalar observables to the physical point, compared to those performed assuming a saturation of the chiral series by their leading order (this is exemplified by the extracted values of F_K/F_π and the $K_{\ell 3}$ form factor $f_+(0)$).

In the course of our study, we have also encountered several interesting features: we have seen the role played by the determination of the lattice spacing, which is generally performed at the same time as the value of the light quark masses, using chiral extrapolations. It seems clear that a change in the formulae used to perform this extrapolation can have a significant impact on the systematics attached to the physical values of an observable computed on the lattice, and that these systematics should be investigated in more detail in the analysis of lattice results. Moreover, we have seen that the topological susceptibility is not the most appropriate topological observable to extract the three-flavour quark condensate in a setting with a quark mass hierarchy similar to the physical case. Indeed, the topological susceptibility is actually sensitive to the two-flavour quark condensate which may differ significantly from the three-flavour one. On the contrary, the fourth cumulant has the potentiality to extract the latter order parameter and should be investigated in closer details by lattice collaborations.

In Chapter 1, we have recalled the main issues concerning QCD and chiral symmetry. Particular emphasis was put on the introduction to spontaneous symmetry breaking, before moving to general considerations concerning the structure of the QCD vacuum. In Chapter 2, we made a general overview of Lattice QCD and Effective Field theories, before introducing in detail Chiral Perturbation Theory from the ground up, for three as well as for two light quark flavours.

Resummed Chiral Perturbation Theory was presented in Chapter 3. In particular, we have applied it to decay constants, masses, electromagnetic and $K_{\ell 3}$ form factors, and in Chapter 4 we performed fits to lattice data. One of the major conclusions we drew was that the leading and next-to-leading order indeed competed in the case of $N_f = 3$ chiral series. Also, there was indeed a suppression of the three-flavour condensate and pseudoscalar decay constants, and this scenario provided a good description of lattice data from two different collaborations.

Finally, Chapters 5 and 6 were devoted to the study of the topological susceptibility χ_t and the fourth cumulant c_4, where they were evaluated up to NLO in Standard and Resummed χPT and their sensibility on the $N_f = 3$ quark condensate probed in the a pre-

liminary study (Chapter 5), before tackling new series of fits that included decay constants, masses and the topological susceptiblity (Chapter 6), which also included finite-volume effects and the determination of the lattice spacing a. The conclusions concerning the pattern of three-flavour chiral symmetry breaking were similar to the previous case, but pointed towards a significant underestimate of the uncertainties attached to the determination of the lattice spacing from a joint fit to the π, K and Ω masses and quark masses.

The study we have made during these three fruitful years could provide indeed a systematic tool to the community, to latticists, chiralists as well as experimentalists, in order to circumvent the potential problems of convergence encountered in $N_f = 3$ chiral series, and to assess the systematic uncertainties associated with chiral extrapolations and determination of lattice spacing in a more detailed way, as our results suggest that these effects can be underestimated if one considers only the standard version of χPT. And, last but not least, it could also help to better understand the very difficult and still unsolved problem of non-perturbative QCD, and to probe the Standard Model in one of its most challenging aspects, i.e. the hadronic sector at low energies.

Appendices

Appendix A

Unitarity integrals and source terms from the generating functional

A.1 The one-loop unitarity integrals $\bar{J}$, K, L and M

One-loop unitarity diagrams lead to the following one-loop integral in d-dimensions:

$$J(k^2) = -i \int \frac{d^d q}{(2\pi)^d} \frac{1}{(M_P^2 - q^2)(M_Q^2 - (k-q)^2)} \tag{A.1}$$

for arbitrary masses M_P and M_Q, P and Q being any light meson. This integral is divergent for $d = 4$ and therefore must be renormalized. We define the substracted integral $\bar{J}(s)$, which is finite at $d = 4$:

$$\bar{J}(s) = J(s) - J(0), \quad s \in \mathbb{R} \tag{A.2}$$

where the quantity $J(0)$ gathers the divergence:

$$J(0) = -2\kappa(\epsilon) - 2k_{PQ} + O(\epsilon), \quad \epsilon = 4 - d \tag{A.3}$$

$$\kappa(\epsilon) = \frac{\mu^{-\epsilon}}{16\pi^2} \left[-\frac{1}{\epsilon} - \frac{1}{2}(\ln 4\pi - \gamma + 1) \right] \tag{A.4}$$

$$k_{PQ} = \frac{1}{32\pi^2} \left(M_P^2 \ln \frac{M_P^2}{\mu^2} - M_Q^2 \ln \frac{M_Q^2}{\mu^2} \right) \tag{A.5}$$

μ being the renormalization scale stemming from the dimensional regularization, and γ the Euler-Mascheroni constant [6, 8].

$\bar{J}(s)$ is expressed as an integral over the Feynman parameter λ:

$$\bar{J}(s) = -\frac{1}{16\pi^2} \int_0^1 d\lambda \ln \frac{M_P^2 - s\lambda(1-\lambda) - \lambda(M_P^2 - M_Q^2)}{M_P^2(1-\lambda) + \lambda M_Q^2} \tag{A.6}$$

which can be reduced to:

$$\bar{J}(s) = \frac{1}{32\pi^2} \left[2 + \ln \frac{M_Q^2}{M_P^2} \left(\frac{\Delta_{PQ}}{s} - \frac{\Sigma_{PQ}}{\Delta_{PQ}} \right) - \frac{\delta}{s} \ln \frac{(s+\delta)^2 - \Delta_{PQ}^2}{(s-\delta)^2 - \Delta_{PQ}^2} \right] \tag{A.7}$$

with the notations $\Sigma_{PQ} = M_P^2 + M_Q^2$, $\Delta_{PQ} = M_P^2 - M_Q^2$ and $\delta^2 = (s-(M_P+M_Q)^2)(s-(M_P-M_Q)^2)$.

We also need the derivatives of $\bar{J}(s)$ at $s=0$:

$$\bar{J}^{'}(0) = \frac{1}{32\pi^2}\left(\frac{\Sigma_{PQ}}{\Delta_{PQ}^2} + 2\frac{M_P^2 M_Q^2}{\Delta_{PQ}^3}\ln\frac{M_P^2}{M_Q^2}\right) \tag{A.8}$$

$$\bar{J}^{''}(0) = \frac{1}{32\pi^2}\left(\frac{2}{3\Delta_{PQ}^4}(3\Sigma_{PQ}^2 - 2\Delta_{PQ}^2) + 4\frac{M_P^2 M_Q^2}{\Delta_{PQ}^5}\ln\frac{M_P^2}{M_Q^2}\right) \tag{A.9}$$

We can now define the combination:

$$\bar{\bar{J}}_{PQ} = \bar{J}(s) - \bar{J}^{'}(0) \tag{A.10}$$

In the expression (2.70) of the one-loop unitarity contribution Z_u of the generating functional Z eq. (2.65), we have the following expressions for the renormalized integrals J, K, L, and M in Fourier space:

$$K_{PQ}(s) = \frac{\Delta_{PQ}}{2s}\bar{J}_{PQ}(s) \tag{A.11}$$

$$L_{PQ}(s) = \frac{\Delta_{PQ}^2}{4s}\bar{J}_{PQ}(s) \tag{A.12}$$

$$M_{PQ}^r(s) = \frac{1}{12s}(s-2\Sigma_{PQ})\bar{J}_{PQ}(s) + \frac{\Delta^2}{3s^2}\bar{\bar{J}}_{PQ}(s) - \frac{1}{6}k_{PQ} + \frac{1}{288\pi^2} \tag{A.13}$$

A.2 Expression for the source terms $\hat{\Gamma}_\mu$ and $\bar{\sigma}$

In Z_u eq. (2.70) we have the source terms $\hat{\Gamma}_\mu$ and $\bar{\sigma}$:

$$\hat{\Gamma}_{PQ}^{\mu} = -\frac{1}{2}Tr([\lambda_P, \lambda_Q^\dagger]\Gamma_\mu) \tag{A.14}$$

$$\bar{\sigma}_{PQ} = \sigma_{PQ}^{\Delta} + \sigma_{PQ}^{\chi} \tag{A.15}$$

$$\sigma_{PQ}^{\Delta} = \frac{1}{2}Tr([\lambda_P, \Delta_\mu][\lambda_Q^\dagger, \Delta^\mu]) \tag{A.16}$$

$$\sigma_{PQ}^{\chi} = \frac{1}{8}Tr(\{\lambda_P, \lambda_Q^\dagger\}(u\chi^\dagger u + u^\dagger\chi u^\dagger)) - \delta_{PQ}\,\mathring{M}_P^{\,2} \tag{A.17}$$

with the following expression for the quantities Γ_μ and Δ_μ:

$$\Gamma_\mu = \frac{1}{2}[u^\dagger, \partial_\mu u] - \frac{1}{2}iu^\dagger r_\mu u - \frac{1}{2}iul_\mu u^\dagger \tag{A.18}$$

$$\Delta_\mu = \frac{1}{2}u^\dagger D_\mu \bar{U} u^\dagger = -\frac{1}{2}u(D_\mu \bar{U})^\dagger u \tag{A.19}$$

where we have $\bar{U} = u^2$ the classical solution of the chiral lagrangian's equations of motion. D_μ is the covariant derivative eq. (2.38). The matrices λ_P are the $SU(3)$ generators, where $P = \pi^0, \pi^+ ... \ \eta$.

Appendix B

Tadpole propagator at finite volume

Periodic boundary conditions lead to quantized momentum: $\vec{p}_{\vec{n}} = \left(2\pi\frac{n_1}{L_1}, 2\pi\frac{n_2}{L_2}, 2\pi\frac{n_3}{L_3}, 2\pi\frac{n_4}{T}\right)$. In the case of the topological susceptibility χ_t and the fourth cumulant c_4, the exterior momenta are zero $p_{ext} = 0$, so only the loops are affected by the quantization. One has then to simply replace their propagators at $V = \infty$ by the propagators in the box. We begin with the general case of a four-dimensional box:

$$\Delta(\vec{x}, M^2)_{|V=\infty} = \frac{1}{(2\pi)^4} \int d^4p \frac{e^{i\vec{p}.\vec{x}}}{p^2 + M^2} \tag{B.1}$$

In the finite case, the periodic boundary conditions allows to write the Fourier transform of the propagator:

$$\Delta(\vec{x}, M^2)_{|V} = \frac{1}{V} \sum_{\vec{n}\in\mathbb{Z}^4} \widetilde{\Delta}\,(\vec{p}_{\vec{n}}, M^2) e^{i\vec{p}_{\vec{n}}.\vec{x}} \tag{B.2}$$

where $V = L^3T$. We define the "4-vector" $\alpha = (L, L, L, T)$. Poisson's resummation [11] formula:

$$\sum_{\vec{n}\in\mathbb{Z}^4} \Delta(\vec{x} + \alpha\vec{n}, M^2)_{|V=\infty} = \frac{1}{V} \sum_{\vec{n}\in\mathbb{Z}^4} \widetilde{\Delta}\,(\vec{p}_{\vec{n}}, M^2) e^{i\vec{p}_{\vec{n}}.\vec{x}} \tag{B.3}$$

implies the following link between $\Delta(\vec{x}, M^2)_{|V}$ and $\Delta(\vec{x}, M^2)_{|V=\infty}$:

$$\Delta(\vec{x}, M^2)_{|V} = \sum_{\vec{n}\in\mathbb{Z}^4} \Delta(\vec{x} + \alpha\vec{n}, M^2)_{|V=\infty} \tag{B.4}$$

We therefore obtain:

$$\Delta(\vec{x}, M^2)_{|V} = \Delta(\vec{x}, M^2)_{|V=\infty} + \sum_{\vec{n}\in(\mathbb{Z}^4)^\star} \Delta(\vec{x} + \alpha\vec{n}, M^2)_{|V=\infty} \tag{B.5}$$

The finite-volume effects are contained in the second term of the above equation (B.5): each term of the sum corresponds to the n-times for which the particle will run around the box. Besides, we can write:

$$\Delta(\vec{x}+\alpha\vec{n},M^2)_{|V=\infty}=\frac{1}{(2\pi)^4}\int d^4p\frac{e^{i\vec{p}.(\vec{x}+\alpha\vec{n})}}{p^2+M^2} \tag{B.6}$$

Putting $\vec{x}=0$, we have the expression of the loop's propagator at finite-volume:

$$\Delta(0,M^2)_{|V}=\frac{1}{(2\pi)^4}\int d^4p\frac{1}{p^2+M^2}+\sum_{\vec{n}\in(\mathbb{Z}^4)^\star}\frac{1}{(2\pi)^4}\int d^4p\frac{e^{i\vec{p}.(\alpha\vec{n})}}{p^2+M^2} \tag{B.7}$$

The second term of the r.h.s. in eq. (B.7) can be re-expressed as a Bessel integral:

$$\begin{aligned}\frac{1}{(2\pi)^4}\int d^4p\frac{e^{i\vec{p}.(\alpha\vec{n})}}{p^2+M^2}&=\frac{1}{(4\pi)^2}\int_0^\infty d\lambda\lambda^{-2}e^{-M^2\lambda}e^{-\frac{|\alpha\vec{n}|^2}{4\lambda}}\\&=\frac{M}{4\pi^2|\alpha\vec{n}|}K_1(M|\alpha\vec{n}|)\end{aligned} \tag{B.8}$$

where $|\alpha\vec{n}|$ is the norm of the euclidean four-vector $\alpha\vec{n}$. We define:

$$\Delta(\alpha\vec{n},M^2)_{|V=\infty}=\frac{M}{4\pi^2|\alpha\vec{n}|}K_1(M|\alpha\vec{n}|) \tag{B.9}$$

Finally, we obtain:

$$\Delta(0,M^2)_{|V}=\Delta(0,M^2)_{|V=\infty}+\sum_{\vec{n}\in(\mathbb{Z}^4)^\star}\Delta(\alpha\vec{n},M^2)_{|V=\infty} \tag{B.10}$$

From that point one only has to make the replacement $\Delta(0,M^2)_{|V=\infty}\to\Delta(0,M^2)_{|V}$ in the expression of the different observables.

• It is possible to proceed in an identical way for a purely spatial box. This is in fact the situation when we evaluate the finite-volume effects in Chapter 5 because the dependence on t is used to extract the observables. The propagator (B.2) is rewritten in that case, with $V=L^3$:

$$\Delta(\tau,\vec{x},M^2)_{|V}=\frac{1}{V}\sum_{\vec{n}\in\mathbb{Z}^3}\int\frac{dp_0}{2\pi}\widetilde{\Delta}\,(p_0,\vec{p}_{\vec{n}},M^2)e^{i(p_0\tau+\vec{p}_{\vec{n}}.\vec{x})} \tag{B.11}$$

where we integrate over the time component p_0 of the momentum which remains continuous, and sum over the spatial components $\vec{p}_{\vec{n}}$. In the spatial box eq. (B.4) then gives:

$$\Delta(\tau,\vec{x},M^2)_{|V}=\sum_{\vec{n}\in\mathbb{Z}^3}\Delta(\tau,\vec{x}+\alpha\vec{n},M^2)_{|V=\infty} \tag{B.12}$$

It is now necessary to evaluate $\Delta(\tau,\vec{x}+\alpha\vec{n},M^2)_{|V=\infty}$. By putting $x=0$:

$$\Delta(0,\alpha\vec{n},M^2)_{|V=\infty}=\int\frac{dp_0d^3\vec{p}}{(2\pi)^4}\frac{e^{i\vec{p}.(\alpha\vec{n})}}{p_0^2+\vec{p}^2+M^2} \tag{B.13}$$

The integral over p_0 is easily calculated:

$$\int_{-\infty}^{+\infty} \frac{dp_0}{2\pi} \frac{1}{p_0^2 + a^2} = \frac{1}{2a}, \quad a > 0 \tag{B.14}$$

All that's left to do is to evaluate the remaining integral:

$$\Delta(0, \alpha\vec{n}, M^2)_{|V=\infty} = \int \frac{d^3\vec{p}}{(2\pi)^3} \frac{e^{i\vec{p}.(\alpha\vec{n})}}{2\sqrt{\vec{p}^2 + M^2}} \tag{B.15}$$

Using the following trick:

$$\frac{1}{\alpha^s} = \frac{1}{\Gamma(s)} \int_0^\infty d\lambda e^{-\alpha\lambda} \lambda^{s-1} \ (\alpha > 0, \ s > 1) \tag{B.16}$$

then, integrating over $\vec{p}^3$, one obtains:

$$\Delta(0, \alpha\vec{n}, M^2)_{|V=\infty} = \int_0^\infty \frac{d\lambda}{16\pi^2} \lambda^{-2} e^{-M^2\lambda} e^{-\frac{|\alpha\vec{n}|}{4\lambda}} \tag{B.17}$$

Finally, we have simply:

$$\Delta(0, M^2)_{|V} = \Delta(0, M^2)_{|V=\infty} + \sum_{\vec{n} \in (\mathbb{Z}^3)^\star} \Delta(\alpha\vec{n}, M^2)_{|V=\infty} \tag{B.18}$$

The result for the propagator in a three-dimensional box is therefore the same as the propagator in a four-dimensional one, up to the fact that the sum only runs over the spatial dimensions. We have the following dictionary between the function $\Xi_P = \xi_{1/2}(L, \mathring{M}_P^2)$ defined in sec. 6.2.2 and the propagator (B.17):

$$\Xi_P \ \longleftrightarrow \ \sum_{\vec{n} \in (\mathbb{Z}^3)^\star} \Delta(\alpha\vec{n}, M^2)_{|V=\infty} \tag{B.19}$$

Appendix C

"Total" fits including additional data points for higher masses and momenta

In sec. 4.3.2, we considered fits to both PACS-CS and RBC/UKQCD data restricted to the low-mass and low-momentum region. We have also performed fits to the whole sets of data available ("Total" data), in order to test the stability of our results, and to illustrate the interest of having larger data sets to determine the higher order remainders in an accurate way. We are aware that some of the data points considered here may stand outside the region of validity for ReχPT, but we found nevertheless interesting to provide these results, showing a good consistency with those obtained with "subset" data (table 4.7).

Our results are summarized in tables C.1 and C.2. The first series of rows corresponds to the outcome of the fit, whereas the lower rows are quantities derived from the results of the fit (leading order and next-to-leading order low-energy constants, quantities in the $N_f = 2$ chiral limit, $K_{\ell 3}$ quantities, relative fraction of LO/NLO/remainders contributions at the minimum for several observables), and the last row is the χ^2 per degree of freedom. Most of the comments made in sec. 4.3.2 can be restated, with a few changes in the case of the RBC/UKQCD data (larger value of F_K/F_π and lower value of $f_+(0)$ than in the case presented in Chapter 4). We notice that the fits are fairly good, and that all higher order remainders turn out to lie within their expected range.

Without $K_{\ell 3}$	RBC/UKQCD Total	PACS − CS Total
r	25.8 ± 0.9	25.7 ± 0.9
$X(3)$	0.44 ± 0.03	0.48 ± 0.04
$Y(3)$	0.77 ± 0.06	0.76 ± 0.07
$Z(3)$	0.56 ± 0.04	0.63 ± 0.05
F_K/F_π	1.214 ± 0.012	1.239 ± 0.011
Rem. at limit	none	none
$\tilde{m}_{s,ref}/m_s$	1.12 ± 0.03	1.21 ± 0.02
$m_s(2\text{ GeV})$[MeV]	110 ± 3	72 ± 2
$m(2\text{ GeV})$[MeV]	4.3 ± 0.1	2.8 ± 0.1
$B_0(2\text{ GeV})$[GeV]	1.75 ± 0.14	2.65 ± 0.20
F_0[MeV]	69.2 ± 2.2	73.0 ± 2.5
$L_4(\mu) \cdot 10^3$	0.7 ± 0.1	0.1 ± 0.2
$L_5(\mu) \cdot 10^3$	1.8 ± 0.2	2.2 ± 0.2
$L_6(\mu) \cdot 10^3$	0.8 ± 0.2	0.5 ± 0.3
$L_8(\mu) \cdot 10^3$	1.2 ± 0.3	1.4 ± 0.3
$X(2)$	0.90 ± 0.01	0.90 ± 0.01
$Y(2)$	1.02 ± 0.01	1.03 ± 0.01
$Z(2)$	0.88 ± 0.01	0.87 ± 0.01
$B(2\text{ GeV})$[GeV]	2.34 ± 0.07	3.58 ± 0.11
F[MeV]	86.7 ± 0.3	86.3 ± 0.3
$\bar{\ell}_3$	3.1 ± 0.6	3.8 ± 0.6
$\bar{\ell}_4$	3.9 ± 0.2	4.2 ± 0.2
Σ/Σ_0	2.07 ± 0.15	1.88 ± 0.14
B/B_0	1.32 ± 0.10	1.35 ± 0.11
F/F_0	1.25 ± 0.04	1.18 ± 0.04
$f_+(0)$	1.006 ± 0.149	1.011 ± 0.149
F_π^2	$0.56 + 0.54 - 0.10$	$0.63 + 0.28 + 0.09$
F_K^2	$0.38 + 0.69 - 0.07$	$0.41 + 0.52 + 0.07$
$F_\pi^2 M_\pi^2$	$0.44 + 0.67 - 0.11$	$0.48 + 0.50 + 0.02$
$F_K^2 M_K^2$	$0.31 + 0.77 - 0.08$	$0.33 + 0.65 + 0.02$
χ^2/N	13.6/7	13.8/15

Table C.1: Results of fits performed on the data from the RBC/UKQCD [99, 100, 101] and PACS-CS [96] collaborations on pseudoscalar masses and decay constants, considering all the available unquenched data (Total). Only statistical errors are shown. The LECs are given at the scale $\mu = m_\rho$. The $K_{\ell 3}$ form factor at zero momentum transfer is a prediction of the fit (with an error combining those obtained from the fit and the maximal contribution allowed for the remainder from dimensional estimation). The penultimate set of rows collects the relative fractions of LO/NLO/remainders for decay constants and masses at the minimum.

With $K_{\ell 3}$	RBC/UKQCD Total I	RBC/UKQCD Total II
r	24.9 ± 0.6	25.2 ± 0.9
$X(3)$	0.43 ± 0.03	0.42 ± 0.03
$Y(3)$	0.80 ± 0.05	0.78 ± 0.06
$Z(3)$	0.53 ± 0.03	0.54 ± 0.04
F_K/F_π	1.199 ± 0.009	1.203 ± 0.011
Rem. at limit	none	none
$\tilde{m}_{s,ref}/m_s$	$1.15^\star$	1.14 ± 0.03
$m_s(2\text{ GeV})$[MeV]	107	109 ± 3
$m(2\text{ GeV})$[MeV]	4.3 ± 0.1	4.3 ± 0.1
$B_0(2\text{ GeV})$[GeV]	1.80 ± 0.12	1.77 ± 0.14
F_0[MeV]	67.1 ± 1.9	67.6 ± 2.1
$L_4(\mu) \cdot 10^3$	0.76 ± 0.10	0.75 ± 0.10
$L_5(\mu) \cdot 10^3$	1.64 ± 0.12	1.71 ± 0.19
$L_6(\mu) \cdot 10^3$	0.71 ± 0.13	0.76 ± 0.17
$L_8(\mu) \cdot 10^3$	1.18 ± 0.22	1.19 ± 0.23
$L_9(\mu) \cdot 10^3$	5.05 ± 2.25	5.08 ± 2.25
$X(2)$	0.90 ± 0.01	0.90 ± 0.01
$Y(2)$	1.02 ± 0.01	1.02 ± 0.01
$Z(2)$	0.88 ± 0.01	0.88 ± 0.01
$B(2\text{ GeV})$[GeV]	2.30 ± 0.06	2.31 ± 0.06
F[MeV]	86.5 ± 0.2	86.6 ± 0.3
$\bar{\ell}_3$	2.7 ± 0.5	2.9 ± 0.6
$\bar{\ell}_4$	4.1 ± 0.2	4.0 ± 0.2
Σ/Σ_0	2.11 ± 0.13	2.14 ± 0.16
B/B_0	1.28 ± 0.07	1.31 ± 0.10
F/F_0	1.29 ± 0.04	1.28 ± 0.04
$f_+(0)$	0.975 ± 0.006	0.975 ± 0.006
$\Delta_{CT} \cdot 10^3$	4.8 ± 5.7	3.8 ± 5.8
$\Delta'_{CT} \cdot 10^3$	-70 ± 28	-68 ± 29
$\langle r^2 \rangle_V^{K^+}$[fm^2]	0.224 ± 0.129	0.225 ± 0.129
$\langle r^2 \rangle_V^{K^0}$[fm^2]	-0.026 ± 0.098	-0.026 ± 0.097
F_π^2	$0.53 + 0.57 - 0.10$	$0.54 + 0.56 - 0.10$
F_K^2	$0.37 + 0.70 - 0.07$	$0.37 + 0.70 - 0.07$
$F_\pi^2 M_\pi^2$	$0.43 + 0.68 - 0.11$	$0.42 + 0.69 - 0.11$
$F_K^2 M_K^2$	$0.30 + 0.78 - 0.08$	$0.30 + 0.78 - 0.08$
$F_\pi F_K f_+(0)$	$0.45 + 0.66 - 0.11$	$0.46 + 0.66 - 0.12$
χ^2/N	33.6/20	33.2/19

Table C.2: Results of two different fits of the data from the RBC/UKQCD [99, 100, 101] on pseudoscalar masses and decay constants, as well as on $K_{\ell 3}$ form factors. We considered all the available unquenched data (Total), and either fixed the lattice strange quark mass (marked then with a star) or let it vary freely. Only statistical errors are shown and LECs are given at the scale $\mu = m_\rho$. The penultimate set of rows collects the relative fractions of LO/NLO/remainders at the minimum for decay constants, masses and $K_{\ell 3}$ form factor at vanishing transfer momentum.

Appendix D

Expressions of Feynman diagrams for topological quantities

D.1 Topological susceptibility χ_t

We use the following notation for the regularized tadpole "bubble" (sec.2.5.4):

$$\Delta^P(0) = \frac{\overset{\circ}{M}_P^{\,2}}{16\pi^2}\left[\log\frac{\overset{\circ}{M}_P^{\,2}}{\mu^2} - \frac{2}{\epsilon} - \ln 4\pi + \gamma - 1 + \ln\mu^2 + O(\epsilon)\right], \quad \epsilon = 4 - d \tag{D.1}$$

The relevant diagrams for the calculation of the topological susceptibility up to next-to-leading order are recalled in figure D.1. The expressions (in the isospin limit) for each of the different diagrams follow.

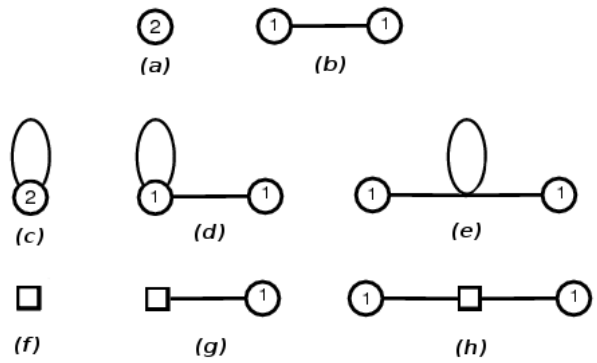

Figure D.1: *Diagrams involved in the evaluation of the topological susceptibility up to NLO. The circles represent the exterior vertices, containing the number of θ derivatives, while the propagating η and π^0 mesons are represented by the solid lines attached to the sources. The loops contain any of the eight Goldstone bosons. The crossing lines correspond to the usual four-point vertex (from $\mathcal{L}^{(2)}$, eq. (2.62)), and the white square in diagrams (f), (g) and (h) to NLO counter-terms (from $\mathcal{L}^{(4)}$, eq. (2.62)).*

- Tree graphs (a) and (b) from $\mathcal{L}^{(2)}$:

$$(a) = -\frac{F_0^2 B_0}{9}(2m + m_s), \quad \text{local term (a)} \tag{D.2}$$

$$(b) = \frac{2}{9}F_0^2 B_0 \frac{(m - m_s)^2}{m + 2m_s}, \quad \text{propagating term (b)} \tag{D.3}$$

• One-loop graphs (c), (d) and (e) from $\mathcal{L}^{(2)}$:

$$(c) = -i\frac{B_0}{9}\left[3m\Delta^\pi(0) + 2(m+m_s)\Delta^K(0) + \frac{1}{3}(m+2m_s)\Delta^\eta(0)\right] \tag{D.4}$$

$$(d) = -i\frac{-4B_0^2}{27}\left[\frac{3(m-m_s)}{2B_0(m+2m_s)}\left(3m\Delta^\pi(0) - 2m_s\Delta^K(0) + \Big(\frac{m}{3} - \frac{4}{3}\Big)\Delta^\eta(0)\right)\right] \tag{D.5}$$

$$(e) = -i\frac{2B_0^3}{27}\frac{9(m-m_s)^2}{4B_0^2(m+2m_s)^2}\left[\frac{2}{3}\Big(3m\Delta^\pi(0) - (10m+3m_s)\Delta^K(0)\Big)\right. \tag{D.6}$$
$$\left. + \frac{1}{9}(2m+16m_s)\Delta^\eta(0)\right]$$

• Tree graphs (f), (g) and (h) from $\mathcal{L}^{(4)}$ (counter-terms):

$$(f) = -\frac{32}{9}B_0^2[(2m+m_s)^2(L_6+L_7) + (2m^2+m_s^2)L_8] \tag{D.7}$$

$$(g) = \frac{128}{9}B_0^2\frac{m-m_s}{m+2m_s}[(L_6+L_7)(m-m_s)(2m+m_s) + L_8(m^2-m_s^2)] \tag{D.8}$$

$$(h) = -\frac{64}{9}B_0^2\frac{(m-m_s)^2}{(m+2m_s)^2}[L_6(2m+m_s)(m+2m_s) + 2L_7(m-m_s)^2 + L_8(m^2+2m_s^2)] \tag{D.9}$$

D.2 Fourth cumulant c_4

As indicated in sec. 5.3.1, there are several classes of diagrams contributing to the chiral expansion of c_4 up to one loop. They are recalled in this appendix. First, there are five leading-order diagrams shown in figure D.2. The tree-diagram 5 is dressed by adding a counter-term or a loop at the level of the vertices or the propagators, the susbsequent diagrams are recalled in figure D.3. Finally there are five additional one-loop diagrams collected in figure D.4 corresponding to the various local terms. In the following, we will give the contribution of the various diagrams with the same distinction for the argument of logarithms coming from tadpole or from unitarity contributions as in eq. (5.28). The relevant diagrams are recalled in the following figures D.2, D.3 and D.4. The expressions (in the isospin limit) for each of the different diagrams follow.

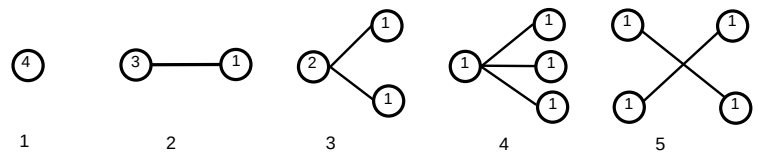

Figure D.2: *Tree diagrams for c_4. The external points stemming from θ derivatives are represented by a circle, containing the relevant number of derivatives.*

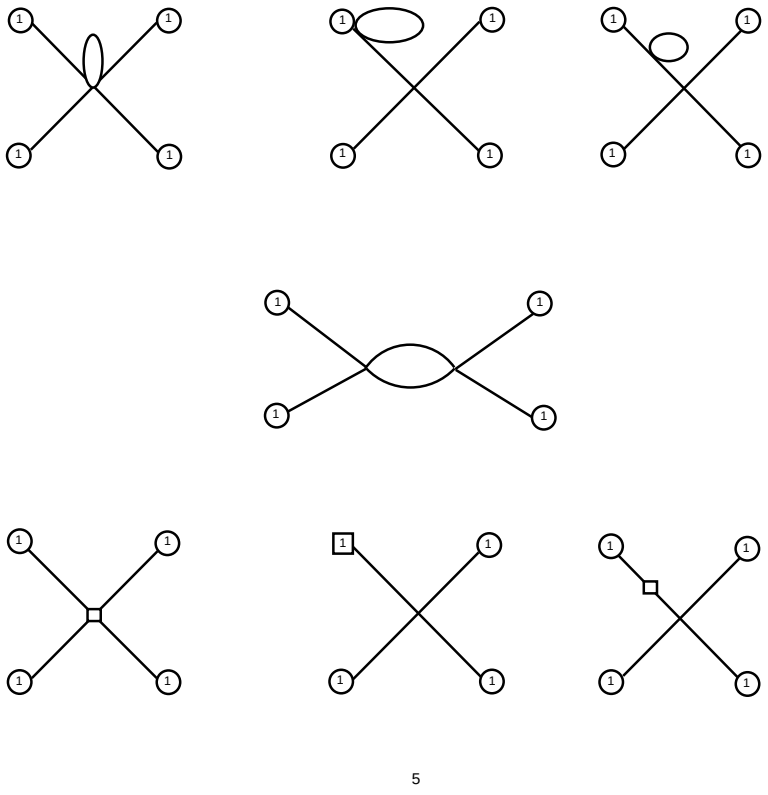

Figure D.3: *Scattering One-loop diagrams for c_4 involving propagation, obtained by dressing the tree-diagram 5. The square correspond to an NLO vertex.*

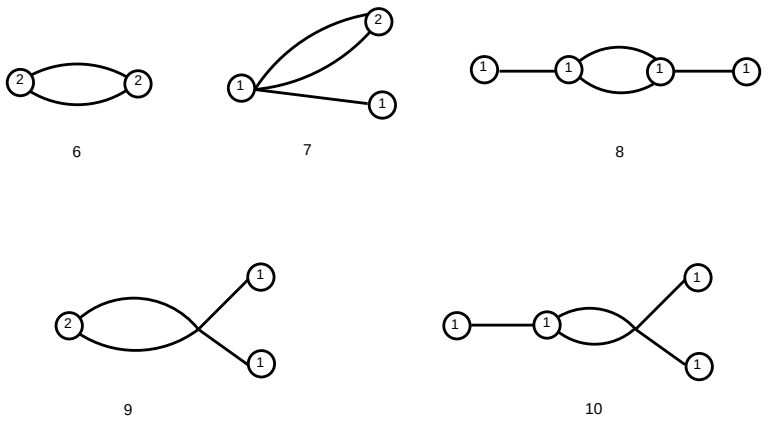

Figure D.4: *One-loop diagrams for c_4 involving local terms.*

- Diagrams 1

$$
\begin{aligned}
&-\frac{1}{81}B_0F_0^2(2m+ms)+\frac{B_0^2m^2}{216\pi^2}\ln\frac{\overset{\circ}{M}_\pi^2}{\mu^2}\\
&+\frac{B_0^2\left(m+m_s\right)^2}{648\pi^2}\ln\frac{\overset{\circ}{M}_K^2}{\mu^2}+\frac{B_0^2\left(m+2m_s\right)^2}{5832\pi^2}\ln\frac{\overset{\circ}{M}_\eta^2}{\mu^2}\\
&-\frac{128}{81}B_0^2\left(m_s+2m\right)^2L_6^r(\mu)-\frac{128}{81}B_0^2\left(m_s+2m\right)^2L_7\\
&-\frac{128}{81}B_0^2\left(2m^2+m_s^2\right)L_8^r(\mu)
\end{aligned}
\tag{D.10}
$$

- Diagrams 2

$$
\begin{aligned}
&\frac{16B_0^2F_0^2(m-m_s)^2}{243M_\eta^2}-\frac{2B_0^3m^2\left(m-m_s\right)}{81\pi^2M_\eta^2}\ln\frac{\overset{\circ}{M}_\pi^2}{\mu^2}+\frac{2B_0^3\left(m-m_s\right)\left(m+m_s\right)^2}{243\pi^2M_\eta^2}\ln\frac{\overset{\circ}{M}_K^2}{\mu^2}\\
&-\frac{2B_0^3\left(m-m_s\right)\left(m-4m_s\right)\left(m+2m_s\right)}{2187\pi^2M_\eta^2}\ln\frac{\overset{\circ}{M}_\eta^2}{\mu^2}\\
&-\frac{256B_0^3\left(m-m_s\right)^2\left(2m+m_s\right)}{243M_\eta^2}L_4^r(\mu)-\frac{256B_0^3\left(m-m_s\right)^2\left(m+2m_s\right)}{729M_\eta^2}L_5^r(\mu)\\
&+\frac{2560B_0^3\left(m-m_s\right)^2\left(2m+m_s\right)}{243M_\eta^2}L_6^r(\mu)+\frac{2560B_0^3\left(m-m_s\right)^2\left(2m+m_s\right)}{243M_\eta^2}L_7\\
&+\frac{2560B_0^3\left(m-m_s\right)^2\left(m+m_s\right)}{243M_\eta^2}L_8^r(\mu)
\end{aligned}
\tag{D.11}
$$

- Diagrams 3

$$
\begin{aligned}
&-\frac{16B_0^2(m-m_s)^2(m+2m_s)}{243M_\eta^4}\\
&+\frac{B_0^4m^2\left(m-m_s\right)\left(m+m_s\right)}{27\pi^2M_\eta^4}\ln\frac{\overset{\circ}{M}_\pi^2}{\mu^2}-\frac{B_0^4\left(m-m_s\right)\left(m+m_s\right)^3}{162\pi^2M_\eta^4}\ln\frac{\overset{\circ}{M}_K^2}{\mu^2}\\
&+\frac{B_0^4\left(m-m_s\right)\left(m+2m_s\right)\left(m^2+mm_s-8m_s^2\right)}{729\pi^2M_\eta^4}\ln\frac{\overset{\circ}{M}_\eta^2}{\mu^2}\\
&+\frac{512B_0^4\left(m-m_s\right)^2\left(2m+m_s\right)\left(m+2m_s\right)}{243M_\eta^4}L_4^r(\mu)+\frac{512B_0^4\left(m-m_s\right)^2\left(m+2m_s\right)^2}{243M_\eta^2}L_5^r(\mu)\\
&-\frac{2040B_0^4\left(m-m_s\right)^2\left(m^2+mm_s+m_s^2\right)}{81M_\eta^4}L_6^r(\mu)-\frac{2040B_0^4\left(m-m_s\right)^2\left(m^2+mm_s+m_s^2\right)}{81M_\eta^4}L_7\\
&-\frac{1024B_0^4\left(m-m_s\right)^2\left(m^2+mm_s+2m_s^2\right)}{81M_\eta^4}L_8^r(\mu)
\end{aligned}
\tag{D.12}
$$

- Diagrams 4

$$
\begin{aligned}
&\frac{64B_0^4F_0^2(m-4m_s)(m-m_s)^3}{2187M_\eta^6}-\frac{4B_0^5m^2\left(4m-13m_s\right)\left(m-m_s\right)^2}{729\pi^2M_\eta^6}\ln\frac{\overset{\circ}{M}_\pi^2}{\mu^2}\\
&+\frac{2B_0^5\left(m+m_s\right)\left(m-m_s\right)^2\left(32m^2-99mm_s-23m_s^2\right)}{10935\pi^2M_\eta^6}\ln\frac{\overset{\circ}{M}_K^2}{\mu^2}\\
&-\frac{4B_0^5\left(m+m_s\right)\left(m-m_s\right)^2\left(4m^2-41mm_s+64m_s^2\right)}{19683\pi^2M_\eta^6}\ln\frac{\overset{\circ}{M}_\eta^2}{\mu^2}
\end{aligned}
$$

$$
\begin{aligned}
&-\frac{1024B_0^5\left(m-m_s\right)^3\left(m-4m_s\right)\left(2m+m_s\right)}{729M_\eta^6}L_4^r(\mu)\\
&-\frac{1024B_0^5\left(m-m_s\right)^3\left(m-4m_s\right)\left(m+2m_s\right)}{2187M_\eta^2}L_5^r(\mu)\\
&+\frac{4096B_0^5\left(m-m_s\right)^3\left(7m^2-11mm_s-14m_s^2\right)}{2187M_\eta^6}L_6^r(\mu)\\
&+\frac{4096B_0^5\left(m-m_s\right)^3\left(7m^2-11mm_s-14m_s^2\right)}{2187M_\eta^6}L_7\\
&+\frac{2048B_0^5\left(m-m_s\right)^3\left(7m^2-9mm_s-28m_s^2\right)}{2187M_\eta^6}L_8^r(\mu)
\end{aligned}
\tag{D.13}
$$

- Diagrams 5

$$
\begin{aligned}
&-\frac{32B_0^5F_0^2(m-m_s)^4(m+8m_s)}{6561M_\eta^8}+\frac{2B_0^6m^2\left(m-m_s\right)^3\left(5m+31m_s\right)}{2187\pi^2M_\eta^8}\ln\frac{\overset{\circ}{M}{}_\pi^2}{\mu^2}\\
&+\frac{2B_0^6\left(m-m_s\right)^3\left(m+m_s\right)\left(m^2-189mm_s+8m_s^2\right)}{32805\pi^2M_\eta^8}\ln\frac{\overset{\circ}{M}{}_K^2}{\mu^2}\\
&+\frac{2B_0^6\left(m-m_s\right)^3\left(m+2m_s\right)\left(5m^2+47mm_s-160m_s^2\right)}{59049\pi^2M_\eta^8}\ln\frac{\overset{\circ}{M}{}_\eta^2}{\mu^2}\\
&+\frac{2B_0^6m^2\left(m-m_s\right)^4}{729\pi^2M_\eta^8}\ln\frac{M_\pi^2}{\mu^2}+\frac{2B_0^6m^2\left(m-m_s\right)^4}{2187\pi^2M_\eta^8}\ln\frac{M_K^2}{\mu^2}\\
&+\frac{2B_0^6\left(m-m_s\right)^4\left(m+8m_s\right)^2}{19683\pi^2M_\eta^8}\ln\frac{M_\eta^2}{\mu^2}\\
&+\frac{2048B_0^6\left(m-m_s\right)^4\left(m+8m_s\right)\left(2m+m_s\right)}{6561M_\eta^8}L_4^r(\mu)\\
&+\frac{2048B_0^6\left(m-m_s\right)^4\left(m+8m_s\right)\left(m+2m_s\right)}{19683M_\eta^8}L_5^r(\mu)\\
&-\frac{1024B_0^2\left(m-m_s\right)^4\left(16m^2+109mm_s+64m_s^2\right)}{6561M_\eta^8}L_6^r(\mu)\\
&-\frac{4096B_0^2\left(m-m_s\right)^4\left(4m^2+7mm_s+16m_s^2\right)}{6561M_\eta^8}L_7\\
&-\frac{4096B_0^2\left(m-m_s\right)^4\left(2m^2+9mm_s+16m_s^2\right)}{6561M_\eta^8}L_8\\
&+\frac{2B_0^6\left(m-m_s\right)^4\left(37m^2+16mm_s+64m_s^2\right)}{19683\pi^2M_\eta^8}
\end{aligned}
\tag{D.14}
$$

- Diagrams 6

$$
\begin{aligned}
&\frac{B_0^2}{72\pi^2}m^2\ln\frac{M_\pi^2}{\mu^2}+\frac{B_0^2}{216\pi^2}\left(m+m_s\right)^2\ln\frac{M_K^2}{\mu^2}+\frac{B_0^2}{1944\pi^2}\left(m+2m_s\right)^2\ln\frac{M_\eta^2}{\mu^2}\\
&+\frac{B_0^2}{1944\pi^2}\left(37m^2+22mm_s+13m_s^2\right)
\end{aligned}
\tag{D.15}
$$

- Diagrams 7

$$
\begin{aligned}
&-\frac{B_0^3m^2\left(m-m_s\right)}{27\pi^2M_\eta^2}\ln\frac{M_\pi^2}{\mu^2}-\frac{B_0^3m_s\left(m_s^2-m^2\right)}{81\pi^2M_\eta^2}\ln\frac{M_K^2}{\mu^2}\\
&-\frac{B_0^3\left(m-4m_s\right)\left(m-m_s\right)\left(m+2m_s\right)}{729M_\eta^2\pi^2}\ln\frac{M_\eta^2}{\mu^2}
\end{aligned}
$$

$$-\frac{B_0^2\,(m-m_s)^{\,2}\,(17m_s+28m)}{729\pi^2 M_\eta^2} \tag{D.16}$$

- Diagrams 8

$$\begin{aligned}&\frac{2B_0^4 m^2\,(m-m_s)^{\,2}}{81\pi^2 M_\eta^4}\ln\frac{M_\pi^2}{\mu^2}+\frac{2B_0^2 m_s^2\,(m-m_s)^{\,2}}{243\pi^2 M_\eta^4}\ln\frac{M_K^2}{\mu^2}\\&+\frac{2B_0^2\,(m-4m_s)^{\,2}\,(m-m_s)^{\,2}}{2187\pi^2 M_\eta^4}\ln\frac{M_\eta^2}{\mu^2}\\&+\frac{2B_0^2\,(m-m_s)^{\,2}\left(28m^2-8mm_s+25m_s^2\right)}{2187\pi^2 M_\eta^4}\end{aligned} \tag{D.17}$$

- Diagrams 9

$$\begin{aligned}&\frac{B_0^4 m^2\,(m-m_s)^{\,2}}{81\pi^2 M_\eta^4}\ln\frac{M_\pi^2}{\mu^2}-\frac{B_0^2 m\,(m-m_s)^2\,(m+m_s)}{243\pi^2 M_\eta^4}\ln\frac{M_K^2}{\mu^2}\\&+\frac{B_0^4\,(m+8m_s)\,(m-m_s)^{\,2}\,(m+2m_s)}{2187\pi^2 M_\eta^4}\ln\frac{M_\eta^2}{\mu^2}-\frac{B_0^4\,(m-m_s)^2\,(m+m_s)^2}{162\pi^2 M_\eta^4}\ln\frac{\overset{\circ}{M}{}_K^2}{\mu^2}\\&+\frac{B_0^4\,(m-m_s)^{\,2}\left(19m^2+mm_s+16m_s^2\right)}{2187\pi^2 M_\eta^4}\end{aligned} \tag{D.18}$$

- Diagrams 10

$$\begin{aligned}&-\frac{4B_0^5 m^2\,(m-m_s)^{\,3}}{243\pi^2 M_\eta^6}\ln\frac{M_\pi^2}{\mu^2}-\frac{4B_0^2 m m_s\,(m-m_s)^{\,3}}{729\pi^2 M_\eta^6}\ln\frac{M_K^2}{\mu^2}\\&-\frac{4B_0^5\,(m-4m_s)\,(m+8m_s)\,(m-m_s)^{\,3}}{6561\pi^2 M_\eta^6}\ln\frac{M_\eta^2}{\mu^2}-\frac{2B_0^5(m+m_s)m_s\,(m-m_s)^{\,3}}{243\pi^2 M_\eta^6}\ln\frac{\overset{\circ}{M}{}_K^2}{\mu^2}\\&-\frac{4B_0^5\,(m-m_s)^{\,3}\left(28m^2+13mm_s-32m_s^2\right)}{6561\pi^2 M_\eta^6}\end{aligned} \tag{D.19}$$

Let us notice that vertices from $\mathcal{L}_{eff}^{(2)}$ with derivatives applied to the internal propagators generate contact terms which yield tadpole contributions even in the case of the scattering diagrams 9 and 10 where such contributions would not be expected naively. One can easily obtain the equivalent contributions with the prescription of eq. (5.27) by setting the LO masses $\overset{\circ}{M}{}_P^{\,2}$ in the argument of all logarithms.

Bibliography

[1] J.Gasser, H. Leutwyler, *Chiral Perturbation Theory to one loop*, *Annals of Physics* **158** 142-210 (1984)

[2] J.Gasser, H. Leutwyler, *Chiral Perturbation Theory : expansions in the mass of the strange quark*, *Nuclear Physics B* **250** 456-516 (1985)

[3] J.Gasser, H. Leutwyler, *Spontaneously Broken Symmetries: Effective lagrangians at finite volumes*, *Nuclear Physics B* **307** 763 (1988)

[4] N.H. Fuchs, H. Sazdjian and J.Stern, *Phys. Lett.* **B269** (1991) 183, *Phys. Rev.* **D47** 3814 (1993)

[5] M. Knecht, B. Moussalam, J.Stern and N.H. Fuchs, *Phys. Lett.* **B269** (1991) 183, *Nuclear Physics* **B457** (1995) 513

[6] M. Peskin, D. Schroeder, *An introduction to quantum field theory*, Advanced Book Program, Westview Press, 1995

[7] J.F. Donoghue, E. Golowich, B.R. Johnson, *Dynamics of The Standard Model*, Cambridge University Press, 1992

[8] L.H. Ryder, *Quantum Field Theory, Second Edition*, Cambridge University Press, 1996

[9] S. Weinberg, *The Quantum Theory of Fields*, Cambridge University Press, 1995

[10] W. Greiner, B. Mueller, *Quantum Mechanics, Symmetries*, Springer, 1994

[11] W. Appel, *Mathématiques pour la Physique et les physiciens !*, Quatrième édition, H&K, 2008

[12] S.B. Treiman, R. Jackiw, B. Zumino and E. Witten *Current Algebra and Anomalies*, World Scientific, 1985

[13] A.Pich, *Effective field theory*, [arXiv:hep-ph/9806303v1], June 1998

[14] G. Colangelo, G. Isidori, *An Introduction to ChPT*, [arXiv:hep-ph/0101264v1], January 2001

[15] G. Ecker, *The Standard Model at Low Energies*, [arXiv:hep-ph/9309268], September 1993

[16] R.D. Peccei, H.R. Quinn, *CP Conservation in the Presence of Instantons*, *Phys.Rev.Lett.* **38** (1977) 1440-1443

[17] R.D. Peccei, H.R. Quinn, *Constraints Imposed by CP Conservation in the Presence of Instantons*, *Phys. Rev.* **D 16** (1977) 1791-1797

[18] K. Fujikawa, *Path-Integral measure of Gauge-Invariant Fermion theories*, *Phys. Rev. Lett.* **42** 18 (1979)

K. Fujikawa, *Path integral for gauge theories with fermions*, *Phys. Rev.* D **21** 10 (1979)

[19] M. F. Atiyah and I.M. Singer, *Dirac Operators Coupled to Vector Potentials*, *Proc. Nat. Acad. Sci.* **81**, 2597-2600, (1984)

[20] C. Vafa and E. Witten, *Eigenvalues Inequalities for fermions in gauge theories*, *Commun. Math. Phys.*, **95**, 257, (1984)

[21] J. Wess, B. Zumino, *Consequences of anomalous Ward identities*, *Phys. Lett. B* **37**, 95, (1971)

[22] E. Witten, *Global Aspects of Current Algebra*, *Nuc. Phys. B* **223**, 422, (1983)

[23] K. G. Wilson, *Confinement of Quarks*, *Phys. Rev. D* **10**, 2445, (1974)

[24] K. G. Wilson, *Quarks and Strings on a Lattice*, (1975)

[25] M. Creutz, *Monte-Carlo Study of Quantized SU(2) Gauge Theory*, *Phys. Rev. D* **21** 2308, (1980)

[26] S. Duane, A.D. Kennedy and B.J. Pendleton, *Hybrid Monte-Carlo*, *Phys. Lett. B* **195**, 216, (1987)

[27] D.B. Kaplan, *A Method for simulating chiral fermions on the lattice*, *Phys. Lett. B*, **288**, 342, (1992), [arXiv:9206013[hep-lat]]

[28] H. Neuberger, *Exactly massless quarks on the lattice*, *Phys. Lett. B.* **417**, 141, (1998), [arXiv:9707022[hep-lat]]

[29] M. Luscher, *Exact chiral symmetry on the lattice and the Ginsparg-Wilson relation*, *Phys. Lett. B* **428**, 342, (1998), [arXiv:9802011[hep-lat]]

[30] B. Sheikholeslami and R. Wohlert, *Improved Continuum Limit Lattice Action for QCD with Wilson fermions*, *Nuc. Phys. B* **259**, 572, (1985)

[31] R. Frezzotti and G. C. Rossi, *Chirally improved Wilson fermions. 1. $O(a)$ improvements*, *JHEP* **0408**, 007, (2004), [arXiv:0306014[hep-lat]]

[32] S. Borsanyi, S. Durr, Z. Fodor, S. Krieg, A. Schafer, E. E. Scholz, K. K. Szabo, *$SU(2)$ chiral perturbation theory low energy constants from 2+1 staggered lattice simulations*, (2012), [arXiv:1205.0788[hep-lat]]

[33] P. Boucaud et al., *Dynamical Twisted Mass Fermions with Light Quarks*, *Phys. Lett. B* **650**, 304 (2007) [arXiv:0701012[hep-lat]]

[34] R. Baron and al. (ETM Collaboration), *Light hadrons from $N_f = 2 + 1 + 1$ dynamical twisted mass fermions*, *PoS*, LATTICE 2010, 123, (2010), [arxiv:1101.0518[hep-lat]]

[35] J. Bijnens, *ChPT beyond one loop*, [arXiv:hep-ph/0604043v2], August 2006

[36] J. Goldstone, *Field Theories with Superconductor Solutions*, Nuovo Cimento, **19**, (1961)

[37] J. Goldstone, A. Salam, S. Weinberg, *Broken Symmetries*, *Phys. Rev.* **127** (1962)

[38] C. G. Callan, S. Coleman, J. Wess, B. Zumino, *Structure of Phenomenological Lagrangians I and II*, *Physical Review*, Volume **177**, Number **5** (1969)

[39] S. Weinberg, *Physica A* 96, (1979), 327

[40] J. Bijnens, I. Jemos, *A new global fit of the L_i^r at next-to-next-to-leading order in Chiral Perturbation Theory*, [arXiv:1103.5945]

[41] G. Ecker, J. Gasser, A. Pich and E. de Rafael, *The Role of Resonances in Chiral Perturbation Theory*, *Nuc. Phys.* **B 321** (1989) 311

[42] S. Descotes-Genon, Jibo He, Emi Kou and Patrick Robbe, *Non-leptonic charmless Bc decays and their search at LHC*, *Phys. Rev. D* **80**, 114031, (2009) [arXiv:0907.2256v1[hep-ph]]

[43] J.Gasser, H. Leutwyler, *Low-energy expansion of meson Form-Factors*, *Nuclear Physics* **B250** (1985) 517

[44] J.Gasser, U.G. Meißner, *Chiral expansion of pion form-factors beyond one loop*, *Nuclear Physics* **B357** (1991) 90

[45] J.Bijnens, P. Talavera, *Pion and kaon electrmagnetic form factors*, *JHEP* **03** (2002) 046 [arXiv:0203049[hep-ph]]

[46] C. G. Callan S. B. Treiman, *Equal Time Commutators and K Meson Decays*, *Phys. Rev. Lett.*, **16** 1966 153

[47] J. Bijnens, K. Ghorbani, $\rightarrow 3$ *at Two Loops In Chiral Perturbation Theory*, *JHEP* **0711** 030 (2007), [arXiv:0709.0230v2[hep-ph]]

[48] V. Cirigliano, M. Giannotti, H. Neufeld, *Electromagnetic effects in Kl3 decays JHEP* **0811** 006 (2008), [arXiv:0807.4507v2[hep-ph]]

[49] V. Bernard, M. Oertel, E. Passemar and J. Stern, *$K^L_{\mu 3}$ decay: A stringent test of right-handed quark currents Phys. Lett.* **B 638** (2006) 480 [arXiv:0603202]

[50] V. Bernard, M. Oertel, E. Passemar and J. Stern, *Dispersive representation and shape of the $K_{\ell 3}$ form factors: robustness Phys. Rev.* **D 80** (2009) 034034 [arXiv:0903.1654]

[51] M. Knecht, B. Moussallam, J. Stern and N.H. Fuchs, *The Low-energy $\pi\pi$ amplitude to one and two loops*, *Nucl. Phys. B* **457** 513 (1995), [arXiv:9507319[hep-ph]]

[52] B. Ananthanarayan, G.Colangelo, J. Gasser and H. Leutwyler, *Roy equation analysis of $\pi\pi$ scattering*, *Phys. Rept.* **353** 207 (2001), [arXiv:0005297[hep-ph]]

[53] G. Colangelo, J. Gasser and H. Leutwyler, *The quark condensate from K_{e4} decays*, *Phys.Rev. Lett.* **86**, 5008 (2001) [arXiv:0103063]

[54] S.Descotes-Genon, N.H. Fuchs, L. Girlanda, J. Stern, *Analysis and interpretation of new low-energy $\pi\pi$ scattering data*, *Eur. Phys. J.* C **24** 469 (2002) [hep-ph/0112088]

[55] J. Bijnens, P. Dhonte, P. Talavera, *$\pi\pi$ scattering in three flavour ChiPT*, *JHEP*, **01**, 050 (2004)

[56] G. Colangelo, J. Gasser and A.Rusetsky, *Isospin breaking in Kl4 decays*, *Eur. Phys. J.* C **59**, 777 (2009) [arXiv:0811.0775]

[57] S. Descotes-Genon, M. Knecht, *Two-loop representations of low-energy pion form factors and pi-pi scattering phases in the presence of isospin breaking*, [arXiv:1202.5886]

[58] V. Bernard, S. Descotes-Genon, M. Knecht, work in progress

[59] A. Lai et al., NA48 collaboration, *Measurement of $K^0_{\mu 3}$ form factors*, *Phys. Lett.* **B 647** (2007) 341 [arXiv:0703002]

[60] F. Ambrosino et al., KLOE collaboration, *Measurement of the $K_L \to \pi\mu\nu$ form factor parameters with the KLOE detector*, *JHEP* **12** (2007) 105 [arXiv:0710.4470]

[61] E. Abouzaid et al., KTEV collaboration, *Dispersive analysis of $K_{L\mu 3}$ and K_{Le3} scalar and vector form factors using KTEV data*, *Phys. Rev.* **D 81** (2010) 341 [arXiv:0703002]

[62] J.R. Batley et al., *New high statistics measurement of K_{e4} decay form factors and $\pi\pi$ scattering phase shifts*, *Eur. Phys. J.* **C 54** (2008) 411

[63] J.R. Batley et al., *Determination of the S-wave $\pi\pi$ scattering lengths from a study of $K^\pm \to \pi^\pm\pi^0\pi^0$ decays*, *Eur. Phys. J.* **C 64** (2009) 589 [arXiv:0912.2165]

[64] H. Leutwyler, *Light quark masses*, Contribution to the Proceedings of the Workshop on Chiral Dynamics, Bern (2009), [arXiv:0911.1416v1[hep-ph]]

[65] S. Descotes-Genon, B. Moussallam, *Radiative corrections in weak semi-leptoni processes at low energy: a two-step matching determination*, *Eur.Phys.J* **C 42**, 403 (2005), [arXiv:0505077v1[hep-ph]]

[66] M. Antonelli et al., FlaviaNet Working Group On Kaon Decays collaboration, *Precision tests of the Standard Model with leptonic and semileptonic kaon decays*, [arXiv:0801.1817]

[67] M. Antonelli et al., *An evaluation of $|V_{us}|$ and precise tests of the Standard Model from world data on leptonic and semileptonic kaon decays*, *Eur. Phys. J.* **C 69** (2010) 399 [arXiv:1005.2323[hep-ph]]

[68] Particle Data Group collaboration, *Review of particle physics*, *Journal of Physics G*, Vol.**37** No.**7A**, (2010), for regular updates see http://pdg.lbl.gov

[69] G. Colangelo et al., (the FLAG working group of FLAVIANET), *Review of lattice results concerning low energy particle physics*, [arXiv:1011.4408[hep-lat]]

[70] B. Moussallam, *N_f dependence of the quark condensate from a chiral sum rule*, (1999), [arXiv:9909292v2[hep-ph]]

[71] B. Moussallam, *Flavour Stability of the Chiral Vacuum and Scalar Mesons Dynamics*, (2000), [arXiv:0005245v2[hep-ph]]

[72] B. Moussallam, *Virtual quarks, vacuum stability and scalar meson physics*, (2001), [arXiv:0111329v2[hep-ph]]

[73] J. Stern *Two alternatives of spontaneous chiral symmetry breaking in QCD* (1998) [arXiv:9801282v1[hep-ph]]

[74] S.Descotes-Genon, J. Stern, *Finite-volume analysis of N_f-induced chiral phase transitions*, *Phys. Rev. D* **62** (2000) 054011, [arXiv:9912234[hep-ph]]

[75] S.Descotes-Genon, J. Stern, *Vacuum fluctuations of $\bar{q}q$ and values of low-energy constants*, *Phys. Lett. B* **488** (2000) [arXiv:0007082]

[76] S.Descotes-Genon *Zweig rule violation in the scalar sector and values of low-energy constants*, *JHEP* **0103** 002 (2001) [arXiv:0012221]

[77] S. Descotes-Genon, L. Girlanda and J. Stern, *Chiral order and fluctuations in multi-flavour QCD*, *Eur. Phys. J.* **C 27** 115 (2003) [hep-ph/0207337]

[78] S. Descotes-Genon, L. Girlanda and J. Stern, *Paramagnetic effects of light quark loops on chiral symmetry breaking*, *JHEP* **0001** (2000) 041 [hep-ph/9910537]

[79] S.Descotes-Genon, N.H. Fuchs, L. Girlanda, J. Stern, *Resumming QCD vacuum fluctuations in three-flavours chiral perturbation theory*, *Eur. Phys. J.* C **34** 201 (2004) [hep-ph/0311120]

[80] S.Descotes-Genon *The role of strange sea quarks in chiral extrapolations on the lattice*, *Eur. Phys. J.* C **40** 81 (2005) [arXiv:0410233]

[81] S.Descotes-Genon *Low-energy pi-pi and pi-K scatterings revisited in three-flavour resummed chiral perturbation theory*, *Eur. Phys. J.* C **52** 141 (2007) [arXiv:0703154[hep-ph]]

[82] S.Descotes-Genon, *Zweig rule violation in the scalar sector and values of low-energy constants*, *JHEP*, **03** (2001) 002 [hep-ph/0012221]

[83] S.Descotes-Genon, *$\pi\pi$ and πK scatterings in three-flavours resummed chiral perturbation theory*, *J. Phys. Conf. Ser.* **110** (2008) 052012 [arXiv:0710.1696]

[84] S.Descotes-Genon, *Le rôle du quark étrange dans la brisure de la symétrie chirale*, *Habilitation à Diriger les Recherches*, http://tel.archives-ouvertes.fr/tel-00678960

[85] M. Kolesar and J. Novotny, *Pi-eta scattering and the resummation of vacuum fluctuation in three-flavour ChPT Eur. Phys. J.* C **56** 231 (2008) [arXiv:0802.1289[hep-ph]]

[86] M. Kolesar and J. Novotny, *The eta decay constant in 'resummed' chiral perturbation theory Fizika* B **17** 57 (2008) [arXiv:0802.1151]

[87] Marian Kolesar, *Analysis of discrepancies in Dalitz plot parameters in eta to 3 pion decay*, *Nucl. Phys.* **B** (Proceedings Supplements) 219-220 C 292-295 (2011), [arXiv:1109.0851v2[hep-ph]]

[88] B. Moussallam, *N_f dependence of the quark condensate from a chiral sum rule*, *Eur. Phys. J.*, **C 14** (2000) 111 [hep-ph/9909292]

[89] B. Moussallam, *Flavor stability of the chiral vacuum and scalar meson dynamics*, *JHEP*, **08** (2000) 005 [hep-ph/0005245]

[90] P. Buettiker, S. Descotes-Genon and B. Moussallam, *A re-analysis of πK scattering à Roy and Steiner*, *Eur. Phys. J.* **C 33** (2004) 409 [hep-ph/0310283]

[91] T. A. Lahde and U.-G. Meißner, *Improved Analysis of J/ψ Decays into a Vector Meson and Two Pseudoscalars*, *Phys. Rev.* **D 74** (2006) 034021 [hep-ph/0606133]

[92] V. Bernard, S. Descotes-Genon and G. Toucas, *Chiral dynamics with strange quarks in the light of recent lattice simulations*, *JHEP*, **1101** (2011) 107 [hep-ph/1009.5066]

[93] V. Bernard, S. Descotes-Genon and G. Toucas, *Topological susceptibility on the lattice and the three-flavour quark condensate*, *JHEP*, **1206** (2012) 051 [hep-ph/1203.0508]

[94] V. Bernard, S. Descotes-Genon and G. Toucas, *Determining the chiral condensate from the distribution of the winding number beyond topological susceptibility*, [arXiv:1209.4367v1[hep-lat]]

[95] G. Colangelo, S. Durr, A. Juttner, L. Lellouch, H. Leutwyler, V. Lubicz, S. Necco, C. T. Sachrajda, *Review of lattice results concerning low energy particle physics*, *Eur. Phys. J.* **C 71** 1695 (2011) [arXiv:1011.4408 [hep-lat]]

[96] S. Aoki et al., (PACS-CS collaboration), *2+1 Flavor Lattice QCD toward the Physical Point*, *Phys. Rev.* **D 79** (2009) 034503, [arXiv:0807.1661]

[97] S. Aoki et al., (PACS-CS collaboration), *Physical Point Simulation in 2+1 Flavor Lattice QCD*, *Phys. Rev.* **D 81** (2010) 074503, [arXiv:0911.2561]

[98] C. Allton et al., (RBC and UKQCD collaboration) *2+1 flavor domain wall QCD on a* $(2fm)^3$ *lattice: light meson spectroscopy with* $Ls = 16$, *Phys. Rev.* **D 76** (2007) 014504, [arXiv:0701013 [hep-lat]]

[99] C. Allton et al., (RBC-UKQCD collaboration) *Physical Results from 2+1 Flavor Domain Wall and* $SU(2)$ *Chiral Perturbation Theory*, *Phys. Rev.* **D 78** (2008) 114509, [arXiv:0804.0473]

[100] P.A. Boyle et al., (RBC-UKQCD collaboration) $K_{\ell 3}$ *semileptonic form factor from 2+1 lattice QCD*, *Phys. Rev. Lett.* **100** (2008) 141601, [arXiv:0710.5136]

[101] P.A. Boyle et al., (RBC-UKQCD collaboration) $K \to \pi$ *form factor with reduced model dependence*, *Eur. Phys. J.* **C 69** 159 (2010) [arXiv:1004.0886]

[102] C. Bernard et al., *Status of the MILC light pseudo-scalar meson project*, *PoS* **Lattice 2007** 090, [arXiv:0710.1118]

[103] The MILC Collaboration, A. Bazavov et al., *Results from the MILC collaboration's* $SU(3)$ *chiral perturbation theory analysis*, *PoS* **Lattice 2009** 079, [arXiv:0910.3618]

[104] S. Durr and al. *The ratio* F_K/F_π *in QCD*, *Phys. Rev.* **D 81** 054507 (2010) [arXiv[1001.4692]]

[105] S. Durr and al. *Ab-Initio Determination of Light Hadron Masses*, *Science* **332** 1224 (2008) [arXiv[0906.3599]]

[106] R. Baron and al. *Light hadrons from lattice QCD with light (u,d), strange and charm dynamical quarks*, *JHEP*, **06**, 111, (2010), [arxiv:1004.5284]

[107] TWQCD collaboration, J. Noaki and al., *Chiral properties of light mesons with* $N_f = 2 + 1$ *overlap fermions*, PoS(LAT2009)096[arXiv:0910.5532]

[108] E. Scholz, private communication

[109] R. Mawhinney (RBC collaboration), *NLO and NNLO chiral fits for 2+1 flavor DWF ensembles*, *PoS* (LAT2009) 081 [arXiv:0910.3194]

[110] J.M. Flynn, C.T. Sachrajda (RBC collaboration), $SU(2)$ *chiral perturbation theory*

[111] J. Bijnens and I. Jemos, *Determination of Low Energy Constants and testing Chiral Perturbation Theory at order* p^6 *(NNLO)*, PoS(CD09)087 [arXiv:0909.4477]

[112] V. Bernard, E. Passemar, *Chiral Extrapolation of the Strangeness Changing* $K\pi$ *Form Factor*, *JHEP*, **04** (2010) 001 [arXiv:0912.3792]

[113] H. Leutwyler, A.V. Smilga, *Spectrum of Dirac operator and role of winding number in QCD*, *Phys. Rev.* D **46** 5607 (1992)

[114] R. Kaiser, H. Leutwyler, *Large N_c in chiral perturbation theory*, *Eur. Phys. J.* C **17** (2000) 623 [arXiv0007101]

[115] J. Bijnens, Jie Lu, *Technicolor and other QCD-like theories at next-to-next-to-leading order*, [arXiv:0910.5424v1[hep-ph]]

[116] P. Herrera-Sikldy, J.I. Latorre, P. Pascual and J. Taron, *Chiral Effective Lagrangian in the large-Nc limit: the nonet case*, *Nucl.Phys. B* **497**, 345-386, (1997), [arxiv:9610549[hep-lat]]

[117] H. Fukaya et al., *Determination of the chiral condensate from QCD Dirac spectrum on the lattice*, *Phys. Rev.* **D 83** (2011) 074501, [arXiv:1012.4052]

[118] S. Aoki, H. Fukaya, S. Hashimoto, T. Onogi, *Finite volume QCD at fixed topological charge*, *Phys. Rev.* **D 76** (2007) 054508, [arXiv:0707.0396]

[119] Y. Mao, T. Chiu, [TWQCD collaboration], *Topological Susceptibility to the One-Loop Order in Chiral Perturbation Theory*, *Phys. Rev.* **D 80** (2009) 034502, [arXiv:0903.2146]

[120] T.W. Chiu, T,H, Hsieh and P.K. Tseng (TWQCD Collaboration),*Topological susceptibility in 2+1 flavors lattice QCD with domain-wall fermions*, *Phys. Lett. B.* **671** 135 (2009) [arXiv:0810.3406]

[121] A. Bazavov et al. (MILC collaboration), *Topological susceptibility with the asqtad action*, *Phys. Rev. D* **81** 114501 (2010) [arXiv:1003.5695]

[122] Y. Aoki and al. (RBC and UKQCD collaborations), *Continuum Limit Physics from 2+1 Flavor Domain Wall QCD*, *Phys. Rev.* **D 83** (2011) 074508, [arXiv:1011.0892 [hep-lat]]

[123] T.W. Chiu, T,H, Hsieh and Y.Y. Mao (TWQCD Collaboration),*Topological Susceptibility in Two Flavors Lattice QCD with the Optimal Domain-Wall Fermion*, *Phys. Lett. B.* **702** 131 (2011) [arXiv:1105.4414]

[124] K. Cichy, V. Drach, E. Garcia-Ramos and K. Jansen *Topological susceptibility and chiral condensate with $N_f = 2 + 1 + 1$ dynamical flavors of maximally twisted mass fermions*, [arXiv:1111.3322s]

[125] S. Durr, Z. Fodor, C. Hoelbling and T. Kurth, *Precision study of the $SU(3)$ topological susceptibility in the continuum*, *JHEP* **0704** 055 (2007) [arXiv:0612021]

[126] L. Giusti, B. Taglienti and S. Petrarca, *Towards a precise determination of the topological susceptibility in the $SU(3)$ Yang-Mills theory*, PoS **LAT 2009** 229 (2009) [arXiv:1002.0444]

[127] R. Baron, P. Boucaud, J. Carbonell, A. Deuzeman, V. Drach, F. Farchioni, V. Gimenez and G. Herdoiza et al., *Light hadrons from lattice QCD with light (u,d), strange and charm dynamical quarks*, *JHEP* **1006** 111 (2010) [arXiv:1004.5284 [hep-lat]].

[128] S.R. Sharpe, *Applications of Chiral Perturbation theory to lattice QCD*, [arXiv:0607016[hep-lat]]

[129] M. Luscher *Volume Dependence of the Energy Spectrum in Massive Quantum Field Theories. 1. Stable Particle States*, *Commun. Math. Phys.* **104** 177 (1986)

[130] D. Becirevic and G. Villadoro, *Impact of the finite volume effects on the chiral behavior of f(K) and B(K)*, *Phys. Rev.* D **69** (2004) 054010 [arXiv:0311028[hep-lat]]

[131] G. Colangelo and S. Durr, *The Pion mass in finite volume*, *Eur. Phys. J.* C **33** 543 (2004) [arXiv:0311023[hep-lat]]

[132] G. Colangelo and C. Haefeli, *An Asymptotic formula for the pion decay constant in a large volume*, *Phys. Lett.* B **590** (2004) 258 [arXiv:0403025[hep-lat]]

[133] F. Bernardoni, P. Hernandez, N. Garron, S. Necco and C. Pena, *Probing the chiral regime of Nf=2 QCD with mixed actions*, *Phys. Rev. D* **83**, 054503, (2011), [arXiv:1008.1870[hep-lat]]

[134] Y. Aoki et al., *Non-perturbative renormalization of quark bilinear operators and B_K using domain wall fermions Phys. Rev.* D **78** 054510 (2008) [arXiv:0712.1061 [hep-lat]]

[135] J. Gasser, C. Haefeli, M. A. Ivanov and M. Schmid, *Integrating out strange quarks in ChPT*, *Phys. Lett. B* **652** 21 (2007) [arXiv:0706.0955[hep-ph]]

[136] J. Gasser, C. Haefeli, M. A. Ivanov and M. Schmid, *Integrating out strange quarks in ChPT: Terms at order p**6*, *Phys. Lett. B* **675** 49 (2009) [arXiv:0903.0801 [hep-ph]]

[137] J. Gasser, C. .Haefeli, M. A. Ivanov and M. Schmid, *Relations between SU(2)- and SU(3)-LECs in chiral perturbation theory Phys. Part. Nucl.* **41** 939 (2010)

[138] L. Del Debbio, H. Panagopoulos and E. Vicari, *theta dependence of SU(N) gauge theories*, *JHEP* **0208** 044 (2002), [hep-th/0204125]

[139] M. D'Elia, *Field theoretical approach to the study of theta dependence in Yang-Mills theories on the lattice*, *Nucl. Phys. B* **661** 139 (2003), [hep-lat/0302007]

[140] L. Giusti, S. Petrarca and B. Taglienti, *Theta dependence of the vacuum energy in the SU(3) gauge theory from the lattice*, *Phys.Rev. D* **76** 094510 (2007), [arXiv:0705.2352 [hep-th]]

[141] E. Vicari and H. Panagopoulos, *Theta dependence of SU(N) gauge theories in the presence of a topological term Phys.Rept.* **470** 93 (2009), [arXiv:0803.1593 [hep-th]]